
# THÈSE

**En vue de l'obtention du**

## DOCTORAT DE L'UNIVERSITÉ DE TOULOUSE

**Délivré par :**
Institut National Polytechnique de Toulouse (INP Toulouse)

**Discipline ou spécialité :**
Génie des Procédés et de l'Environnement

---

**Présentée et soutenue par :**
Santiago SEPTIEN STRINGEL

**le :** 21 novembre 2011

**Titre :**

High temperature gasification of millimetric wood particles between 800°C and 1400°C

---

**Ecole doctorale :**
Mécanique, Energétique, Génie civil et Procédés (MEGeP)

**Unité de recherche :**
RAPSODEE (Ecole des Mines d'Albi-Carmaux)

**Directeur(s) de Thèse :**

Pr. Sylvain SALVADOR (EMAC)

**Rapporteurs :**
Pr. Wim VAN SWAAIJ, Université de Twente, Pays-Bas
Pr. Frédéric MARIAS, Université de Pau et des Pays de l'Adour

**Autre(s) membre(s) du jury**
Pr. Yann ROGAUME, Université Henri Poincaré, Nancy, Cxaminateur
Dr. Marine PEYROT, CEA Grenoble, Cxaminateur
Dr. Sylvie VALIN, CEA Grenoble, Cv_kgl_rcsp

*High temperature gasification of millimetric wood particles between 800°C and 1400°C*

*By Santiago SEPTIEN STRINGEL*

*Gazéification à haute température des particules millimétriques de bois entre 800°C et 1400°C*

*Par Santiago SEPTIEN STRINGEL*

*“The imagination is more*
*important than the knowledge”*

*A. Einstein*

# Remerciements !!!!!!!!!!

Ma thèse, qui aboutit avec la publication de cet ouvrage, a constitué une période très importante de ma vie, marquée par de nombreux apprentissages et de très agréables souvenirs qui vont rester toujours en moi. Trois années se sont déjà écoulées, trop rapidement pour pouvoir m'en apercevoir. Mais si le temps passe si vite c'est parce qu'on vit des moments plaisants et riches, et c'est ainsi que je pourrais résumer cette période de ma vie qui vient de s'achever.
Mes travaux de thèse ont débouché sur des résultats très satisfaisants et ont été l'objet de critique très positive. Cela n'aurait pas pu être possible sans la précieuse participation d'un grand nombre de personnes, chacune ayant apportée à sa manière une pierre à l'édifice. Après tout, cette thèse a été un travail en équipe et les fruits de nos efforts sont présentés dans ce manuscrit. Ainsi donc, j'ai une liste très étendue de personnes à remercier...

Un grand merci à ma responsable, Sylvie Valin, pour ton excellent rôle d'encadrant et pour ton énorme patience envers moi. Tu m'as permis de bien orienter la thèse dès le début, alors que c'est justement à ce niveau qu'on est le plus désorienté. A tout moment, tu t'es montrée intéressée et attentive à mon travail, et n'a jamais hésité à m'apporter ton aide et à mettre à ma disposition ton temps. Lors de la rédaction du mémoire de thèse, période qui s'est avérée assez rude, tu as partagé ma souffrance et mon stress, surtout à la fin, en suivant avec acharnement l'évolution de ma rédaction (même pendant tes journées libres !!!) et en apportant des corrections très pertinentes qui sont essentielles à la qualité de ce document.

Un grand merci à Sylvain Salvador, notre « Einstein » de la combustion et gazéification, pour ton excellent rôle de directeur de thèse. Je te remercie pour ta grande disponibilité et ta direction scientifique d'excellence, sur laquelle l'épine dorsale du présent travail repose. Un grand merci pour ton accueil chaleureux lors de mes campagnes d'essais à l'Ecole de Mines. Nos discussions sur la science, sur mes anecdotes en Albi, sur tes vols en ULM, ou sur n'importe quel autre sujet entre chaque expérience vont me manquer. Je regrette de n'avoir pas eu l'occasion de me frotter à tes talents de badmintoneurs. Il paraît qu'en plus d'être un scientifique de qualité, tu es aussi un très bon joueur de badminton, redouté dans l'EMAC.

Un grand merci à Bertrand Spindler, Marine Peyrot et Capucine Dupont. Merci d'avoir assurer avec la meilleure disponibilité, le relais de l'encadrement de mes travaux de thèse

pendant les congés de maternité de Sylvie Valin. Votre contribution à la thèse est indéniable du point de vue expérimental comme de modélisation. Merci à Bertrand et Marine pour être toujours prêt à transposer mes idées, même les plus folles, dans GASPAR. Merci à Marine pour ton énorme générosité et ton admirable gentillesse. Merci à Capucine d'avoir toujours cru dans mes capacités scientifiques lors de mon stage et de m'avoir recommandé pour cette thèse (et allez le PSG, même si vous allez regretter de n'avoir pas pris à Guillermo Ochoa comme gardien de but ;-) ).

Un grand merci aux membres du jury de thèse d'avoir accepté de relire ce manuscrit et par votre assistance dans ma soutenance de thèse. Vos remarques ont été d'une valeur précieuse pour l'amélioration de ce document.

Un grand merci à tout le personnel technique qui est derrière cette thèse et les gens qui m'ont donné un coup de main lors de mes expériences.
Merci Bernard Auduc pour maintenir en « bonne forme » l'installation du four à chute et de veiller à sa constante amélioration. Tes multi-compétences techniques et tes interventions chirurgicales dans l'équipement expérimental m'ont toujours impressionné beaucoup, en plus d'être une personne très agréable et avec un très bon sens de l'humour imprégné par l'accent du sud-ouest.
De même, je voudrais rendre hommage à tous les anciens utilisateurs de l'installation du four à chute qui m'ont précédé (Van De Steene, Commandré, Couhert, Dupont, Li) : vous avez permis d'arriver vers l'outil expérimental performant et fiable d'aujourd'hui.
Je voudrais également remercier Younes Chhiti, mon ami doctorant de l'EMAC réalisant une thèse « jumelée » à la mienne. Merci de m'avoir prêté, dans des nombreuses occasions, tes bras lors de mes expériences dans le four à chute, en plus de me montrer des gestes de ta générosité au quotidien (merci pour toutes les fois que tu m'as raccompagné à la gare quand je partais d'Albi, et par tes nombreuses invitations chez toi pour manger un tajine, fumer le narguilé et boire du thé à la menthe).
Je ne voudrais pas oublier de remercier à Sylvain Jacob, mon Padawan du four à chute : lors de ma dernière campagne d'essais, tu m'as apporté une aide plus que précieuse me permettant ainsi d'accomplir un programme très chargé qui paraissait irréalisable dans le temps imparti (Sylvain, j'espère que Ganesh sera de ton côté pour la fin de ta thèse, et surtout pour tes expériences en ATG ☺).
Merci Christelle Verne - Tournon pour ton aide et ton support technique lors des mes expériences au CEA.

Un grand merci à tous les membres du LTB pour votres aides et conseils, et surtout pour votre amitié. L'ambiance du laboratoire a été toujours très agréable, épanouissante et

professionnelle, ce qui m'a permis de travailler dans les meilleures conditions. Quelle meilleur manière de commencer la journée de travail qu'après notre traditionnelle « rencontre café » de 9 heures, avec vous tous, dans la salle Bethsy, et se demander c'était qui le prochain à apporter les croissants !!!!!!
Un grand merci à Karine Froment de m'avoir donné l'opportunité de rester dans le laboratoire après mon stage (tu as vu, finalement j'ai tenu ma promesse de bien me tenir ☺).
Un grand merci à tous les gens avec lequel j'ai partagé un espace au cours de mes trois années de thèse : mon cher collègue de bureau, Timothée Nocquet (ou Tim), je te souhaite bon courage pour la fin de ta thèse, et je suis sûr que tu vas très bien t'en sortir grâce à tes grandes compétences et à ton appareil de massage de crâne (tu verras que tu en auras besoin à la fin de la thèse); Sébastien Thierry, le plus grand fan de Miss Mexico 2010 et passionné des grosses vagues (il se prétend aussi bon surfeur que Brice de Nice), avec lequel j'ai eu le grand plaisir de partager la salle d'analyse et l'animer un peu de temps en temps (Séb, j'attends encore que tu me fasses goûter le saucisson de ta famille du 2011, j'espère qu'il soit aussi bon que celui des éditions précédentes !).

Un grand merci aux gens qui ont fait partie de mon quotidien en dehors du cadre du travail. Merci à ma copine Sam-Soan, tu m'as toujours donné son appui, surtout dans les périodes difficiles de la thèse et après-thèse. Merci pour m'avoir nourri et éviter de manger que des Kebab à la fin de thèse, de m'avoir partagé tes fortes compétences organisationnelles lors de mon pot de thèse, et aussi pour apporter des corrections de syntaxe à ces remerciements☺. Ton soutien a été crucial... Merci, je tiens fort à toi.
Un grand merci à mes colocs du 1 rue de Vicat (Brigitte, Martin, Dieguito, Pierrot, Nat, Cha), nous avons donné de la vie à cet appartement et vous m'avez permis de me sentir en famille. Je vais garder précieusement dans ma mémoire le grand nombre de repas que nous avons partagé, les fêtes que nous avons organisées et où plus de 100 personnes ont assisté (à notre grande surprise !), le grand nombre de squatteurs qui ont connu les confortables fauteuils de la coloc, entre autres souvenirs... De même, merci beaucoup Cha, Pierrot, Poule, Achille, Sergio, Suzie et Soan, vous m'avez permis d'alléger la part qui me correspondait lors du déménagement, à la veille de rendre mon manuscrit de thèse.
Un grand merci à mes camarades connus dans le cadre du CEA (Matteo, Giorgio, Sergio, Kavita, Malek, Yan, Rob, JC, Manon, Erik...) et en dehors (Anna, Ali et Jean, Adéline, Adrian, Victor, Manolo...) pour votre soutien et pour tous les moments inoubliables que nous avons passé ensemble. Les épiques repas à midi en H1 ou H3 avec mes collègues stagiaires et thésards , où on parlait de tout et n'import quoi, me manquent déjà trop.
Un grand merci pour l'amitié et soutien de mes camarades, éparpillés un peu partout en France et dans le monde (Caio, Sam, Ricky, Palo, Désir, Luis, Inès, les Carlos, Oliver, Inma,

Changh...). J'ai eu vraiment la chance de vous croiser dans un instant précieux de nos chemins.

Maintenant je vais changer de continent et donc de langue. Je passe à l'espagnol (CARAMBA !!!) ...
« Muchas gracias a TODA mi familia y a mis viejos camaradas (Raúl, Layin, Isabel, Esteban, Danielito...) que han seguido de lejos mi aventura en Francia y nunca me han dejado de mandar sus bendiciones. Muchas gracias por su apoyo y por creer en mí. A pesar de la distancia y el tiempo, los traigo conmigo en mi espíritu.
En especial, agradezco del fondo de mi corazón y expreso mi máxima gratitud para Cuaya y Mamá Ana, gracias por haberme brindado todo el apoyo y los medios para poder realizar mis estudios universitarios en Francia.
Muchas gracias a la tía Ana Maria por haberme caucionado para todos mis tramites un sin números de veces y así haberme facilitado mi estancia en Francia. Muchas gracias por recibirme siempre con los brazos abiertos y mantener la puerta de tu casa en Paris abierta.
Muchas gracias a la Madrina Osa, pudiste superar una terrible infección estomacal y liberarte de las obligaciones de tu chamba para poder estar presente el día de la presentación de mi doctorado. Tu presencia me inyecto muchos ánimos durante la charla. Y ni hablar, lastima que no pudo venir Enrique, será para la próxima.
Este trabajo se lo dedico a la Abuela Olvido que seguramente me estará mirando desde el mas allá con esa gran sonrisa que nos acostumbró durante toda su vida. Y a mi abuelo Septien y a Tita, que se nos fueron este 2011... »

Merci à tous pour votre soutien, les apprentissages que vous m'avez réparti et les beaux moments que nous avons partagé ensemble. Cela a été le véritable moteur qui m'a motivé à progresser et arriver au bout de cette thèse.

Merci de tout mon cœur

*Santiago Septien Stringel*

Optons une attitude éco-responsable: renseignons nous, réfléchissons et agissons ensemble! Le changement climatique peut se combattre avec un changement de conscience ...

## ABSTRACT

Biomass gasification was studied in the conditions of an entrained flow reactor, namely at high heating rate and temperature. Experiments in a drop tube reactor were performed between 800°C and 1400°C, with wood particles of 0.35 mm and 0.80 mm size, under inert and steam containing - 25 mol% of $H_2O$ - atmospheres. These experiments were also simulated with a 1D model which gave good predictions. The collected solids, soot and char, were analyzed and characterized.

This study highlights the importance of gas phase reactions on the yields of the final products, mainly gaseous compounds, in these conditions. These reactions are hydrocarbons cracking, reforming and polymerization, leading to soot formation, and water-gas shift.

Char graphitization and deactivation were experimentally demonstrated. However, these phenomena have a negligible influence on char evolution in the drop tube reactor.

Finally, the particle size was shown to have almost no influence on experimental results.

**Keywords:** Gasification; biomass; drop tube reactor; entrained flow reactor; soot; modeling

## RESUME

La gazéification de la biomasse a été étudiée dans les conditions d'un réacteur à flux entraîné, à savoir à vitesse de chauffage et à température élevées. Des expériences ont été réalisées dans un four à chute entre 800°C et 1400°C, à partir de particules de bois de taille 0,35 mm et 0,80 mm, dans une atmosphère inerte (100% molaire de $N_2$), ou contenant de la vapeur d'eau (25% molaire). Les expériences ont également été simulées grâce à un modèle 1D avec des résultats positifs, ce qui a permis de mieux comprendre les phénomènes mis en jeu. Les solides obtenus (suies et char) ont été analysés et caractérisés.

Des rendements élevés en gaz et goudrons, et un faible rendement en char ont été mesurés. Par conséquent, l'évolution de la phase volatile est déterminante pour les rendements des produits finaux. Au-dessus de 1000°C, la formation de suies devient importante. Les suies sont formées à partir de $C_2H_2$ et de HAP. En présence de vapeur d'eau, le rendement en suies est nettement moins élevé, ce qui s'explique essentiellement par le vaporeformage des précurseurs de suie, mais aussi par leur gazéification. La réaction de water-gas shift joue un rôle important dans la distribution des gaz majoritaires. La gazéification du char a été mise en évidence à 1200°C et 1400°C sous atmosphère humide. L'ensemble de ces réactions conduit à un gaz riche en $H_2$, CO et $CO_2$. L'équilibre thermodynamique est presque atteint à 1400°C avec une concentration de 25% molaire de $H_2O$ dans l'atmosphère.

La graphitisation et la désactivation du char porté à haute température ont été mises en évidence expérimentalement. Néanmoins, ces phénomènes ont une influence négligeable sur l'évolution du rendement en char lors des expériences en four à chute.

Enfin, la taille des particules n'a presque aucune influence sur les résultats expérimentaux.


**Mots clés:** Gazéification; biomasse; four à chute; réacteur à flux entraîné; suies; modélisation

## Table of contents

TABLE OF CONTENTS ..... I
LIST OF TABLES ..... VI
LIST OF FIGURES ..... VII
NOMENCLATURE ..... XI

INTRODUCTION ..... 2
INTRODUCTION EN FRANÇAIS ..... 7

CHAPTER 1: FUNDAMENTAL CONCEPTS ..... 10
1. DESCRIPTION OF WOOD ..... 11
1.1. MACROSCOPIC STRUCTURE ..... 11
1.2. CHEMICAL COMPOSITION ..... 12
*1.2.1. Elementary composition ..... 12*
*1.2.2. Moisture content ..... 13*
*1.2.3. Constitution ..... 13*
2. DESCRIPTION OF WOOD PYROLYSIS ..... 15
2.1. PHYSICAL PHENOMENA ..... 15
2.2. CHEMICAL PHENOMENA ..... 16
2.3. PYROLYSIS REGIMES ..... 17
3. DESCRIPTION OF THE GAS PHASE EVOLUTION AND SOOT FORMATION ..... 17
3.1. CRACKING AND POLYMERIZATION REACTIONS ..... 17
*3.1.1. Generalities about cracking and polymerization reactions ..... 17*
*3.1.2. From hydrocarbon cracking and polymerization to soot formation ..... 18*
*3.1.3. Tar cracking, light hydrocarbon decomposition and formation of PAHs ..... 18*
*3.1.4. Formation and growth of soot particles ..... 20*
3.2. REFORMING REACTIONS ..... 21
3.3. WATER GAS SHIFT ..... 21
4. DESCRIPTION OF GASIFICATION ..... 22
4.1. CHARACTERISTICS OF THE CARBONACEOUS SOLIDS ..... 22
*4.1.1. Char characteristics ..... 22*
*4.1.2. Soot characteristics ..... 22*
4.2. DESCRIPTION OF THE PHENOMENA INVOLVED IN GASIFICATION ..... 23
*4.2.1. Physical phenomena ..... 23*
*4.2.2. Chemical phenomena ..... 25*
4.3. REACTION REGIME ..... 26
4.4. REACTIVITY OF CHAR AND SOOT ..... 26
5. INFLUENCE OF THE HEATING RATE ON WOOD GASIFICATION ..... 27
6. SUMMARY ..... 27
RESUME DU CHAPITRE 1 : CONCEPTS FONDAMENTAUX ..... 28
CHAPTER 2: STATE OF THE ART ..... 30
1. EXPERIMENTAL LITERATURE REVIEW ..... 31
1.1. EXPERIMENTAL APPROACHES USED IN LITERATURE ..... 31
*1.1.1. Pyrolysis experiments ..... 31*
*1.1.2. Gas phase reactions experiments ..... 33*
*1.1.3. Solid residue gasification experiments ..... 34*

*1.1.4. Direct biomass gasification experiments* ..... *35*
*1.1.5. Summary* ..... *35*
1.2. EXPERIMENTAL RESULTS OBTAINED UNDER HIGH HEATING RATES AND HIGH TEMPERATURES ..... 35
*1.2.1. Experimental results obtained under an inert atmosphere* ..... *35*
*1.2.1.1. Evolution of the yields with temperature* ..... *35*
*1.2.1.2. Evolution of char and soot yields with temperature* ..... *36*
*1.2.1.3. Influence of particle size during wood pyrolysis* ..... *36*
*1.2.2. Experimental results obtained under a wet atmosphere* ..... *36*
*1.2.3. Structural modifications of char and soot with temperature* ..... *37*
*1.2.4. Summary* ..... *38*
**2. MODELING APPROACH ..... 38**
2.1. PYROLYSIS MODELING ..... 39
*2.1.1. Chemical kinetics of biomass pyrolysis* ..... *39*
*2.1.1.1. Global and semi-global models* ..... *39*
*2.1.1.2. Other modeling approaches* ..... *40*
*2.1.2. Modeling of physical phenomena during biomass pyrolysis* ..... *41*
*2.1.2.1. Transport model* ..... *41*
*2.1.2.2. Shrinking core model* ..... *41*
2.2. GAS PHASE AND SOOT FORMATION MODELING ..... 42
*2.2.1. Gas reactions modeling* ..... *42*
*2.2.2. Representation of tar for modeling* ..... *44*
*2.2.3. Soot formation modeling* ..... *44*
2.3. GASIFICATION REACTION MODELING ..... 45
*2.3.1. Chemical kinetics of gasification* ..... *46*
*2.3.1.1. Determination of the intrinsic kinetics* ..... *46*
*2.3.1.2. Determination of f(X)* ..... *48*
*2.3.2. Modeling of physical phenomena* ..... *49*
*2.3.3. Modeling of additional phenomena for char gasification* ..... *50*
*2.3.3.1. Fracturing and peripheral fragmentation* ..... *50*
*2.3.3.2. Thermal deactivation* ..... *50*
2.4. OTHER MODELING APPROACHES ..... 52
2.5. SUMMARY ..... 52
**3. CHARACTERISTIC TIME ANALYSIS ..... 53**
3.1. PRINCIPLE OF THE APPROACH ..... 53
3.2. RESULTS OBTAINED IN LITERATURE FROM CHARACTERISTIC TIME ANALYSIS ..... 54
*3.2.1. Pyrolysis characteristic time analysis* ..... *54*
*3.2.2. Gasification characteristic time analysis* ..... *54*
3.3. SUMMARY ..... 55
**4. CONCLUSION AND THESIS FOCUS ..... 55**
**RESUME DU CHAPITRE 2 : ETAT DE L'ART ..... 56**
**CHAPTER 3: MATERIALS AND METHODS ..... 60**
**1. EXPERIMENTAL SETUP ..... 61**
1.1. RAW MATERIAL ..... 61
1.2. DROP TUBE REACTOR FACILITY ..... 63
*1.2.1. Description of the drop tube reactor* ..... *63*
*1.2.2. Operating conditions* ..... *65*
*1.2.3. Validation of the experimental conditions in the DTR* ..... *66*
*1.2.3.1. Temperature field* ..... *66*
*1.2.3.2. Steady-state regime in the DTR* ..... *68*
1.3. SOLID RESIDUE CHARACTERIZATION ..... 69
*1.3.1. Composition analysis* ..... *69*
*1.3.2. Observations by scanning electron microscopy* ..... *69*
*1.3.3. Reactivity measurements* ..... *69*
*1.3.3.1. Description of the experimental device* ..... *69*
*1.3.3.2. Description of the experimental procedure* ..... *71*
*1.3.3.3. Reactivity determination* ..... *72*

1.4. PRODUCTS YIELDS DETERMINATION ..... 72
*1.4.1. Gas compounds yields determination ..... 73*
*1.4.2. Char yield determination ..... 74*
*1.4.3. Tar and soot yields estimation ..... 74*
**2. PRELIMINARY CHARACTERIZATION OF THE EXPERIMENTS IN THE DROP TUBE REACTOR BY THEORETICAL STUDIES ..... 74**
2.1. CHARACTERISTIC TIME ANALYSIS ..... 74
*2.1.1. Calculation of the characteristic times ..... 75*
*2.1.1.1. Characteristic times related to physical phenomena ..... 75*
*2.1.1.2. Characteristic times related to chemical phenomena ..... 80*
*2.1.2. Results of the characteristic time analysis ..... 82*
*2.1.2.1. Heating and devolatilisation of the wood particles ..... 82*
*2.1.2.2. Mass transfer and gasification in the case of a char particle ..... 83*
*2.1.2.3. Mass transfer and gasification in the case of soot ..... 85*
*2.1.3. Summary ..... 86*
2.2. CALCULATIONS AT THE THERMODYNAMIC EQUILIBRIUM ..... 86
**RESUME DU CHAPITRE 3 : OUTILS ET METHODES ..... 89**
**CHAPTER 4: EXPERIMENTAL RESULTS ..... 92**
**1. THERMAL DECOMPOSITION OF 0.35 MM BEECH PARTICLES BETWEEN 800°C AND 1400°C ..... 93**
1.1. THERMAL DECOMPOSITION UNDER AN INERT ATMOSPHERE ..... 93
*1.1.1. Gas, tar, soot and char yields ..... 93*
*1.1.2. Individual gas yields ..... 94*
*1.1.3. Discussion ..... 96*
*1.1.3.1. Tar and soot evolution with temperature ..... 96*
*1.1.3.2. Char evolution with temperature ..... 97*
*1.1.3.3. Gas evolution with temperature ..... 97*
1.2. THERMAL DECOMPOSITION UNDER A WET ATMOSPHERE ..... 98
*1.2.1. Gas, tar, soot and char yields ..... 98*
*1.2.2. Individual gas yields ..... 99*
*1.2.3. Discussion ..... 101*
*1.2.3.1. Influence of temperature ..... 101*
*1.2.3.2. Influence of steam in the atmosphere ..... 101*
1.3. COMPARISONS WITH THE THERMODYNAMIC EQUILIBRIUM ..... 102
1.4. SUMMARY ..... 104
**2. INFLUENCE OF RESIDENCE TIME AND PARTICLE SIZE ON THE BEECH PARTICLES THERMAL DECOMPOSITION ..... 105**
2.1. INFLUENCE OF RESIDENCE TIME OF 0.35 MM PARTICLES ..... 105
*2.1.1. Products yields under an inert atmosphere ..... 105*
*2.1.2. Products yields under a wet atmosphere ..... 106*
*2.1.3. Discussion ..... 107*
2.2. INFLUENCE OF PARTICLE SIZE ..... 107
*2.2.1. Influence of particle size on products yields in a inert atmosphere ..... 107*
*2.2.2. Influence of particle size on products yields under a wet atmosphere ..... 108*
*2.2.3. Discussion ..... 109*
2.3. SUMMARY ..... 110
**3. CHARACTERIZATION OF SOOT AND CHAR ..... 110**
3.1. CHARACTERIZATION OF SOOT ..... 111
*3.1.1. Soot morphology ..... 111*
*3.1.2. Soot composition ..... 111*
*3.1.3. Soot reactivity ..... 112*
*3.1.3.1. Influence of temperature and residence time on soot reactivity ..... 112*
*3.1.3.2. Influence of particle size on soot reactivity ..... 112*
3.2. CHARACTERIZATION OF CHAR ..... 113
*3.2.1. Char morphology ..... 114*

*3.2.2. Char composition ... 117*
*3.2.2.1. Influence of temperature on char composition ... 117*
*3.2.2.2. Influence of residence time on char composition ... 118*
*3.2.2.3. Influence of particle size on char composition ... 118*
*3.2.2.4. Discussion ... 119*
*3.2.3. Char reactivity ... 120*
*3.2.3.1. Influence of temperature on char reactivity ... 120*
*3.2.3.2. Influence of residence time on char reactivity ... 121*
*3.2.3.3. Influence of particle size on char reactivity ... 121*
3.3. SUMMARY ... 123
**4. CONCLUSION ... 123**
**RESUME DU CHAPITRE 4 : RESULTATS EXPERIMENTAUX ... 125**
**CHAPTER 5: MODELING ... 128**
**1. DESCRIPTION OF GASPAR SOFTWARE ... 129**
1.1. DESCRIPTION OF THE ORIGINAL MODEL ... 129
*1.1.1. Origins ... 129*
*1.1.2. Basic principles ... 129*
*1.1.3. Modeling of physical and chemical processes ... 130*
*1.1.4. Input and output data of the model ... 130*
*1.1.5. Limitation of the model ... 131*
1.2. MODIFICATIONS IN GASPAR ... 131
*1.2.1. Modeling of tar evolution ... 131*
*1.2.2. Modeling of soot formation and gasification ... 131*
*1.2.2.1. Modeling of soot formation ... 131*
*1.2.2.2. Modeling of soot gasification ... 132*
*1.2.3. Modeling of char gasification ... 133*
*1.2.3.1. Modeling of the intrinsic kinetics ... 134*
*1.2.3.2. Modeling of the surface function ... 134*
1.3. SUMMARY ... 134
**2. VALIDATION AND RESULTS OF THE MODELING ... 135**
2.1. DETERMINATION OF VARIABLES OF THE MODEL FOR THE CALCULATIONS ... 135
2.2. SELECTION OF THE MODEL TAR COMPOUNDS ... 136
2.3. VALIDATION OF GASPAR ... 137
*2.3.1. Validation of the devolatilization coefficients choice ... 137*
*2.3.2. Validation of the soot modeling approach ... 138*
*2.3.3. Validation of char gasification modeling approach ... 139*
2.4. RESULTS OF THE SIMULATION ... 141
*2.4.1. Results of the simulation for $C_2H_2$, PAHs and soot ... 141*
*2.4.1.1. Simulation of experiments under an inert atmosphere ... 141*
*2.4.1.2. Simulation of experiments under a wet atmosphere ... 144*
*2.4.2. Results of the simulation for major gas ... 147*
*2.4.2.1. Simulation of experiments under an inert atmosphere ... 147*
*2.4.2.2. Simulation of experiments under a wet atmosphere ... 149*
2.5. SUMMARY ... 151
**3. CONCLUSION AND PERSPECTIVES ... 151**
**RESUME DU CHAPITRE 5 : MODELISATION ... 153**

**CONCLUSION ... 156**
**CONCLUSION GENERALE ET PERSPECTIVES ... 159**

**REFERENCES ... 162**

APPENDIXES ..... 176
APPENDIX A: SUMMARY OF ACTUAL ENERGETIC SITUATION ..... 177
APPENDIX B: BIOMASS GASIFICATION PROCESS ..... 180
APPENDIX C: LIST OF THE MAIN SOOT PRECURSORS ..... 181
APPENDIX D: PARTICLE RESIDENCE TIME DURING EXPERIMENTS IN THE DROP TUBE REACTOR ..... 182
APPENDIX E: REGIMES OF PYROLYSIS AND GASIFICATION DURING PARTICLES THERMAL DECOMPOSITION ..... 185
APPENDIX F: EXPERIMENTAL PRODUCTS YIELDS RESULTS ..... 187
APPENDIX G: SEM OBSERVATIONS OF SOOT AND CHAR FROM DTR EXPERIMENTS ..... 189
APPENDIX H: INFLUENCE OF A WET ATMOSPHERE ON CHAR CHARACTERISTICS ..... 195
APPENDIX I: KINETIC PARAMETERS CALCULATION FOR SOOT AND CHAR GASIFICATION ..... 198

## List of Tables

Table 1. Elementary mean composition of wood (Mermoud, 2006) ..... 12
Table 2. Chemical composition of some wood species (Sjostrom, 1993) ..... 13
Table 3. Tar classification proposed by Evans and Milne ..... 18
Table 4. Typical operating parameters of reactors for pyrolysis experiments under high heating fluxes ... 32
Table 5. Main dimensionless numbers related to biomass gasification ..... 53
Table 6. Different regimes of pyrolysis and gasification ..... 54
Table 7. Sample size distribution ..... 61
Table 8. Biomass composition ..... 62
Table 9. Composition of biomass ash obtained at 550°C ..... 62
Table 10. Gas analyzers used during experiments ..... 65
Table 11. Gas and particle residence time for experiments in the DTR ..... 66
Table 12. Error bar for the yield of each gaseous compound ..... 73
Table 13. Values from the literature of physical properties of wood, char and soot ..... 79
Table 14. Expression of the physical properties of pure gas in function of temperature (Perry, 1997) ..... 79
Table 15. Kinetic parameters of fast pyrolysis ..... 81
Table 16. Kinetic parameters of gasification of biomass char from fast pyrolysis ..... 82
Table 17. Kinetic parameters of soot gasification (De Soete, 1988) ..... 82
Table 18. Characteristic times and dimensionless numbers relative to heat transfer and pyrolysis ..... 83
Table 19. Characteristic times and dimensionless numbers relative to mass transfer and char gasification with 25 mol% of $H_2O$ ..... 84
Table 20. Characteristic times and dimensionless numbers relative to mass transfer and char gasification with 1 mol% of $H_2O$ ..... 84
Table 21. Characteristic times relative to mass transfer and soot gasification ..... 85
Table 22. Range of the temperature decomposition of light hydrocarbons under an inert atmosphere ..... 98
Table 23. Comparison of the temperature of complete conversion (temperature from which hydrocarbons are undetectable) for $CH_4$, $C_2H_2$ and $C_6H_6$ between an inert atmosphere and a wet atmosphere composed 25 mol% of $H_2O$ (Hiblot, 2010; Valin et al., 2009) ..... 102
Table 24. Molar composition (daf) of soot samples from the 0.35 mm particles thermal decomposition at 1200°C and 1400°C, after 2 s and 4 s of gas residence time ..... 111
Table 25. Molar composition (daf) of char samples from the 0.35 mm particles thermal decomposition at 1000°C, 1200°C and 1400°C, after 4 s of residence time ..... 117
Table 26. Molar composition (daf) of char samples from the 0.35 mm particles thermal decomposition 1000°C and 1200°C, after 2 s and 4 s of residence time ..... 118
Table 27. Molar composition (daf) of char samples from the 0.35 mm and 0.80 mm particles thermal decomposition at 1000°C, 1200°C and 1400°C, by sampling at the bottom of the reactor ..... 119
Table 28. Molar composition of tar from Hinoki cypress sawdust thermal decomposition experiments at 800°C in a DTR (Zhang et al., 2010) ..... 136
Table 29. Indicators concerning fossil fuels exploitation ..... 178
Table 30. Potential of biomass as a source of energy in France ..... 179
Table 31. Operating conditions of a fluidized bed reactor and an entrained flow reactor ..... 180
Table 32. Molar composition (daf) of chars samples from the 0.35 mm particle thermal decomposition under inert and wet atmospheres at 1000°C ..... 197

## List of Figures

Figure 1. Scheme of an entrained flow reactor (Marsh et al., 1971) ..... 4
Figure 2. Anatomy of a tree trunk ..... 11
Figure 3. Gross structure of softwood (a) and hardwood (b) (Siau, 1984) ..... 12
Figure 4. Structure of cellulose (Sjostrom, 1993) ..... 13
Figure 5. Structure of hemicellulose molecule (Ibañez, 2002) ..... 14
Figure 6. Example of a lignin polymer structure (Sudo & Takahashi, 1989) ..... 14
Figure 7. Microstructure of wood fibers ..... 15
Figure 8. External radiative, convective and convective transfer modes for a wood particle ..... 15
Figure 9. Evolution of the normalized mass of an eucalyptus sample during its pyrolysis at atmospheric pressure and at a heating rate of 5°C/min (Kifani-Sahban et al., 1996) ..... 16
Figure 10. Temperature gradient inside a wood particle during its heating ..... 17
Figure 11. Formation of free radicals from thermal cracking (H atom: blue; C atom: black; electron: red) ..... 18
Figure 12. Light hydrocarbon maturation chemical scheme (Khan & Crynes, 1970) ..... 19
Figure 13. Mechanisms for PAH formation HACA mechanism (a) and the mechanism considering addition of benzenic rings (b) (Frenklach & Wang, 1994) ..... 19
Figure 14. Tar maturation scheme as a function of temperature (Elliott, 1988) ..... 19
Figure 15. Scheme of soot formation (Svensson, 2005) ..... 20
Figure 16. Logarithmic value of water gas shift equilibrium constant versus temperature ..... 21
Figure 17. Diesel soot spherules microstructure (Ishiguro et al., 1997) ..... 22
Figure 18. Representation of mass transfer phenomena in gasification of a char particle – note: the boundary layer is delimited by a dotted line ..... 23
Figure 19. Diffusion coefficient in function of pore size (Oliveira & Kaviany, 2001) ..... 24
Figure 20. Representation of mass transfer phenomena in gasification of a soot particle – note: the boundary layer is delimited by a dotted line ..... 24
Figure 21. Chemical phenomena in solid gasification ..... 25
Figure 22. Scheme of the functioning principle of an EFR and a DTR ..... 33
Figure 23. Schematic diagram of a TGA ..... 34
Figure 24. Incomplete pyrolysed wood particles obtained at 800°C and 950°C (Dupont, 2006) ..... 36
Figure 25. Representation of the graphitization of a char structure in function of pyrolysis temperature (Bunsell, 1988) ..... 37
Figure 26. Comparison of the reactivity of graphite and of a charcoal at two pyrolysis temperatures at 50% of conversion (Russell et al., 1999) ..... 37
Figure 27. TEM images of soot obtained from the pyrolysis of $C_2H_2$ at 1250°C (a) and 1650°C (b) (Vander Wal & Tomasek, 2004) ..... 38
Figure 28. Empirical models for primary pyrolysis ..... 39
Figure 29. Empirical models including secondary reactions ..... 40
Figure 30. Shrinking core model principle ..... 41
Figure 31. Cross section of coal particle after pyrolysis at 850°C for about 30 s (a) (Chern & Hayhurst, 2004) and beech wood particle after pyrolysis at 1000°C for 3 s (b) (Burghoffer, 2009) – Note: a fictive pyrolysis front is represented by a white line ..... 42
Figure 32. Kinetic scheme of the main reactions used in a model for the combustion of hydrocarbons and PAHs formation (Durán et al., 2004) ..... 43
Figure 33. Most common tar model compounds (Hiblot 2010) ..... 44
Figure 34. Chemical scheme used for the soot mass growth with $C_2H_2$ and oxidation ..... 45
Figure 35. Representation of fracturing and fragmentation of a char particle ..... 50
Figure 36. Pyrolysis regimes in function of temperature and particle size (Dupont, 2006) – note: the hatched zones correspond to the uncertainty of the characteristic time calculations ..... 54

Figure 37. Beech sawdust ..... 61
Figure 38. Microscopic view of wood particles from the 0.35 mm sample ..... 62
Figure 39. Experimental facilities at EMAC ..... 63
Figure 40. Scheme of the drop tube reactor (DTR) ..... 64
Figure 41. Simulation of temperature field in the DTR for the experiments at 1000°C (a), 1200°C (b) and 1400°C (c). Note: the sampling heights are represented by white dotted lines ..... 67
Figure 42. Mass evolution of the beech sawdust in the feeding system ..... 68
Figure 43. Measurement of the gas concentration of $CO_2$ by NDIR (a) and $H_2$ by TCD (b) ..... 68
Figure 44. ATG (right of the picture) coupled to a wet gas generator (left of the picture) ..... 70
Figure 45. Scheme of the TGA facility ..... 70
Figure 46. Evolution of the temperature during the gasification experiments with char (a) and soot (b) ... 71
Figure 47 Mass yields of the products from beech particles thermal decomposition under an inert atmosphere at thermodynamic equilibrium ..... 87
Figure 48 Mass yields of the products from beech particles thermal decomposition under a wet atmosphere at thermodynamic equilibrium ..... 87
Figure 49. Mass yields of the products from the 0.35 mm particles thermal decomposition under an inert atmosphere at 800°C, 1000°C, 1200°C and 1400°C ..... 93
Figure 50. Mass fraction of C, H and O in the products from the 0.35 mm particles thermal decomposition under an inert atmosphere at 800°C, 1000°C, 1200°C and 1400°C ..... 94
Figure 51. Molar yields of non hydrocarbon gas (a) and light hydrocarbons (b) from the 0.35 mm particles thermal decomposition under an inert atmosphere at 800°C, 1000°C, 1200°C and 1400°C ..... 95
Figure 52. Mass yields of the products from the 0.35 mm particles thermal decomposition under inert and wet atmospheres at 1000°C, 1200°C and 1400°C ..... 99
Figure 53. Molar yields of non hydrocarbon gas (a) and light hydrocarbons (b) for the 0.35 mm particles thermal decomposition under inert and wet atmospheres at 1000°C, 1200°C and 1400°C ..... 100
Figure 54. Carbon repartition in the products from the 0.35 mm particles thermal decomposition under a wet atmosphere at 1000°C, 1200°C and 1400°C ..... 101
Figure 55. Molar yields of the products from the particles thermal decomposition experiments and from thermodynamic equilibrium calculations under inert (a) and wet (b) atmospheres ..... 103
Figure 56. WGS constant calculated from the experiments under inert and wet atmospheres, and from the thermodynamic equilibrium ..... 104
Figure 57. Mass yields of the products from the 0.35 mm particles thermal decomposition under an inert atmosphere at 1000°C and 1200°C, after 2 s and 4 s of residence time ..... 106
Figure 58. Mass yields of the products from the 0.35 mm particles thermal decomposition under a wet atmosphere at 1000°C and 1200°C, after 2 s and 4 s of residence time ..... 106
Figure 59. Mass yields of the products from the 0.35 mm and 0.80 mm particles thermal decomposition under an inert atmosphere at 1000°C, 1200°C and 1400°C, after short (a) and long (b) residence times ..... 108
Figure 60. Mass yields of the products from the 0.35 mm and 0.80 mm particles thermal decomposition under a wet atmosphere at 1000°C, 1200°C and 1400°C, after short (a) and long (b) residence times ..... 109
Figure 61. SEM observations of soot samples from the 0.80 mm particles thermal decomposition at 1200°C (a) and 1400°C (b), after 4 s of residence time ..... 111
Figure 62. Reactivity in two conversion ranges of soot samples from the 0.35 mm particles thermal decomposition at 1200°C and 1400°C, after 2 s and 4 s of gas residence time ..... 112
Figure 63. Reactivity in two conversion ranges of soot samples from the 0.35 mm and 0.80 mm particles thermal decomposition at 1200°C (a) and at 1400°C (b), after 4 s of gas residence time ..... 113
Figure 64. SEM observations of char samples from the 0.35 mm particles thermal decomposition at 1000°C (a) and 1400°C (b), after 4 s of residence time ..... 114

Figure 65. SEM observations of char samples from experiments at 1000°C (a, b, c), 1200°C (d,e) and 1400°C (f) ..... 115
Figure 66. XRD analysis of char samples from 1400°C experiments, without grains (a) and with grains (b) on its surface ..... 116
Figure 67. Soot particles observed in char samples from 1000°C (a) and 1200°C (b) experiments ..... 117
Figure 68. H/C and O/C ratios versus temperature ..... 118
Figure 69. Triangular diagram with the char molar composition from the 0.35 mm particles pyrolysis of at 800°C, 1000°C and 1200°C after different residence times ..... 119
Figure 70. Reactivity in two conversion ranges of char samples from the 0.35 mm particles thermal decomposition at 800°C, 1000°C, 1200°C and 1400°C, after 4 s of residence time ..... 120
Figure 71. Reactivity in two conversion ranges of char samples from the 0.35 mm particles thermal decomposition at 1200°C, after 2 s and 4 s of residence time ..... 121
Figure 72. Reactivity in two conversion ranges of char samples from the 0.35 mm and 0.80 mm particles thermal decomposition at 1000°C (a), 1200°C (b) and 1400°C (c), after 4 s of residence time ..... 122
Figure 73. Representation of the gas and solid flows in a DTR in GASPAR ..... 129
Figure 74. Modeling principle of GASPAR software ..... 135
Figure 75. Experimental and simulated molar yields of permanent gas from the particles thermal decomposition under an inert atmosphere at 800°C, versus reactor length ..... 137
Figure 76. Simulated molar yields of $CH_30H$ and $C_{10}H_8$ from the particles thermal decomposition under an inert atmosphere at 800°C, versus reactor length ..... 138
Figure 77. Experimental and simulated (by using different modeling approaches) mass yields of soot from the particles thermal decomposition under an inert atmosphere at 800°C, 1000°C, 1200°C and 1400°C ..... 138
Figure 78. Mass yields of PAHs and $C_2H_2$ yields from the simulation of experiments at 1200°C and 1400°C under an inert atmosphere without considering soot formation, versus reactor length ..... 139
Figure 79. Experimental and simulated mass yields of char from the particles thermal decomposition under inert (a) and wet (b) atmospheres at 1000°C, 1200°C and 1400°C ..... 140
Figure 80. Experimental and simulated mass yields of $C_2H_2$, PAHs and soot from the particles thermal decomposition under an inert atmosphere at 1000°C (a), 1200°C (b) and 1400°C (c), versus reactor length ..... 142
Figure 81. Example of soot surface mass growth with PAHs (a) and $C_2H_2$ (b) ..... 143
Figure 82. Experimental and simulated (by considering soot gasification) mass yields of $C_2H_2$, PAHs and soot from the particles thermal decomposition under a wet atmosphere at 1000°C (a), 1200°C (b) and 1400°C (c), versus reactor length ..... 145
Figure 83. Experimental and simulated (without considering soot gasification) mass yields of $C_2H_2$, PAHs and soot from the particles thermal decomposition under a wet atmosphere at 1000°C (a), 1200°C (b) and 1400°C (c), versus reactor length ..... 146
Figure 84. Experimental and simulated molar yields of permanent gas from the particles thermal decomposition under an inert atmosphere at 1000°C (a), 1200°C (b) and 1400°C (c), versus reactor length ..... 148
Figure 85. Experimental and simulated molar yields of permanent gas from the particles thermal decomposition under a wet atmosphere at 1000°C (a), 1200°C (b) and 1400°C (c), versus reactor length ..... 150
Figure 86. Energetic worldwide supply in 2008 (*"other" includes geothermal, solar, wind, heat, etc…) ..... 177
Figure 87. Worldwide energy demand ..... 177
Figure 88. Distribution of the proven and undiscovered oil reserves in the globe ..... 178
Figure 89. Different scenarios about the increase of temperature on Earth due to global warming ..... 178
Figure 90. Different routes of energetic valorization of biomass ..... 179
Figure 91. Biomass gasification plant prototype for a BtL or BtG application ..... 180

Figure 92. Residence times of gas, 0.35 mm and 0.80 mm particles during experiments under an inert atmosphere at 1000°C (a), 1200°C (b) and 1400°C (c), versus reactor length ..... 183
Figure 93. Slip velocity of 0.35 mm and 0.80 mm particles during experiments under an inert atmosphere at 1000°C, 1200°C and 1400°C, versus reactor length ..... 184
Figure 94: Regimes of pyrolysis considering kinetic parameters set from Brink (1978) (a) and Shuaning et al. (2006) (b), as a function of temperature and particle size ..... 185
Figure 95. Regimes of gasification under atmospheres containing 1 mol% (a) and 25 mol% (b) of $H_2O$, as a function of temperature and particle size ..... 186
Figure 96. SEM observations of char samples from experiments under a wet atmosphere at 1200°C (a) and 1400°C (b -c) with their respective XRD analysis spectrum ..... 196
Figure 97. Reactivity in two conversion ranges of char samples from the 0.35 mm particles thermal decomposition under inert and wet atmospheres at 1000°C and 1200°C ..... 197
Figure 98. Graphs [$\ln(R_{X=10-70\%})=f(1/T)$] (a) and [$\ln(R_{X=10-70\%}) = f(\ln(P_{H2O})$] (b) for soot ..... 199
Figure 99. Graphs [$\ln(R_{X=10-70\%})=f(1/T)$] (a) and [$\ln(R_{X=10-70\%}) = f(\ln(P_{H2O})$] (b) for char ..... 199

# Nomenclature

## Latin letters

| | | |
|---|---|---|
| $Bi_M$ | Mass Biot number | - |
| $Bi_T$ | Thermic Biot number | - |
| $C_p$ | Heat capacity | $J.kg^{-1}.K^{-1}$ |
| $d$ | Diameter | m |
| $D_{eff}$ | Effective gas diffusion coefficient | $m^2.s^{-1}$ |
| $D_{Knudsen}$ | Knudsen diffusion coefficient | $m^2.s^{-1}$ |
| $D_{mol}$ | Molecular diffusion coefficient | $m^2.s^{-1}$ |
| $Ea$ | Activation energy | $J.mol^{-1}$ |
| $f(X)$ | Surface function | - |
| $F$ | Molar flow rate | $mol.s^{-}$ |
| $g$ | Gravitational constant | $m.s^{-2}$ |
| $k$ | Intrinsic kinetic parameter | $s^{-1}$ |
| $k_0$ | Pre-exponential factor | $s^{-1}.bar^{-n}$ |
| $h_m$ | Mass exchange coefficient | $m.s^{-1}$ |
| $h_t$ | Heat exchange coefficient | $W.m^{-2}.K^{-1}$ |
| $m$ | Mass | kg |
| $M$ | Molar mass | $g.mol^{-1}$ |
| $n$ | Order of the reaction | - |
| $Nu$ | Nusselt number | - |
| $L_0$ | Pore length | m |
| $P$ | Pressure | bar or Pa |
| $Pr$ | Prandtl number | - |
| $Py$ | Pyrolysis number | - |
| $Q$ | Volume flow rate | $m^3.s^{-1}$ |
| $r$ | Radius | m |
| $R$ | Constant of ideal gas | $J.mol^{-1}.K^{-1}$ |
| $Re$ | Reynolds number | - |
| $Sh$ | Sherwood number | - |
| $S_0$ | Pore surface area per unit of solid volume | $m^2/m^3$ |
| $t$ | Time | s |
| $t_i$ | Characteristic time of $i$ | s |
| $T$ | Temperature | K |
| $Tc$ | Critical temperature | K |
| $x$ | Ash mass content | - |
| $X$ | Conversion | - |
| $y$ | Molar content | - |
| $Y$ | Molar yield | $mol.mol^{-1}$ dry biomass |
| $V_{slip}$ | Particle slip velocity | $m.s^{-1}$ |
| $V_t$ | Terminal velocity of free fall | $m.s^{-1}$ |

## Greek letters

| | | |
|---|---|---|
| $\omega$ | Emissivity | - |
| $\sigma$ | Boltzmann constant | $W.m^{-2}.K^{-4}$ |

| | | |
|---|---|---|
| $\lambda$ | Thermal conductivity | $W.m^{-1}.K^{-1}$ |
| $\varepsilon$ | Porosity | - |
| $\tau$ | Tortuosity | - |
| $(\Sigma v)$ | Volume diffusion | $m^3.mol^{-1}$ |
| $\Psi$ | Surface function | - |
| $\xi$ | Annealing coordinate or coefficient | - |

**Subscripts**

| | |
|---|---|
| *conv* | External convection |
| *cond* | Internal conduction |
| *deact* | Deactivated |
| g | Gas |
| *gas* | Gasification |
| *mass ext* | External mass transfer |
| *mass int* | Internal mass transfer |
| *p* | Particle |
| *pyr* | Pyrolysis |
| *rad* | Radiation |

**Acronyms**

| | |
|---|---|
| BtL | Biomass - to - Liquid |
| BtG | Biomass - to - Gas |
| daf | Dry, ash free basis |
| DTR | Drop Tube Reactor |
| EFR | Entrained Flow Reactor |
| FID | Flame Ionization Detector |
| FTIR | Fourier Transformed InfraRed spectrometer |
| HR | Heating Rates |
| LM | Langmuir - Hinshelwood |
| NDIR | Non – Dispersive InfraRed spectrometer |
| PAH | PolyAromatic Hydrocarbon |
| RPM | Random Pore Model |
| SCM | Shrinking Core Model |
| SEM | Scanning Electronic Microscope |
| TCD | Thermal Conductivity Detector |
| TEM | Transmission Electronic Microscope |
| TGA | ThermoGravimetric Analyzer |
| VRM | Volume Reaction Model |
| WGS | Water – Gas Shift |
| µ-GC | Micro – Gas Chromatograph |

Chemical nomenclature of main compounds

| | |
|---|---|
| Ar | Argon |
| $CH_4$ | Methane |
| $CH_3OH$ | Methanol |
| $C_2H_2$ | Acetylene |

| | |
|---|---|
| $C_2H_4$ | Ethylene |
| $C_2H_6$ | Ethane |
| $C_6H_6$ | Benzene |
| $C_6H_6O$ | Phenol |
| $C_7H_8$ | Toluene |
| $C_{10}H_8$ | Napthalene |
| $C_{12}H_8$ | Acenaphtalene |
| $C_{14}H_{10}$ | Phenanthrene |
| $C_{16}H_{10}$ | Pyrene |
| CO | Carbon monoxide |
| $CO_2$ | Carbon dioxide |
| $H_2$ | Hydrogen |
| $H_2O$ | Water |
| $N_2$ | Nitrogen |

# Introduction

Energy has always had an indispensable role in the society. Before the industrial age, Man used rustic means to accomplish its diverse activities, such as animals for locomotion or wind mills for cereal milling. Industrialization, starting at the beginnings of the XIX$^{e}$ century, changed the phase of the human civilization which deeply mutated in the space of two centuries of technological progress. This change was based on development of the energy sector, leading to revolutionary improvements in the electrical and transport areas, which could not be possible without fossil fuels, namely petroleum, coal and natural gas.

In counterpart, the use of fossil fuels left disastrous traces in the environment. At local scale, it led to the pollution of air, water and soil. At large scale, it is considered as mainly responsible for global warming by the greenhouse gas emissions. Besides, the actual civilization has created a hazardous dependence with respect to petroleum, in particular in the transport sector where no alternatives to fuels derived from oil really exist nowadays, while the reserves are declining and the demand is growing everyday. This resource is estimated to arrive to its depletion in the next decades and it may be accompanied by an unprecedented energy crisis.

Measures must be taken now for the transition to a more sustainable system which is not dependant on fossil fuels, such as:

- decrease of the consumption;
- increase of efficiency;
- use of clean and sustainable sources of energy, as renewable energy.

For this, biomass is a very interesting alternative. This resource is the oldest source of energy in mankind history, originally used to make fire, which provides light, heat and protection. As an energy resource, biomass has the advantages to be abundant and well distributed in the globe, to be neutral with respect to greenhouse gas emissions, to be renewed in the human time scale and to offer several applications of use. Among these, biomass can be burnt for direct heat and electricity production, or it can be used as raw material to synthesize biofuels. The last option needs a chemical transformation of the biomass by the means of biological or thermochemical treatment.

In the biological treatment, the biofuels can be directly extracted from the plant, as in the case of biodiesel, or obtained by microbial transformation, for bioethanol or biogas. For this purpose, the alimentary part of the plant can be used to produce what is called first generation biofuels, or the lignocellulosic part can be transformed into second generation fuels. The production of first generation biofuels is a very controversial practice, as it is in direct competition with the alimentary sector and leads to food price rise.

In the thermochemical treatment, the lignocellulosic biomass is decomposed by the means of heat. This decomposition can occur under an inert atmosphere in order to produce bio-oils or bio-char, or under an atmosphere containing a reagent such as $O_2$ in stoechiometric default, $H_2O$ and/or $CO_2$, in order to produce syngas - $H_2$ and CO - through gasification process. Syngas can be used for a highly efficient electricity production or for the production of second generation biofuels via Biomass-to-Liquid (BtL) or Biomass-to-Gas (BtG) processes. More information about the actual energetic context and the high potential of biomass can be seen in Appendix A.

The main advantages of gasification process are the high flexibility towards feedstock and its ability to decompose the whole lignocellulosic matter. Besides, a large variety of hydrocarbons, similar to those obtained from the petroleum refinement, can be synthesized from syngas via the Fischer-Tropsch process. In this case, the biofuels would be compatible with the actual engines and would not require the development of new vehicle fleet.

Gasification process dates from the beginning of the XIX$^{e}$ century with the invention of the first gasifier, initially developed to produce town gas for lightening and cooking from coal and peat, until be replaced by electricity and natural gas. This process was then used for chemical synthesis since the 1920s, notably for the production of synthetic fuel from coal during the Second World War, due to a shortage of petroleum. For the same last reason, at this time, biomass was for the first time used for a gasification application: wood gas generators, called gasogenes, were used to power motorized vehicles in Europe. After the reintroduction of petroleum, the

industrial use of gasification was abandoned until today, at the exception of South Africa in the 1950s where the process was developed to produce a wide synthetic hydrocarbons variety from coal, in order to face to the stop of oil supply from the other countries by political reasons. During the next decades, the interest of gasification gained ground during short episodes of crisis where the oil distribution was menaced, more particularly during the oil crisis in the 1970s. The increase of interest for gasification process was reflected by the development of several R&D programs which were quickly abandoned with reestablishment of the oil situation. Since the last 20 years, the imminent petroleum depletion has forced the nations to research alternative fuels, which has led to new researches in the gasification field, at the beginning for coal and more recently for biomass, a more environmentally friendly alternative.

The biomass thermal decomposition during gasification involves different stages. The first step is the particle drying, followed then by pyrolysis, which consists in the solid devolatilization under the effect of heat, leading to the formation of tar (hydrocarbons > $C_6$), gas, and a char (solid residue). Subsequently, the oxidizing molecules, $O_2$, $H_2O$ and/or $CO_2$, react with the carbonaceous solid through gasification reaction and/or with tar and gas through reforming reaction. The products from the thermal decomposition can also react among themselves. Note the difference between the terms “biomass gasification” and “gasification of the carbonaceous solid”: the first refers to the whole transformation whereas the other is specific to the chemical reaction between the gaseous reagent and the carbonaceous solid. The operating conditions in the gasifier are fixed in order to maximize the syngas production, and to minimize the pollutants emission and the production of fouling compounds, as tar. At the present time, several gasification technologies are under development, as the fluidized bed reactor, the fixed bed reactor and the entrained flow reactor. Appendix B gives a description of a typical gasification plant, and compares the operating characteristics between an entrained flow reactor and a fluidized bed reactor.

The French research center, CEA (“Commissariat à l’Energie Atomique et aux Energies Alternatives”) located in Grenoble, started to work on a R&D program about biomass gasification about ten years ago. The research is carried out at different scales, from the experimental and modeling study of physicochemical phenomena at lab scale, to the implementation and piloting of demonstration plants at semi-industrial scale, and is focused on two main gasifier technologies, fluidized bed reactor and entrained flow reactor.

The entrained flow reactor (Figure 1) is one of the most promising gasifier technologies. Its main advantage is the high conversion of biomass into a syngas almost free of tar and gaseous hydrocarbons. The typical process conditions are as follows: high temperature (> 1300°C), short particle residence time (< 5 s) and extremely high heat flux at the particles surface (> $10^6$ $W.m^{-2}$). The feedstock, in a pulverized solid form (< 200 µm), and the carrier gas are introduced into the reactor from the top. At the outlet of the reactive zone, the gas is quenched and sent to the process, while the ash is recovered at the bottom of the reactor. A burner, located at the top of the reaction zone and producing a flame by the combustion of part of the feedstock, provides the heat required for the process, which is highly endothermic. The entrained flow reactor is autothermal, and so has a high energetic efficiency. However, as part of the feedstock is combusted in the burner, the process loses mass efficiency.

Steam can also be injected at the top of the reactor, and is then added to the $H_2O$ produced in the burner through biomass combustion.

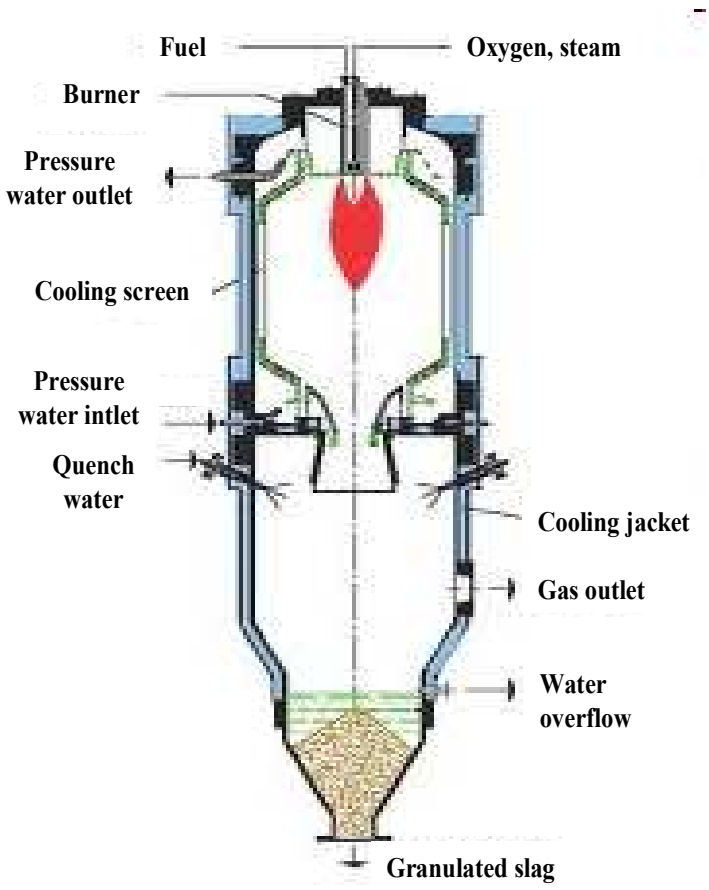


**Figure 1. Scheme of an entrained flow reactor (Schingnitz & Mehlose, 2005)**

The objective of this thesis is precisely to better understand the phenomenology of biomass steam gasification in an entrained flow reactor. This type of reactor has been the subject of a wide number of researches for coal but its application for biomass is relatively new.

Our work also includes the study of the influence of biomass particle size. As said before, biomass is generally introduced in a pulverized form, with particles with a size lower than 200 µm. As raw biomass is a material difficult to grind, this step is costly, and the use of larger particles would be of interest. A study about the design of a biomass gasification plant using an entrained flow reactor (Van der Drift, 2004) found that the greatest efficiency would be achieved using 1 mm biomass particles as feedstock. A costly biomass pre-treatment operation, like an advanced grinding and/or a thermal treatment, as torrefaction to facilitate grinding or fast pyrolysis for the production of bio-oil, could then be avoided. However, studies are necessary to investigate the behavior of millimetric particles in such a process.

In order to reach the objectives of the study, the influence of several operating parameters on biomass gasification was investigated with experiments in a drop tube reactor. This type of analytical reactor can approach the conditions of an entrained flow reactor at a lab scale. The feedstock selected here was beech sawdust. The variables of the study were temperature - 800°C, 1000°C, 1200°C and 1400°C - , steam content in the atmosphere - 0 mol% and 25 mol% - , residence time - 2 s and 4 s - and beech particle size - 0.35 mm and 0.80 mm -. A particular attention was paid to the characterization of the solids, char and soot, obtained from these experiments.

Moreover, a model representing biomass gasification in a drop tube reactor was developed based on an existing model that was implemented for combustion applications. The experimental and modeling results put together allow establishing an integral description of the phenomena involved during wood particles gasification.

In the first Chapter of this study, the fundamental physical and chemical concepts about steam gasification are presented.

The second Chapter provides a literature review about the experimental results in the conditions of interest, i.e. high temperature and high heating rate, and about the different approaches for biomass gasification modeling.

The third Chapter is dedicated to the description of the materials and methods used in the study. The drop tube reactor is described as well as the experimental setup of the tests performed. The solids collected during the experiment, soot and char, were characterized in detail. In particular, the reactivity measurements performed in the thermogravimetric analyzer are described. The second part of the chapter concerns preliminary studies, namely a characteristic time analysis and calculations at the thermodynamic equilibrium, which are useful for the interpretation of the experimental results and the modeling in the following chapters.

In the fourth Chapter, the experimental results are shown and discussed. The influence of temperature, $H_2O$ content in the atmosphere, particles size and residence time on products yields are put into evidence. Moreover, the soot and char characterization results are given and discussed in function of the operating parameters in the drop tube reactor.

In the last chapter, the GASPAR software, used for the simulation of the experiments, is described. The modifications brought to the software to better represent the high temperatures experiments are presented. These include a better representation of tars, soot and char, based on the experimental results. The modeling of the experiments and the confrontation with the experimental results are presented.

Finally, the experimental and modeling results are brought together in order to arrive to a general conclusion which provides new elements of comprehension of the phenomena occurring during the biomass gasification in the conditions of an entrained flow reactor.

# Introduction en français

Face à l'épuisement des combustibles fossiles et aux contraintes environnementales actuelles, l'utilisation de la biomasse comme source d'énergie apparaît comme une alternative très sérieuse. Parmi les différentes voies de valorisation énergétique de la biomasse, la gazéification permet de transformer les composés lignocellulosiques en un mélange de gaz de synthèse ($H_2$ et CO), à partir desquels on peut synthétiser des hydrocarbures d'intérêt, comme le diesel ou le kérosène.

Cette thèse a été réalisée dans le cadre d'une collaboration entre le CEA (Commissariat à l'Energie Atomique et aux Energies Alternatives) de Grenoble et l'Ecole de Mines d'Albi – Carmaux. Son objectif est de mieux comprendre la phénoménologie liée à la gazéification de la biomasse dans un réacteur à flux entraîné, une des technologies de gazéifieur les plus prometteuses. Les conditions typiques de fonctionnement des réacteurs à flux entraînés sont : une température élevée, supérieure à 1300°C, un temps de séjour des particules court, inférieur à 5 s environ, et un flux de chaleur à la surface des particules très important, supérieur à $10^6$ $W.m^{-2}$. Ce type de réacteur a fait l'objet d'un grand nombre de recherches pour le charbon, mais son application pour la biomasse est relativement nouvelle. Une des problématiques liée à l'utilisation de biomasse dans un réacteur à flux entraîné est celle de l'injection de biomasse dans le réacteur. En effet, la biomasse est généralement introduite sous une forme pulvérisée dans le réacteur (particules de taille inférieure à 200 µm). Comme la biomasse brute est un matériau difficile à broyer, l'étape de broyage est coûteuse, et l'utilisation de particules de plus grosse taille permettrait de réduire ces coûts. Cependant, des études sont nécessaires pour mieux comprendre le comportement des particules millimétriques dans un tel procédé.

Pour atteindre les objectifs de cette thèse, l'influence de diverses conditions opératoires sur la gazéification de la biomasse a été étudiée par des expériences dans un four à chute. Ce type de réacteur analytique peut reproduire les conditions d'un réacteur à flux entraîné à l'échelle du laboratoire. La biomasse utilisée est de la sciure de hêtre. Les variables d'étude sont la température (800°C, 1000°C, 1200°C et 1400°C), la teneur en vapeur d'eau dans l'atmosphère (0% et 25% molaire), le temps de séjour (2 s et 4 s) et finalement la taille de particules (0,35 mm et 0,80 mm). Une attention particulière a été portée à la caractérisation des solides, char et suies, récupérés pendant les expériences en four à chute. Par ailleurs, un modèle représentant la gazéification de la biomasse dans un four à chute a été développé en se basant sur les résultats des expériences. Les résultats expérimentaux et de la modélisation ont permis d'établir une description intégrale des phénomènes mis en jeu lors de la gazéification de la biomasse.

Dans le premier chapitre de cette étude, les concepts physiques et chimiques fondamentaux sur la gazéification sont présentés.

Le deuxième chapitre donne un état de l'art des résultats expérimentaux obtenus dans nos conditions d'intérêt, c'est-à-dire à haute température et pour une vitesse de chauffage élevée, et sur les différentes approches abordées pour la modélisation de la gazéification de la biomasse.

Le troisième chapitre est consacré à la description du protocole expérimental suivi dans cette étude. Le fonctionnement du four à chute est décrit ainsi que les conditions expérimentales des essais réalisés. Le solide récupéré pendant les expériences, c'est-à-dire les suies et le char, a été caractérisé en détail. En particulier, les mesures de réactivités effectuées dans un analyseur thermogravimétrique (ATG) y sont décrites. La deuxième partie de ce chapitre est consacrée à une étude préliminaire sur les temps caractéristiques et sur des calculs à l'équilibre thermodynamique, lesquelles ont été utiles plus tard pour l'interprétation des résultats expérimentaux et de modélisation.

Dans le chapitre suivant, les résultats expérimentaux sont présentés et discutés. L'influence de la température, de la teneur en vapeur d'eau dans l'atmosphère, de la taille des particules et du temps de séjour sur les rendements des produits issus de la gazéification de la biomasse dans le four à chute y sont étudiés. En outre, les résultats sur la

caractérisation des suies et du char sont présentés et analysés afin d'établir un lien avec les conditions expérimentales de leur obtention.

Dans le dernier chapitre, le logiciel GASPAR, utilisé pour la simulation des expériences, est décrit. Les modifications apportées au logiciel afin de mieux représenter les expériences y sont également présentées. Cela consiste notamment en une meilleure représentation des goudrons, des suies et du char. Les résultats de la modélisation sont ensuite confrontés avec les résultats expérimentaux.

Enfin, les résultats expérimentaux et de modélisation sont rassemblés afin d'arriver à une conclusion générale qui fournit de nouveaux éléments de compréhension des phénomènes se produisant lors de la gazéification de la biomasse dans les conditions d'un réacteur à flux entraîné.

# Chapter 1: Fundamental concepts

# 1. Description of wood

Wood has been largely chosen in literature as raw material for biomass gasification study in a first approach to the process understanding, because of its worldwide abundance and its less heterogeneous structure compared to another type of biomass. It is of high importance to have a thorough knowledge of wood constitution from the macroscopic to the microscopic scale, in order to better understand how its transformation proceeds during gasification process. In this part, the wood will be described from the trunk anatomy to its molecular structure.

## 1.1. Macroscopic structure

Wood is the principal component of the trunk of a tree. As observed in Figure 2, it is located in the heart of the trunk. This part, considered as dead matter, is bordered by two slight layers, which are the life part of the tree. The first one represents the sapwood, where the sap circulates within the tree; the second one is the cambium, a set of living cell ensuring the cell division. Finally, a slight layer of bark, a protection barrier, covers the ensemble.

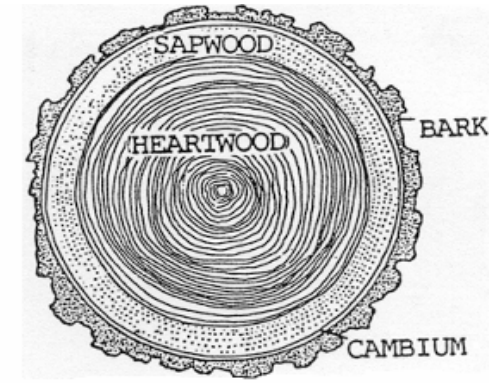


**Figure 2. Anatomy of a tree trunk**

Wood is formed during the tree growth: after a trunk diameter enlargement, the sap progressively stops to circulate in the heart of the tree, causing the death of this part. Wood cells, named as tracheids, are composed of vessels for sap used for transportation in the earlier stages of the tree, and also of fibers for its mechanical resistance.

Two groups of wood exist: softwood (ex: spruce) and hardwood (ex: eucalyptus). The term softwood is used to describe wood from the trees whose seeds are developed “naked”, like pine cones, and then fall on the ground. These trees are known as gymnosperm. Hardwood trees, said to be angiosperm, produce seeds with a covering on their surfaces. Hardwood structure is much more complex than softwood one: the number of components is higher and their arrangement much more variable. Typical structures of softwood and hardwood are depicted in Figure 3.

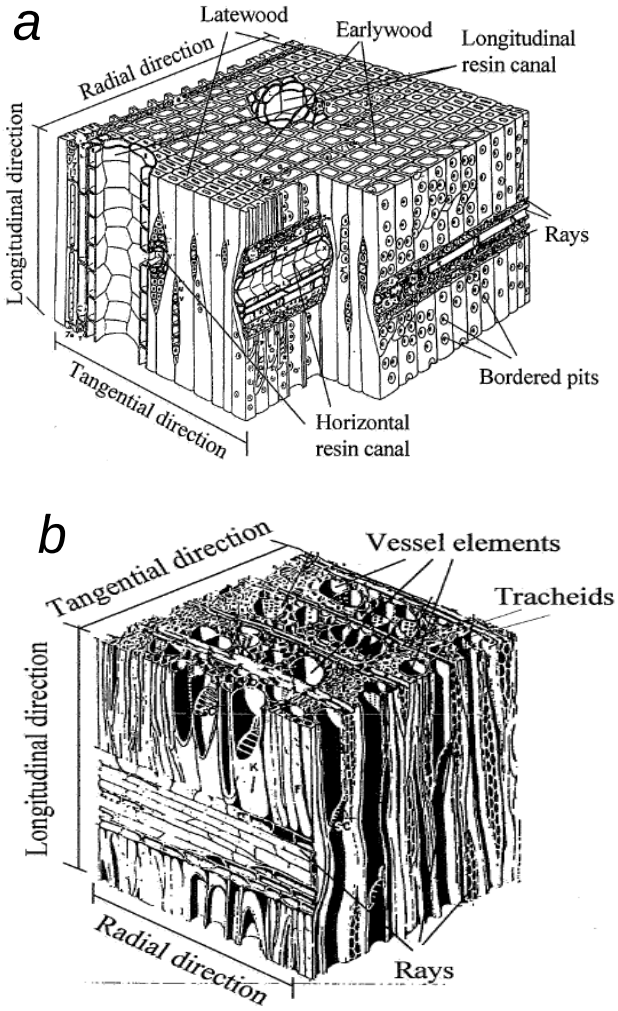


**Figure 3. Gross structure of softwood (a) and hardwood (b) (Siau, 1984)**

## 1.2. Chemical composition

### *1.2.1. Elementary composition*

Wood is mostly composed of C, H, O and N. It also contains a minor part of mineral matter found in the form of ash. The proportions between these compounds are different from a type of wood to another, but the general trends are conserved. Table 1 provides the mean elementary composition of woods.

**Table 1. Elementary mean composition of wood (Mermoud, 2006)**

| | %w, dry basis | |
|---|---|---|
| **C** | 50.9 | ± 2.0 |
| **H** | 6.1 | ± 0.4 |
| **O** | 42.6 | ± 2.6 |
| **N** | 0.4 | ± 0.4 |
| **ash** | 3.5 | ± 4.4 |

The ash composition differs from a wood type to another, but the major components are the same: Ca, K, Mg and Na.

### 1.2.2. Moisture content

Raw wood can contain up to 50 w% of water. After a natural drying, moisture can be decreased to about 10 w% to 20 w%, in function of the storage conditions. Because of its hygroscopic properties, wood is very sensitive to the temperature and ambient hygrometry. In raw harvested wood, moisture can exist in three forms: water vapour in the pores, capillary or free water (liquid) in the pores and hygroscopic or bound water in the solid structure (Siau, 1984).

### 1.2.3. Constitution

About 95 % of the wood cells are composed of three molecular components: cellulose, hemicellulose and lignin. Additionally, wood contains some low-molecular weight organic compounds know as extractives, which gather a thousand of species extractible by solvents. Some examples of extractives are: aliphatic aromatic and alicyclic compounds, aromatic hydrocarbons, alcohols, ketones, organic acids, esters, phenolic compounds, resins and terpenes.

As displayed in Table 2, the repartition of cellulose, hemicellulose and lignin is slightly variable among the wood species. However, a general trend is always respected: cellulose is the major component - 40 to 45 w% daf -, followed by hemicellulose and lignin in comparable amounts - 20 to 30 w% daf -.

**Table 2. Chemical composition of some wood species (Sjostrom, 1993)**

| **Components** | **SOFTWOOD** | | **HARDWOOD** | |
|---|---|---|---|---|
| w%, dry, ash free basis | Scot Pine | Spruce | Eucalyptus | Silver Birch |
| Cellulose | 40.0 | 39.5 | 45.0 | 41.0 |
| Hemicellulose | 28.5 | 30.6 | 19.2 | 32.4 |
| Lignin | 27.7 | 27.5 | 31.3 | 22.0 |
| Extractives | 3.5 | 2.1 | 2.8 | 3.0 |

Cellulose is a glucose polymer (Figure 4), composed of (1, 4)-D-glucopyranose and represented by the elementary formula $(C_6H_{10}O_5)_n$. The value of *n*, the degree of polymerization, reaches even more than 10000 units in an unaltered wood (Sudo & Takahashi, 1989). The linear conformation of cellulose explains the wood fibrous aspect.

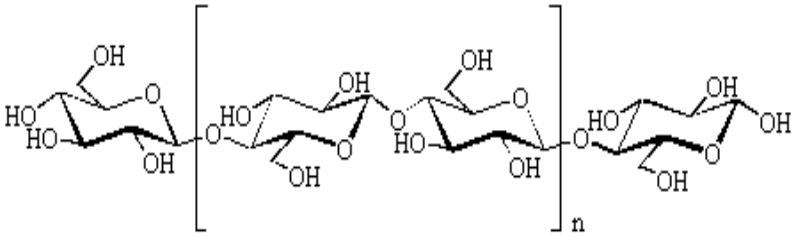


**Figure 4. Structure of cellulose (Sjostrom, 1993)**

Hemicellulose is a mixture of polysaccharides of 50 to 200 units, entirely composed of sugars such as glucose, mannose, arabinose, methylglucuronic acid, galacturonic acid and mostly xylose. Its structure is similar to that of cellulose but it exhibits a branched rather than a linear structure (Gronli, 1996). Hemicellulose polymers are usually located perpendicularly to microfibrils. Their constitution depends on the type of wood. An example of a hemicellulose polymer is given in Figure 5.

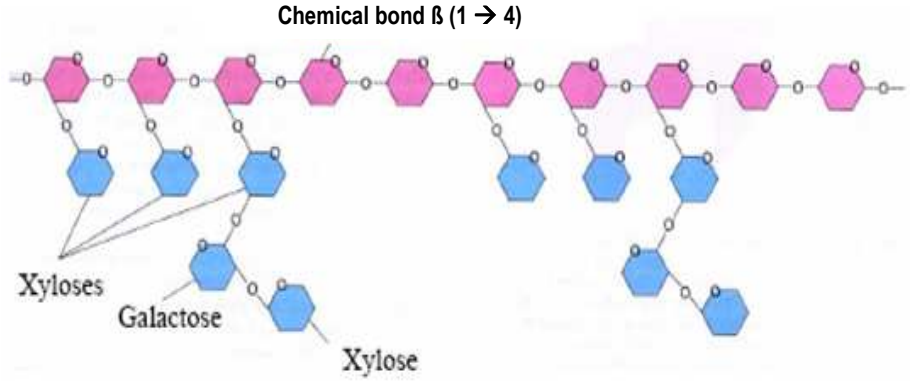


**Figure 5. Structure of hemicellulose molecule (Ibañez, 2002)**

Lignin is a three-dimensional polymer, mostly constituted of phenolic units of nature highly dependent on the type of wood. As a lignin polymer is severely impacted by the extraction mode, its complex structure is very difficult to define and thus it is not still well known in the scientific community. One possible structure is proposed in Figure 6.

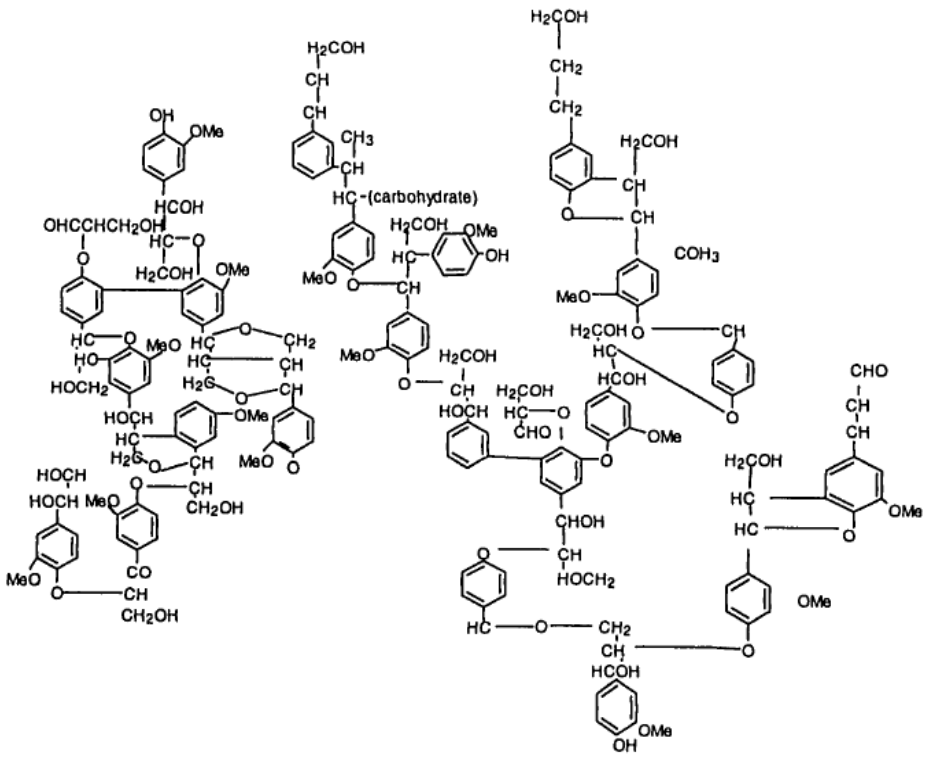


**Figure 6. Example of a lignin polymer structure (Sudo & Takahashi, 1989)**

Cellulose, hemicellulose and lignin have together a structural role in the wood. Cellulose molecules are linked together via hydrogen bonds to form micelles and at larger scale microfibrils, which are very long cables of a few microns in diameter. Microfibrils, ensuring the strength of the structure, are mixed with a smooth resin of hemicellulose and lignin, where lignin molecules link the cellulose fibers together and hemicellulose molecules link the lignin to cellulose. Figure 7 displays this arrangement. Extractives are not structural components, but they contribute to the properties of a wood, such as color, odor, taste, decay resistance, etc (Miller, 1999).

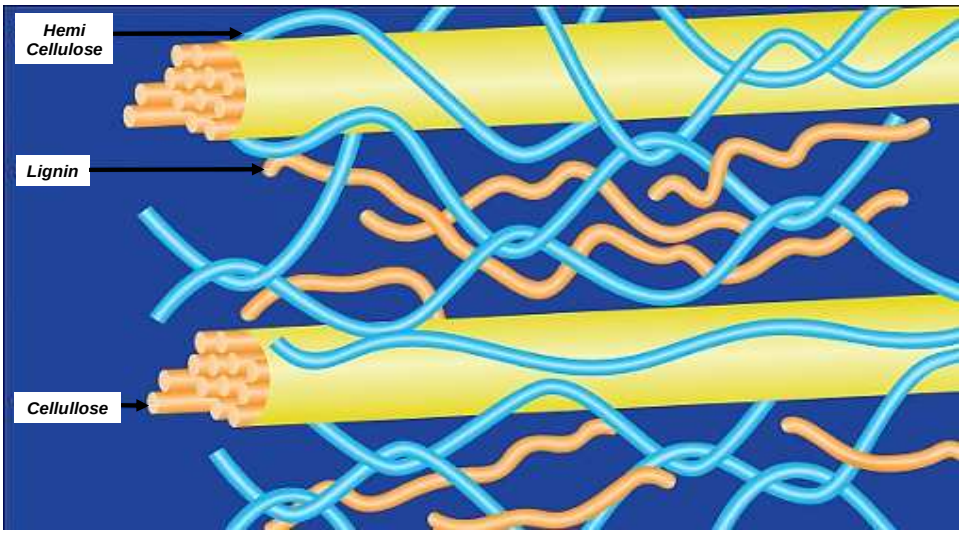


**Figure 7. Microstructure of wood fibers**

## 2. Description of wood pyrolysis

Now that wood constitution has been globally described, it is important to understand the mechanisms of lignocellulosic matter transformation during gasification process. The first step corresponds to pyrolysis, and is then followed by gas reactions and gasification reaction.

When wood is exposed to high temperatures, its structure is thermally decomposed by the cleavage of several chemical bonds. This decomposition leads to the formation of an important number of volatiles and a solid residue. This complex process involves both physical and chemical phenomena.

### 2.1. Physical phenomena

As pyrolysis occurs at temperatures above 250°C, heating is the first step. The heating of the wood particle begins on its external surface and the heat is then conducted to the heart of the particle.

The particle is externally heated by radiation and/or convection or conduction. Radiation exchange is done mainly between the radiative heat source and the particle. Some gas compounds in the atmosphere, such as steam, also participate in the radiation exchange. Convective heating is ensured by the hot gas flow around the wood particle, whereas conduction rather occurs when the hot gas is in static motion with respect to the particle. Figure 8 illustrates these three heat transfer modes.

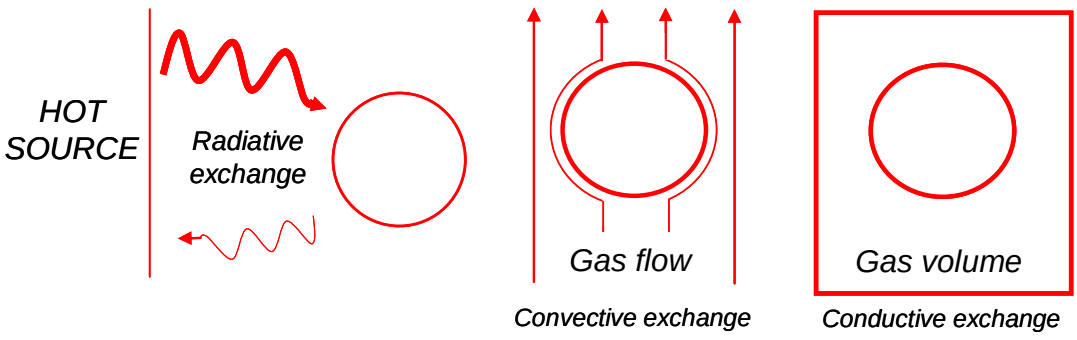


**Figure 8. External radiative, convective and convective transfer modes for a wood particle**

Heat is then transferred from the external surface of the sample into the inside by internal conduction, which corresponds to the diffusion of heat from the hot zones to the cold ones. As wood is a porous solid, radiation between pores can also take part of the internal heating of the sample.

Additional transfer processes are also present during pyrolysis. In fact, the release of volatiles during pyrolysis involves mass and momentum transfer phenomena. The formation of volatiles can create local overpressurized zones within the sample, leading to a gas flow from inside the sample to outside it which can transport mass and heat by advection. Volatiles can also move inside the particle by mass diffusion within the pores.

Other phenomena can couple mass and heat transfer: Dufour effect describes an internal heat transport by the means of the gas flow within the pores. The thermodiffusion effect, also called Soret effect, corresponds to a mass transfer of gas resulting from a temperature gradient inside the sample.

## 2.2. Chemical phenomena

The zones of the wood sample which have reached a high enough temperature can be then decomposed by the cleavage of several chemical bonds in its structure. Figure 9 gives an example of wood degradation versus temperature. The sample is firstly dried between 100°C and 200°C and then the degradation of its main components starts at higher temperature. It can be noticed that hemicellulose decomposes at the lower temperatures, followed by cellulose and then lignin, which appears as the most thermally resistant component of wood.

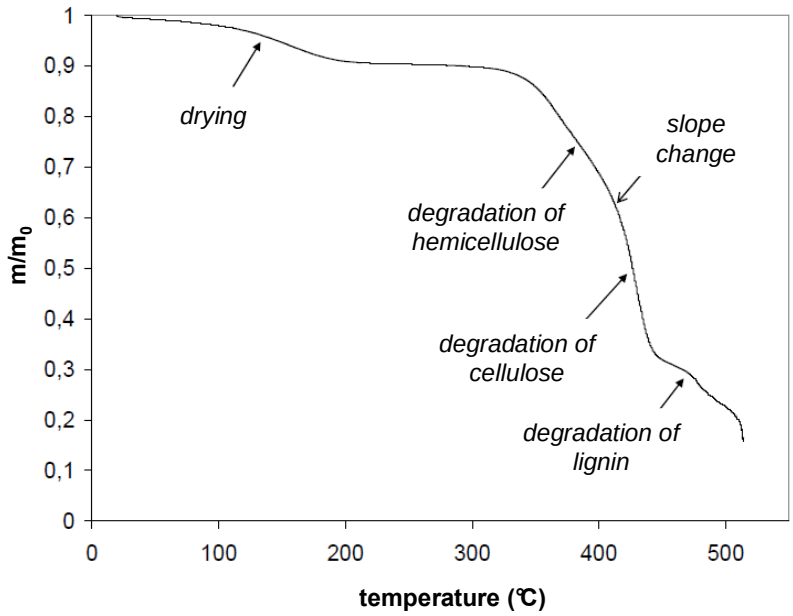


**Figure 9. Evolution of the normalized mass of an eucalyptus sample during its pyrolysis at atmospheric pressure and at a heating rate of 5°C/min (Kifani-Sahban et al., 1996)**

This thermochemical decomposition releases a huge number of volatile compounds: permanent gases as CO, $CO_2$, $H_2O$ and $CH_4$; tar which is usually defined as a sum of organic components with boiling points higher than 150°C (Baker et al., 1988), or with a molecular weight larger than $C_6H_6$ (Neeft et al., 1999). Even if $C_6H_6$ is excluded from these definitions, some authors consider it as a tar (Kajitani et al., 2006; Zhang et al., 2006). Therefore, the use of the term "tar" is confusing in literature because its definition can differ from an author to another.

An unvolatilised fraction of the wood, called the char, usually remains. It is presumed to come from the cellulose and the lignin fractions.

### 2.3. Pyrolysis regimes

The conversion time of pyrolysis depends on the sample heating and the chemical kinetics. Depending on the rate of each phenomenon, pyrolysis can take place under three different regimes:

- When heat transfer is much slower than chemical reactions, pyrolysis can be considered to be in a thermal regime or regime controlled by internal and/or external heat transfer. In this regime, chemical phenomena can be considered to occur instantaneously compared to physical phenomena.
- When heat transfer is much faster than chemical reactions, pyrolysis is in a kinetically controlled regime. This means that physical phenomena can be considered to occur instantaneously with respect to chemical phenomena.
- When heat transfer and chemical reactions take place on the same time scale, pyrolysis is in an intermediary regime.

When heat transfers are slow enough, a gradient of temperature can be observed in the sample (Figure 10).

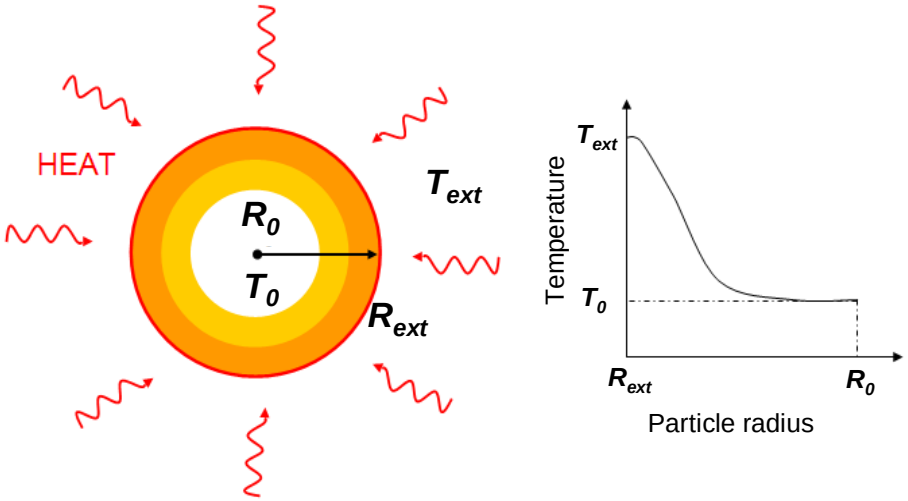


**Figure 10. Temperature gradient inside a wood particle during its heating**

## 3. Description of the gas phase evolution and soot formation

The volatiles released from pyrolysis can react between them or with an oxidant agent present in the atmosphere, as $H_2O$ or $CO_2$. The gas reactions responsible for the evolution of volatile phase can be grouped into 4 groups: cracking reactions, polymerization reactions, reforming reactions and water gas shift reaction. These chemical reactions strongly depend on the temperature, pressure, and atmosphere composition. The gas compounds temperature can evolve with the endothermicity or exothermicity of reactions, and by heat transfers with the surrounding.

### 3.1. Cracking and polymerization reactions

#### *3.1.1. Generalities about cracking and polymerization reactions*

Cracking reactions are a complex process whereby organic molecules are broken down into smaller molecules. During this process, the C-C bonds or C-H bonds from a hydrocarbon are cleaved by the effect of a heat input, so that some carbon atoms end up with a single electron (Figure 11). In other words, free radicals are formed. Reactions of the free radicals lead to a rearrangement of the fragments from the cracked molecule into various molecules. Note that several molecules containing double bond carbon, namely olefins, are formed during this process.

Cracking reactions especially concern large hydrocarbons as tar, but do not exclude small hydrocarbon molecules.

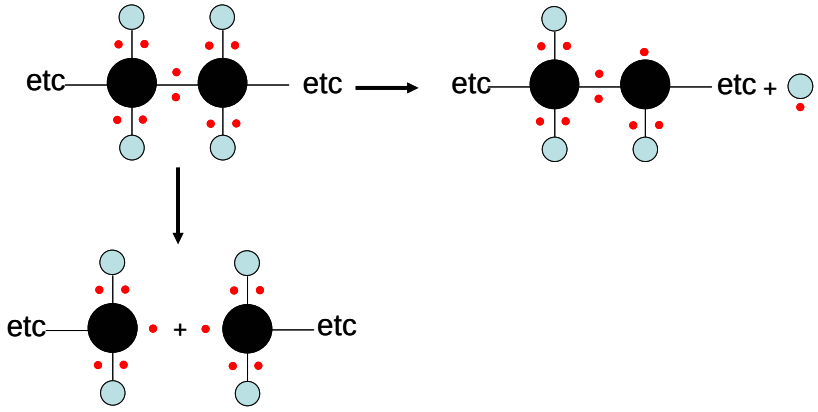


**Figure 11. Formation of free radicals from thermal cracking (H atom: blue; C atom: black; electron: red)**

Hydrocarbon polymerization is the opposite reaction of cracking and also involves free radicals. In this case, large hydrocarbon chains are formed from small molecules.

### *3.1.2. From hydrocarbon cracking and polymerization to soot formation*

The hydrocarbons chains resulting from the wood pyrolysis, which are fragments of the initial structure of the solid, are destroyed with temperature. As a first stage, they are cracked into smaller fragments, which at higher temperature polymerize to form new large molecules. The polymerization can lead to the formation of soot particles, which continue to grow through a complex series of physical and chemical processes in interaction with the gas phase.

### *3.1.3. Tar cracking, light hydrocarbon decomposition and formation of PAHs*

Tars from the solid devolatilization, referred to as primary tars, can be decomposed into secondary and tertiary tars with the increase of reaction severity, which means an increase of temperature or residence time. A classification into primary, secondary and tertiary tars has been proposed (Evans & Milne, 1987a; 1987b), as shown in Table 3.

**Table 3. Tar classification proposed by Evans and Milne**

| Primary tars | Secondary tars | Tertiary tars | |
|---|---|---|---|
| | | Substituted | Condensed |
| Derived products from cellulose and hemicellulose (levoglucosan, furfural…)<br><br>Derived products from lignin (metoxyphenol) | Olefins and phenolics | Methyl derived aromatics (methyl acenaphtylene, toluene) and indene | Aromatic hydrocarbons without substitute (benzene, naphtalene, acenaphthylene, phenanthrene, pyrene) |

The decomposition of tar is due to cracking reactions occurring in the gas phase and converting oxygenated tar compounds into phenolics which subsequently are cracked into small aromatic rings. Light hydrocarbons, mainly

$CH_4$ and olefins such as $C_2H_4$, are produced during this process, as well as non hydrocarbon gases among which $H_2$ and CO.

Light hydrocarbons compounds can also be decomposed by the effect of heat. Figure 12 shows the most often used chemical scheme to describe the evolution of the major light hydrocarbons: $CH_4$ can be polymerized into $C_2H_6$, which can subsequently suffer from successive cracking, more specifically dehydrogenations, to give $C_2H_4$ and finally $C_2H_2$. Indeed, the light hydrocarbon decomposition tends to the formation of $C_2H_2$, which is the basis compound for the synthesis of aromatic compounds, as described below.

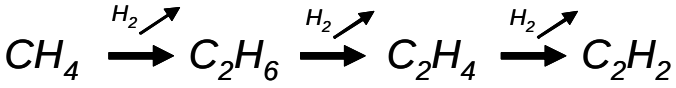


**Figure 12. Light hydrocarbon maturation chemical scheme (Khan & Crynes, 1970)**

At a high temperature enough (> 900°C), benzenic rings, resulting from tar cracking or from light hydrocarbons polymerization, grow with the addition of $C_2H_2$ or another $C_6H_6$ molecule to form PAH, which will continue to grow to a larger PAH molecule. A detailed and comprehensive mechanism of $C_6H_6$ formation from aliphatic hydrocarbons is given by Richter and Howard (2000). Figure 13 gives two examples of mechanism for PAH formation: the HACA mechanism (H abstraction – $C_2H_2$ addition), which is the most accepted in literature, and a mechanism based on the addition of two benzenic rings.

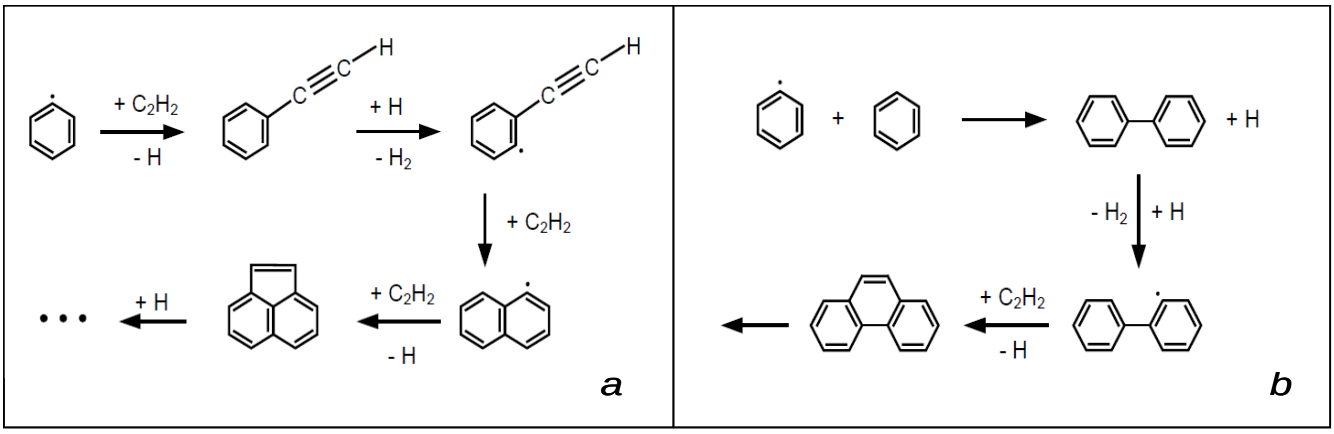


**Figure 13. Mechanisms for PAH formation HACA mechanism (a) and the mechanism considering addition of benzenic rings (b) (Frenklach & Wang, 1994)**

A scheme of the whole process of tar maturation in function of temperature – from 400°C to 900°C - is given in Figure 14.

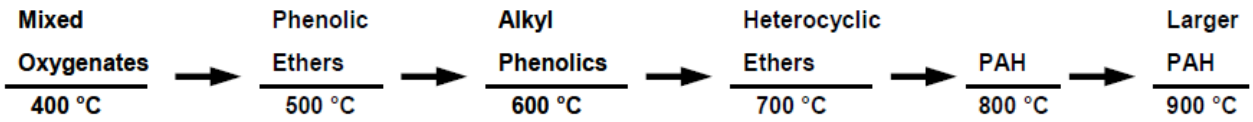


**Figure 14. Tar maturation scheme as a function of temperature (Elliott, 1988)**

### 3.1.4. Formation and growth of soot particles

When a critical size of PAH is reached, the nucleation of the primary soot particles, known as spherules, can take place through the inception process, which can be seen as the transition from the homogeneous phase to the heterogeneous one. The inception process forms soot particles with a rather small mass, which is reported to be about $3.10^{-21}$ g (Krestinin et al., 2000). At this point, the soot particle size is increased mainly by surface growth mechanism, which can represent up to 98% of total growth and can be then recognized as a key of soot formation understanding (D'Alessio et al., 2000; Kronholm & Howard, 2000; Woods & Haynes, 1994). Two relevant mechanisms, proceeding in parallel in interaction with the homogeneous phase, have been identified: surface growth by the addition of $C_2H_2$ (Equation 1 and Equation 2), proposed by Frenklach & Wang (1990), and with the addition of PAH. During this process, the $C_2H_2$ and PAHs molecules are polymerized with the surface of soot particles, by the means of radical reactions in the case of $C_2H_2$ or by molecule collision in the case of PAHs.

$$C_{soot}H + H\cdot \rightarrow C_{soot}\cdot + H_2 \qquad \textbf{Equation 1}$$

$$C_{soot}\cdot + C_2H_2 \rightarrow C'_{soot}H + H \qquad \textbf{Equation 2}$$

With: $C_{soot}H$ as an active site on soot surface on which $C_2H_2$ can polymerize

Soot primary particles can also grow through coagulation, representing the collision of two particles from which a new nearly spherical particle emerges.

Finally, particles can agglomerate by sticking to each other to form cluster-like or chain-like structure. If the diameter of a spherule is in the range of 10 - 80 nanometers, the particle issued from primary particles agglomeration, that is called secondary particle, can reach the scale of micrometers.

Figure 15 summarizes the soot formation process from the fuel pyrolysis to the particles agglomeration. Appendix C shows a list of possible soot precursors.

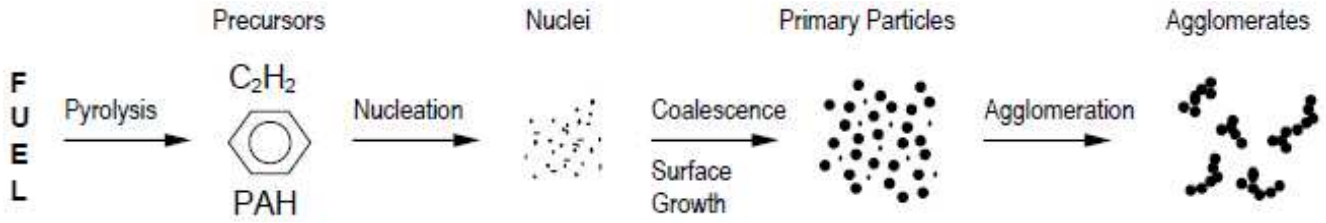


**Figure 15. Scheme of soot formation (Svensson, 2005)**

Soot is also sometimes named "coke" (Kajitani et al., 2006; Zhang et al., 2006). However, the use of this term is confusing in literature because it is also used as a synonym of secondary char (Antal & Gronli, 2003; Branca et al., 2005). Nonetheless, soot and secondary char have completely different paths of formation and properties. Secondary char is formed through polymerization reactions of lignin and cellulose derived tars, which are primary tars, at a lower temperature than soot. The latter requires temperatures higher than 900°C whereas secondary char formation occurs at temperatures lower than 600°C.

### 3.2. Reforming reactions

Hydrocarbons can be reduced into $H_2$ and CO in the presence of $CO_2$ and $H_2O$. During this process, the radical OH● reacts with a hydrocarbon through its single electron site (Equation 3). This radical is formed during the cleavage of an O-H bond in water molecule (Equation 4) or through the donation of an oxygen atom from the $CO_2$ molecule to a radical H● (Equation 5).

$$n\,OH\cdot + C_nH_m \rightarrow n\,CO + (\frac{m+n}{2})\,H_2$$ **Equation 3**

$$H_2O \rightarrow H\cdot + OH\cdot$$ **Equation 4**

$$CO_2 + H\cdot \rightarrow CO + OH\cdot$$ **Equation 5**

Reforming mechanisms are summarized by Equation 6 and Equation 7. Reforming reactions are endothermic, thus they generally need high temperatures to occur.

$$n\,CO_2 + C_nH_m \rightarrow 2\text{n}\,CO + \frac{m}{2}\,H_2$$ **Equation 6**

$$n\,H_2O + C_nH_m \rightarrow n\,CO + (n+\frac{m}{2})H_2$$ **Equation 7**

### 3.3. Water gas shift

Water gas shift is a reaction between permanent gases through which an O atom is exchanged between $H_2/H_2O$ and $CO/CO_2$ (Equation 8).

$$H_2O + CO \leftrightarrow H_2 + CO_2$$ **Equation 8**

This reaction is reversible. The direct path, producing $CO_2$ and $H_2$ from $H_2O$ and CO, is exothermic, so it is favored at low temperatures. The indirect path is endothermic and thus rather favored at high temperatures. Figure 16 shows that the indirect path is favored for temperatures higher than 800°C. This graph was plotted using a simple temperature dependent equilibrium constant correlation given by Moe (1962).

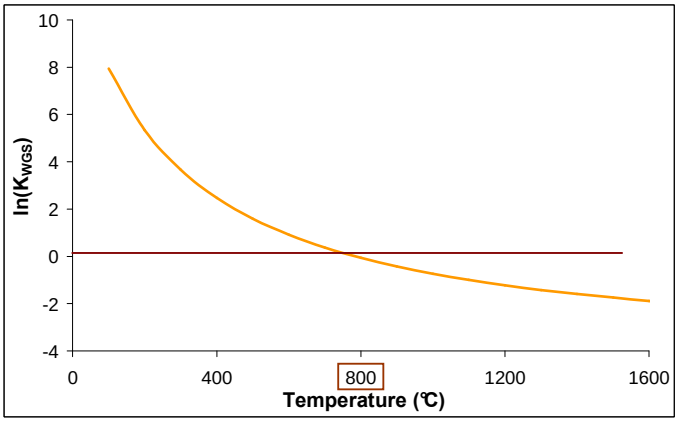


**Figure 16. Logarithmic value of water gas shift equilibrium constant versus temperature**

## 4. Description of gasification

Carbonaceous solids which can be formed during wood pyrolysis, such as char and soot, can be reduced by $H_2O$ (Equation 9) and $CO_2$ (Equation 10). These reduction reactions, named as gasification reactions, produce $H_2$ and CO in the case of gasification with $H_2O$, and only CO in the case of gasification with $CO_2$.

$$C_{solid} + H_2O \rightarrow H_2 + CO \qquad \textbf{Equation 9}$$

$$C_{solid} + CO_2 \rightarrow 2\,CO \qquad \textbf{Equation 10}$$

### 4.1. Characteristics of the carbonaceous solids

#### *4.1.1. Char characteristics*

Char (primary char) is a porous and amorphous solid essentially composed of carbon with small amounts of hydrogen, oxygen and minerals. Its pores can be grouped by their size: micropores of size inferior to 10 nm, mesopores of 10 nm to 50 nm size and macropores of size superior to 50 nm. The size of the char particle usually has the same order of magnitude as that of the wood sample from which it is issued.

#### *4.1.2. Soot characteristics*

Soot is a black solid material mainly composed of carbon and hydrogen, and also of some traces of oxygen, sulfur and nitrogen. The general chemical formula $(C_8H)_n$ was proposed in literature (Palmer & Cullis, 1965).

As mentioned in section 3.1.2.2, soot can be considered as an agglomeration of elementary primary particles, named as spherules. While the sizes from these primary particles mostly vary between 10 nm and 40 nm and can reach a maximal value of 80 µm (Lahaye & Prado, 1981), the agglomerates have a size of some micrometers. The porosity at these two scales of observation is also very different: spherules have a very low porosity, which is between 8% and 14%, with a maximal pore size of 1 nm, whereas agglomerates have a high porosity up to 95% with pore sizes in the magnitude order of 10 nm to 100 nm.

Several works in literature have been dedicated to the spherules microstructure study (Dobbins & Subramaniasivam, 1994; Lahaye & Prado, 1981; Smekens et al., 2000; Wu, 2004). The spherules structure can be essentially divided in two parts: an inner core composed of several fine particles with a spherical nucleus surrounded by carbon networks; the outer shell consisting in concentric layer of graphitic crystallites, which are chemically and structurally very stable. The disposition of such structure is dependent on the particular conditions present during soot formation, namely: temperature, pressure, oxidant concentration, residence time, fuel composition.

Figure 17 shows an illustration of a diesel soot microstructure.

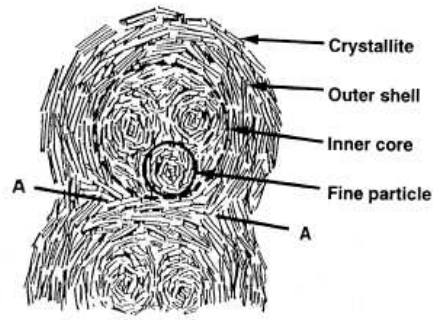


**Figure 17. Diesel soot spherules microstructure (Ishiguro et al., 1997)**

## 4.2. Description of the phenomena involved in gasification

Gasification, as a heterogeneous solid – gas reaction, involves both physical and chemical phenomena. The transfer of reactive molecules from the atmosphere to the inside of the particle and the heating of this latter are required steps before the chemical reaction can occur. Once gasification reaction has taken place, product gas flows from inside the particle to outside.

### *4.2.1. Physical phenomena*

Figure 18 represents the main mass transfer phenomena during the gasification of a char particle around which a fictive gas boundary layer is drawn.

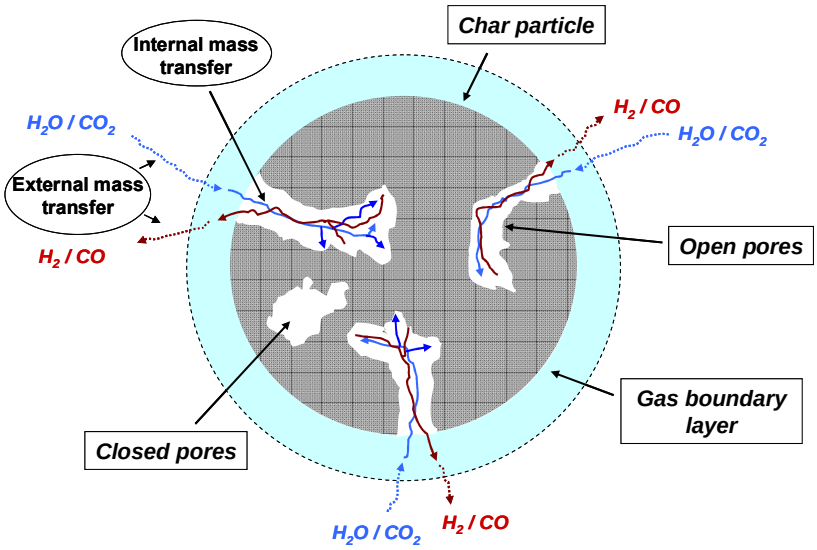


**Figure 18. Representation of mass transfer phenomena in gasification of a char particle – note: the boundary layer is delimited by a dotted line**

At the first step of gasification process, the reactive gas molecules present in the atmosphere have to reach the surface of the particle. This step needs an external mass transfer, which is ensured by convection of the gas moving around the particle or molecular diffusion in the case of a static gas. Once gasifying molecules arrive to the particle surface, they penetrate into it through the pores where they move along until finding a reaction site. The same phenomenon takes place for the release of the product gas, but in the opposite way: the gas molecules head towards the char particle outside through the pores and then they are incorporated into the surrounding gas. Note that the release of gasification products, $H_2$ and CO, can interfere with the transfer of $H_2O$ and $CO_2$ inside the particle. The gas flow inside the particle is ensured by internal mass diffusion, by pressure differences at the interior of the solid and by Soret effect.

Mass diffusion mechanism depends on the pore size, as it can be observed in Figure 19: Knudsen diffusion is predominant for pore sizes between 1 nm and 100 nm, and molecular diffusion for pore sizes higher than 100 nm.

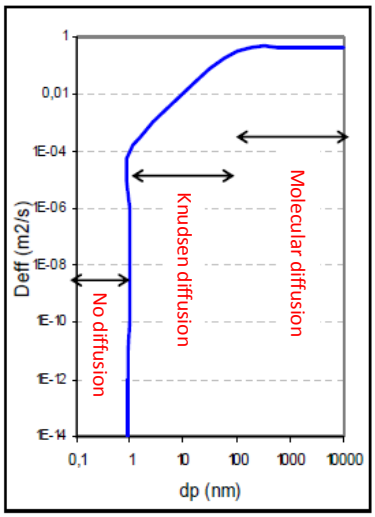


**Figure 19. Diffusion coefficient in function of pore size (Oliveira & Kaviany, 2001)**

The same mass transfer phenomena during gasification as those for char occur for soot, as shown in Figure 20 which shows a soot particle surrounded by a fictive gas boundary layer during its gasification.

Note that the internal mass diffusion in soot particles occurs within the pores which are created from the spacing between the spherules. The reactive gas cannot diffuse inside a spherule because of the too small pore size (< 1 nm), which suggests gasification reaction occurs on the surface of the spherules.

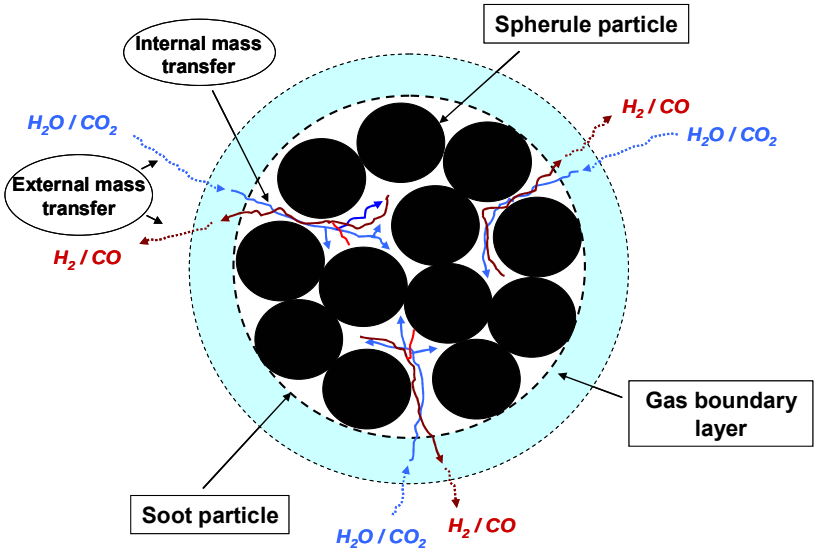


**Figure 20. Representation of mass transfer phenomena in gasification of a soot particle – note: the boundary layer is delimited by a dotted line**

Gasification is an endothermic reaction, which is possible at temperatures above 700°C. Thereby, the carbonaceous solid needs to be heated if it is not at a high enough temperature for gasification to occur. The heating mechanisms are the same as those occurring in wood heating during pyrolysis: external convection and radiation; internal conduction and radiation; advection and Dufour effect (refer to section 2.1).

### 4.2.2. Chemical phenomena

Gasification reaction is a surface reaction between a solid and a gas, which involves sorption phenomena. Different types of sorption exist, in function of the nature of the bond linking the reactive gas to the active sites or site of reaction, which are assumed to be located in the micropores in the case of char.

Physisorption or physical adsorption is due to the electric attraction between a gas molecule and an active site. In the case of gasification, as $CO_2$ and $H_2O$ are electrically neutral molecules but present a difference of electronegativity within their structure, Van Der Waals interactions are the only source of physisorption. Because of the weakness of the involved forces, this phenomenon is reversible. During physisorption, the adsorbed compounds are not affected by a cleavage of their molecular structure.

Concerning chemisorption or chemical adsorption, a gas molecule is linked to an active site through a bond of chemical origin, for instance a covalent bond. In this case, the involved interaction is very strong, thus chemisorption phenomena are never or rarely reversible.

Once reacting gas has reached the site of reaction, gasification takes place in three stages (Figure 21):

- Adsorption of the gas molecule on the surface of the solid, by the means of physisorption or chemisorption;
- Chemical reaction between the adsorbed compound and the carbon present in the site;
- Desorption of the product formed by physisorption.

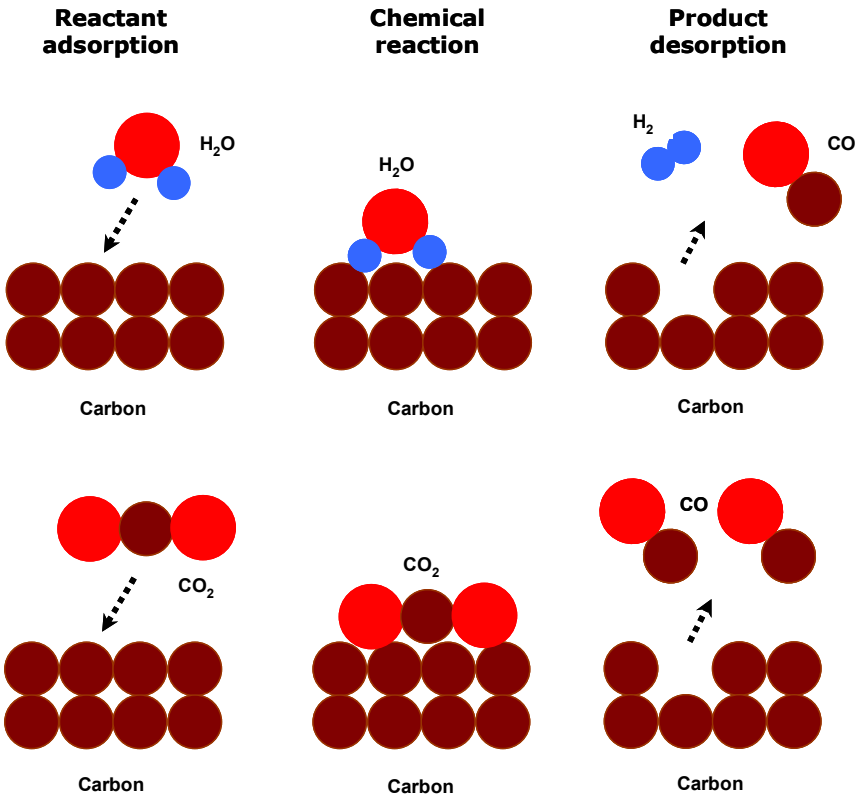


**Figure 21. Chemical phenomena in solid gasification**

As reported in literature (Roth, 2006), soot can also be oxidized with the radical OH●, which can be formed from $H_2O$ (Equation 4).

$$C_{soot}H + OH\cdot \rightarrow C_{soot}\cdot + CO + H_2$$ **Equation 11**

Soot conversion can occur in parallel to the formation process or successively. In the first case, gasification then competes against surface growth by $C_2H_2$ and PAHs addition.

### 4.3. Reaction regime

As mentioned in the case of pyrolysis (section 2.3), gasification reaction can occur under three regimes:

- regime controlled by heat or/and mass transfer;
- kinetically controlled regime;
- intermediary regime.

In an intermediary regime or in a regime controlled by transfers, a gradient of reagent concentration and/or temperature exist in the particle: the maximal concentration and higher temperature are located on the particle surface and they decrease when heading toward the center.

### 4.4. Reactivity of char and soot

In literature, gasification reaction rate is very often characterized by the reactivity, which refers to the evolution of the loss of carbonaceous solid mass *m* at an instant *t* with respect to its mass at this instant during gasification (Equation 12). It is important to make the distinction between intrinsic and apparent reactivity. The first term applies to a kinetically controlled regime, whereas the second one has to be used when transfer rates cannot be neglected.

$$R(t) = -\frac{1}{m(t)}\frac{dm(t)}{dt}$$ **Equation 12**

The degree of conversion *X* expresses the degree of advancement of the reaction (Equation 13). Reactivity can be written as a function of *X* (Equation 14).

$$X(t) = 1 - \frac{m(t)}{m(t=0)}$$ **Equation 13**

$$R(t) = \frac{1}{1 - X(t)}\frac{dX(t)}{dt}$$ **Equation 14**

The intrinsic reactivity of a carbonaceous solid depends on the number of reactive sites and on the reactivity of each individual site, both influenced by different external conditions. For example in the case of char, the pyrolysis heating rate and pressure (Cetin et al., 2005; 2004) determine the reactive sites number whereas the temperature (Gronli et al., 2002; Ollero et al., 2003), the composition of the atmosphere (Barrio et al., 2001; Roberts & Harris, 2007) and the biomass composition, especially the ash content (Mitsuoka et al., 2011; Moilanen, 2006), have a direct influence on the reactive sites reactivity. In the case of soot, the conditions of its formation have an influence on its structural ordering, and thus possibly on its intrinsic reactivity.

The apparent reactivity can also be influenced by factors related to the physical transfers, as characteristics of the particles (physical properties, size, tortuosity, porosity…) and those of the surrounding gas (physical properties, temperature, gas flowrate….).

## 5. Influence of the heating rate on wood gasification

The heating rate is very influent on pyrolysis and leads to a classification of this process into two main types. Slow pyrolysis operates at a heating rate of several 10°C.min$^{-1}$ and favors the production of char. Fast pyrolysis is characterized by a heating rate higher than 10°C.s$^{-1}$ and a high yield in volatile compounds, including gas and tar, to the detriment of char.

The differences between slow and fast pyrolysis yields can have different explanations:

- At the contrary of slow pyrolysis, fast pyrolysis does not give enough time for the transformation of cellulose into a more thermo-stable molecule, the anhydrocellulose, which is known to give higher yields in char (Zanzi et al., 1996).
- The brutal expulsion of volatiles during fast pyrolysis decreases the possibility of a tar polymerization into secondary char in contact of primary char (Fushimi et al., 2003; Kumar & Gupta, 1994), which can catalyze the process (Boroson et al., 1989). Besides, cracking reactions, which are in competition with secondary char formation (Antal & Gronli, 2003), are favored under high heating rates.
- Fast pyrolysis favors endothermic phenomena, like volatiles formation, rather than exothermic phenomena, as primary char formation (Milosavljevic et al., 1996).

On another side, char from fast pyrolysis is much more reactive than char from slow pyrolysis (Mermoud et al., 2006b). This can be explained by the difference of their structure: while char from fast pyrolysis is highly damaged by the brutal release of volatiles, slow pyrolysis is so progressive that volatiles can escape from the particle through the pores without destroying the structure. The damaged structure of char from fast pyrolysis then presents a high porosity (Cetin et al., 2005; 2004), with more micropores, mesopores, macropores and cavities. Formation of micropores means formation of reactive sites, which leads to a high intrinsic reactivity. Besides, a high porosity in general facilitates the gas diffusion within the particle, which leads to a higher mass transfer rate.

## 6. Summary

During wood gasification process, lignocellulosic matter is firstly decomposed into a wide variety of compounds, which continue to evolve through gas phase and heterogeneous reactions. This complex transformation involves both physical and chemical phenomena, which are coupled, like: heat and mass diffusion, heat and mass convective transport, radiation exchange, chemical reactions as devolatilisation, cracking, polymerization, reforming, water gas-shift and gasification. The main products of this transformation, which can be final or intermediate products, are: char, light hydrocarbons ($CH_4$, $C_2H_2$, $C_2H_4$, $C_2H_6$, $C_6H_6$), tar (> 6 C), soot and permanent gases ($H_2O$, $CO_2$, $H_2$, CO).

As wood is a resistant material, this decomposition requires an important input of heat. The way heat is brought, determined by the operating conditions, influences the pyrolysis products and their further evolution. In the case of rapid heating rate and high temperature, pyrolysis is expected to produce high yields in gas and tar, and low yields of a very reactive char. Note that tar polymerization into secondary char seems to be improbable because tar cracking and polymerization into soot are favored at high temperatures.

Next chapter will present the experimental results in literature obtained under the conditions of interest, which are those of an entrained flow reactor, namely high heating rates and high temperatures, and about the modeling of biomass gasification phenomena.

# Résumé du Chapitre 1 : Concepts fondamentaux

Le bois est largement utilisé dans la littérature pour l'étude de la gazéification de la biomasse, en raison de son abondance et de sa structure moins hétérogène que celle des autres types de biomasse. Le bois est le principal constituant du tronc de l'arbre et il est considéré comme de la matière morte. Environ 95% des cellules du bois sont composées de trois composants moléculaires: la cellulose, l'hémicellulose et la lignine, lesquels ont un rôle structural. De plus, le bois contient d'autres composés inorganiques de plus faible taille, les extractibles, lesquels contribuent aux propriétés du bois (odeur, couleur, etc.…).

Lorsque le bois est exposé à des températures élevées, de nombreuses liaisons chimiques sont rompues sous l'effet de la chaleur. Cette décomposition du bois, connue sous le nom de pyrolyse, conduit à la formation d'un nombre important de composés volatiles et d'un résidu solide, le char. Ce processus complexe implique des phénomènes physiques et chimiques.

Comme la pyrolyse se produit à des températures élevées, le chauffage de la particule est la première étape du processus. La particule est chauffée sur sa surface externe puis la chaleur se propage vers le cœur du solide par convection et/ou conduction. Les transferts de chaleur se font principalement par convection, conduction et rayonnement. Des transferts de masse et de quantité de mouvement sont liés au dégagement du gaz produit.

Au cours de la montée en température, la particule est séchée entre 100°C et 200°C, puis la dégradation de ses principaux composants commence à des températures plus élevées. Les principaux produits de cette transformation sont: les gaz permanents ($CO_2$, CO, $H_2O$, $CH_4$, hydrocarbures en $C_2$, benzène), les goudrons (hydrocarbures de masse moléculaire supérieure à celle du benzène), les suies et le char.

Les composés volatiles dégagés lors de la pyrolyse peuvent réagir entre eux ou avec un agent oxydant présent dans l'atmosphère, comme $H_2O$ ou $CO_2$. Les réactions responsables de l'évolution de la phase gazeuse peuvent être classées en 4 groupes: réactions de craquage, de polymérisation, de reformage et de water-gas shift (WGS). Ces réactions chimiques dépendent fortement de la température, de la pression et de la composition de l'atmosphère.

A des températures suffisamment élevées, le processus de craquage des goudrons et des hydrocarbures légers produit d'importantes quantités de noyaux benzéniques et de $C_2H_2$, lesquels peuvent ensuite se polymériser en hydrocarbures polyaromatiques (HAP). A partir des HAP et du $C_2H_2$, des particules solides, les suies, peuvent être synthétisées. Les hydrocarbures peuvent être oxydés en $H_2$ et CO en présence des oxydants $CO_2$ et $H_2O$ lors des réactions de reformage. La réaction de WGS, réaction réversible, permet d'échanger des atomes d'oxygène entre les composés $H_2/H_2O$ et $CO/CO_2$ suivant la constante d'équilibre.

Les solides carbonés provenant de la pyrolyse, à savoir le char et les suies, peuvent réagir avec les gaz oxydant, $H_2O$ et $CO_2$. Ces réactions, dites de gazéification, produisent du $H_2$ et du CO. La gazéification, réaction hétérogène et endothermique, fait intervenir des phénomènes physiques et chimiques. Ainsi, la gazéification nécessite un chauffage de la particule, et implique des transferts de masse de réactifs et de produits de la réaction entre l'environnement et la particule. La réaction chimique se fait par des phénomènes d'adsorption – désorption des espèces gazeuses sur les sites actifs du solide.

Comme le bois est un matériau résistant, sa décomposition nécessite un apport important de chaleur. La façon dont la chaleur est apportée détermine la distribution des produits de pyrolyse et influence leur évolution. Dans le cas de vitesses de chauffe rapides et à des températures supérieures à 700°C, la pyrolyse produit de grandes quantités de composes volatiles et de faibles quantités de char, lequel est très poreux dans ces conditions. La formation de char secondaire à partir de la polymérisation des goudrons est peu probable puisque les réactions de craquage et la formation des HAP et suies sont privilégiées dans ces conditions.

# Chapter 2: State of the art

# 1. Experimental literature review

Literature presents a large collection of studies about the effect of different parameters on gasification of coal or biomass as feedstock. This section defines the effect of the parameters estimated as the most sensitive under the conditions of an entrained flow reactor, which are high temperature and rapid heating rate.

## 1.1. Experimental approaches used in literature

Gasification can be studied by two different approaches. In the first one, the different stages during gasification are experimentally decoupled: pyrolysis, gas phase reactions and carbonaceous solid gasification are treated separately. In the second case, gasification process is integrally studied in one step.

### *1.1.1. Pyrolysis experiments*

The study of pyrolysis is performed in a furnace under an inert atmosphere, composed of nitrogen, helium or argon. The sample heating conditions depend on the furnace technology: there are analytical reactors for both slow and fast heating rates (HR).

Table 4 lists the different reactors that can operate at high heat flux with their respective operating parameters. These devices are designed to study only pyrolysis, also referred as primary pyrolysis, or pyrolysis with secondary reactions, also referred as secondary pyrolysis.

Among the experimental devices to study fast pyrolysis, pyroprobe, screen heater, xenon arc lamp and tubular reactor have a similar functioning principle: the sample is introduced in a room where it is exposed to a high heating flux. All of these reactors minimize their gas residence time in order to limit gas phase reactions, especially tar cracking, and thus to study only particles pyrolysis. In practice, it is very difficult to completely avoid secondary reactions because cracking reactions are very fast at the operating temperatures.

**Table 4. Typical operating parameters of reactors for pyrolysis experiments under high heating fluxes**

| | Pyroprobe | Screen heater | Xenon arc lamp | Tubular reactor | Drop tube reactor | Fluidized bed reactor |
|---|---|---|---|---|---|---|
| **Maximum heat flux ($W.m^{-2}$)** | ~$2x10^6$ | ~$2x10^6$ | ~$1.3x10^6$ | ~$5x10^4$ | ~$2x10^5$ | ~$1.3x10^3$ |
| **Maximum temperature (°C)** | 1400 | 1000 | 1000 | 1000 | 1500 | 1000 |
| **Run mode** | Constant HR | Constant HR | Constant HR | Isothermal | Isothermal | Isothermal |
| **Feeding type** | Batch | Batch | Batch | Batch | Continuous | Batch or continuous |
| **Sample mass** | 0.002 g | ~ 0.1 g | 1 – 4 g | 0.3 – 2 g | 0.5 – 1 g/min | > 5 g or g/min |
| **Particle size (mm)** | < 0.01 – 0.1 | 0.1 – 0.5 | 10 – 30 | 10 – 20 | 0.1 - 1 | 10 - 20 |
| **Solid residence time** | 0.1 - 1 s | 1 s – 1 h | 1 s – 1 h | 1 s – 1 h | 0.1 s – 5 s | 1 min – 1 h |
| **Example** | (Hajaligol, 1982), (Nunn, 1985) | (Font, 1994), (Fisher, 2002) | (Gronli, 1996), (Boutin et al., 2002), | (Couhert, 2007; Girods et al., 2009) | (Dupont et al., 2008), (Zanzi et al., 1996) | (Guerrero et al., 2005), (Kojima et al., 1993) |

The drop tube reactor (DTR) and the fluidized bed reactor, also operating at high heating rates, are closer to real processes than the other experimental tools. Contrary to the other reactors, they work in a continuous mode that allows measuring the product yields in a steady state regime. In these kinds of reactor, the primary pyrolysis cannot be decoupled from secondary reactions, particularly tar cracking, mainly at temperatures higher than 600°C, because the volatiles residence time in the hot environment of the reactor is of several seconds, which is an enough time for gas reactions to take place.

The functioning principle of the DTR is very close to the one of the entrained flow reactor (EFR). This leads to a similar particle thermal history for both reactors: as it is schematized in Figure 22, the particles are entrained by a gas flow from the top to the bottom of the reactor, passing for several seconds through a hot zone where the transformation takes place. However, the heat source is different in a DTR compared to an EFR: while the heat is provided in a DTR by electrically heated walls, the EFR is heated by a flame.

Most of the works in DTRs found in literature take place at a maximum temperature of 950°C for biomass (Chen, 2009; Dupont et al., 2008; Shuangning et al., 2006; Zanzi et al., 1996), at the exception of some authors (Wei et al., 2006; Zhang et al., 2006).

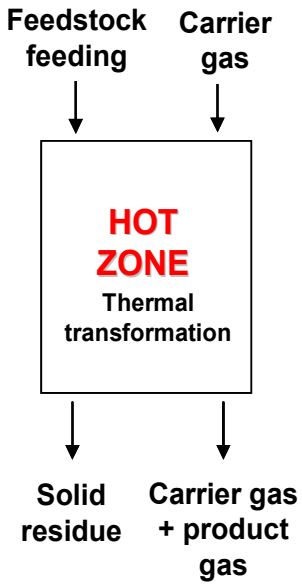


**Figure 22. Scheme of the functioning principle of an EFR and a DTR**

The fluidized bed reactor, which is originally one of the industrial reactor technologies for biomass gasification, can also be found at lab scale. Biomass transformation takes place in an inert or catalytic bed, which is fluidized in order to homogenize the heat within the reactor.

Other analytical reactors operating at high HR have been designed by some authors (Bellais, 2007; Lu, 2006).

### *1.1.2. Gas phase reactions experiments*

In literature, some authors have studied gas reactions to characterize the behavior of the gas phase during the thermochemical conversion of a solid, liquid or gas. The topics more investigated in this field are the decomposition of light hydrocarbons (Makarov & Pechik, 1974; Skinner & Ruehrwein, 1959), the formation of aromatic compounds (Bohm & Jander, 1999; Skjøth-Rasmussen et al., 2002) and the formation of soot (Dworkin et al., 2011; Mendiara et al., 2005). Even if the research on these topics is mostly oriented for a combustion application, many data can be useful in the gasification context, especially the one obtained from experiments under an inert atmosphere.

For a more specific gasification application, some authors have also studied the gas reactions in an reactive atmosphere of $H_2O$ and/or $CO_2$ (Hiblot, 2010; Valin et al., 2009). However, most of the researches in this field are in the presence of catalyst or $O_2$ (Gutierrez et al., 2005).

The most common gas phase reactor in literature is the tubular reactor or laminar flow reactor (Hiblot, 2010; Valin et al., 2009), consisting in a heated alumina tube through which a gas flows and reacts in the hot zone. Two other reactors are very used to study soot formation: the shock wave reactor (Bhaskaran & Roth, 2002) and the laminar flame reactor (Li et al., 2011).

### *1.1.3. Solid residue gasification experiments*

In literature, several studies about the heterogeneous reaction of gasification can be found. Most of the char gasification works have been performed with char from biomass pyrolysis obtained under slow HR (Barrio et al., 2001; Klose & Wölki, 2005) or with charcoal (Cetin et al., 2004; Roberts & Harris, 2006). Only few works deal with gasification of char obtained from biomass pyrolysis at high heating rates and high temperatures (Fermoso et al., 2009; Yuan et al., 2011).

In the case of soot, gasification studies are rare in literature. Nevertheless, a review about soot oxidation with $O_2$ (Stanmore et al., 2001) provides general data about soot behavior during heterogeneous reactions.

The thermogravimetric analyzer (TGA) is doubtlessly the most used analytical reactor for gasification or oxidation study. Figure 23 gives a simplified scheme of a TGA. The sample is put in a crucible, which is suspended in a hot environment swept by a gas flux and linked to a balance measuring the variation of the mass on line.

Gasification can be performed during the rise of temperature or when an isothermal plateau is reached. For a TGA experiment, a few milligrams of sample have to be placed in the crucible and the particle size has to be inferior to the mm, in order to avoid transfer limitations and then to operate in a kinetically controlled regime. Macro-TG offers the possibility to study gasification in a regime limited by transfers, by using a higher mass sample (10 – 75 g) or with a larger particle size (6 – 22 mm) than is allowed in a standard TGA (Mermoud et al., 2006a; Tagutchou, 2008).

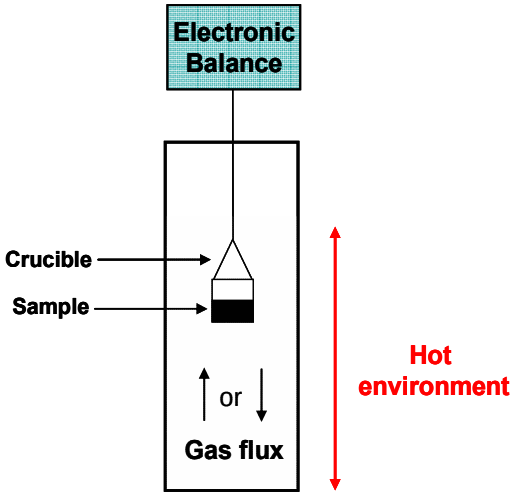


**Figure 23. Schematic diagram of a TGA**

Other furnaces can also be used for char gasification studies, like a DTR (Kajitani et al., 2002) or an analytical fluidized bed (Matsui et al., 1987), which present the advantage to work in a steady state regime. However, in a TGA the thermal conditions are better controlled and the online measurement of the sample mass evolution leads to a more precise determination of reaction kinetics. A problem in TGA may be a bad reproducibility between

experiments, mainly because the low mass samples used in TGA experiments can be not representative of the whole sample.

#### 1.1.4. Direct biomass gasification experiments

Some authors have studied the whole thermal decomposition of the biomass in a gasification atmosphere with $H_2O$ or $CO_2$, using reactors such as DTRs (Hallgren, 1993; Wolfesberger et al., 2009; Zhang et al., 2010) or analytical fluidized bed reactors (Wolfesberger et al., 2009). In the case of the DTR, this approach has not been yet really well explored in the case of biomass, even if an extensive collection of works exists in the case of coal (Ouyang et al., 1998; Shin et al., 2000).

#### 1.1.5. Summary

Among the different laboratory devices described in literature, the DTR seems to be the most suitable analytical reactor to study the pyrolysis and gasification of biomass in an EFR. This experimental device can work at high temperatures and high heating rates in a continuous mode, in a similar way to EFR. However, as it was not designed to study primary pyrolysis, the particles residence time is largely enough for gas reactions to occur. Therefore, the pyrolysis experimental study in a DTR includes secondary reactions. Other pyrolysis lab reactors with significantly lower residence time could be better adapted to study primary pyrolysis, but even in these conditions the separation between devolatilisation and gas phase reactions is not sure.

Other analytical reactors can be useful and complementary to the DTR, as the TGA to characterize the carbon solid reactivity or the tubular reactor to focus on gas phase reactions.

### 1.2. Experimental results obtained under high heating rates and high temperatures

Now that the experimental devices available to study biomass gasification under high heating rates have been described, the existing experimental results in the bibliography are reviewed in this section, which focuses on the results obtained in a DTR under different experimental conditions: atmosphere composition, reaction temperature and particle diameter. A particular attention is paid to the structural changes of carbonaceous solid at high temperatures.

#### 1.2.1. Experimental results obtained under an inert atmosphere

##### 1.2.1.1. Evolution of the yields with temperature

Rapid pyrolysis produces mainly tar at a medium temperature range (400 – 500°C) and gas at temperatures higher than 700°C (as mentioned in section 5 of Chapter "Fundamental Concepts"). Tar yield starts to decrease from 500°C, where it reaches its maximum value (Bridgwater et al., 1999). Besides, a detailed analysis of tar composition (Ogi et al., 2010; Zhang et al., 2006) shows that the latter changes with temperature: around 600°C, tar is mainly composed of oxygenated and phenolic compounds, whereas from 800°C aromatic compounds are majority. These changes in tar composition with temperature, due to cracking and polymerization reactions (refer to section 3.1 of Chapter "Fundamental Concepts"), are accompanied of an increase of gas yield: increase of $CH_4$, $H_2$ and CO yields, formation of $C_2$, $C_3$ compounds and $C_6H_6$. Within $C_2$ species, $C_2H_6$ has a very fast apparition and $C_2H_4$ yield begins to decrease after reaching its maximum value at 800°C, at the same time as $C_2H_2$ formation starts (Chen, 2009; Ekstrom & Rensfelt, 1980).

From 1000°C, a decrease of hydrocarbons yields and a high soot formation can be observed (Qin et al., 2009; Zhang et al., 2006). At the same time, an increase of $H_2$ and CO yields, and a decrease of $H_2O$ and $CO_2$ yields with temperature are measured. Around 1400°C, tars are totally converted and only low amounts of gaseous hydrocarbons still remain, consisting essentially in $CH_4$ and $C_2H_2$ (Zhang et al., 2010).

#### 1.2.1.2. Evolution of char and soot yields with temperature

Pyrolysis under a high heating flux gives a low char yield. At 600°C, char represents around 10 - 15% of the initial biomass mass and at 800°C this yield slightly decreases to 5 - 10 % where a plateau is attained (Wei et al., 2006; Zhang et al., 2006). However, for temperatures higher than 1100°C, char may be partially gasified by the $H_2O$ and $CO_2$ released during the devolatilisation process, leading to a new decrease in char yield with the increase of temperature (Zhang et al., 2006).

Soot, another solid product of the hydrocarbon reactions, starts its formation since 900°C – 1000°C by polymerization of the hydrocarbons compounds (refer to section 3.1 of Chapter "Fundamental Concepts"). Its yield increases until a maximum is reached around 1200°C and then it slightly decreases because of gasification with pyrolytic $H_2O$ and $CO_2$ (Qin et al., 2009; Zhang et al., 2006).

#### 1.2.1.3. Influence of particle size during wood pyrolysis

Some authors include in their study the effect of particle size on pyrolysis in the temperature range of 700°C to 950°C in a DTR (Chen, 2009; Dupont et al., 2008; Wei et al., 2006; Zanzi et al., 1996). All of them agree that pyrolysis cannot completely be achieved in the case of particles larger than about 0.50 mm at 800°C and 0.70 mm at 950°C. This limitation leads to a higher solid yield for large particles than for small ones and was confirmed by the aspect of the particle cross-section: the particle external surface presents a black color, sign of a complete pyrolysis, whereas the color of the core is rather brown, which shows that wood has not finished to transform into char (Figure 24).

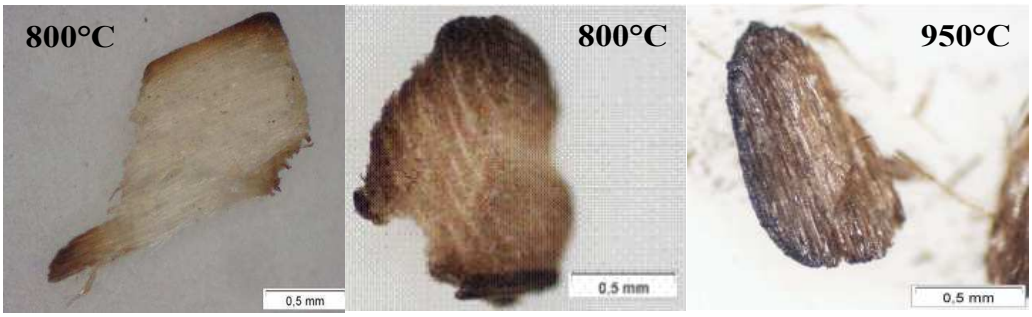


**Figure 24. Incomplete pyrolysed wood particles obtained at 800°C and 950°C (Dupont, 2006)**

Only one work on biomass particle size effect at higher temperature than 950°C has been found (Bitowft et al., 1989). In this study, it was shown that particles with a size between 0.250 mm and 0.355 mm pyrolyze faster than particles with a size between 0.500 mm and 0.630 mm. The latter seem to be incompletely pyrolysed at 1000°C for a residence time of 1 s, at the contrary of the smaller particles. Above 1000°C, complete pyrolysis seems to be finally achieved for both particle sizes.

### 1.2.2. Experimental results obtained under a wet atmosphere

Only few works in literature are dedicated to the study of biomass gasification in a DTR (Dupont et al., 2007; Qin et al., 2009; Zhang et al., 2010). Through these works, it has been observed that an atmosphere rich in $H_2O$ leads to a faster decrease in char, soot and hydrocarbons yields with temperature, compared to an atmosphere with a poor content in $H_2O$, typically a pyrolysis atmosphere (Qin et al., 2009; Zhang et al., 2010). However, the effect of $H_2O$ is observable only for temperatures higher than 1000°C for a residence time of some seconds. For temperatures lower than 1000°C, only a little part of hydrocarbons seems to be affected by the presence of $H_2O$ and the water gas shift equilibrium is modified (Dupont et al., 2007). The use of a catalyst lowers the temperature of hydrocarbons conversion in the presence of $H_2O$ (Wei et al., 2007).

### 1.2.3. Structural modifications of char and soot with temperature

Several authors have observed that char formed at temperatures higher than 1000°C loses a part of its reactivity with the increase of temperature. This reactivity decrease, known as thermal deactivation or thermal annealing, has been widely studied in the case of coal pyrolysis under high heating flux (Liu et al., 2003; Russell et al., 1999; Shim & Hurt, 2000).

Char graphitization or carbonization process is assumed to be the main responsible for the reactivity decrease. Indeed, this phenomenon leads to the ordering of char structure which tends towards that of graphite as temperature increases (Figure 25). As graphitization degree is higher, the number and reactivity of the reactive sites is lower, leading to the decrease of char reactivity (Figure 26).

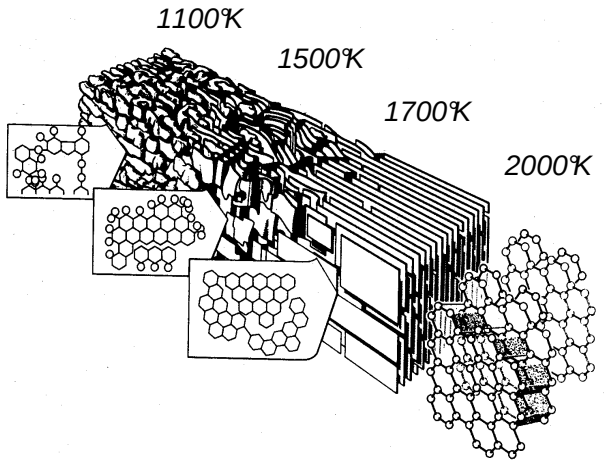


**Figure 25. Representation of the graphitization of a char structure in function of pyrolysis temperature (Bunsell, 1988)**

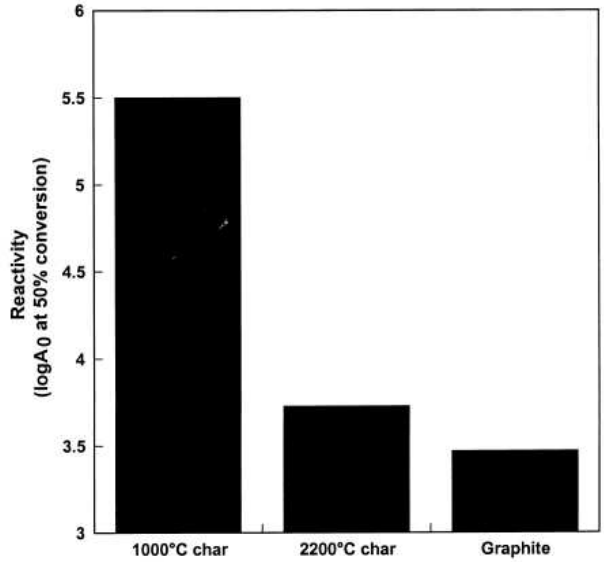


**Figure 26. Comparison of the reactivity of graphite and of a charcoal at two pyrolysis temperatures at 50% of conversion (Russell et al., 1999)**

In the case of biomass, only few studies of char deactivation have been found in literature (Kumar & Gupta, 1994; Shim & Hurt, 2000). The results from these works highlight that char from biomass also suffers from thermal deactivation but in a moderate intensity compared to charcoal.

The decrease of reactivity with temperature has also been observed in the case of soot (Ruiz et al., 2007). However, this cannot be related to the graphitization process, as no appreciable changes in soot structure can be observed below 1800°C according to some experimental experiments in very high temperature devices (Leung et al., 1991; Marsh et al., 1971). Nevertheless, temperature during soot formation can indirectly influence the ordering degree of the solid structure (Vander Wal & Tomasek, 2004): below 1300°C, PAHs are likely the dominant species during soot mass growth, whereas at higher temperatures their decomposition into $C_2H_2$ is enhanced, which leads to a more important contribution of $C_2H_2$ on soot mass growth. As soot surface growth with the addition of $C_2H_2$ gives a graphite structure whereas that from PAHs gives an amorphous one, the soot structure order is increased with temperature. Figure 27 shows a more ordered disposition of the soot graphite layers in the soot obtained from the $C_2H_2$ pyrolysis at 1650°C compared to soot obtained at 1250°C.

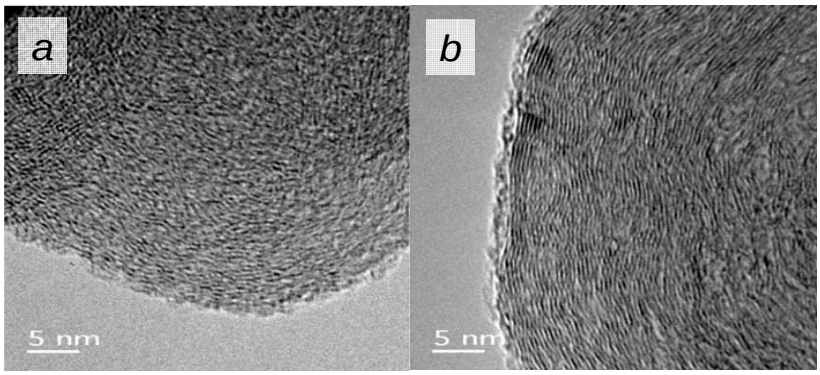


**Figure 27. TEM images of soot obtained from the pyrolysis of $C_2H_2$ at 1250°C (a) and 1650°C (b) (Vander Wal & Tomasek, 2004)**

### *1.2.4. Summary*

Most of the experimental works in a DTR concern coal pyrolysis and gasification, or biomass pyrolysis in a temperature range of 700°C to 950°C. In the case of biomass, only few works go beyond 1000°C, as the DTR has been primarily used for the research of biomass gasification in a fluidized bed reactor, which mainly operates between 800°C and 950°C.

It has been observed in literature that the yield of syngas ($H_2$ and CO) increases with temperature, at the same time as hydrocarbons and solid carbon yields decrease. In the case of an inert atmosphere, important soot formation can also be observed above 1000°C. The addition of $H_2O$ to the reaction atmosphere above 1000°C lowers the yields of soot, char and hydrocarbons. In counterpart, high temperature can also induce the graphitization of solid carbon structure, which leads to a decrease of its reactivity.

## 2. Modeling approach

Modeling, which is complementary to the experimental analysis, is a necessary step for biomass gasification study. The development of a model provides a prediction of the conversion time and the product distribution, as the operating conditions are varied. This enables to better understand the phenomena occurring during the experiments. In the other way, the experiments should validate the model.

This section is dedicated to the description of gasification models. The main steps of the process have to be identified and then considered separately. This brings us to the modeling of pyrolysis, gas phase reactions and gasification reaction.

## 2.1. Pyrolysis modeling

As pyrolysis is a complex phenomenon which involves many physical and chemical phenomena (refer to section 2 of Chapter "Fundamental concepts"), its modeling should include chemical kinetics coupled with the description of physical phenomena, and variations of physical properties of the fuel. The first step during biomass pyrolysis is the moisture evaporation step, which is highly endothermic, and is followed by the thermal degradation, which includes heat, momentum and mass transfer coupled to chemical kinetics.

In the case of coal, morphological modifications of the particle, as for example swelling and softening, have been modelled by some authors (Oh et al., 1989; Shurtz et al., 2011). In the case of biomass, no models including such aspects have been found in literature.

Extensive reviews of biomass pyrolysis modeling can be found in literature (Chen, 2009; Di Blasi, 2008).

### *2.1.1. Chemical kinetics of biomass pyrolysis*

#### *2.1.1.1. Global and semi-global models*

Modeling of pyrolysis kinetics can be performed by the means of global models and semi-global models. A very simple approach, the one – step global model, considers pyrolysis as a single step reaction (Figure 28a). However, this model is not able to predict the influence of temperature on the final product yields as a fixed char yield is imposed for all temperatures.

Among the semi-global models, the multi-step scheme (Shafizadeh & Chin Peter P, 1977) lumps the pyrolysis products into three groups: gas, tar and char. As shown in Figure 28b, this model describes pyrolysis by three competing reaction, thus the prediction of the yields of char, tar and gas becomes possible by assigning kinetics constant for each reaction. Another semi-global model, the independent parallel reactions model assumes that the biomass directly decomposes into individual products *i* by single independent reactions of first – order with respect to biomass mass (Figure 28- c). Indeed, this model can predict the yields of different volatile products, as for example $CH_4$, $C_2$ and $C_3$ compounds, $H_2$, CO, $H_2O$, $CO_2$… (Hajaligol, 1982).

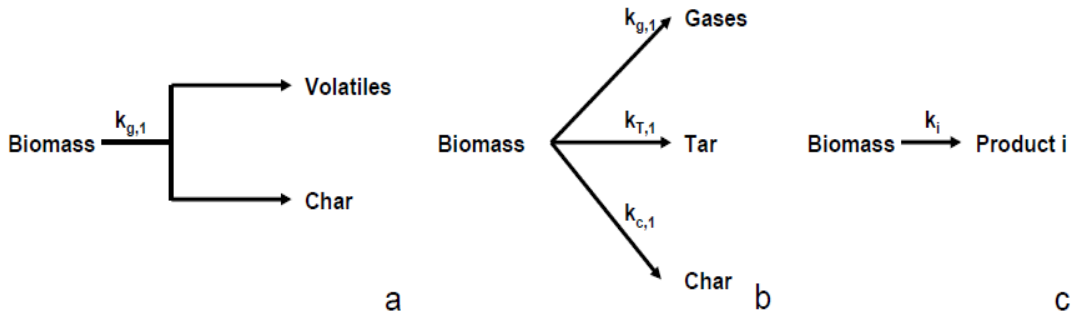


**Figure 28. Empirical models for primary pyrolysis**

These models are supposed to describe only the primary pyrolysis and exclude the secondary reactions. However, as primary pyrolysis is very difficult to be isolated from secondary reactions, some models include further stages in their mechanisms, especially tar cracking reactions. Figure 29 shows a typical scheme of biomass pyrolysis which includes tar cracking (Janse et al., 2000; Mousquès et al., 2001). Contrary to a large amount of

experimental studies on biomass devolatilisation, very few studies have been performed to quantify the kinetics of tar reactions (Di Blasi, 1993).

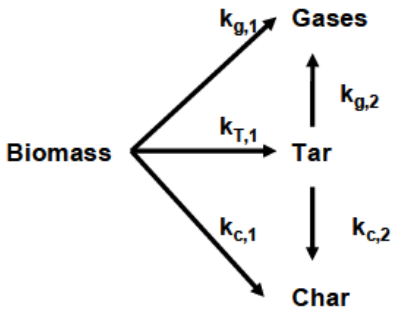


**Figure 29. Empirical models including secondary reactions**

Note that the reaction rate constants in global and semi-global models are usually expressed by an Arrhenius law:

$$k = k_0 \cdot e^{\frac{Ea}{R \cdot T}}$$ **Equation 15**

With:

| | | |
|---|---|---|
| $k$ | Chemical kinetics rate | $s^{-1}$ |
| $k_0$ | Pre-exponential factor | $s^{-1}$ |
| $Ea$ | Activation Energy | $J.mol^{-1}$ |
| $R$ | Constant of ideal gas | $J.mol^{-1}.K^{-1}$ |
| $T$ | Temperature | K |

#### 2.1.1.2. *Other modeling approaches*

Some researchers have attempted to predict biomass behavior during pyrolysis, by the sum of the contribution of its main components, namely cellulose, hemicellulose and lignin (Miller & Bellan, 1997; Orfão et al., 1999; Ranzi et al., 2008). However, the use of a superposition model is based on a quite hazardous assumption where the interaction between biomass components is not taken into account. Nevertheless, some superposition models have shown acceptable predictions (Ranzi et al., 2008).

Some other approaches, initially focused on coal pyrolysis modeling, have been adapted for the case of biomass.

The distributed activation energy model or DAEM (Feng et al., 2003; Maki et al., 1997; Please et al., 2003) assumes an infinite number of irreversible first – ordered parallel reactions with different activation energy to occur simultaneously, where the distribution in activation energies is represented by a distribution function.

The network structural models (De Jong et al., 2007; Niksa, 2000; Sheng & Azevedo, 2002) consider that biomass structure is composed of macromolecules lumped into different groups, which suffer from structural changes during devolatilization, especially from chemical bonds breaks, leading to the formation of gas, tar and char.

Both types of models are able to predict mass loss and gas yields. However, the DEAM and network structural models present respectively a high degree of mathematical and physical complexity.

### 2.1.2. Modeling of physical phenomena during biomass pyrolysis

#### 2.1.2.1. Transport model

Transport models usually include external heat transfer and intraparticle transport. For a precise heat balance, pyrolysis enthalpy has to be considered, but this parameter is very difficult to determine, as pyrolysis process occurs through an important number of unknown reactions and involves several unidentified intermediary species. For this cause, different alternative approaches to calculate pyrolysis enthalpy (Mok & Antal, 1983; Rath et al., 2003) are used in literature.

Extra-particle phenomena, as the gas carrier heating, are not always taken into consideration except for some cases where they are treated in a simplified way. External heat transfer, including convection and radiation, is determined by the more appropriate exchange coefficients to the operating conditions. For instance, the value of the external heat transfer is about 400 – 1180 $W/m^2/K$ in a fluidized-bed reactor versus 100 – 200 $W/m^2/K$ in moving and stirred bed reactors (Yang et al., 2000).

Intraparticle processes are much more difficult to model because of the coexistence of various phenomena: heat transport by conduction, diffusion of gas within the pores, radiation exchange between the internal pores, pressure and velocity variations, etc…. Moreover, the medium where the intraparticle phenomena take place is a complex mixture of solid and gas, whose properties are very difficult to characterize. Several simplifications are usually made and some of the phenomena are neglected, in order to simplify the modeling.

Transport processes depend very closely on the physical properties of the solid, such as thermal conductivity, specific heat capacity, mass diffusivity, permeability…Through a model sensibility analysis (Di Blasi, 1997; Gronli, 1996), thermal conductivity and solid density were determined as the most sensitive parameters in the transport processes: the conversion time becomes longer as the density of the biomass increases and/or the thermal conductivity decreases.

#### 2.1.2.2. Shrinking core model

An approach used in wood pyrolysis modeling consists in the shrinking core model which is based on the principle schematized in Figure 30: as pyrolysis proceeds, an infinitely thin reaction front where pyrolysis takes place propagates from the surface of the particle towards the centre; the particle size is usually reduced during this process. The pyrolyzing particle then presents two zones: a char region and a virgin wood core separated by the pyrolysis front. The solid properties (density, porosity, thermal conductivity…) vary from the initial wood values to the final char values, passing through intermediary values during the transformation (Di Blasi, 2008).

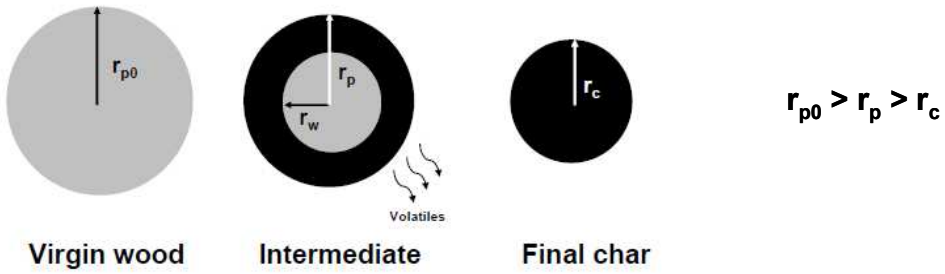


**Figure 30. Shrinking core model principle**

It has been noticed that the thickness of the reaction zone is proportional to $[\Delta T \cdot \lambda / Q]$ with $\lambda$ as the solid thermal conductivity, $\Delta T$ as the characteristic temperature difference across the reaction front and $Q$ as the heat flux at the reaction front (Maa & Bailie, 1973). In order to verify the assumption of an infinitely thin pyrolysis front, this model can only be valid for a fuel with low thermal conductivity, as wood, and with an apparatus presenting a high heating flux, such as a DTR. During fast pyrolysis experiments on millimetric coal and wood particles, a boundary

between the char region and the wood core can be observed (Figure 31), which proves that the shrinking core model can be used to describe fast pyrolysis in these cases.

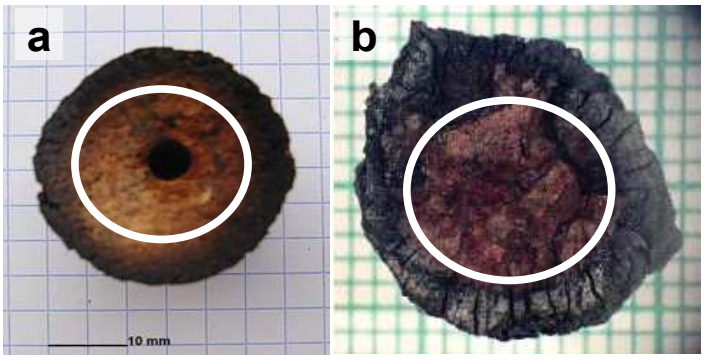


**Figure 31. Cross section of coal particle after pyrolysis at 850°C for about 30 s (a) (Chern & Hayhurst, 2004) and beech wood particle after pyrolysis at 1000°C for 3 s (b) (Burghoffer, 2009) – Note: a fictive pyrolysis front is represented by a white line**

Usually, the shrinking core model is associated with the assumptions of no moisture content and one-dimensional system. More recently, this model has been modified to include the effects of moisture (Galgano & Di Blasi, 2004), assuming that the moist region is separated from the dry region by an infinitely thin constant-temperature front.

## 2.2. Gas phase and soot formation modeling

The gas phase composition is susceptible to be modified in function of the surrounding conditions, as temperature, pressure, the type of the atmosphere, which can be inert or oxidant, and the residence time. Therefore, modeling of gas phase behavior is necessary for an accurate prediction of the product distribution at the outlet of the reactor.

### *2.2.1. Gas reactions modeling*

For the modeling of gas phase composition, the chemical reactions between the main gaseous compounds have to be firstly identified. Then, each reaction can be represented by a simple single step model, or by a complex series of interconnected reactions, which presents several intermediary reactions and species. An example of this last approach, which is closer to the reality than a global model, is shown in Figure 32.

As the chemical reactions depend on the surrounding conditions, the physical evolution of the gas stream has to be included in the modeling.

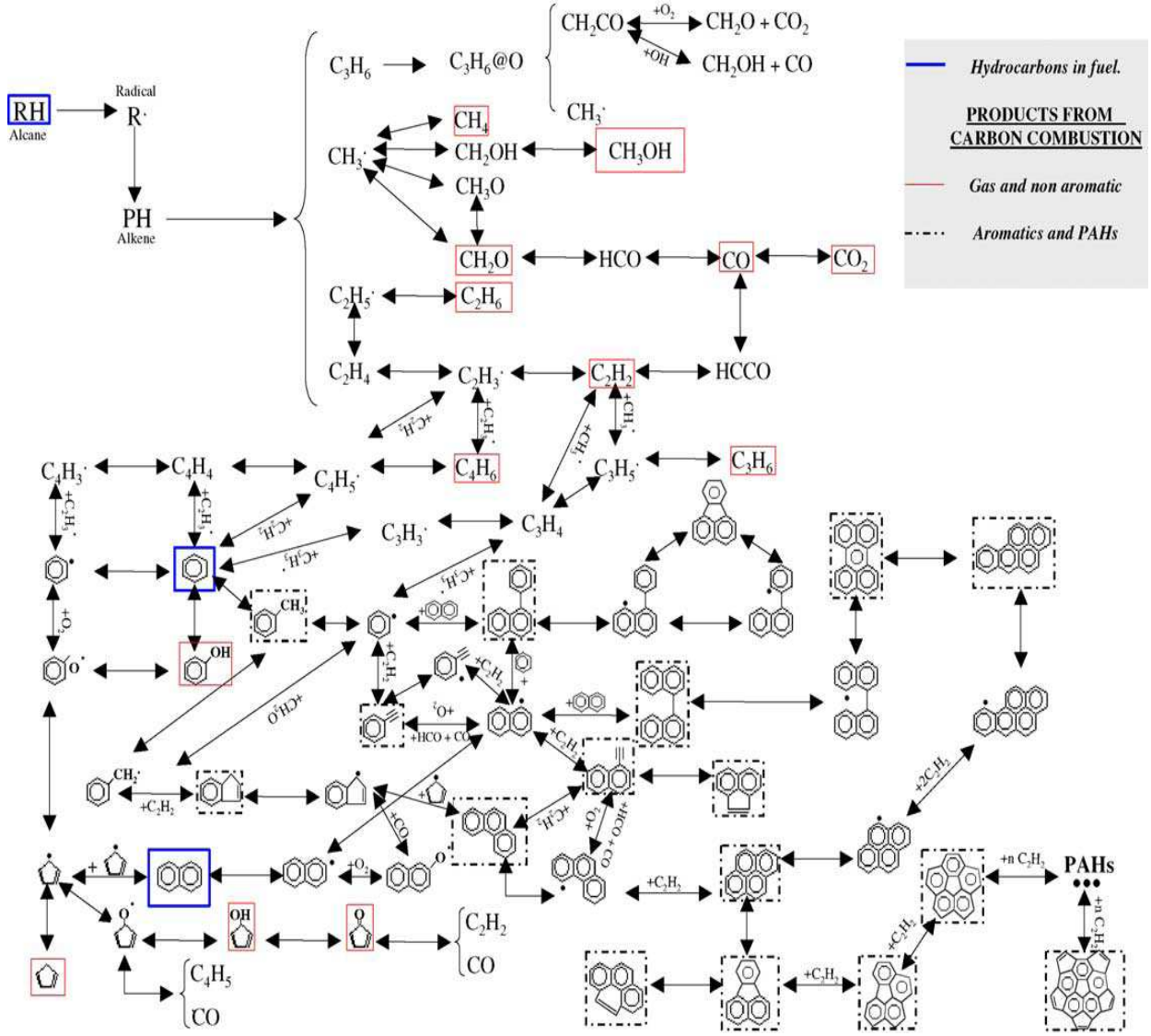


**Figure 32. Kinetic scheme of the main reactions used in a model for the combustion of hydrocarbons and PAHs formation (Durán et al., 2004)**

Modeling of the gas phase by a kinetic scheme can be undertaken by using CHEMKIN (Kee et al., 1989; Kee et al., 1990), a software specially developed for this purpose, which considers gas reactions taking place in a Perfectly Stirred Reactor (PSR) at each time step. This assumption simplifies the calculations, because the gaseous reagents are considered to have a perfect contact and then no mixing limitation has to be included. CHEMKIN contains thermodynamic data of all the involved reactions, thus it can calculate the enthalpy of the involved reactions.

Each kinetic scheme is determined from a chemical mechanism which is validated with experiments. A lot of detailed chemical mechanisms, published in the literature, are devoted to combustion. Among them, some mechanisms seem of great interest in the case of biomass gasification, as for example the Konnov's mechanism (Coppens et al., 2007), with 127 species and 1207 reactions, and the Skjoth-Ramussen mechanism (Skjøth-Rasmussen et al., 2004; Skjøth-Rasmussen et al., 2002), with 159 species and 773 reactions.

The first cited mechanism, built to precisely describe the oxidation of light gases up to $C_3$ species, is expected to be reliable in the prediction of light species (Konnov, 2000). It has been validated for a wide range of temperature and pressure conditions, and for a large number of species (Konnov, 2000). The second mechanism is more suitable

for the prediction of soot precursors, especially PAHs, for which it takes into account the last progress in this field, and has been validated through a series of experiments on oxidation of light hydrocarbons (< $C_4$). Both mechanisms have already been tested with an acceptable accuracy for a biomass gasification application, through gas phase experiments with a composition representative of the biomass pyrolysis one (Valin et al., 2009).

A few chemical mechanisms have been specifically developed for a biomass gasification application. Ranzi et al. (2008) have included a kinetic scheme for the evolution of gas phase in their model of biomass pyrolysis (130 species, 2808 reactions). The DCPR mechanism (186 species, 1116 reactions) has been adapted to predict the behavior of a gas from biomass pyrolysis (Hiblot, 2010). These mechanisms lead to good prediction of the gas phase behavior for a biomass gasification application.

### 2.2.2. Representation of tar for modeling

Tar is a mixture of a high number of compounds, thus its detailed modeling is very difficult. In order to simplify the modeling, model tar compounds can be selected to represent all tar species. The most common compounds used in literature (Hiblot, 2010) are: benzene ($C_6H_6$), toluene ($C_7H_8$), indene ($C_9H_8$), naphthalene ($C_{10}H_8$) and phenol ($C_6H_5OH$), which are shown in Figure 33. These compounds can be then taken into account in a chemical scheme in CHEMKIN, such as Skjoth – Rasmussen chemical scheme.

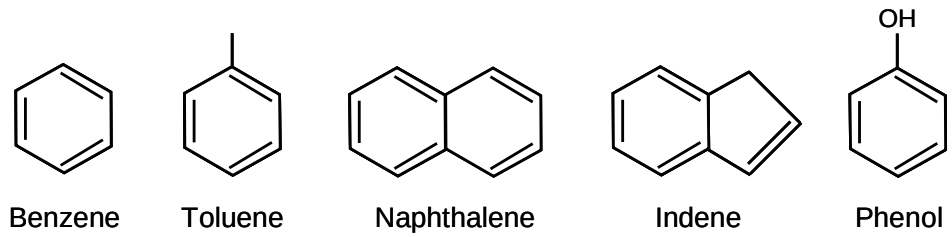


**Figure 33. Most common tar model compounds (Hiblot 2010)**

### 2.2.3. Soot formation modeling

Different approaches exist to model soot formation, from empirical to detailed models (Roth, 2006).

Among the models based on physical concepts, the simplest one assumes that soot is formed from the $C_2H_2$ decomposition through one single step reaction (Hiblot, 2010; Ziegler, 2004), which can only predict soot mass yield.

$$C_2H_2 \rightarrow 2C_{soot} + H_2 \qquad \textbf{Equation 16}$$

However, the representation of soot formation by this approach is incomplete as it does not include PAHs, while these compounds also play an important role in soot formation. Besides, it assumes that soot is only composed of carbon, which is a rough approximation as hydrogen content in typical soot is about 10 mol% (Stanmore et al., 2001).

Other authors use semi-global models which represent soot formation through multi-step reactions and enable to predict soot mass yield and particle density. In this kind of model, each of these reactions represent an elementary step during soot formation, namely particle inception and surface mass growth, which can be coupled or not to coagulation and oxidation modeling phenomena. Usually, each step is described in a simplified way and then soot is also assumed to be only carbon. An example of semi-global models is the one developed by Lindstedt (1994), derived from that of Leung & al. (1991) and including:

- particle inception by the means of $C_2H_2$;
- surface growth by the means of $C_2H_2$;
- soot oxidation with molecular $O_2$;
- particle coagulation.

This model, was shown to accurately predict soot mass yield with respect to experimental measurements but its prediction of particle density is less satisfactory (Vandsburger et al., 1984). Other models based on Lindstedt's one were developed (Fusco et al., 1994).

More detailed models about soot formation can also be found in literature, as the one developed by Roth (2006) and based on that of Frencklach (Frenklach & Wang, 1990). This one considers all the chemical and physical steps during soot formation, which are:

- soot particle inception through the collision of two pyrene molecules;
- surface mass growth by the addition of $C_2H_2$, which is represented by the chemical scheme shown in Figure 34;
- surface mass growth by the addition of PAHs - here naphthalene, acenaphtalene, phenanthrene and pyrene -, represented by the collision of PAH molecules with soot primary particles;
- particle coagulation;
- oxidation with $O_2$ and OH ●, which is competing with soot mass growth (Figure 34).

This type of model, able to predict mass yield, particle density, and even soot composition, can be applied in a wide range of combustion conditions. However, its development is long and complex, and requires the knowledge of an important number of parameters.

| Number | Reaction |
|---|---|
| R1 | $C_{Soot}$-H + H → $C_{Soot}$· + $H_2$ |
| R-1 | $C_{Soot}$· + $H_2$ → $C_{Soot}$-H + H |
| R2 | $C_{Soot}$· + H → $C_{Soot}$-H |
| R3 | $C_{Soot}$· + $C_2H_2$ → $C_{Soot}$-H + H |
| R4 | $C_{Soot}$· + $O_2$ → $C_{Soot}$ + CO + CO |
| R5 | $C_{Soot}$-H + OH → $C_{Soot}$· + CO + $H_2$ |

**Figure 34. Chemical scheme used for the soot mass growth with $C_2H_2$ and oxidation**

## 2.3. Gasification reaction modeling

It is essential that biomass gasification modeling includes the evolution of the solid phase - char and soot - during the thermochemical transformation. The formation of char and soot is described in the previous sections. In the same way, their gasification has also to be considered.

As gasification reaction involves physical and chemical phenomena (refer to section 4 of Chapter "Fundamental concepts"), its modeling should consider both aspects. In the case of char, most of the works in literature are only focused on the modeling of the chemical kinetics and the understanding of intrinsic parameters (Barrio et al., 2008; Khalil et al., 2008; Klose & Wölki, 2005). Less authors show interest in the contribution of the physical process parameters (Gómez-Barea et al., 2005; Mermoud et al., 2006a). Note that an extensive number of works about charcoal gasification modeling precedes the research about biomass char (Liu et al., 2000; Molina & Mondragón, 1998; Roberts & Harris, 2006).

Concerning soot gasification modeling with $H_2O$ and $CO_2$, only a few works can be found in literature (De Soete, 1988; Harris & Smith, 1990). At the contrary, several works in literature focus on the modeling of soot oxidation with $O_2$ (Du et al., 1991; Gilot et al., 1993; Lee et al., 1962). Two approaches for soot oxidation modeling exist: one involving $O_2$ and OH ●, put into competition with the surface mass growth by $C_2H_2$ addition (Figure 34); the other using the classical approach for heterogeneous reaction, as described below.

### 2.3.1. Chemical kinetics of gasification

The gasification reaction rate can be expressed as the variation of the char mass $m_{char}$ during a time interval $dt$ (Equation 17).

$$-\frac{dm_{char}}{dt} = k(T, P_i) \cdot S_{reactive} \cdot m_{char} \qquad \textbf{Equation 17}$$

The variable $k$ [$m^{-2}.s^{-1}$] refers to the intrinsic kinetics of the reaction, which depends on the temperature $T$ and the partial pressure $P_i$ of the gaseous compounds - $H_2O$, $CO_2$, $H_2$, CO-. The variable $S_{reactive}$ [$m^2$] refers to the reactive (microporous) surface of the solid and depends on the quantity and availability of reactive sites. As the reactive surface is very difficult to determine and changes all along the transformation, a new term was introduced: the surface function $f(X)$, which implicitly contains the reactive surface and considers the evolution of the solid morphological structure in function of the conversion $X$. The reaction rate can be then rewritten in function of the conversion (Equation 18).

$$\frac{dX}{dt} = k(T, P_i) \cdot f(X) \qquad \textbf{Equation 18}$$

With: $k$ [$s^{-1}$]

#### 2.3.1.1. Determination of the intrinsic kinetics

The simpler approach to express the intrinsic reactivity of a carbonaceous solid is an Arrhenius kinetic law of $n^{th}$ order with respect to the partial pressure of the reactive gas, $H_2O$ (Barrio et al., 2001) or $CO_2$ (DeGroot & Shafizadeh, 1984), as shown in Equation 19.

$$k(T, P_i) = k_0 \cdot e^{\frac{-Ea}{R \cdot T}} \cdot P_i^n \qquad \textbf{Equation 19}$$

When both $H_2O$ and $CO_2$ are involved in gasification reaction, alternative equations for the intrinsic reactivity have been proposed, as for example Equation 20 (Groeneveld & van Swaaij, 1980).

$$k(T, P_i) = k_0 \cdot e^{\frac{-Ea}{R \cdot T}} \cdot (P_{H_2O} \cdot P_{CO_2})^{0.7} \qquad \textbf{Equation 20}$$

As this approach gives global models which are not able to describe the complexity of the real phenomena involved, several authors have used more realistic kinetic models based on a Langmuir-Hinshelwood (LH) reaction mechanism, which comes from the fundamental theory of gas adsorption on a solid (refer to section 4.2.2 of

Chapter "Fundamental Concepts"), proposed in 1918 by the American chemist, Langmuir (1881-1957). The LH approach is based on the following assumptions:

- All surface sites are equivalent.
- Only one adsorbed atom can be accommodated on a reactive site at the same time.
- Adsorption is monolayer.
- There are no interactions between gas molecules on neighboring sites.

Here is the most usual gasification chemical scheme based on a LH mechanism in literature:

- Chemisorption + Oxygen exchange step

$$C_f + H_2O \xleftrightarrow{k_1,k_2} C(O) + H_2$$ **Equation 21**

(Steam gasification)

$$C_f + CO_2 \xleftrightarrow{k_1,k_2} C(O) + CO$$ **Equation 22**

(Boudouard reaction)

Where $C_f$ is an active site and C(O) a carbon – oxygen complex.

- Desorption

$$C(O) \xrightarrow{k_3} CO + C_f$$ **Equation 23**

- Adsorption of $H_2$

$$C_f + H_2 \xrightarrow{k_4} C(H_2)$$ **Equation 24**

$$C_f + 1/2H_2 \xrightarrow{k_5} C(H)$$ **Equation 25**

Where $C(H_2)$ and C(H) are carbon – hydrogen complexes.

This chemical scheme takes the inhibition of gasification by $H_2$ and CO into account, as the presence of these species tend to decrease the formation of C(O) complex intermediates (Equation 21 - 22). Besides, $H_2$ competes against $H_2O$ for the occupation of the active sites by the formation of C(H) and $C(H_2)$ complex, as shown in Equation 24 – 25 (Hüttinger & Merdes, 1992; Lussier et al., 1998a), which reduces the availability of reactive surface.

The LH model considers a quasi equilibrium between the adsorption and desorption phenomena. In other words, a dynamic equilibrium is established between the molecules which reach the reactive surface and the ones which leave it. After taking these considerations into account, the reaction rate of gasification can be written as Equation 26.

$$k = \frac{k_1 \cdot P_{H_2O}}{1 + (k_1 / k_3) \cdot P_{H_2O} + f(k_2, k_4, k_5) \cdot P_{H_2}}$$ **Equation 26**

(Case of steam gasification)

With $f(k_2,k_4,k_5)$ as a combination of rate constants depending on the relative influence of the two inhibition processes.

At low pressures, the inhibition of gasification by $H_2$ and CO can be neglected (Roberts & Harris, 2006), which leads to $k_2, k_4$ and $k_5 = 0$. Equation 26 can be then rewritten as Equation 27.

$$k = \frac{k_1 \cdot P_{CO_2}}{1 + (k_2 / k_3) \cdot P_{CO} + (k_1 / k_3) \cdot P_{CO_2}}$$ **Equation 27**

(Case of Boudouard reaction)

Other kinetic models of LH type assuming different gasification mechanisms can be found in literature, as for example:

- the Blackwood and McGrory mechanism, which considers the formation of methane at high pressures from the methanation reaction between $C_f$ and the $H_2$ produced during the gasification (Mühlen et al., 1985);
- a mechanism considering the competition between $CO_2$ and $H_2O$ for the same reactive sites during the gasification with both reagents (Roberts & Harris, 2007);
- a mechanism that considers that the reactive sites of $H_2O$ and $CO_2$ are different during the gasification with both reagents (Tagutchou, 2008).

#### *2.3.1.2. Determination of f(X)*

Three basic models can be applied to study the evolution of the reactive surface during heterogeneous reaction: the volume reaction model (VRM), the shrinking core model (SCM) and the random pore model (RPM).

The VRM, also named homogenous model (Molina & Mondragón, 1998), assimilates the heterogeneous reaction of gasification to a homogeneous reaction: the reaction takes place at the totality of the active sites and the structure of the particle is assumed not to change.

The surface function corresponding to this model, which decreases as gasification proceeds, is expressed as Equation 28.

$$f(X) = (1 - X)$$ **Equation 28**

The SCM assumes that the reaction initially occurs at the external surface of the particle and gradually moves inside it. As the particle size is reduced during the transformation, the reactive surface also decreases, but the particle density remains unchanged. At the intermediate conversion of solid, the char represents a shrinking core of non-reacted solid.

The surface function for this model can be visualized in Equation 29.

$$f(X) = (1 - X)^{2/3}$$ **Equation 29**

The RPM considers that gasification takes place on the inside surface of the micropores, which occupy most of the surface area of the particle. As a function of the reaction progress, the reactive surface initially increases due to the pores growth, and then it decreases by the coalescence of adjacent pores.

The surface function for this model can be expressed as Equation 30.

$$f(X) = (1 - X) \cdot \sqrt{1 - \psi \cdot \ln(1 - X)} \qquad \textbf{Equation 30}$$

Where $\Psi$ is a surface function parameter related to the pore structure of the non reacted sample ($X = 0$), which can be calculated through Equation 31.

$$\psi = \frac{4 \cdot \pi \cdot L_0 \cdot (1 - \varepsilon_0)}{S_0^{\,2}} \qquad \textbf{Equation 31}$$

With:

| | | |
|---|---|---|
| $S_0$ | Pore surface area per unit of solid volume | $m^2/m^3$ |
| $L_0$ | Pore length | m |
| $\varepsilon_0$ | Solid porosity | - |

The $\Psi$ parameter is very difficult to measure directly. Therefore, authors have employed alternative methods to determine it: through the experimental curves [$S(t)/S_f = f(X)$] (Matsumoto, 2009) or [$dX/d\,t = f(X)$] (Seo et al.) or by simple fitting with experimental profiles (Fermoso et al., 2009).

The RPM model, initially developed for charcoal gasification (Bhatia & Perlmutter, 1980), is known to be one of the more accurate model to describe gasification of biomass chars surely because the characteristic porous structure of char is taken into account into the model (Matsumoto, 2009). The SCM also gives accurate predictions (Fermoso et al., 2009). In the case of soot, only RPM surface function has been found in literature (Song, 2010).

Most of the times, the surface function is associated with intrinsic kinetics of $n^{th}$ order to calculate the reaction rate.

An extensive collection of additional surface functions, which are based on physical or empirical assumptions, is available in literature (Gøbel et al., 2008; Lussier et al., 1998b; Struis et al., 2002).

### 2.3.2. Modeling of physical phenomena

Physical phenomena during gasification consist in heat and mass transport phenomena, which are responsible for the particle heating to the reaction temperature and the mass transport of gasification reagents and products between the particle and the surroundings. The description of such phenomena has to derive from the classical equations of mass, momentum and energy conservation.

The external heat and mass transport can be modelled using the exchange coefficient which shows to be the most adapted to the surrounding conditions and particle characteristics. The internal mass transport inside the char and soot particles is modeled considering a combination of the molecular diffusion and Knudsen diffusion. The internal heat transport results from conduction and internal radiation. Besides, because of the porosity characteristic of char and soot, the flow inside the carbonaceous solid has to be described by the Darcy law from which the pressure and velocity fields inside the solid can be calculated. As in the case of pyrolysis, the complexity of the solid matrix geometry and the sensibility of the thermal conductivity to the solid local conditions can complicate the internal phenomena modeling.

Other transfer modes, like the Dufour and the Soret effects, are usually neglected in gasification modeling.

A shrinking core model, similar to that for biomass pyrolysis (refer to section 2.1.2.2), can be used to describe the gasification under a regime controlled by transfer, in which only mass transport phenomena is considered (Levenspiel, 1997).

### 2.3.3. Modeling of additional phenomena for char gasification

Literature presents some additional models considering char structure changes during gasification process, which can modify the apparent reactivity.

#### 2.3.3.1. Fracturing and peripheral fragmentation

Char structure can be damaged because of mechanical constraints appearing during gasification, leading to fracturing and peripheral fragmentation (Figure 35). Both of these phenomena are assumed to increase the concentration of reactive sites and to favor the gas diffusion (Manocha et al., 2002; Struis et al., 2002), which result in an increase of the char reactivity.

Fragmentation, which seems to appear in the range of 80 to 90% of char conversion (Bar-Ziv & Kantorovich, 2001; Feng & Bhatia, 2000) due to the structure weakness at this conversion level, is modelled through a "critical porosity" (Marbán & Fuertes, 1997; Wang & Bhatia, 2001), beyond which this phenomenon can occur. However, this phenomenon can only occur under a regime controlled by internal transfers, because in a kinetically controlled regime the whole char structure suddenly collapses at high conversion level.

Fracturing has not been modelled for the moment because of its unpredictable character. In fact, its modeling would require the knowledge of the local geometry of char structure and its evolution during gasification, which is extremely difficult to measure.

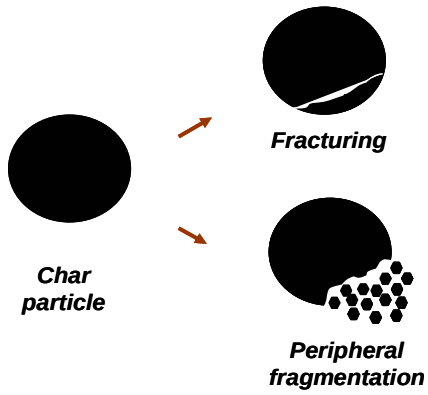


**Figure 35. Representation of fracturing and fragmentation of a char particle**

#### 2.3.3.2. Thermal deactivation

High temperatures can induce the thermal annealing of a carbonaceous solid structure (refer to section 1.2.3). Through this phenomenon, the reactivity of the active sites and the reactive surface are both decreased, leading to a lower apparent reactivity of the solid. An important number of works exist in literature about the modeling of the intrinsic reactivity decrease by thermal annealing. Most of these works were performed for coal combustion application.

The most common approach so far for thermal annealing modeling has been the use of an annealing factor (Hurt et al., 1998; Liu & Niksa, 2004; Niksa et al., 2003). The oxidation reaction rate of the annealed char is then equal to the product of the reaction rate of the non annealed char by the annealing factor. This approach lies on two main assumptions:

- Thermal annealing occurs with the same intensity for all the elementary steps of oxidation - chemisorption, oxygen exchange step, desorption-. For the moment, this assumption has not been proved: the oxygen adsorption has been verified to be affected by thermal annealing (Senneca et al., 2007) but no influence could be observed on the other oxidation steps.
- Thermal annealing is much faster than oxidation, thus a single value of the thermal deactivation factor can express the loss of char reactivity along the oxidation process. This assumption can be verified in some devices, as in reactors where the char is exposed to a flame during a very short residence time, but is more difficult to prove in other cases, as in a fluidized bed reactor.

Another approach consists in a simple model of thermal annealing kinetics assuming that the evolution of annealing could be quantified by the progress of an internal reaction which describes the transformation of active sites into deactivated ones (Salatino et al., 1999):

$$C_f \xrightarrow{r_{deact}} C_{f,deact} \qquad \textbf{Equation 32}$$

Where $C_f$ and $C_{f,deact}$ represent the active sites and the deactivated sites respectively.

For instance, Senneca & Salatino (2011) suggest the following expression for the deactivation reaction rate $r_{deac}$:

$$r_{deact} = k_{deact} \cdot (1-\xi)^n \cdot [C_f] \qquad \textbf{Equation 33}$$

With: $\xi$ referring to an annealing coordinate or coefficient, equal to 0 for the young char and 1 for the fully annealed char.

The deactivation reaction is usually introduced into a chemical scheme of oxidation including both annealed and non annealed carbon (Blyholder et al., 1958; Senneca & Salatino, 2011).

The distribution of activation energy (DAE) is a more complicated approach also used for thermal deactivation modeling (Hurt & Calo, 2001; Russell et al., 1999; Zolin et al., 2000). This type of model describes annealing with several first order reactions occurring in parallel. The number of deactivated sites can be obtained from the calculation of the energy distribution.

Finally, other different approaches for modeling the kinetics of thermal annealing were proposed by Feng & al. (2002):

- A superposition model, which correlates the evolution of physical properties of the carbonaceous solid with the thermal annealing degree, as for instance the electric resistivity which decreases with the progress of annealing.
- A diffusion model, which assumes that the graphitization reaction rate is controlled by the diffusion kinetics of the iron atoms into the char matrix, based on the experimental observation that iron catalyzes the formation of graphite layers. This model shows accurate predictions for the annealing of charcoal with high iron content.

A more detailed review of annealing models is given by Senneca & Salatino (2011).

## 2.4. Other modeling approaches

Some authors use empirical correlations to predict the pyrolysis products yields or the conversion time in function of operating temperature (Gonzalez Saiz, 1988; Singh et al., 1986), biomass properties (Passé-Coutrin et al., 2005), particle characteristics (De Diego et al., 2002)… In addition to their simplicity, empirical correlations can emphasize the effects of one or several parameters during pyrolysis. However, they are not based on physics fundaments and their use is limited to the experimental conditions in which they have been obtained.

Another type of modeling is based on the calculation of the thermodynamic equilibrium by the minimization of the Gibbs energy by considering the system as closed. This simple model only requires a few information, which are: the amounts of C, H and O in the system, the temperature, and the pressure. Indeed, it does not depend on a reaction mechanism or a reactor configuration, although it is based on physical fundaments. This model is coupled to thermodynamic tables containing the formation enthalpy of an important variety of gaseous products and graphite. However, this approach can only be used under conditions where the thermodynamic equilibrium can be reached, namely high temperatures.

More information about empirical and thermodynamic models are provided by Dupont (2006).

## 2.5. Summary

Modeling of biomass gasification process at the particle scale has to take into account the coupling between the physical and chemical phenomena involved.

A great number of chemical reactions participate in the thermochemical process: devolatilization (pyrolysis), gas – gas reactions, gas – solid reactions (gasification). Each transformation can be modelled by a single reaction or by series of reactions included in a chemical mechanism. The reaction rate can be then calculated from the chemical kinetics of the considered reactions. In the case of heterogeneous reactions, another important parameter has to be considered: the reactive surface, which is represented by a function varying with the conversion. This surface function takes into account the morphological changes of char and soot during the gasification reaction.

During the biomass gasification process, several physical phenomena occur in parallel with chemical phenomena: gas and particle heating, gaseous molecules transport in the atmosphere and inside the particle. The occurrence of these physical phenomena depends on mass, heat and momentum transfers between the particle, the gas and the heating source. The physical exchange between the particle surface and the atmosphere does not present any particular challenge for modeling: it can be determined by well known equations which can be easily found in literature. However, the intraparticle phenomena are much more delicate to model, because their description refers to a very complex science, the physics of porous media. In order to limit the complexity of physical phenomena modeling, some simplifying models have been proposed in literature, as the shrinking core model.

Additional phenomena occurring during biomass gasification can be added to the modeling: moisture evaporation, fragmentation and fracturing, thermal annealing of carbonaceous solid structure…

The important number of phenomena involved and the complexity of their coupling make biomass gasification very difficult to model. Very detailed models are usually hard to develop and their calculation time can be very consuming. Therefore, simplifications are recommended. However, a simplification has always to be performed with caution and has to be preferably justified, in order to avoid a lost in accuracy for the model. For this cause, a characteristic time analysis can be useful.

# 3. Characteristic time analysis

## 3.1. Principle of the approach

The characteristic time of a phenomenon is the theoretical time needed for the process to occur entirely when this is only controlled by the involved phenomenon. In the case of gasification and pyrolysis, the more usual phenomena considered in characteristic time analysis are:

- External convection or conduction, radiation and internal conduction at particle heating stage;
- External mass transfer by convection or diffusion and internal diffusion of reagents into the particle;
- Chemical reactions of devolatilization and gasification.

The use of characteristic time analysis can be of great interest in the case of pyrolysis and carbonaceous solid gasification. This approach has already been used by different authors for a thermochemical application (Van de Steene, 1999; Villermaux & Antoine, 1980).

The comparison between the characteristic times enables to determine the limiting phenomena of the process. The limiting phenomena are characterized by a much higher characteristic time than the other phenomena.

The analysis can be performed by direct comparison of the different characteristic times or by the intermediary of their ratio, to which some dimensionless numbers have been associated (Damköhler, 1936). This last procedure is practical to put the limiting phenomena into evidence, but it hides the time scale of the phenomena. Therefore, both approaches are complementary.

Table 5 provides the main dimensionless numbers related to biomass gasification.

**Table 5. Main dimensionless numbers related to biomass gasification**

| | |
|---|---|
| Number of thermic Biot $Bi_T$ | $t_{cond}/t_{conv}$ |
| Number of Damkohler Da | $t_{pyro}/t_{conv}$ |
| Number of pyrolysis Py | $t_{pyro}/t_{cond}$ |
| Ratio between external radiation and convection | $t_{rad}/t_{conv}$ |
| Number of mass Biot $Bi_M$ | $t_{mass\ int}/t_{mass\ ext}$ |
| Ratio between gasification and external mass transfer | $t_{gas}/t_{mass\ ext}$ |
| Ratio between gasification and internal mass transfer | $t_{gas}/t_{mass\ int}$ |
| Ratio between gasification and pyrolysis | $t_{gas}/t_{pyro}$ |

With:

| | | |
|---|---|---|
| $t_{cond}$ | Characteristic time of internal heat conduction | s |
| $t_{conv}$ | Characteristic time of external heat convection | s |
| $t_{rad}$ | Characteristic time of external radiation | s |
| $t_{pyro}$ | Characteristic time of pyrolysis | s |
| $t_{mass\ int}$ | Characteristic time of internal mass transfer | s |
| $t_{mass\ ext}$ | Characteristic time of external mass transfer | s |
| $t_{gas}$ | Characteristic time of gasification | s |

In function of the values of the dimensionless numbers, the regime in which the transformation takes place can be determined (refer to section 2.3 and 4.3. of Chapter "Fundamental Concepts"), as figured in Table 6. Note that this analytical procedure, coming from the Chemical Engineering domain, has been adapted into the thermochemical domain. For example, the number of pyrolysis *Py*, non existent term in the Chemical Engineering glossary, is the inverse number of Thiele thermal modulus.

A more detailed description about characteristic time analysis has been performed by Dupont (2006).

**Table 6. Different regimes of pyrolysis and gasification**

| $Bi_T << 1$<br>$Bi_M << 1$ | | $Bi_T >> 1$<br>$Bi_M >> 1$ | |
|---|---|---|---|
| $Da << 1$<br>$t_{gas}/t_{mass\ ext} << 1$ | $Da >> 1$<br>$t_{gas}/t_{mass\ ext} >> 1$ | $Py >> 1$<br>$t_{gas}/t_{mass\ int} >> 1$ | $Py << 1$<br>$t_{gas}/t_{mass\ ext} << 1$ |
| Regime limited by external transfer | Pure kinetic regime | | Regime limited by internal transfer |

## 3.2. Results obtained in literature from characteristic time analysis

### *3.2.1. Pyrolysis characteristic time analysis*

According to several characteristic time analyses found in literature (Dupont, 2006; Koufopanos et al., 1989; Miller & Bellan, 1997; Simmons & Gentry, 1986), the critical particle size under which pyrolysis is in pure kinetic regime, is between 100 µm and 1000 µm for a pyrolysis temperature between 500°C and 1000°C. This critical particle size seems to decrease as temperature increases. This tendency is illustrated in Figure 36, which displays the pyrolysis regimes under fluidized bed conditions (Dupont, 2006).

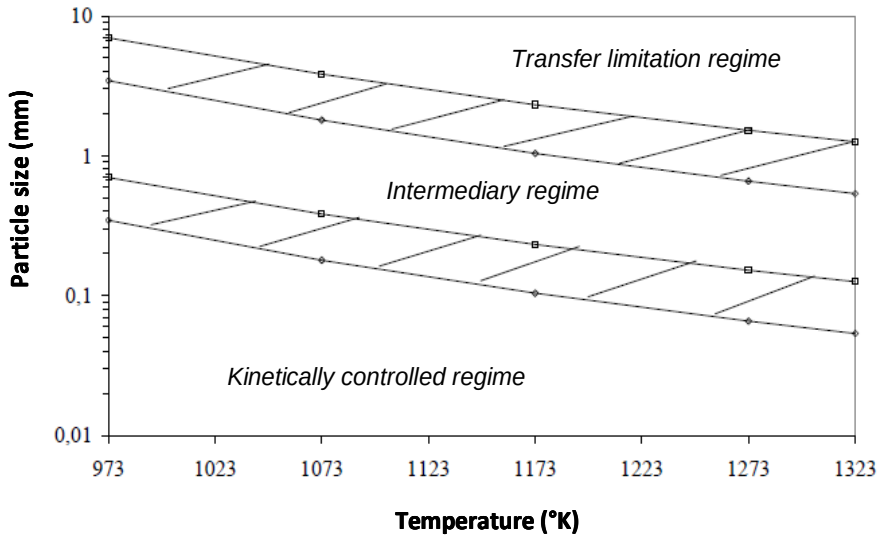


**Figure 36. Pyrolysis regimes in function of temperature and particle size (Dupont, 2006) – note: the hatched zones correspond to the uncertainty of the characteristic time calculations**

### *3.2.2. Gasification characteristic time analysis*

Van de Steene (1999) performed a characteristic time analysis of several phenomena concerning coal combustion at 900°C. He concluded that the oxidation is controlled by chemical kinetics for particles with a size lower than 100 µm and by mass transfers for particles with a size higher than 1 mm.

No characteristic time analysis applied to gasification of char from biomass was found in literature.

### 3.3. Summary

A characteristic time analysis enables to identify the preponderant phenomena and to estimate the order of magnitude of the conversion time. By consequence, it can be used as a simplification tool for modeling and for the analysis of experimental results. Note that as this approach is very approximate, only the order of magnitude can be taken into consideration.

## 4. Conclusion and thesis focus

By an experimental literature review, the interest to operate during gasification at high temperature (>1000°C) and high heating rates has been highlighted: low amounts of tar are measured, the conversion of light hydrocarbons and char is high, and the yields of $H_2$ and CO are elevated. These results are obtained even for a residence time of a few seconds. However, literature has also revealed some possible undesirable phenomena: the formation of soot; the char deactivation, which could reduce the char gasification rate, and the incomplete conversion for almost millimetric biomass particles. These problems could lead to a lower biomass conversion into syngas than expected. Literature does not give clear answers about these points in the context of interest: the studies on soot formation and gasification, and on the gasification kinetics of biomass char from rapid pyrolysis are very rare. The char deactivation has been studied mostly for coal combustion. Moreover, most studies about the influence of particle size have been performed at temperatures below 1000°C. Besides, the researches about biomass gasification under the conditions of an EFR are not enough explored, unlike coal gasification.

The objective of this thesis is to bring a better comprehension of biomass gasification at high temperature for an EFR application.

For this purpose, experiments will be performed in a DTR, the more representative device of an EFR at the lab scale, under several temperatures and atmosphere compositions, and for several particle sizes and residence times. The products yields, gaseous phase composition and solid residue characteristic will be determined.

The comprehension of biomass gasification at high temperatures and high heating rates will also lead to improve an existing model to simulate gasification experiments. This model takes into consideration the physicochemical phenomena occurring during devolatilisation, carbonaceous solid gasification and the gas phase reactions. Such a model has not been yet reported in literature in the case of biomass, but precious data about the modeling of each of the gasification aspects taken individually is provided. In order to avoid complex models which become very difficult to develop, the preponderant phenomena have to be distinguished from the negligible one.

# Résumé du Chapitre 2 : Etat de l'art

Parmi les différents dispositifs de laboratoire décrits dans la littérature, le four à chute semble être le réacteur analytique le mieux approprié pour étudier la gazéification de la biomasse dans les conditions proches de celles d'un réacteur à flux entraîné (RFE). Ce dispositif expérimental peut fonctionner en mode continu à des températures et vitesses de chauffage élevées, d'une manière similaire au RFE. Dans un four à chute comme dans un RFE, le temps de séjour des particules étant largement supérieur à la durée de la pyrolyse, les réactions secondaires ont suffisamment de temps pour s'y dérouler également. D'autres réacteurs analytiques peuvent être utiles et complémentaires au four à chute, comme la thermobalance pour caractériser la réactivité du carbone solide ou le réacteur tubulaire pour étudier les réactions en phase gazeuse.

La plupart des travaux expérimentaux en four à chute se focalisent sur la gazéification du charbon ou sur la pyrolyse de la biomasse dans une plage de température de 700°C à 950°C. Dans ce cas, seuls quelques travaux ont été menés au-delà de 1000°C. En effet, le four à chute a été principalement utilisé pour la recherche sur la gazéification de la biomasse dans un réacteur à lit fluidisé, qui fonctionne dans une gamme de température comprise entre 800°C et 950°C.

Les quelques travaux sur la décomposition thermique de la biomasse au-delà de 1000°C montrent que le rendement en gaz de synthèse ($H_2$ et CO) augmente avec la température, alors que les rendements en hydrocarbures et char diminuent, et que des suies sont formées. L'ajout de vapeur d'eau dans l'atmosphère au-dessus de 1000°C réduit les rendements en suie, en char et en hydrocarbures. En contrepartie, une température élevée peut également induire la graphitisation de la structure solide du char, ce qui conduit à une diminution de sa réactivité.

Très peu de travaux s'intéressent à l'influence de la taille de particules sur la gazéification du bois au-delà de 1000°C.

La modélisation des phénomènes liés à la gazéification de la biomasse débute à l'échelle des particules et doit prendre en compte le couplage entre les phénomènes physiques et chimiques impliqués.

Un grand nombre de réactions chimiques participent à la transformation: dévolatilisation (pyrolyse), réactions gaz - gaz, réactions gaz – solide (gazéification). Chaque transformation peut être modélisée par une réaction unique ou par une série de réactions incluses dans un schéma cinétique. Les vitesses de réaction peuvent alors être calculées à partir des paramètres cinétiques des réactions considérées. Dans le cas des réactions hétérogènes, un autre paramètre important est à considérer: la surface réactive, qui est représentée par une fonction variant avec le taux de conversion. Cette fonction de surface prend en compte les changements morphologiques du résidu carboné lors de la réaction de gazéification.

Pendant le processus de gazéification de la biomasse, plusieurs phénomènes physiques se produisent en parallèle aux phénomènes chimiques: le chauffage des particules et du gaz, le transport des molécules gazeuses dans l'atmosphère et à l'intérieur de la particule. Ces phénomènes physiques dépendent donc des transferts de masse, de chaleur et de mouvement entre la particule, le gaz et la source de chauffage. Les échanges de chaleur ou de masse entre la surface des particules et l'atmosphère ne présentent pas de défi particulier pour la modélisation: ils peuvent être déterminés par des équations classiques. Toutefois, les phénomènes intraparticulaires sont beaucoup plus délicats à modéliser, parce que leur description se réfère à une science très complexe, la physique des milieux poreux.

D'autres phénomènes survenant pendant la gazéification de la biomasse peuvent être ajoutés à la modélisation: évaporation de l'humidité, fragmentation et fracturation, désactivation thermique...

Le nombre important de phénomènes impliqués et la complexité de leur couplage rendent difficiles la modélisation de la gazéification de biomasse dans son ensemble. Des modèles très détaillés sont généralement difficiles à développer et leur temps de calcul peut être conséquent. Ainsi donc, des simplifications sont

souhaitables, comme par exemple le modèle à cœur rétrécissant qui permet de limiter la complexité de la modélisation des phénomènes physiques. Toutefois, une simplification doit toujours être effectuée avec prudence et doit se baser sur des fondements réels autant que possible afin d'éviter une perte de signification physique pour le modèle.

L'analyse des temps caractéristiques permet ainsi d'identifier les phénomènes prépondérants et d'estimer l'ordre de grandeur du temps de conversion associé. Par conséquent, elle peut être utilisée comme un outil de simplification pour la modélisation, et d'analyse des résultats expérimentaux. Cette approche étant approximative, seul l'ordre de grandeur des résultats doit être pris en considération.

# Chapter 3: Materials and Methods

## 1. Experimental setup

This Chapter describes the experimental setup used for the study of biomass gasification under the conditions of an entrained flow reactor, namely high heating rates ($10^5$ - $10^6$ W.m$^2$), high temperatures (> 1000°C) and short residence time (< 5 s) for particle sizes of several hundreds of micrometers.

### 1.1. Raw material

The feedstock selected for the experiments is commercial beech sawdust (Figure 37), provided by the firm SPPS (*www.sppsfrance.com*) and mainly used for food smoking. Beech wood, one of the most available resources in France, is a potential feedstock for future gasification industrial units.


**Figure 37. Beech sawdust**

After sieving, two ranges of particle sizes were selected for the experiments: 0.313 - 0.400 mm and 0.710 - 0.900 mm (Table 7). The difference of particle sizes between the two samples was verified through optical measurements, which gave an equivalent diameter of the particles by assimilating them to spherical particles. This experimental analysis was conducted with "Mastersizer", an instrument which is provided by the Malvern Instruments firm (*www.malverninstruments.fr*).

**Table 7. Sample size distribution**

| Sample Name | Particle size (mm) by a sieve classification | Equivalent diameter (mm) measured by "Mastersizer" |
|---|---|---|
| 0.35 mm | 0.313 - 0.400 | 0.277 – 0.592<br>average = 0.423 |
| 0.80 mm | 0.710 - 0.900 | 0.545 – 1.195<br>average = 0.953 |

Note the difference between the particle sizes determined by sieve classification and optical measurement in Table 7. This deviation can be attributed to the shape of the particles. In reality, the wood particles are not spherical but rather cubic or flake-like, as shown in Figure 38. Particles with a flake-like shape can pass through sieve orifices smaller than their equivalent diameter if they are positioned in a perpendicular orientation. So, a particle size range determined by sieving can contain larger particles than expected.

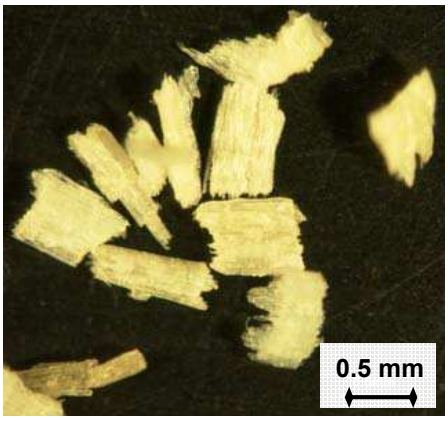


**Figure 38. Microscopic view of wood particles from the 0.35 mm sample**

The proximate analysis - ash, moisture, volatile matter and fixed carbon -, and the ultimate analysis - C, H, O, N, S - of the two samples are shown in Table 8.

The measurements of moisture and volatile matter were performed following the French Standards: NF-M-03-002 (AFNOR 1995), NF-M-03-003 (AFNOR 1994), NF-M-03-004 (AFNOR 2003). The ash content was measured at 550°C following the standard CEN/TS 14775. The fixed carbon content was determined by difference (% fixed carbon = 100 - % ash - % volatile matter - % moisture).

The C and H contents were determined from an ultimate analysis following the standard CEN/TS 15104, performed by the laboratory SOCOR (*www.socor-sp.com*). The O content was deduced by difference (% O = 1 - % H - % C - % ash).

Chemical composition of both samples is quite the same.

**Table 8. Biomass composition**

| Sample Name | C | H | N | S | O * | Volatile matter | Fixed carbon* | Ash | Moisture |
|---|---|---|---|---|---|---|---|---|---|
| | %mass, dry | | | | | %mass, dry | | | % mass |
| 0.35 mm | 50.8 | 5.9 | 0.3 | 0.02 | 42.8 | 85.3 | 14.3 | 0.4 | 7 |
| 0.80 mm | 50.4 | 5.9 | 0.3 | 0.02 | 43.3 | 85.3 | 14.3 | 0.4 | 7 |

* by difference

Ash composition, which was determined by SOCOR following the standard CEN/TS 15290, is presented in Table 9. Note that the sum of the measured inorganic contents in ash does not reach 100% but approximately 80%, maybe because of the presence of inorganic carbon. Again chemical composition of ash from both samples is quite the same.

**Table 9. Composition of biomass ash obtained at 550°C**

| Sample name | Ash composition (%mass, dry) | | | | | | | | | | | Total |
|---|---|---|---|---|---|---|---|---|---|---|---|---|
| | Si | Al | Fe | Ti | Ca | Mg | K | Na | S | P | Mn | |
| 0.35 mm | 9.4 | 2.1 | 1.3 | 0.1 | 27.7 | 9.0 | 17.7 | 0.8 | 2.9 | 2.7 | 5.3 | 79.0 % |
| 0.80 mm | 9.3 | 2.4 | 1.2 | 0.2 | 27.5 | 8.7 | 16.2 | 0.8 | 5.5 | 2.6 | 5.3 | 79.7 % |

## 1.2. Drop tube reactor facility

The experimental facility is located in a research center (RAPSODEE), in Albi, a southwestern city of France. The laboratory owns two similar drop tube reactors (DTRs), whose main difference is the operating temperature. The DTR on the left of Figure 39 operates at a maximum temperature of 1050°C, whereas the other one on the right of Figure 39 can operate at higher temperature, up to 1600°C. The first cited reactor was used for previous biomass gasification research works in our laboratory, focused on fluidized bed reactor application (Chen, 2009; Dupont, 2006). For the present study, the second reactor was operated.


**Figure 39. Experimental facilities at EMAC**

### *1.2.1. Description of the drop tube reactor*

The drop tube reactor, depicted in Figure 40, consists in an alumina tube inserted in a vertical electrical heater with three independent heating zones. A thermocouple measuring the wall temperature of the alumina tube is placed in each of the heating zones and is used for temperature regulation. The dimensions of the tube are 2.3 m in length and 0.075 m in internal diameter. The heated zone is 1.2 m long. This DTR works at atmospheric pressure and can reach a maximum temperature of 1600°C.

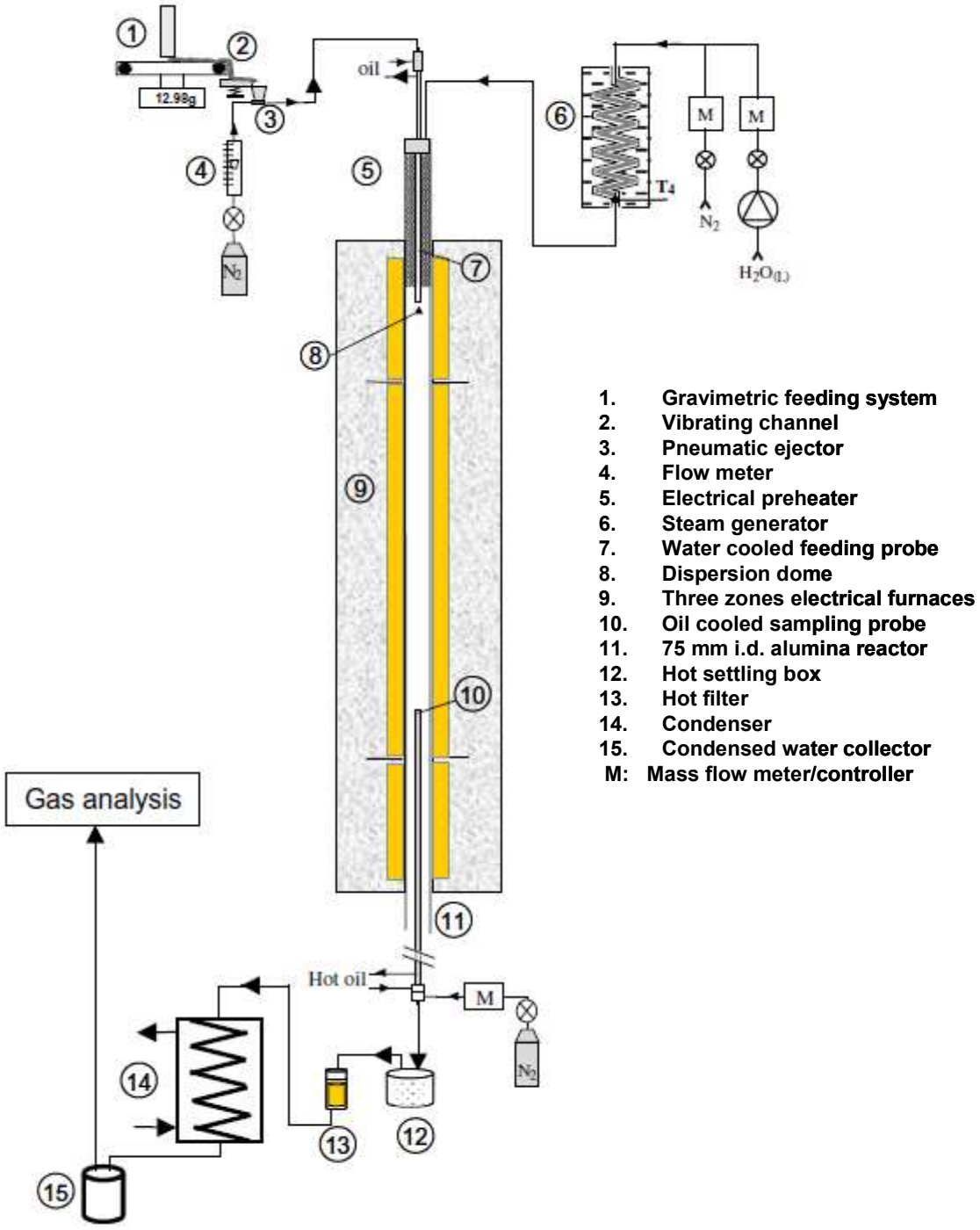


**Figure 40. Scheme of the drop tube reactor (DTR)**

The wood particles are continuously fed into the reactor using a gravimetric feeding system, which consists in a feedstock hopper on a conveyor belt. The overall is placed on a balance and is connected to a computer, which controls the conveyor belt velocity from the online mass loss measured by the balance so as to follow the set point of the feeding flow rate. The feedstock, initially introduced in the hopper, is entrained by the conveyor belt to a vibrating channel from which the particles pass into a Venturi box and are then injected into the reactor with a 2 $NL.min^{-1}$ transport nitrogen stream through a water-cooled feeding probe at 30°C.

A dispersion dome is placed at the outlet of the feeding probe to distribute the solid particles over the reactor cross section. The main gas stream, which can be $N_2$ or a mixture of $N_2$ and $H_2O$, passes through an electrical pre-heater where it attains a temperature of 900°C and then meets the mixture of cold wood particles and transport stream at the dispersion dome. Note that the outlet of the injection probe is about 15 cm above the electrical furnace, in order to protect it from the high heating flux which could damage it. For the introduction of $H_2O$ into the DTR, a steam generator working at 180°C is linked to the reactor inlet.

An oil-cooled sampling probe at 100°C can be inserted at different heights in the reactor to collect gas and the remaining solid. A fraction of the exhaust gas is then sucked in the sampling probe and passes successively through a settling box and a filter. This part of the experimental facility is heated to avoid steam and tar condensation. After the filter, the sampled gas passes through several analyzers (Table 10). If steam is introduced into the reactor, a condenser has to be placed between the filter and the analyzers.

**Table 10. Gas analyzers used during experiments**

| Analyzer | $H_2$ | CO | $CO_2$ | $H_2O$ | $CH_4$ | $C_2H_4$ | $C_2H_2$ | $C_2H_6$ | $C_3H_8$ | $C_6H_6$ | THC* | $O_2$ |
|---|---|---|---|---|---|---|---|---|---|---|---|---|
| µ-GC[1] | X | X | X | | X | X | X | X | X | X | | |
| FTIR[2] | | X | X | | X | X | X | X | X | X | | |
| TCD[3] | X | | | | | | | | | | | |
| FID[4] | | | | | X | | | | | | X | |
| NDIR[5] | | X | X | | | | | | | | | |
| Psychrometer | | | | X | | | | | | | | |
| Paramagnetic analyzer | | | | | | | | | | | | X |

[1] *Micro-Gas Chromatograph*
[2] *Fourier Transformed InfraRed spectrometer*
[3] *Thermal Conductivity Detector*
[4] *Flame Ionization Detector*
[5] *Non-Dispersive InfraRed spectrometer*
* *Total Hydrocarbon*

Each main gaseous compound was measured twice with different analyzers, apart from steam and $O_2$, as presented in Table 10. The relative differences between the measurements of two analyzers ranged between 5% and 20% for the major compounds. In general, the µ-GC concentration values showed to be more reliable and less fluctuant than the other analyzers ones. So, these ones were considered for each individual gaseous species in the experimental analysis, except for $C_2$ hydrocarbons for which this analyzer had some detection problems and presented high deviations during the measurement of low concentrations. For these compounds, the FTIR values were considered more accurate.

Note that the $O_2$ concentration was also measured in order to check the absence of this oxidant in the atmosphere during the experiments, which could lead to undesirable phenomena.

### *1.2.2. Operating conditions*

Experiments were performed under an inert atmosphere composed of $N_2$ or a steam containing atmosphere with 25 mol% of $H_2O$ and 75 mol% of $N_2$. For both cases, experiments were conducted at several temperatures - 1000°C, 1200°C and 1400°C -, and with the two particle sizes (Table 7). Experiments at 800°C were also performed for a particle size of 0.35 mm under an inert atmosphere.

The total introduced gas flow rates were 18.8 $NL.min^{-1}$, 15.9 $NL.min^{-1}$, 13.8 $NL.min^{-1}$ and 12.1 $NL.min^{-1}$ for experiments at 800°C, 1000°C, 1200°C and 1400°C respectively, in order to keep a constant gas velocity and thus a

constant gas residence time as temperature was changed. The DTR is considered to operate under diluted condition: the released gas from the biomass thermal decomposition did not considerably change the total gas flow rate.

Biomass feeding rate varied between 0.3 g/min and 1.3 g/min. In general, it was adjusted in order to keep the same gas/biomass mass ratio. No influence of the feeding rate was observed during preliminary experiments (Septien, 2009). In the case of a steam containing atmosphere, steam is in a large stoechiometric excess, about 30 to 35 times higher than the minimum quantity needed for the gasification of all the carbon introduced into the reactor.

About 4/5$^{th}$ of the gas flow was sampled at two different heights in the DTR: at the bottom and in some cases at the middle of the heated zone. At 1400°C, no experiments could be performed with sampling at the middle of the heated zone, because the sampling probe material was not able to resist to such a high temperature.

The gas and particle residence times are shown in Table 11. The particle residence time was calculated taking into account the particle slip velocity varying along the reactor. To represent this variation, a shrinking core model developed by Chen (2009) was used, which takes into account changes in the particle outside diameter and density along the pyrolysis. This model, suitable for the pyrolysis modeling at high HR (refer to section 2.1.2.2. of Chapter "State of the Art"), was experimentally validated at 800°C and 950°C in a DTR. The results thus have to be taken with caution for higher temperatures. Besides, as self-gasification of char with pyrolytic $H_2O$ and $CO_2$ becomes possible above 1000°C for a residence time of a few seconds, the density and size of the carbonaceous solid could be modified, leading to a decrease of the slip velocity. The residence time in Table 11 could be then overestimated.

The whole results obtained from the shrinking core model can be observed in Appendix D.

**Table 11. Gas and particle residence time for experiments in the DTR**

| T (°C) | Sampling height from the DTR bottom (m) | Gas flow rate (Nl.min$^{-1}$) | Residence time (s) | | |
|---|---|---|---|---|---|
| | | | Gas | Char from 0.35 mm particle | Char from 0.80 mm particle |
| 1000 | 0 | 15.9 | 4.4 | 3.8 | 2.6 |
| | 0.6 | | 2.2 | 1.9 | 1.3 |
| 1200 | 0 | 13.8 | 4.4 | 3.8 | 2.7 |
| | 0.6 | | 2.2 | 1.9 | 1.3 |
| 1400 | 0 | 12.1 | 4.4 | 3.8 | 2.7 |

The gas and char from the 0.35 mm wood particles have close residence times (Table 11). This is not the case for the char from the 0.80 mm particles. Note that there is no considerable effect of temperature on the char residence time in these conditions.

### *1.2.3. Validation of the experimental conditions in the DTR*

#### *1.2.3.1. Temperature field*

A thermohydraulic simulation of the DTR by the FLUENT software (*www.ansys.com*) was performed in order to characterize the temperature field in the reactor for our experimental conditions (Luis et al., 2011). This simulation was based on the following assumptions:

- The gas flow in the DTR is laminar, which has been verified with the calculation of a Re number of about 100.
- Gas is a non participative medium with respect to radiation.
- The wall temperature of each heated zone is fixed to the set point temperature.

- The temperature of the walls located above the injection probe outlet, corresponding to the pre-heating gas zone, is set to 900°C.
- The walls of the dispersion dome and the external walls of the injection probe outlet are heated by radiative flux, as radiation exchange between faces is considered.
- All the walls are considered as adiabatic ($Q_{conduction} = 0$), apart of the dispersion dome which can be heated from the inside by conduction.
- The simulation was carried out only in the case of experiments under an inert atmosphere, because the contribution of steam radiation is very difficult to take into account in the simulation.

The simulation results of the temperature field in a cross section of the DTR, from the particle injection zone (left of the figure) to the reactor bottom (right of the figure), are presented in Figure 41 for 1000°C, 1200°C and 1400°C.

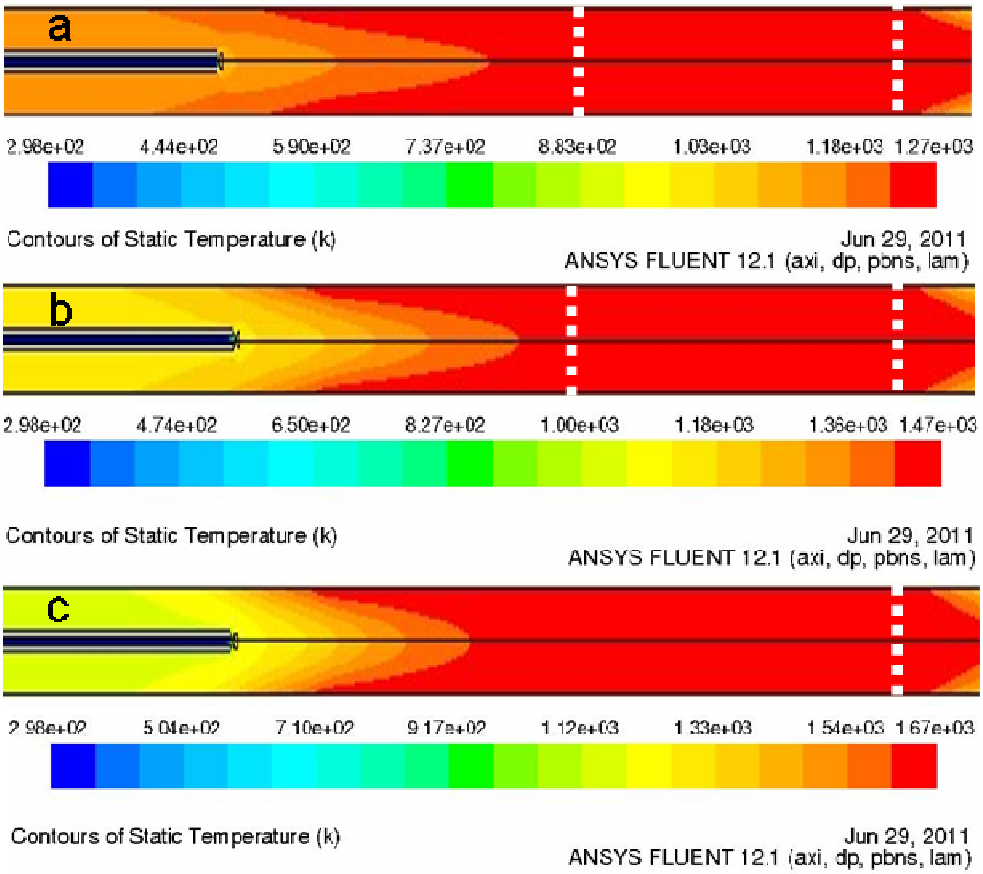


**Figure 41. Simulation of temperature field in the DTR for the experiments at 1000°C (a), 1200°C (b) and 1400°C (c). Note: the sampling heights are represented by white dotted lines**

The results of the thermohydraulic simulation show a temperature gradient from the inlet of the reactor to approximately the middle of the reaction zone, from which the temperature set point is reached. Within the gradient area, the temperature varies from 700°C to 1000°C for the experiments at 1000°C, from 850°C to 1200°C for the experiments at 1200°C and from 950°C to 1400°C for the experiments at 1400°C. Therefore, the wood decomposition can start at a lower temperature than expected. This is one limitation of the DTR during experiments. In the case of a steam containing atmosphere, the temperature set point should be reached more quickly than under an inert atmosphere, as steam can also be heated by radiation, unlike $N_2$.

### 1.2.3.2. *Steady-state regime in the DTR*

Another assumption that has to be verified is the steady state regime during the experiments. Figure 42 shows that the mass loss of the beech sawdust in the feeding system (described in section 1.2.1.) varies linearly with time during a typical experiment. This means the feedstock is introduced in the reactor at a constant rate. This feeding system gives very accurate results, with a relative deviation between the measured feeding rate and the feeding rate set point inferior to 3%.

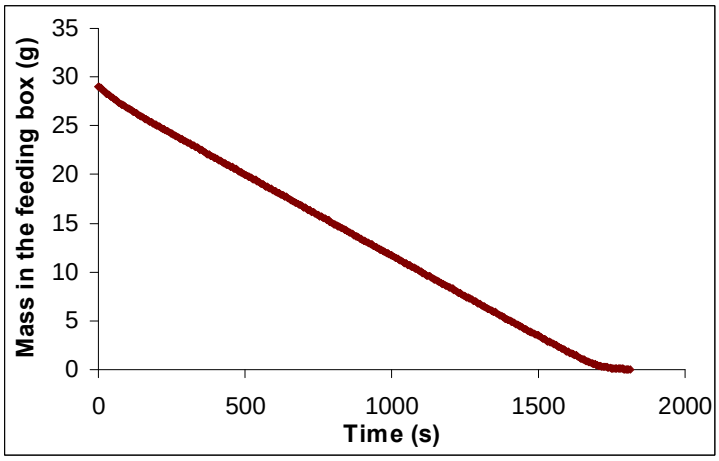


**Figure 42. Mass evolution of the beech sawdust in the feeding system**

Through the online measurement of the gas concentrations which is possible with some of the analyzers - FID, TCD, NDIR, Psychrometer -, it was observed that the steady state regime is reached during the experiments in the DTR a few minutes after the experiment beginning. This behavior is illustrated in Figure 43 by a typical online measurement of $H_2$ and $CO_2$ concentrations respectively obtained by TCD and NDIR.

The gas concentration measurements with µ-GC and FTIR used for experimental analysis were started after having reached the steady state regime.

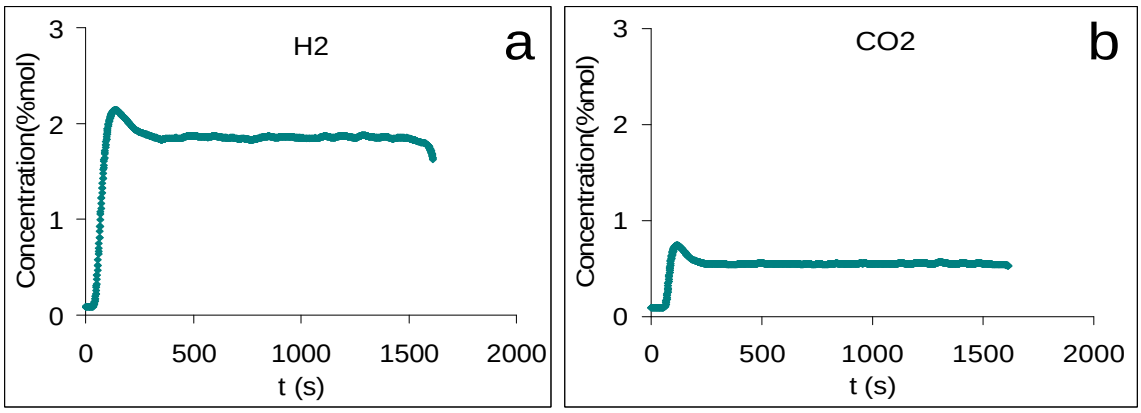


**Figure 43. Measurement of the gas concentration of $CO_2$ by NDIR (a) and $H_2$ by TCD (b)**

## 1.3. Solid residue characterization

Solid was collected after each experiment in the sampling probe, the settling box and the filter.

Through preliminary experiments, it was observed that solid in the sampling probe is a mixture of char and soot, whereas solid in the settling box and in the filter is respectively char and soot. This solid repartition in the experimental installation may be explained by the particle history in the sampling line. When passing through the sampling probe, some soot sticks on the wall of the probe and forms a growing film which can retain part of the char. In the settling box, char is separated from the gas by gravity whereas soot continues to be entrained by the gas stream until the filter, due to its very small size. This type of particle segregation was also observed by other authors (Zhang et al., 2006) during DTR experiments similar to the one of the present study.

Three types of analyses were conducted on the char and soot that were collected:

- composition analysis;
- observation of the structure by Scanning Electron Microscopy;
- reactivity measurement.

Note that not enough amounts of soot could be collected at 1000°C for its characterization.

### *1.3.1. Composition analysis*

A composition analysis was performed in order to measure the elemental composition in C, H, O and ash of the sampled char and soot. The same procedure used for the elemental composition measurement of the beech sawdust (refer to section 1.1) was followed.

### *1.3.2. Observations by scanning electron microscopy*

The structure of selected solid samples was observed by Scanning Electron Microscopy (SEM), which was coupled to X-Ray Diffraction (XRD) technique to analyze the elemental composition of a selected area with a 4 to 5 µm width penetration in the solid particle. Note that H is an invisible element for the XRD analysis. The maximum zoom that the SEM could reach with a correct resolution was about 100 nm.

The microscopic observations were conducted with the technical support of SERMA Technologies (*www.serma-technologies.com*).

### *1.3.3. Reactivity measurements*

#### *1.3.3.1. Description of the experimental device*

The reactivity to steam gasification of soot and char was determined from experiments in a ThermoGravimetric Analyzer (TGA) which was coupled to a wet gas generator (Figure 44).

**Figure 44. ATG (right of the picture) coupled to a wet gas generator (left of the picture)**

The TGA furnace can reach a maximal temperature of 1600°C and the steam generator can produce a gas with a maximum steam content of about 27 mol%. Both devices, designed by SETARAM (*www.setaram.com*), operate at atmospheric pressure. Figure 45 provides a scheme of the TGA facility.

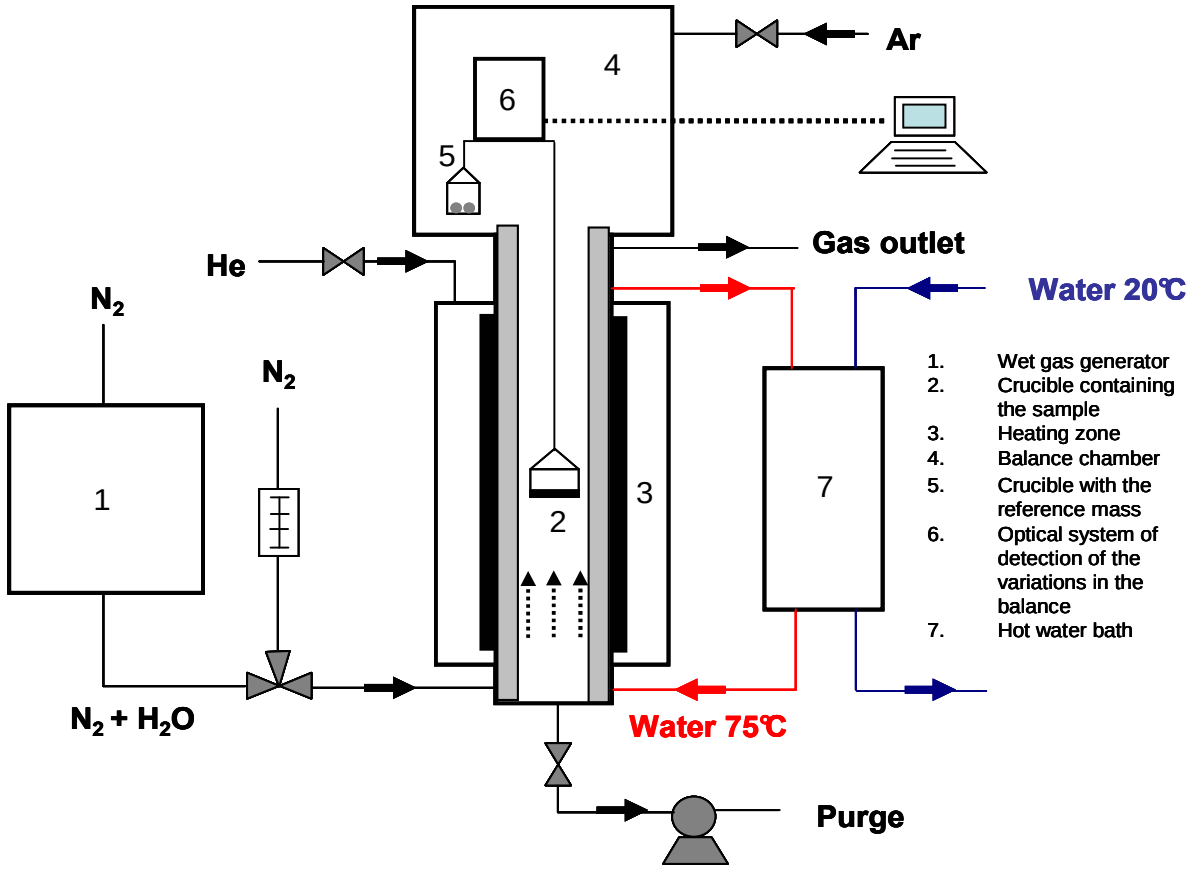


**Figure 45. Scheme of the TGA facility**

The TGA is constituted of an alumina tube heated by electric resistances made of graphite. An argon stream flows in the electric zone in order to protect the graphite against oxidation with air. The crucible, which contains the sample, is suspended in the heated zone of the reactor by the branch of a balance, which is located in a chamber in the head of the reactor. The other branch of the balance is linked to a reference mass, which remains constant during all the experiments. The mass variation of the sample is measured through a system which transmits an electrical signal, which is then converted into a numeric signal so as to visualize the mass sample online on a computer.

The carrier gas flows from the bottom to the top of the reactor. A manual valve enables to switch the source of the carrier gas between the gas coming from a $N_2$ bottle and the wet gas coming from the wet gas generator. The head of the reactor is slightly pressurized by a helium flow at 10 ml/min, in order to protect the electric system of the balance against the steam introduced into the reactor. All the lines are heated to 80°C in order to avoid steam condensation. Besides, water from a bath at 70°C flows around the walls of the reactor so as to avoid steam condensation in the non heated zones and to evacuate the heat from the reactor core.

Before each experiment, a purge system enables to change the initial atmosphere in the reactor, corresponding to the ambient atmosphere, into an inert one in order to remove all the humidity traces and oxygen.

#### *1.3.3.2. Description of the experimental procedure*

During TGA experiments, gasification takes place in isothermal mode. The reactor is heated at 24°C/min under a nitrogen atmosphere. Once the gasification temperature plateau is reached, the $N_2$ carrier gas flow is stopped and it is substituted by the wet gas. The gasification experiment is considered to begin at this instant. The flow rate of the carrier gas is fixed at 50 ml/min for all experiments. The gasification temperature is in the range of 750 to 850°C for char and 910 to 980°C for soot. The steam concentration is 20 mol% or 5 mol%. The length of the gasification tests varies from a few minutes to about one hour, in function of the operating conditions and the sample.

When the sample is char, the temperature in the TGA is first set at 950°C under $N_2$, before decreasing it to the gasification temperature, in order to release most of the remaining volatile matter from the solid.

Figure 46 shows the evolution of the temperature set point during the gasification experiments with char and soot.

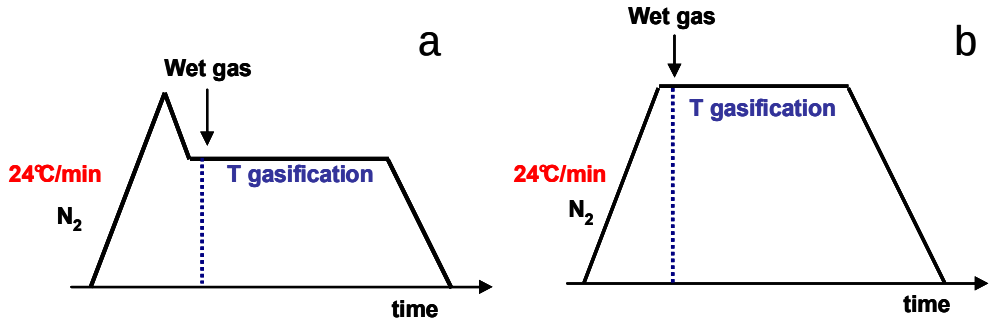


**Figure 46. Evolution of the temperature during the gasification experiments with char (a) and soot (b)**

Gasification or oxidation experiments in a TGA can be subject to mass transfer limitations, more particularly in the case of soot. Several works in literature have reported that oxidation experiments in a TGA could be limited by diffusion phenomena of $O_2$ into the soot particles bed contained in the crucible (Song, 2010; 2006). This limitation can be avoided with a very low particles bed thickness. So, a large crucible offering an important surface for a good spreading of soot particles was selected. The absence of any mass limitation during the soot gasification experiments was experimentally verified, for sample masses varying in the range of 1 mg to 5 mg. However, the contribution of intraparticle mass diffusion in measured kinetics cannot be discarded, even if it is not very likely to occur due to the small size of soot particles (agglomerates).

In the case of char, an experimental study performed in the same facility shows that no mass limitation is observed below 6 mg for a char prepared in a fluidized bed reactor (Septien, 2007).

Therefore, the char and soot mass during TGA experiments was about 3 to 4 mg, which offers the maximum of representativeness of the sample and enables to be in a kinetically controlled regime in order to study the intrinsic reactivity.

No grinding of char samples was applied because this could reduce the representativeness of the char from the DTR experiments. Besides, it has been demonstrated that the particle size is not limiting below 1 mm for a char prepared in a fluidized bed reactor (Septien, 2007), at a lower heating rate than the one in the DTR. As char porosity is more important with the increase of the HR, internal mass diffusion is supposed to be slower in the fluidized bed char than in the DTR one. By consequence, no internal mass diffusion limitation is supposed to appear during the gasification experiments of any of the char samples.

#### *1.3.3.3. Reactivity determination*

The reactivity, which refers here to the reaction rate of char or soot sample gasification, can be calculated from the mass loss measured in the TGA (Equation 12 of section 4.4 of Chapter "Fundamental concepts"). In literature, there is no agreement about how to define one representative value of reactivity for an experiment. It is most frequently obtained as the average reactivity between two degrees of conversion, as for instance: 0 – 50% (Chen et al., 1997), 0 – 95% (Moilanen, 2006), 60 – 80% (DeGroot & Shafizadeh, 1984), 20 – 80% (Barrio et al., 2001). It can also correspond to the reactivity at a specific conversion, as for instance 50% (Ollero et al., 2003; Zhang et al., 2008). The range of conversion chosen depends on the criteria taken by the author.

In this work, two conversion ranges were chosen: 10 - 70%, in order to study the reactivity at the middle of the transformation, and 0 - 95%, in order to have a global reactivity of the transformation.

Through the repeatability of experiments, the error bar of reactivity was estimated to be about 30% for char and 20% for soot. These high uncertainties could be caused by a high heterogeneity within each sample, as well as a very low sample mass used in experiments.

### 1.4. Products yields determination

The yield of each product is determined from the ratio between the flow rate of the product at the reactor outlet and the feeding rate of the dry biomass (Equation 34).

$$Y_i = F_i / \left( F_{biomass} \times (1 - y_{moisture}) \right)$$ **Equation 34**

With:

| | | |
|---|---|---|
| $Y_i$ | Yield of product *i* | $mol.mol^{-1}$ db |
| $F_i$ | Molar flow rate of *i* | $mol.s^{-1}$ |
| $F_{biomass}$ | Molar flow rate of the biomass | $mol.s^{-1}$ |
| $y_{moisture}$ | Molar moisture content of the biomass | - |

Note that the yield can be expressed on a mass basis.

### 1.4.1. Gas compounds yields determination

The flow rate of each gaseous compound is obtained from the gas concentration measured by the analyzers and from the total flow rate of the permanent gases (Equation 35). The gas analysis is performed on a "dry" gas, which contains $H_2O$ in a so low content, inferior to 2 mol%, that no condensation can occur at the ambient temperature.

$$F_i = y_i \times F_{gas}$$ **Equation 35**

With:

| | | |
|---|---|---|
| $y_i$ | Molar fraction of *i* in the dry gas | - |
| $F_{gas}$ | Molar flow rate of the total dry gas | $mol.s^{-1}$ |

The total dry gas flow rate before the analyzers can be calculated with Equation 36 and 37, which are based on the following assumptions: the gas follows the ideal gas law, and all the gaseous species are quantified by the analyzers. This last assumption is verified since a considerable part of tar, which is not experimentally quantified, is condensed before the analyzers during experiments at 1000°C, and no tar is detected at 1200°C and 1400°C. Note that the $H_2O$ fraction measured by the psychrometer is included in Equation 36 for the calculation of the total gas flow rate.

$$F_{N_2} = y_{N_2} \times F_{gas} = \left(1 - \sum_{i \neq N_2} y_i\right) \times F_{gas}$$ **Equation 36**

$$F_{N_2} = \frac{P \times y_{N_2} \times Q_{N_2}}{R \times T}$$ **Equation 37**

With:

| | | |
|---|---|---|
| $F_{N2}$ | Molar flow rate of $N_2$ | $mol.s^{-1}$ |
| $y_{N2}$ | Molar concentration of $N_2$ in the dry gas | - |
| $P$ | Total pressure of dry gas | Pa |
| $Q_{N2}$ | Volume flow rate of $N_2$ | $m^3.s^{-1}$ |
| $R$ | Constant of ideal gas | $J.kg^{-1}.K^{-1}$ |
| $T$ | Gas temperature | K |

The gas fractions used for yields calculations are mean values obtained from the repeatability experiments performed at several days and months of interval. The uncertainty on the gas yields is estimated from the maximal difference observed between different measurements. Table 12 presents the estimated error bar for the yield of each gaseous compound.

The uncertainties for the $C_2$ species and $C_6H_6$ are the highest - 20 % -, which is probably due to their very low amounts in the released gas.

**Table 12. Error bar for the yield of each gaseous compound**

| **Compound** | $H_2$ | CO | $CO_2$ | $H_2O$ | $CH_4$ | $C_2H_2$ | $C_2H_4$ | $C_2H_6$ | $C_6H_6$ |
|---|---|---|---|---|---|---|---|---|---|
| **Error bar** | 5% | 5% | 10% | 10% | 10% | 20% | 20% | 20% | 20% |

### 1.4.2. Char yield determination

The char yield is calculated by the ash tracer method (Chen, 2009; Dupont, 2006; Zanzi et al., 1996), shown in Equation 38.

$$F_{char} \times M_{char} \times x_{ash,char} = F_{biomass} \times (1 - y_{moisture}) \times M_{dry\ biomass} \times x_{ash,biomass} \quad \textbf{Equation 38}$$

With:

| | | |
|---|---|---|
| $F_{char}$ | Molar flow rate of char | $mol.s^{-1}$ |
| $M_{char}$ | Molar mass of char (≈ carbon) | $g.mol^{-1}$ |
| $x_{ash,\ char}$ | Ash mass content in char | - |
| $M_{dry\ biomass}$ | Molar mass of dry biomass | $g.mol^{-1}$ |
| $x_{ash,\ biomass}$ | Ash mass content in dry biomass | - |

Equation 38 is based on the assumption that ash from biomass remains in the char and is neither consumed nor transformed. The error bar of this method is estimated at 25% and comes from the uncertainty of the ash content measurements of wood and char samples.

The study of Misra et al. (1993) showed that biomass ash prepared at 350°C loses about 20 % to 50 % of its mass above 1000°C. This mass loss is mainly due to the decarbonatation of ash between 600°C and 900°C, and to the volatilization of sulfur - 7 to 55% - and potassium - 63 to 90% - between 900°C and 1100°C. Hence, based on the elemental composition of the wood sample ash used in this study (Table 9), ash in char could lose up to 40% of its weight during experiments in the worst case. So, the char yield determined from the experiments could be overestimated.

### 1.4.3. Tar and soot yields estimation

"Tar" here and in the following text refers to all the organic compounds with a molecular weight larger than benzene, excluding soot and char, and condensing at ambient temperature.

Tar and soot yields cannot be directly quantified but they can be estimated by difference through a mass balance (Equation 39).

$$F_{tar/soot} = F_{biomass} - F_{gas} - F_{char} \quad \textbf{Equation 39}$$

The uncertainty for tar and soot yields is estimated to be about 40%.

## 2. Preliminary characterization of the experiments in the drop tube reactor by theoretical studies

This chapter presents a preliminary study, which consists in a characteristic time analysis and calculations at the thermodynamic equilibrium. The analysis of the results from these theoretical studies will be useful for the interpretation of the experimental results and the modeling in next chapters.

### 2.1. Characteristic time analysis

A characteristic time analysis (refer to section 3 of Chapter "State of the art") under the experimental conditions of this work (described in section 1.2.2) was performed in two cases: wood pyrolysis and carbonaceous solid gasification. The main objectives of this approach are the determination of the regimes during the experiments

and the estimation of the timescales of the phenomena in order to compare them to the residence time of the particles.

The phenomena considered in the characteristic time analysis are:

- For wood pyrolysis: heating of the particle by external convection and radiation, internal conduction, and devolatilisation of wood. The wood initial temperature is considered to be at the ambient conditions.
- For char and soot gasification: external mass transfer of the reactive gas, $H_2O$ and $CO_2$, to the particle surface by convection, internal mass transfer by gas diffusion inside the particle and gasification. Note that char and soot are supposed to be at the reactor temperature at the instant of their formation.
- The gaseous atmosphere surrounding the particles is supposed to be at the reactor wall temperature and the particles are considered to be spherical.

Characteristic times are considered to be in the same order of magnitude if their ratio is inferior to a factor of 10.

### 2.1.1. Calculation of the characteristic times

#### 2.1.1.1. Characteristic times related to physical phenomena

- External mass and convective heat transfers

The characteristic time related to the external convective heat and mass transfers for isotherm and iso-concentration spherical particles are respectively shown in Equation 40 and 41.

$$t_{conv} = \frac{\rho_p \times Cp_p \times d_p}{6 \times h_t} \qquad \textbf{Equation 40}$$

$$t_{mass\ ext} = \frac{\rho_p \times R \times T \times d_p}{6 \times h_m \times P_{H_2O} \times M_{CO}} \qquad \textbf{Equation 41}$$

With:

| | | |
|---|---|---|
| $t_{conv}$ | Characteristic time of heat convection | s |
| $t_{mass\ ext}$ | Characteristic time of external mass transfer | s |
| $\rho_p$ | Particle density | $kg.m^{-3}$ |
| $Cp_p$ | Particle heat capacity | $J.kg^{-1}.K^{-1}$ |
| $d_p$ | Particle diameter | m |
| $h_t$ | Heat exchange coefficient | $W.m^{-2}.K^{-1}$ |
| $h_m$ | Mass exchange coefficient | $m.s^{-1}$ |
| $P_{H2O}$ | Partial pressure of $H_2O$ | Pa |
| $M_{CO}$ | Molar mass of CO | $kg.mol^{-1}$ |

The heat and mass exchange coefficients can be determined from dimensionless numbers: the Nusselt number (*Nu*) in the case of heat transfer (Equation 42) and the Sherwood number (*Sh*) in the case of mass transfer (Equation 43).

$$Nu = \frac{h_t \times d_p}{\lambda_g}$$ **Equation 42**

$$Sh = \frac{h_m \times d_p}{D_{mol}}$$ **Equation 43**

With:

| | | |
|---|---|---|
| $\lambda_g$ | Gas conductivity | $W.m^{-1}.K^{-1}$ |
| $D_{mol}$ | Molecular diffusion coefficient | $m^2.s^{-1}$ |

Each of these numbers can also be expressed as a combination of other dimensionless numbers: the Reynolds particle number ($Re_p$) and Prandtl number ($Pr$) in the case of Nu, the $Re_p$ and Schmidt number ($Sc$) in the case of $Sh$.

The $Re_p$, $Pr$ and $Sc$ numbers are respectively shown in Equation 44, 45 and 46.

$$\mathrm{Re}_p = \frac{\rho_g \times V_{slip} \times d_p}{\mu_g}$$ **Equation 44**

$$\mathrm{Pr} = \frac{\mu_g \times Cp_g}{\lambda_g}$$ **Equation 45**

$$Sc = \frac{\mu_g}{\rho_g \times D_{mol}}$$ **Equation 46**

With:

| | | |
|---|---|---|
| $\rho_g$ | Gas density | $kg.m^{-3}$ |
| $V_{slip}$ | Particle slip velocity | $m.s^{-1}$ |
| $\mu_g$ | Gas dynamic viscosity | $Pa.s^{-1}$ |
| $Cp_g$ | Gas heat capacity | $J.kg^{-1}.K^{-1}$ |

The particle slip velocity $V_{slip}$ is supposed to be equal to the terminal velocity of free fall in a Stokes regime ($Re_p << 1$), which is expressed in Equation 47.

$$V_t = \frac{g \times {d_p}^2 \times (\rho_p - \rho_g)}{18 \times \mu_g}$$ **Equation 47**

With:

| | | |
|---|---|---|
| $V_t$ | Terminal velocity of free fall | $m.s^{-1}$ |
| $g$ | Gravitationnel constant | $m.s^{-2}$ |

Different correlations of $Nu$ = f($Rep$, $Pr$) and $Sh$ = f($Re_p$,$Sc$) can be found in literature in function of the hydrodynamic conditions of the particle in the surrounding gas. Equation 48 and Equation 49 show correlations that can be used in the case of a laminar gas flow around a spherical particle (Whitaker, 1972), which is the case of our experimental study. It can be noticed both correlations are the same because of the Chilton and Colburn (1934) analogy between heat and mass transfers.

$$Nu = 2 + 0{,}6 \times \mathrm{Re}_p^{1/2} \times \mathrm{Pr}^{1/3}$$ **Equation 48**

$$Sh = 2 + 0{,}6 \times \mathrm{Re}_p^{1/2} \times Sc^{1/3}$$ **Equation 49**

- External radiative heat transfer

The characteristic time of radiative heat transfer can be expressed as Equation 50.

$$t_{rad} = \frac{\rho_p \times Cp_p \times d_p}{6 \times \omega_p \times \sigma \times (Tg + Tp) \times (Tg^2 + Tp^2)}$$ **Equation 50**

With:

| | | |
|---|---|---|
| $t_{rad}$ | Characteristic time of radiative heat transfert | s |
| $\omega_p$ | Particle emissivity | - |
| $\sigma$ | Boltzmann constant | $W.m^{-2}.K^{-4}$ |
| $T_p$ | Initial particle temperature | K |

- Heat conduction inside the particles

The characteristic time of conductive heat transfer inside the particles can be expressed as:

$$t_{cond} = \frac{\rho_p \times Cp_p \times dp^2}{36 \times \lambda_p}$$ **Equation 51**

With:

| | | |
|---|---|---|
| $t_{cond}$ | Characteristic time of internal heat conduction | s |
| $\lambda_p$ | Particle thermal conductivity | $W.m^{-1}.K^{-1}$ |

- Internal mass diffusion

The characteristic time of internal mass diffusion is shown in Equation 52.

$$t_{\text{mass int}} = \frac{dp^2}{36 \times D_{eff}}$$ **Equation 52**

With:

| | | |
|---|---|---|
| $t_{mass\ int}$ | Characteristic time of internal mass diffusion | s |
| $D_{eff}$ | Effective gas diffusion coefficient | $m^2.s^{-1}$ |

Gas diffusion inside char and soot particles depends on the structure of the solid, as well as on the diffusion characteristics of $H_2O$ and $CO_2$. Equation 53 takes into consideration both aspects (Wheeler, 1955).

$$D_{eff} = \left(\frac{\varepsilon_p}{\tau_p}\right) \times D$$ **Equation 53**

With:

| | | |
|---|---|---|
| $\varepsilon_p$ | Particle porosity | - |
| $\tau_p$ | Particle tortuosity | - |
| $D$ | Gas diffusion coefficient | $m^2.s^{-1}$ |

The gas diffusion inside char and soot particles is controlled by both molecular (Equation 54) and Knudsen diffusion (Equation 55).

$$D_{mol} = \frac{0{,}001 \times T^{1,75} \times \left(\frac{1}{M_i} + \frac{1}{M_{N_2}}\right)^{1/2}}{P_g \times \left((\sum v)_i^{1/3} + (\sum v)_{N_2}^{1/3}\right)^2} \quad \textbf{Equation 54}$$

$$D_{Knudsen} = \frac{2}{3} \times r_{pore} \times \sqrt{\frac{2 \times R \times T}{\pi \times M_c}} \quad \textbf{Equation 55}$$

With:

| | | |
|---|---|---|
| $D_{mol}$ | Molecular diffusion coefficient | $m^2.s^{-1}$ |
| $M_i$ | Molar mass of $i$ ($H_2O$ or $CO_2$) | $kg.mol^{-1}$ |
| $M_{N2}$ | Molar mass of $N_2$ | $kg.mol^{-1}$ |
| $P_g$ | Total gas pressure | Pa |
| $(\Sigma v)_i$ | Volume diffusion of $i$ ($H_2O$ or $CO_2$) | $m^3.mol^{-1}$ |
| $(\Sigma v)_{N2}$ | Volume diffusion of $N_2$ | $m^3.mol^{-1}$ |
| $D_{Knudsen}$ | Knudsen diffusion coefficient | $m^2.s^{-1}$ |
| $r_{pore}$ | Pore size | m |
| $M_c$ | Molar mass of carbon | $kg.mol^{-1}$ |

The global diffusion coefficient $D$ can be then deduced from Equation 56:

$$D = \left(\frac{1}{D_{mol}} + \frac{1}{D_{Knusden}}\right)^{-1} \quad \textbf{Equation 56}$$

- Solid and gas physical properties

As observed through Equation 40 – 56, the characteristic times of physical phenomena depend on the physical properties of the gas and the solid.

The values used for the solid physical properties were obtained from the literature (Table 13). The wood thermal conductivity is a mean value between the conductivities in parallel and perpendicular directions with respect to the wood fibers.

No values of tortuosity for char from rapid pyrolysis were found in literature. However, tortuosity can be deduced from the ratio $\varepsilon_p/\tau_p$, which is estimated to be 0.15 for biomass char (Gómez-Barea et al., 2005; Groeneveld & van Swaaij, 1980), and from the value of the porosity $\varepsilon_p$, which corresponds to the value measured for a char from beech rapid pyrolysis in a DTR by Chen (2009).

**Table 13. Values from the literature of physical properties of wood, char and soot**

| Physical properties | Wood | Char | Soot |
|---|---|---|---|
| $\rho_p$ (kg.m$^{-3}$) | 710 (Chen, 2009) | 170 (Chen, 2009) | 1087 (Song, 2006) |
| $Cp_p$ (J.kg$^{-1}$.K$^{-1}$) | 1522 (Miller, 1999) | - | - |
| $\lambda_p$ (W.m$^{-1}$.K$^{-1}$) | 0.11 (Miller, 1999) | - | - |
| $\omega_p$ | 0.9 (Gronli, 1996) | - | - |
| $\varepsilon_p$ | - | 0.9 (Chen, 2009) | 0.26 (Song, 2006) |
| $\tau_p$ | - | 6 (estimated) | 2.8 (Song, 2006) |
| $r_{pore}$ ($10^{-9}$ m) | - | 50 (Tagutchou, 2008) | 15 (Song, 2006) |

The properties of gas considerably vary with temperature. Table 14 shows the physical properties of $N_2$ and $H_2O$ in function of temperature. Note that the density is determined from the ideal gas law.

**Table 14. Expression of the physical properties of pure gas in function of temperature (Perry, 1997)**

| Physical properties | $N_2$ | $H_2O$ (steam) |
|---|---|---|
| $\rho_g$ (kg.m$^{-3}$) | $\frac{P_g \times M_{N_2}}{R \times T}$ | $\frac{P_g \times M_{H_2O}}{R \times T}$ |
| $\mu_g$ (Pa.s$^{-1}$) | $1.781\times10^{-5} \times \frac{(300{,}55+111)}{111+T} \times \left(\frac{T}{300.55}\right)^{3/2}$ | $(-4.9554\times10^{-6} \times T^2 + 0.043895 \times T - 1.0143)\times10^{-6}$ |
| $\lambda_g$ (W.m$^{-1}$.K$^{-1}$) | $\frac{\mu_{N2}}{Cp_{N2}} \times (1.3 \times (T \times M_{N2} - R) + 14644 - \frac{2928.8}{T/Tc_{N2}})$ | $\frac{\mu_{H2O}}{M_{H2O}} \times (1.15 \times (Cp_{H2O} \times M_{H2O} - R) + 14644 - \frac{2928.8}{T/Tc_{H2O}})$ |
| $Cp_g$ (J.kg$^{-1}$.K$^{-1}$) | $\frac{(6.5+0.001\times T)}{M_{N_2}} \times 4.18$ | $Cp_{H2O} = (8{,}22 + 0{,}0015 \times T + 0{,}00000134 \times T) / M_{H2O} \times 4{,}18$ |

With:

| | | |
|---|---|---|
| $Tc_{N2}$ | Critical temperature of $N_2$ | K |
| $Tc_{H2O}$ | Critical temperature of $H_2O$ | K |

In the experiments under a wet atmosphere, the physical properties of the gases are a combination of the properties of $N_2$ and $H_2O$. This mixture can be assimilated as an ideal gaseous phase. This assumption simplifies the calculations of density (Equation 57) and heat capacity (Equation 58).

$$\rho_g = \sum_i (y_i \times \rho_i) \qquad \textbf{Equation 57}$$

$$Cp_g = \sum_i (x_i \times Cp) \qquad \textbf{Equation 58}$$

With: $x_i$ as the mass concentration of $i$ and $i = H_2O$ or $N_2$

In the case of thermal conductivity and viscosity, the relation of Wilke (Equation 59 and Equation 60) can be used (Gosse, 1991).

$$\mu_g = \sum_i \left( \frac{y_i \times \mu_i}{y_i + \sum_{j \neq i} \left( y_j \times \phi_{ij} \right)} \right) \quad \textbf{Equation 59}$$

$$\lambda_g = \sum_i \left( \frac{y_i \times \lambda_i}{y_i + \sum_{j \neq i} \left( y_j \times \phi_{ij} \right)} \right) \quad \textbf{Equation 60}$$

With:

$$\phi_{ij} = \left[ 8 \times \left( 1 + \frac{M_i}{M_j} \right) \right]^{-1/2} \left[ 1 + \left( \frac{\lambda_i \text{ or } \mu_i}{\lambda_j \text{or } \mu_i} \right)^{1/2} \left( \frac{M_j}{M_i} \right)^{1/4} \right]^2 \quad \textbf{Equation 61}$$

$i = H_2O$ or $N_2$; $j = N_2$ or $H_2O$

#### *2.1.1.2. Characteristic times related to chemical phenomena*

- Characteristic time of pyrolysis

The characteristic time of pyrolysis is obtained from the chemical kinetics of the devolatilisation reaction (Equation 62), which is represented by a one-step reaction.

$$t_{pyr} = \frac{1}{k_{pyr}} = \frac{1}{k_0 \times \exp\left( -E_a / R \times T \right)} \quad \textbf{Equation 62}$$

With:

| | | |
|---|---|---|
| $t_{pyr}$ | Characteristic time of pyrolysis | s |
| $k_{pyr}$ | Pyrolysis reaction rate | $s^{-1}$ |
| $k_0$ | Pre-exponential factor | $s^{-1}$ |
| $E_a$ | Energy of activation | $J.mol^{-1}$ |

The kinetic parameters used here are based on the study of rapid pyrolysis kinetics performed in a DTR by Brink (1978) and Shuaning et al. (2006). Table 15 describes the experimental setup and the results from this kinetic study. These kinetic parameters have to be taken with a lot of caution as they were obtained for fast pyrolysis at temperatures below 1000°C.

**Table 15. Kinetic parameters of fast pyrolysis**

| Source | Brink (1978) | Shuaning et al. (2006) |
|---|---|---|
| Temperature | 647 – 871°C | 476 – 627°C |
| Pressure | 1 bar | 1 bar |
| Type of biomass | White fir | Wheat straw |
| Particle size | < 0.175 mm | 0.05 - 0.070 mm |
| Kinetic parameters | | |
| $E_a$ | 105 kJ.mol$^{-1}$ | 32 kJ.mol$^{-1}$ |
| $k_0$ | 2.64 x 10$^5$ s$^{-1}$ | 1.05 x 10$^3$ s$^{-1}$ |

- Characteristic time of gasification

The characteristic time of gasification reaction is obtained from the chemical kinetics of an n-order reaction with respect to the reagents $H_2O$ and $CO_2$ partial pressures (Equation 63).

$$t_{gas} = \frac{1}{k_{gas}} = \frac{1}{k_0 \times P_i^n \times \exp\left(-E_a / R \times T\right)}$$ **Equation 63**

With:

| | | |
|---|---|---|
| $t_{gas}$ | Characteristic time of gasification | s |
| $k_{gas}$ | Gasification reaction rate | s$^{-1}$ |
| $k_0$ | Pre-exponential factor | Pa$^{-n}$.s$^{-1}$ |
| $P_i$ | Partial pressure of *i* ($H_2O$ or $CO_2$) | Pa |
| $n$ | Order of the reaction | - |

Only two works about gasification kinetics of wood char prepared in a DTR have been found in literature (Fermoso et al., 2009; Matsumoto, 2009). Characteristics and kinetic parameters derived from these studies are presented in Table 16. Note that chars in these works could be partially oxidized during their preparation due to the presence of a few percents of $O_2$ in the atmosphere. Therefore, the measured kinetics could be different from the kinetics of a non-reacted char prepared in the same conditions without oxygen introduction.

**Table 16. Kinetic parameters of gasification of biomass char from fast pyrolysis**

| Source | Matsumoto (2009) | | Fermoso et al. (2009) |
|---|---|---|---|
| Gasification experiment | | | |
| Reagent | $H_2O$ and $CO_2$ | | $CO_2$ |
| Experimental device | DTR | | TGA |
| Temperature | 900°C – 1200°C | | 750°C – 900°C |
| Solid preparation | | | |
| Experimental device | EFR pilot | | DTR |
| Temperature | 900°C – 1000°C | | 1000°C |
| Pressure | 1 bar | | 1 bar |
| Wood specie | Japanese cedar | | Slash pine |
| Particle size | Not specified | | 0.075 – 0.11 mm |
| Kinetic parameters | **$H_2O$** | **$CO_2$** | **$CO_2$** |
| $E_a$ | 136 kJ/mol | 93.9 kJ/mol | 184 kJ/mol |
| $k_0$ | $1.5 \times 10^4$ $s^{-1}$ | $2.24 \times 10^3$ $s^{-1}$ | $1.5 \times 10^6$ $s^{-1}$ |
| $n$ | 0.22 | 0.22 | 0.34 |

In the case of soot gasification kinetics, only one reference was found in literature (De Soete, 1988). Kinetic parameters derived from this study are presented in Table 17. Note that soot in this study was obtained by the pyrolysis of hydrocarbon molecules, thus the gasification kinetic parameters could be different from those for soot from biomass pyrolysis.

**Table 17. Kinetic parameters of soot gasification (De Soete, 1988)**

| **Reagent** | **$H_2O$** | **$H_2O$** | **$CO_2$** |
|---|---|---|---|
| Experimental device | Fixed bed reactor | Fixed bed reactor | Fixed bed reactor |
| Fuel used for soot preparation | α – ethylnaphtalene | N - hexadecane | α – ethylnaphtalene |
| Kinetic parameters | | | |
| $E_a$ | 23.5 kJ/mol | 21.7 kJ/mol | 30.9 kJ/mol |
| $k_0$ | 100 $s^{-1}$ | 19 $s^{-1}$ | 8100 $s^{-1}$ |
| $n$ | 1 | 1 | 1 |

### 2.1.2. Results of the characteristic time analysis

The characteristic times analysis corresponding to the experimental conditions of this work in the DTR (described in section 1.1.2.) is presented below. As pyrolysis is the first stage during biomass gasification, the characteristic times related to heating and devolatilisation of the wood particles are firstly discussed. Then an analysis of the characteristic times related to gasification of the char and soot, and to mass transfer of the reagents $H_2O$ and $CO_2$ into the carbonaceous solids is performed.

#### 2.1.2.1. Heating and devolatilisation of the wood particles

The results of characteristic time calculations relative to particle heating and devolatilisation, and the associated dimensionless numbers, are given in Table 18. Note that the reported values apply both for an inert and a wet atmosphere.

**Table 18. Characteristic times and dimensionless numbers relative to heat transfer and pyrolysis**

| Temperature (°C) | | 1000 | | 1200 | | 1400 | |
|---|---|---|---|---|---|---|---|
| Particle diameter (mm) | | 0.35 | 0.80 | 0.35 | 0.80 | 0.35 | 0.80 |
| Characteristic times (s) | External heat transfer by convection | 0.09 | 0.3 | 0.08 | 0.3 | 0.08 | 0.3 |
| | External heat transfer by radiation | 0.5 | 1.1 | 0.3 | 0.7 | 0.2 | 0.5 |
| | Internal heat transfer by conduction | 0.03 | 0.2 | 0.03 | 0.2 | 0.03 | 0.2 |
| | Pyrolysis* | 0.04 | | 0.01 | | 0.008 | |
| | Residence time of the particle (s) | 3.8 | 2.7 | 3.8 | 2.7 | 3.8 | 2.7 |
| Dimensionless numbers | $Bi_t$ ($t_{cond}/t_{conv}$) | ~ 1 | ~ 1 | ~ 1 | ~ 1 | ~ 1 | ~ 1 |
| | $t_{rad}/t_{conv}$ | ~ 1 | ~ 1 | ~ 1 | ~ 1 | ~ 1 | ~ 1 |
| | $Da$ ($t_{pyr}/t_{conv}$) | ~ 1 | ~ 1 | ~ 1 | ~ $10^{-1}$ | ~ 1 | ~ $10^{-1}$ |

* Mean value obtained from the pyrolysis kinetics of Brink (1978) and Shuaning et al. (2006)

It can be observed that characteristic times of the heat transfer phenomena increase with particle size by a factor of 2 to 7. The characteristic times of heat transfer by radiation and of pyrolysis decrease with temperature, whereas the characteristic times of heat transfer by conduction and convection are hardly sensitive to this parameter.

The three thermal transfer modes and the pyrolysis have characteristic times of the same order of magnitude, as shown with the dimensionless numbers ($Bi_t$, $t_{rad}/t_{conv}$ and $Da$ ~ 1). The only exception is for 0.80 mm particles at 1200°C and 1400°C, where devolatilisation is much faster than the particle heating ($Da$ ~ $10^{-1}$). From these observations, the following points can be deduced:

- None of heat transfer modes should be neglected.
- Wood pyrolysis should be controlled by both chemical kinetics and heating rate, except for 0.80 mm particles at 1200°C and 1400°C where pyrolysis should then be only controlled by heat transfer.

It can also be seen that the overall pyrolysis process characteristic time is less than one second. Therefore, the particle residence time, which is of several seconds, appears to be sufficiently long for complete biomass pyrolysis conversion to be achieved under the experimental conditions.

#### *2.1.2.2. Mass transfer and gasification in the case of a char particle*

Table 19 and Table 20 present the results of characteristic time calculations relative to mass transfer phenomena and to char gasification for two different reagent concentration: 25 mol% and 1 mol%. The 25 mol% value corresponds to the $H_2O$ content in the atmosphere during experiments under a wet atmosphere. The 1 mol% value is the order of magnitude of the $H_2O$ concentration measured during experiments under an inert atmosphere, and of the $CO_2$ concentration for both types of experiments. The characteristic times relative to gasification with 1 mol% of $H_2O$ and $CO_2$ were found to be similar. Therefore, only the results with $H_2O$ are shown in Table 20.

The initial char particle diameters were estimated from the shrinking core model developed by Chen (2009): the initial wood particles sizes of 0.35 mm and 0.80 mm are reduced to 0.25 mm and 0.50 mm respectively after pyrolysis. This same model was used for the determination of the char particle residence time.

**Table 19. Characteristic times and dimensionless numbers relative to mass transfer and char gasification with 25 mol% of $H_2O$**

| Temperature (°C) | | 1000 | | 1200 | | 1400 | |
|---|---|---|---|---|---|---|---|
| Char particle diameter (mm) | | 0.25 | 0.50 | 0.25 | 0.50 | 0.25 | 0.50 |
| Characteristic times (s) | Diffusion internal mass transfer | $7.10^{-4}$ | $3.10^{-3}$ | $7.10^{-4}$ | $3.10^{-3}$ | $6.10^{-4}$ | $2.10^{-3}$ |
| | Convective external mass transfer | 0.04 | 0.1 | 0.03 | 0.1 | 0.03 | 0.1 |
| | Gasification reaction | 9 | | 1.5 | | 0.5 | |
| | Residence time of char (s) | 3.8 | 1.8 | 3.8 | 1.8 | 3.8 | 1.8 |
| Dimensionless numbers | $Bi_M$ ($t_{mass\ int}/t_{mass\ ext}$) | $\sim 10^{-2}$ | $\sim 10^{-2}$ | $\sim 10^{-2}$ | $\sim 10^{-2}$ | $\sim 10^{-2}$ | $\sim 10^{-2}$ |
| | $t_{gas}/t_{mass\ ext}$ | $\sim 10^{2}$ | $\sim 10^{2}$ | $\sim 10$ | $\sim 10$ | $\sim 10$ | $\sim 1$ |

**Table 20. Characteristic times and dimensionless numbers relative to mass transfer and char gasification with 1 mol% of $H_2O$**

| Temperature (°C) | | 1000 | | 1200 | | 1400 | |
|---|---|---|---|---|---|---|---|
| Char particle diameter (mm) | | 0.25 | 0.50 | 0.25 | 0.50 | 0.25 | 0.50 |
| Characteristic times (s) | Diffusion internal mass transfer | $7.10^{-4}$ | $3.10^{-3}$ | $7.10^{-4}$ | $3.10^{-3}$ | $6.10^{-4}$ | $3.10^{-3}$ |
| | Convective external mass transfer | 0.9 | 3.1 | 0.8 | 2.8 | 0.8 | 2.7 |
| | Gasification reaction | 17 | | 3 | | 1 | |
| | Residence time of char (s) | 3.8 | 1.8 | 3.8 | 1.8 | 3.8 | 1.8 |
| Dimensionless numbers | $Bi_M$ ($t_{mass\ int}/t_{mass\ ext}$) | $\sim 10^{-3}$ | $\sim 10^{-3}$ | $\sim 10^{-3}$ | $\sim 10^{-3}$ | $\sim 10^{-3}$ | $\sim 10^{-3}$ |
| | $t_{gas}/t_{mass\ ext}$ | $\sim 10$ | $\sim 10$ | $\sim 1$ | $\sim 1$ | $\sim 1$ | $\sim 1$ |

Table 19 and Table 20 show that mass transfer characteristic times increase with particle size by a factor 4 – 5 but do not vary significantly with temperature. External mass transfer also appears to be strongly dependent on the reagent concentration: a decrease of the $H_2O$ concentration leads to the increase of the external mass transfer characteristic time by a factor higher than 10. As expected, an increase of temperature or oxidant partial pressure leads to a decrease of gasification characteristic time.

As can be seen with the dimensionless number $t_{gas}/t_{mass\ ext}$, the gasification characteristic time is higher or has the same order of magnitude as that of external mass transfer, depending on the temperature, on the concentration of the reactive gas and on the particle size. In all the cases, internal mass transfer occurs much faster than the chemical and external mass transfer phenomena ($Bi_M \sim 10^{-3}$ - $10^{-2}$), thus it can be neglected.

Through the previous observations, the following regimes for char gasification in function of the operating conditions and of the sample size can be deduced:

- Under a wet atmosphere, gasification is controlled only by chemical kinetics ($t_{gas}/t_{mass\ ext} \sim 10$ - $10^2$), except at 1400°C for 0.50 mm char particles where gasification is also controlled by external mass transfer ($t_{gas}/t_{mass\ ext} \sim 1$).

- Under an inert atmosphere, gasification is controlled only by chemical kinetics at 1000°C ($t_{gas}/t_{mass\ ext} \sim 10$) or by both kinetics and external mass transfer at 1200°C and 1400°C ($t_{gas}/t_{mass\ ext} \sim 1$), for both particle sizes.

Complete gasification conversion may be achieved at 1400°C in the case of a wet atmosphere, as the required time for a complete gasification, inferior to 1 s, is much lower than the particle residence time. For experiments at 1200°C under a wet atmosphere or 1400°C under a inert atmosphere, the characteristic times of chemical and/or mass transfer phenomena have the same order of magnitude as the particle residence time: char gasification seems then to be possible but a complete conversion is uncertain. At 1000°C, char gasification is not likely to occur, as the chemical kinetics is too slow.

#### *2.1.2.3. Mass transfer and gasification in the case of soot*

The results of characteristic time calculations relative to mass transfer phenomena and to soot gasification with $H_2O$ and $CO_2$ are presented in Table 21. The reagent concentration considered for the calculations of the characteristic times for soot were the same as those used for char gasification analysis. As in the case of char gasification, the type of reagent - $H_2O$ and $CO_2$ - does not have a significant influence on the characteristic times, thus gasification with 1 mol% $CO_2$ is not shown in Table 21.

Soot particle is here considered as an agglomerate of spherules with a size of 100 µm, which is the highest one found in literature (Fujita & Ito, 2002; Zhang et al., 2006). It was selected in order to study gasification in the less favored situation for transfers. Due to its low density, soot behaves like an aerosol in the gas stream, thus the particles are not subjected to slipping in the gas. Soot particles have then the same residence time as the gas released during the pyrolysis of 0.35 mm and 0.80 mm beech particles, which is about 4.0 s. This supposes that soot is formed at the top of the reactor.

**Table 21. Characteristic times relative to mass transfer and soot gasification**

| Temperature (°C) | | | 1000 | 1200 | 1400 |
|---|---|---|---|---|---|
| Characteristic times (s) | Internal mass transfer | 25 mol % $H_2O$ | $3.10^{-4}$ | $6.10^{-4}$ | $6.10^{-4}$ |
| | | 1 mol % $H_2O$ | $3.10^{-4}$ | $6.10^{-4}$ | $6.10^{-4}$ |
| | External mass transfer | 25 mol % $H_2O$ | 0.01 | 0.01 | 0.009 |
| | | 1 mol % $H_2O$ | 0.2 | 0.3 | 0.3 |
| | Gasification * reaction | 25 mol % $H_2O$ | 45 | 4 | 0.7 |
| | | 1 mol % $H_2O$ | 1000 | 100 | 17 |
| Residence time of the particle (s) | | | 4.0 | | |
| Dimensionless numbers | $Bi_M\ (t_{mass\ int}/t_{mass\ ext})$ | 25 mol % $H_2O$ | $\sim 10^{-2}$ | $\sim 10^{-2}$ | $\sim 10^{-2}$ |
| | | 1 mol % $H_2O$ | $\sim 10^{-3}$ | $\sim 10^{-3}$ | $\sim 10^{-3}$ |
| | $t_{gas}/t_{mass\ ext}$ | 25 mol % $H_2O$ | $\sim 10^{3}$ | $\sim 10^{2}$ | $\sim 10$ |
| | | 1 mol % $H_2O$ | $\sim 10^{3}$ | $\sim 10^{2}$ | $\sim 10$ |

* Mean value obtained from the soot gasification kinetics of De Soete (1988)

The same trends about the evolution of the characteristic times in function of temperature, particle size and reagent partial pressure are observed for soot and for char gasification related phenomena.

With the dimensionless $Bi_M$ number, it can be observed that the characteristic time of external mass transfer is higher than that of internal mass transfer ($Bi_M \sim 10^{-2}$ - $10^{-3}$) for a $H_2O$ concentration of 1 mol% and 25 mol %. In all the cases, the gasification characteristic time is higher than that of the external mass transfer ($t_{gas}/t_{mass\ ext} \sim 10 - 10^5$) and so than that of the internal mass transfer. Therefore, soot gasification is kinetically controlled.

A complete conversion of soot particles can only be expected at 1400°C with 25 mol% of $H_2O$, where the gasification characteristic time is inferior to one second. At lower temperature or lower $H_2O$ concentration, soot gasification is very unlikely to occur.

Comparing Table 19, Table 20 and Table 21, one can see that the characteristic time of gasification for soot is higher than the characteristic times of gasification and external mass transfer for char. It can be then expected that char gasification occurs more rapidly than soot gasification.

Note that the integral pyrolysis and char gasification regimes in a temperature range of 1000°C to 1500°C, and a particle size range of 0.1 mm to 1 mm are presented in Appendix E.

### *2.1.3. Summary*

Through a characteristic time analysis, the wood pyrolysis and char/soot gasification were characterized under the experimental conditions of the DTR.

Heat transfer and chemical phenomena linked to pyrolysis appear to be very fast, needing less than one second to occur, which is an enough time for complete conversion of wood into char under the explored conditions. The particle heating is mainly controlled by external convection and internal conduction. When temperature and particle size are increased, pyrolysis tends to pass from an intermediary regime into a regime controlled by heat transfers.

Char or soot gasification is in most of the cases a slower phenomenon than pyrolysis. An incomplete conversion of char is expected under almost every experimental condition, due to a limitation from its low chemical kinetics and also from a low external mass transfer rate, which is the case of experiments under an inert atmosphere. A complete conversion of char or soot is expected to occur only at 1400°C for a steam concentration of 25 mol%. In this case, gasification may occur almost simultaneously as wood pyrolysis.

In function of the experimental conditions, char gasification can be controlled only by chemical kinetics, or by both external mass transfer and chemical kinetics. A kinetically controlled regime is favored when the temperature and the reagent concentration are increased, and the particle size is decreased. At 1200°C and 1400°C for experiments under an inert atmosphere or at 1400°C with the 0.50 mm char particles, the external mass transfer should also control the process. Note that the internal mass transfer can be neglected in all the cases. Concerning soot gasification, the process is always kinetically controlled.

This characteristic time analysis will be compared with the experimental results in next chapter and be used as a support for the interpretation of the phenomena occurring during the experiments. Besides, it will also help for the modeling of these phenomena.

## 2.2. Calculations at the thermodynamic equilibrium

The thermodynamic equilibrium calculations (refer to section 2.4. of Chapter “State of the Art”) were performed with the GEMINI software that proceeds by minimization of the free enthalpy: a solver minimizes the Gibbs energy of the closed system to give the composition of the mixture. The input data are the amount of elements C, H, O in the system, temperature and pressure.

This tool relies on thermodynamic databases that contain the values of the standard Gibbs energy of a complete collection of components:

- hydrocarbons up to $C_{35}$, which can contain oxygen or nitrogen groups;
- a large list of non hydrocarbon gas from the combination of C, H, O and N;
- graphite.

The major gases involved in biomass gasification are included in this database: $CH_4$, $C_2$ species, $C_6H_6$, $H_2O$, $H_2$, CO, $CO_2$. Note that in thermodynamic calculations, both char and soot are assumed to be pure carbon in graphitic form.

Figure 47 and Figure 48 show the product yields from the calculations at the thermodynamic equilibrium under the experimental conditions under an inert atmosphere and a wet atmosphere respectively. In Figure 48, $H_2O$ was not represented because its concentration is much higher than the other products ones.

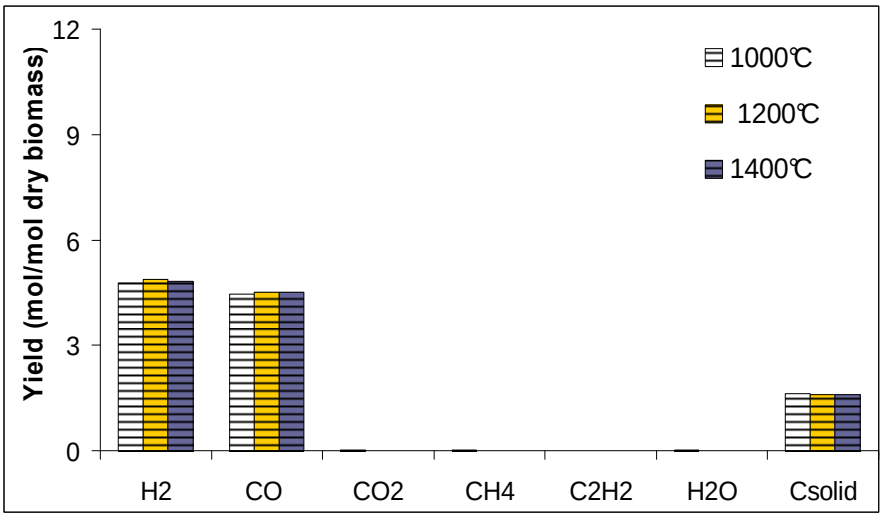


**Figure 47 Mass yields of the products from beech particles thermal decomposition under an inert atmosphere at thermodynamic equilibrium**

Under an inert atmosphere, the decomposition of biomass mainly leads to the formation of $H_2$, CO and carbonaceous solid, whose yields remain almost unchanged between 1000°C and 1400°C. Only traces of $CH_4$, $CO_2$ and $H_2O$ are calculated at 1000°C. Therefore, the complete conversion of biomass into $H_2$, CO and solid during its decomposition can be then considered as achieved from 1000°C.

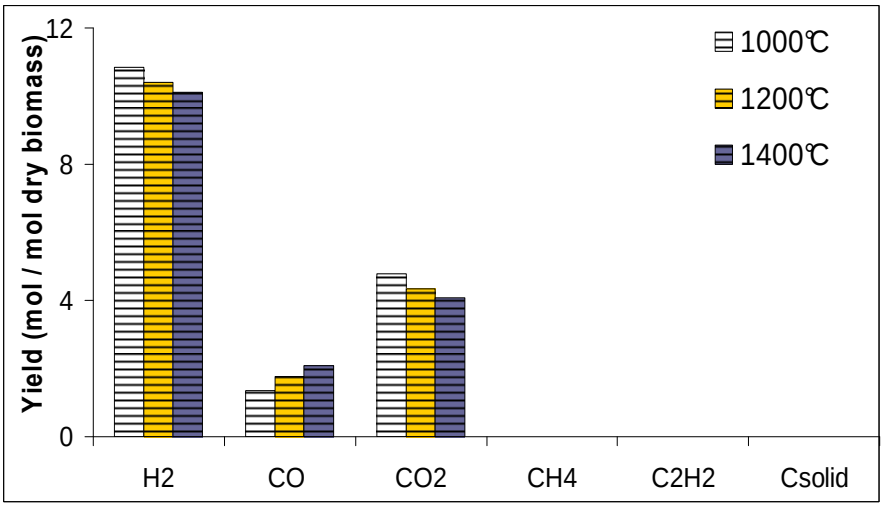


**Figure 48 Mass yields of the products from beech particles thermal decomposition under a wet atmosphere at thermodynamic equilibrium**

The products from the biomass decomposition under a wet atmosphere are $H_2$, CO and $CO_2$, which are different from those obtained under an inert atmosphere: under a wet atmosphere, $CO_2$ is observed unlike $C_{solid}$. The $H_2$ yield is almost tripled and the CO yield decreases by a factor 2 under a wet atmosphere compared to an inert one. A slight effect of the temperature can also be noticed: as temperature is increased, the yields of $H_2$ and $CO_2$ decrease whereas the yield of CO increases. These variations can be attributed to the water gas shift reaction whose indirect path is favored at higher temperature.

In summary, the complete decomposition of biomass into syngas seems to be thermodynamically possible from 1000°C. The products from this decomposition are different depending on the steam content in the atmosphere: $H_2$, CO and $C_{solid}$ under an inert atmosphere, $H_2$, CO and $CO_2$ in the case of a wet atmosphere. The concentrations of $H_2$, CO and $CO_2$ change with temperature in relation with the modification of the WGS constant equilibrium. This reaction is then the only one which can induce an evolution of the system at the thermodynamic equilibrium under the explored conditions.

Thermodynamic equilibrium calculations will be compared in next chapter to the experimental results obtained in the DTR in order to determine if the overall system reaches thermodynamic equilibrium and if not, to identify the reasons why.

# Résumé du Chapitre 3 : Outils et Méthodes

Ce chapitre décrit l'installation expérimentale utilisée pour l'étude de la gazéification de la biomasse dans les conditions d'un réacteur à flux entraîné, à savoir des vitesses de chauffage et des températures élevées, un temps de séjour court (< 5 s), et une taille de particules de quelques centaines de micromètres.

La décomposition thermique de bois (ici sciure de hêtre) est étudiée dans un four à chute localisé à l'Ecole des Mines d'Albi - Carmaux. Les expériences sont effectuées sous atmosphère inerte ou sous atmosphère contenant 25%mol de vapeur d'eau, à plusieurs températures (1000°C, 1200°C et 1400°C) et avec deux tailles de particules (0,35 mm et 0,80 mm).

Le débit total de gaz introduit dans le réacteur est de 18,8 $NL.min^{-1}$, 15,9 $NL.min^{-1}$, 13,8 $NL.min^{-1}$ et 12,1 $NL.min^{-1}$ pour les expériences à 800°C, 1000°C, 1200°C et 1400°C respectivement, de manière à conserver une vitesse des gaz constante et donc un temps de séjour constant quelle que soit la température. Les conditions dans le four à chute sont considérées comme diluées: le gaz produit par la décomposition thermique de la biomasse ne change ni le débit total de gaz ni la température. Le débit d'alimentation de la biomasse est compris entre 0,3 $g.min^{-1}$ et 1,3 $g.min^{-1}$.

L'échantillonnage de gaz et de solide dans le four à chute est réalisé à deux hauteurs différentes: à la sortie et au milieu de la zone réactionnelle. A 1400°C, aucun échantillonnage n'a pu être réalisé au milieu de la zone réactionnelle, car le matériau de la canne d'échantillonnage n'était pas en mesure de résister à une telle température.

Le temps de séjour du gaz est de 2 s et 4 s en échantillonnant respectivement à la moitié et à la fin de la zone réactionnelle. Les temps de séjour des particules de 0,35 mm et 0,80 mm sont respectivement de 3,8 s et 2,7 s à la sortie du réacteur, et de 1,9 s et 1,3 s à la moitié du réacteur.

Le gaz échantillonné passe par plusieurs analyseurs (µGC, IRND, IRTF, psychromètre, catharomètre, FID, analyseur paramagnétique) qui mesurent la fraction molaire de plusieurs espèces gazeuses ($H_2$, CO, $CO_2$, $H_2O$, $CH_4$, $C_2H_2$, $C_2H_4$, $C_2H_6$, $C_6H_6$). Le résidu solide récupéré lors des expériences, composé de suies et de char, est caractérisé grâce à des analyses de composition (C, H, O, cendres), des observations au microscope électronique à balayage, et des mesures de réactivité par analyse thermogravimétrique.

Ce dernier type d'analyse est réalisé dans une thermobalance en mesurant la perte de masse d'un échantillon lors de sa gazéification à une température donnée. Pour cela, la gazéification a été étudiée entre 750°C et 850°C pour le char, et 910°C et 980°C pour les suies, à une pression partielle de vapeur d'eau de 0,05 bar ou 0,20 bar, avec quelques mg d'échantillon.

Par ailleurs, ce chapitre présente une étude préliminaire, comprenant d'une part une analyse des temps caractéristiques et d'autre part, des calculs à l'équilibre thermodynamique. L'analyse des résultats obtenus par ces études théoriques est utile pour l'interprétation des résultats expérimentaux et de modélisation présentés dans les chapitres suivants.

Les temps caractéristiques relatifs à la pyrolyse du bois et à la gazéification du char et des suies ont été déterminés dans les conditions expérimentales du four à chute:

- Les phénomènes physiques et chimiques liés à la pyrolyse semblent être très rapides, nécessitant moins d'une seconde pour se produire, ce qui est un temps suffisant pour une conversion complète au cours des expériences. Le chauffage des particules est principalement contrôlé par convection externe et conduction interne. Lorsque la température et la taille des particules augmentent, la pyrolyse passe d'un régime intermédiaire à un régime limité par les transferts de chaleur.
- La gazéification du char et des suies est dans la plupart des cas plus lente que la pyrolyse. Une conversion incomplète du char est prévue dans presque toutes les conditions expérimentales, en raison d'une cinétique chimique limitante et éventuellement de transferts externes de masse ralentis sous une faible pression partielle de vapeur d'eau. Une gazéification complète du char et suies n'est prévue qu'à 1400°C pour une pression partielle de vapeur

de 0,25 bar. En fonction des conditions expérimentales, la gazéification du char peut se produire en régime chimique, ou en régime limité par la cinétique chimique et le transfert de masse externe.

D'après les calculs à l'équilibre thermodynamique, la décomposition complète de la biomasse en gaz de synthèse serait possible à partir de 1000°C. Les produits de cette décomposition sont différents selon la teneur en vapeur d'eau dans l'atmosphère: $H_2$, CO et $C_{solide}$ sous atmosphère inerte; $H_2$, CO et de $CO_2$ dans le cas d'une atmosphère humide. Les concentrations en $H_2$, CO et $CO_2$ changent avec la température en suivant la constante d'équilibre de la réaction de water – gas shift. Cette réaction est alors le seul phénomène qui peut provoquer l'évolution du système à l'équilibre thermodynamique.

# Chapter 4: Experimental Results

This chapter presents the results of beech particles gasification experiments in a drop tube reactor. The gas yields were measured during the experiments and the collected solid residues, char and soot, were characterized later.

In the first two parts of this chapter, the thermal decomposition of 0.35 mm and 0.80 mm beech particles is studied under inert and wet atmospheres, by sampling at the middle and the bottom of the reactor. This study highlights the effect of temperature, steam content, residence time and particle size on wood gasification.

The second part of this chapter is dedicated to the description of soot and char characteristics, such as morphology, composition and reactivity, which are studied as a function of the operating conditions.

Note that the term "particles thermal decomposition", used here to describe the experiments under inert and wet atmospheres, respectively refer to the classical terms "biomass pyrolysis" and "biomass gasification" used in literature. The use of the "thermal decomposition" term in the present study avoids confusing the whole process to the elementary steps, i.e. particles devolatilisation and char gasification.

## 1. Thermal decomposition of 0.35 mm beech particles between 800°C and 1400°C

Note that the results of the DTR experiments are expressed in mass yields ("g/g dry biomass" or "$g/g_{db}$") or molar yields ("mol/mol dry biomass" or "$mol/mol_{db}$") with respect to the dry biomass.

### 1.1. Thermal decomposition under an inert atmosphere

#### *1.1.1. Gas, tar, soot and char yields*

Figure 49 shows the mass yields of the products of the thermal decomposition of 0.35 mm wood particles under an inert atmosphere as a function of temperature. We remind that the residence time of gas and 0.35 mm particles is 4 s. The elemental repartition of C, H and O in the products is provided in Figure 50.

The term "tar + soot" corresponds to the unmeasured compounds, whose yields were determined by difference from a mass balance, as explained in section 1.4.3 of "Materials and Methods". These compounds are assumed to be tar and/or soot but no direct distinction between them was experimentally possible. Note that the gas yield in Figure 49 includes the initial moisture of the beech particles, that is of 7 w%.

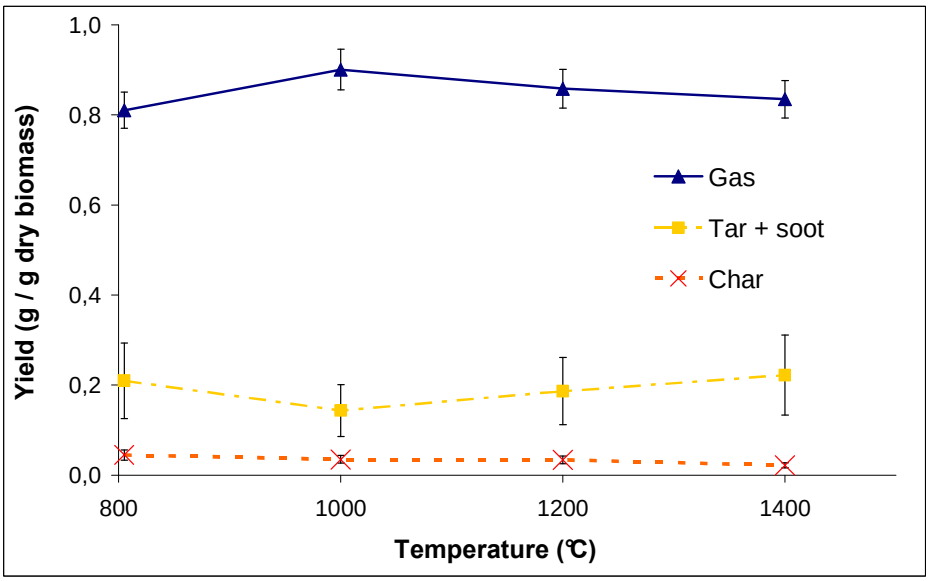


**Figure 49. Mass yields of the products from the 0.35 mm particles thermal decomposition under an inert atmosphere at 800°C, 1000°C, 1200°C and 1400°C**

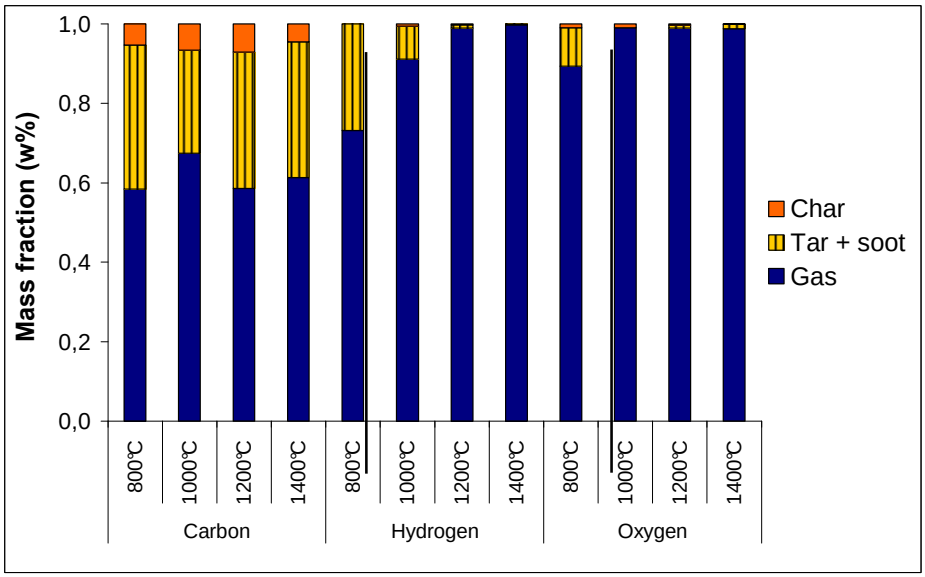


**Figure 50. Mass fraction of C, H and O in the products from the 0.35 mm particles thermal decomposition under an inert atmosphere at 800°C, 1000°C, 1200°C and 1400°C**

Figure 49 shows that the thermal decomposition of 0.35 mm beech particles produces mainly gas, more than 0.80 $g/g_{db}$, and char in lower amount, less than 0.05 $g/g_{db}$. The sum of tar and soot yields is about 0.20 $g/g_{db}$.

These yields remain almost unchanged as temperature varies, even if some slight differences can be observed. At 1000°C, the gas yield reaches its maximum value - 0.90 $g/g_{db}$ - and consequently the sum of tar and soot yields reaches its minimum value - 0.15 $g/g_{db}$ -. These differences are however in the limit of the error bar and have to be considered with caution. The char yield at 1400°C - 0.025 $g/g_{db}$ - seems to be slightly inferior to the yields measured at lower temperatures - 0.04 to 0.05$g/g_{db}$ -.

With Figure 50, it can be seen that the carbon fraction in the products remains almost similar at the different temperatures, whereas the hydrogen and oxygen contents vary with temperature. As temperature increases, the hydrogen and oxygen fractions in "tar + soot" are lower and their fractions in gas are higher. Above 1200°C, more than 95 w% of oxygen and hydrogen are measured in gas.

A mean formula for "tar + soot" can be established from the mass balance presented in Figure 50 at each temperature. This gives $C_nH_nO_{0.2n}$ at 800°C, $C_nH_{0.4n}$ at 1000°C and a compound almost only composed of carbon at 1200°C and 1400°C.

### *1.1.2. Individual gas yields*

Figure 51a and b displays the molar yields versus temperature of respectively non hydrocarbon gases and light hydrocarbons, for experiments under an inert atmosphere with 0.35 mm particles.

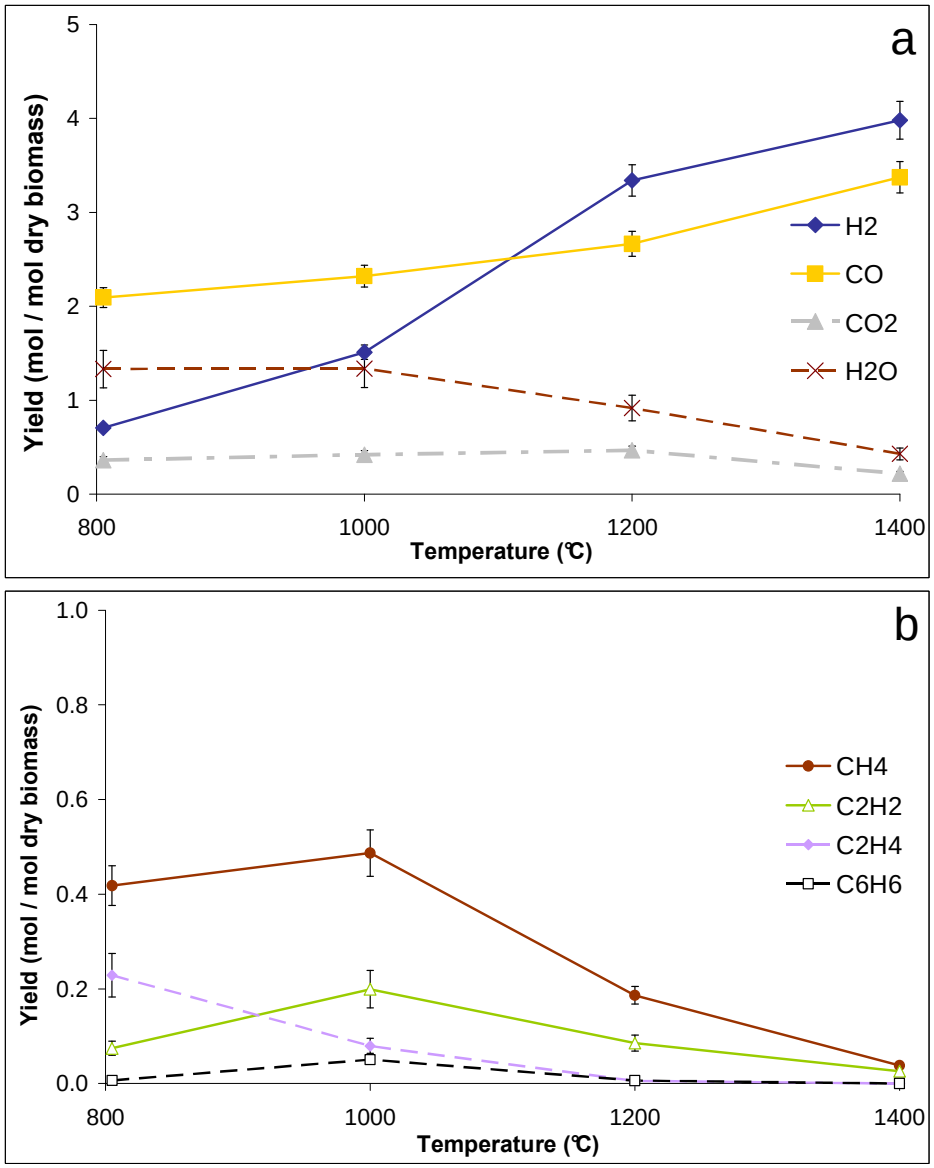


**Figure 51. Molar yields of non hydrocarbon gas (a) and light hydrocarbons (b) from the 0.35 mm particles thermal decomposition under an inert atmosphere at 800°C, 1000°C, 1200°C and 1400°C**

The main gases from the thermal decomposition of biomass are: $H_2$, CO, $CO_2$, $H_2O$, $C_2H_2$, $C_2H_4$ and $C_6H_6$ as classically observed in the literature. Note that a very low $C_2H_6$ yield - 0.03 mol/$mol_{db}$ - was measured at 800°C.

The comparison between Figure 51a and Figure 51b shows that the non hydrocarbon gases yields are higher than the hydrocarbon gases yields with yields respectively higher and lower than 0.5 mol/$mol_{db}$. The major gas is CO at 800°C and 1000°C, and $H_2$ at 1200°C and 1400°C. Among the hydrocarbons, $CH_4$ is the major one.

As often observed in literature, temperature has an important influence on the gas compounds yields. Indeed, the increase of temperature leads to higher $H_2$ and CO yields. In particular, the $H_2$ yield is multiplied by about 4 between 800°C and 1400°C. The CO yield increase is more moderate, and is 50% higher at 1400°C than at 800°C. The $H_2O$ yield is steady between 800°C and 1000°C, and then decreases between 1000°C and 1400°C. This result is very similar for $CO_2$ yield which remains steady between 800°C and 1200°C, and then decreases between 1200°C and 1400°C.

It can be observed that the $CH_4$, $C_2H_2$ and $C_6H_6$ yields are higher at 1000°C than at 800°C, and then drastically decrease between 1000°C and 1400°C. On the contrary, the $C_2H_4$ yield continuously decreases in the temperature range of experiments. At 1200°C, almost no $C_2H_4$ and $C_6H_6$ are measured. At 1400°C, only $CH_4$ and $C_2H_2$ can still be quantified - 0.05 $mol/mol_{db}$ -.

### 1.1.3. Discussion

As shown in Figure 49, the thermal decomposition of 0.35 mm beech particles produces mainly gas and very low amounts of char, which is typical of biomass rapid pyrolysis (refer to section 5 of Chapter "Fundamental concepts").

At 800°C, the gas composition is the result of the early stage of pyrolysis phenomena, which are particle drying and devolatilisation, as well as secondary gas reactions. Figure 49, Figure 50 and Figure 51 show that above 800°C product yields significantly change with temperature. All of these changes can find an explanation in the reactions which are summarized below:

- cracking reactions, consisting in the decomposition of large molecules into smaller units;
- polymerization reactions, consisting in the formation of a large molecule from smaller ones, which can lead to soot formation and release high amounts of $H_2$;
- reforming reactions, whereby $H_2$ and CO are formed from hydrocarbons;
- gasification reactions, whereby $H_2$ and CO are formed from carbonaceous solid.

These reactions are well described in Section 3 and section 4 of Chapter "Fundamental Concepts".

Note that the wood moisture - 0.075 $g/g_{db}$ - is lower than the $H_2O$ yield measured during the experiments at 800°C - 1.3 $g/g_{db}$ -. This means that $H_2O$ during the experiments comes from both initial moisture evaporation and thermal decomposition reactions. This compound is produced in a high enough amount to react with 1/5 of the carbon contained in the wood and to completely gasify the char.

#### 1.1.3.1. Tar and soot evolution with temperature

In Figure 49, it can be seen that the sum of tar and soot yields varies between 0.15 $g/g_{db}$ and 0.20 $g/g_{db}$ in the temperature range of 800 - 1400°C. Even if this variation is slight, important changes in composition occur as a function of temperature, as it can be appreciated from the "tar + soot" mean formula established from Figure 50.

At 800°C, the mean formula $C_nH_nO_{0.2n}$ presents a low O/C ratio, 0.2, and a similar content in carbon and hydrogen. As no soot formation has been reported in literature at this level of temperature, "tar + soot" is assumed to be only tar, which can be composed of a mixture of aromatic and, in a lower proportion, of oxygen containing hydrocarbons according to the mean formula.

At 1000°C, the mean formula $C_nH_{0.4n}$ contains no oxygen and has a quite low H/C ratio, 0.4, which could correspond to a mixture of PAHs and soot. The presence of a few soot at 1000°C is confirmed by SEM observations of our solid samples, even if no soot could be collected at the outlet of the reactor at this temperature.

At 1200°C and 1400°C, the "tar + soot" mean formula mainly contains carbon, like soot whose carbon content is higher than 95 w%, which suggests that only soot is present at these temperatures. This hypothesis is verified by experimental observations: no condensed tar could be observed in the experimental unit. Besides, the sum of $CH_4$, $C_2$ species and $C_6H_6$ molar fractions in the exhaust gas, measured by µ-GC and FTIR analyzers, was the same than the molar fraction of the total hydrocarbons measured by FID analyzer. This means that no significant amounts of hydrocarbons, apart from the light hydrocarbons, were detected at 1200°C and 1400°C. The assumption of no tar from 1200°C can also be seen in the tar composition analysis performed by Zhang (2010) during wood thermal decomposition experiments in a DTR.

The evolution of tar and soot yields with temperature can be explained by the cracking and polymerization reactions. It is well known that tar cracking is the first gas phase reaction which occurs during the biomass thermal decomposition for temperatures higher than 600°C, and that it mainly concerns oxygen containing hydrocarbons. The cracking of oxygen containing hydrocarbons seems to be completely achieved from 1000°C, as no oxygen in hydrocarbon is then determined. At 1000°C, the influence of polymerization can be clearly seen through the formation of PAHs and soot. At 1200°C and 1400°C, polymerization is highly favored and leads to the formation of soot only.

#### *1.1.3.2. Char evolution with temperature*

In Figure 49, the char yield for experiments at 800°C, 1000°C and 1200°C is about 0.04 – 0.05 $g/g_{db}$, which corresponds to the yield of a char from completely pyrolysed beech particles, according to the results of Chen (2009). So the 0.35 mm particles are supposed to be completely pyrolysed in our conditions. This result was expected from the pyrolysis characteristic time analysis (refer to section 2.1.2.1 of Chapter "Materials and Methods"), which predicts pyrolysis occurs in less than 1 s due to the high heating rate and chemical kinetics.

The char yield at 1400°C, 0.025 $g/g_{db}$, is lower than the yields determined below this temperature, which is probably due to its gasification with the $H_2O$ and $CO_2$ released during pyrolysis. The gasification characteristic time analysis, performed in section 2.1.2.2 of Chapter "Materials and Methods", suggests that a possible gasification of char for 0.35 mm particles could occur at 1400°C.

#### *1.1.3.3. Gas evolution with temperature*

As it can be observed in Figure 49, gas yield exhibits very low variations - 0.80 to 0.90 $g/g_{db}$ - between 800°C and 1400°C. However, Figure 51 shows that the yields of each individual gas compound considerably change with temperature. As temperature increases, light hydrocarbons, $H_2O$ and $CO_2$ yields tend to decrease, whereas $H_2$ and CO yields tend to increase. Most of these variations are a consequence of the reactions involving hydrocarbons, namely cracking, polymerization and reforming. This is discussed in details below.

Tar cracking can be verified by the presence of light hydrocarbons at 800°C, especially $CH_4$ and $C_2H_4$. From 1000°C, all the oxygen containing hydrocarbons are cracked (section 1.1.3.1), which explains the higher CO yield at 1000°C compared to 800°C (Figure 51a).

As discussed in section 1.1.3.1, polymerization is possible from 1000°C. This type of reaction can explain the hydrocarbons yields decrease and the $H_2$ yield increase as temperature increases. Note that the maximum gas yield is measured at 1000°C, which surely corresponds to the highest production of gas by cracking reactions combined to the lowest consumption of light hydrocarbons by polymerization.

In order to better understand the evolution of each light hydrocarbon yield with temperature, Table 22 summarizes the studies found in literature about the thermal decomposition of these compounds under an inert atmosphere.

**Table 22. Range of the temperature decomposition of light hydrocarbons under an inert atmosphere**

| Compounds | Main decomposition product(s) | Range of conversion temperature (Hiblot, 2010; Valin et al., 2009) |
|---|---|---|
| $CH_4$ | $C_2$ | 1000 – 1600°C |
| $C_2H_6$ | $C_2H_4$ | <1000°C |
| $C_2H_4$ | $C_2H_2$ | 900 – 1300°C |
| $C_2H_2$ | $C_6H_6$, PAH | 900 – 1600°C |
| $C_6H_6$ | $CH_4$, $C_2H_4$, PAH | 900 – 1300°C |

In Table 22, it can be seen that above 1000°C, the decomposition of all hydrocarbons is possible, and that a complete conversion at 1400°C can be expected for $C_2H_6$, $C_2H_4$ and $C_6H_6$ only. The hydrocarbons $C_2H_2$ and $CH_4$ need a higher temperature, at minimum 1600°C, for their complete conversion. Note that the decomposition of $C_2H_6$ is completely achieved at 1000°C. These trends agree with the experimental results presented in Figure 51b.

The decomposition of $CH_4$, $C_2H_6$ and $C_2H_4$ can, as shown in Table 22, lead directly or indirectly to the formation of $C_2H_2$ from which $C_6H_6$ is produced. Subsequently, $C_2H_2$ and $C_6H_6$ polymerize into PAHs, and finally soot can be synthesized from $C_2H_2$ and PAHs, as introduced in section 3.1 of Chapter "Fundamental concepts". The $C_2H_2$ and $C_6H_6$ yields peaks observed at 1000°C can be correlated to a lower soot formation at this temperature than at 1200°C and 1400°C.

The hydrocarbons yields decrease observed with temperature may also be attributed to hydrocarbon reforming reactions for experiments at 1200°C and 1400°C. Reforming reactions are put into evidence by the higher CO yield and the lower $H_2O$ and $CO_2$ yields at 1200°C and at 1400°C. Nevertheless, these variations are much slighter than the $H_2$ and soot yields variations observed from 1200°C. Therefore, the contribution of reforming reactions in hydrocarbons conversion is minor in comparison with polymerization.

The slight char gasification observed at 1400°C (section 1.1.3.2) may also contribute to the decrease of $H_2O$ and $CO_2$ yields and to the increase of CO and $H_2$ yields.

Note that the yields of the permanent gases are susceptible to be modified via water gas shift reaction. The reverse path of this reaction is favored at high temperatures. No visible influence of the WGS has been observed in the experimental results.

## 1.2. Thermal decomposition under a wet atmosphere

### *1.2.1. Gas, tar, soot and char yields*

Figure 52 compares the mass yields of the products from the thermal decomposition of 0.35 mm particles under a wet atmosphere - 25 mol% of $H_2O$ - and an inert atmosphere at three temperatures - 1000°C, 1200°C and 1400°C -. The latter results were already described and discussed in section 1.1. For all experiments, the residence time of gas and particles was about 4 s.

Note that the gas yields in Figure 52 concern dry gas, which implies that the $H_2O$ yield measured during experiments under an inert atmosphere is not included.

The thermal decomposition of wood particles under a wet atmosphere produces mainly gas, superior to 0.90 $g/g_{db}$. The total gas yield increases with temperature, especially between 1000°C and 1200°C. The sum of tar and soot yields is about 0.08 $g/g_{db}$ at 1000°C under a wet atmosphere. As for experiments under an inert atmosphere

(refer to section 1.1.3.1), the assumption is made that no more tar is present at 1200°C and 1400°C. The soot yield is then about 0.05 $g/g_{db}$ at these temperatures.

Char yield is very low, inferior to 0.04 $g/g_{db}$, and decreases as temperature increases. At 1400°C no char was observed.

Through the comparison of the products yields under an inert and a wet atmosphere in Figure 52, it can be seen that, at each temperature, the gas yield is higher whereas the "tar + soot" and char yields are lower for experiments under a wet atmosphere. These differences are enhanced at 1200°C and 1400°C.

At 1200°C and 1400°C, the sum of all products yields is much higher for wet atmosphere experiments, around 50% more. At 1000°C, the differences in yields between the two atmospheres are more moderate, and char yield is approximately the same for both types of experiments.

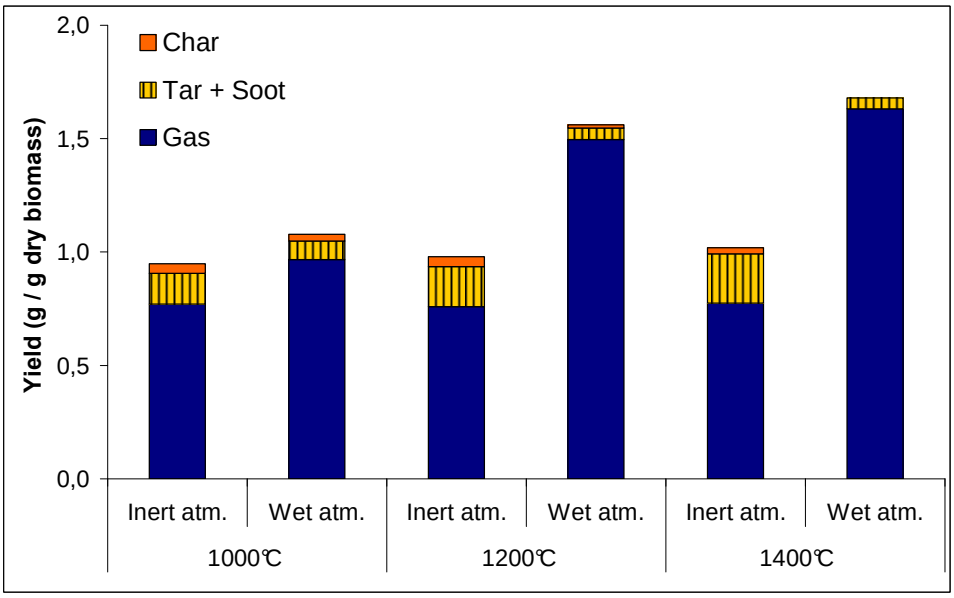


**Figure 52. Mass yields of the products from the 0.35 mm particles thermal decomposition under inert and wet atmospheres at 1000°C, 1200°C and 1400°C**

### *1.2.2. Individual gas yields*

The molar yields of the gas compounds produced by the thermal decomposition of 0.35 mm particles under a wet and an inert atmosphere are compared in Figure 53a for $H_2$, CO, $CO_2$ and Figure 53b for light hydrocarbons. The species $H_2O$ is not included in this comparison, as it is in high excess with respect to the other compounds under a wet atmosphere.

The gas produced under a wet atmosphere is mainly composed of non hydrocarbon gases: $H_2$, CO and $CO_2$ represent more than 90 mol% of the gas species represented in Figure 53a and b. The $H_2$ and $CO_2$ yields tend to increase with temperature, even if the $CO_2$ yield seems to reach a plateau above 1200°C. Note that the $H_2$ and $CO_2$ yields are almost three times higher at 1200°C than at 1000°C. The CO yield is lower at 1200°C than at 1000°C but then higher at 1400°C than at 1200°C.

$CH_4$ is the major species among the hydrocarbon gases, representing more than 75 mol% of the hydrocarbon gases at 1000°C and 1200°C, and is followed by $C_2H_2$. Each hydrocarbon yield decreases as temperature increases. At 1200°C, $C_2H_4$ and $C_6H_6$ are not detectable, and at 1400°C no hydrocarbon gas at all is measured under a wet atmosphere.

Through Figure 53, the yields of permanent gases obtained from the wood particles thermal decomposition under a wet atmosphere can be compared to those obtained under an inert atmosphere.

The $CO_2$ and $H_2$ yields are at least twice as high under a wet atmosphere as under an inert one. At 1200°C and 1400°C, the $CO_2$ yield is even 15 times higher. On the contrary, the CO yields are the same at 1000°C in the two atmospheres, and lower at 1200°C and 1400°C under a wet atmosphere.

The yields of all hydrocarbons, except $CH_4$ at 1000°C and 1200°C, are the same or lower under a wet atmosphere than under an inert one. The $CH_4$ yield is rather surprisingly higher under an inert atmosphere at 1000°C and even more at 1200°C.

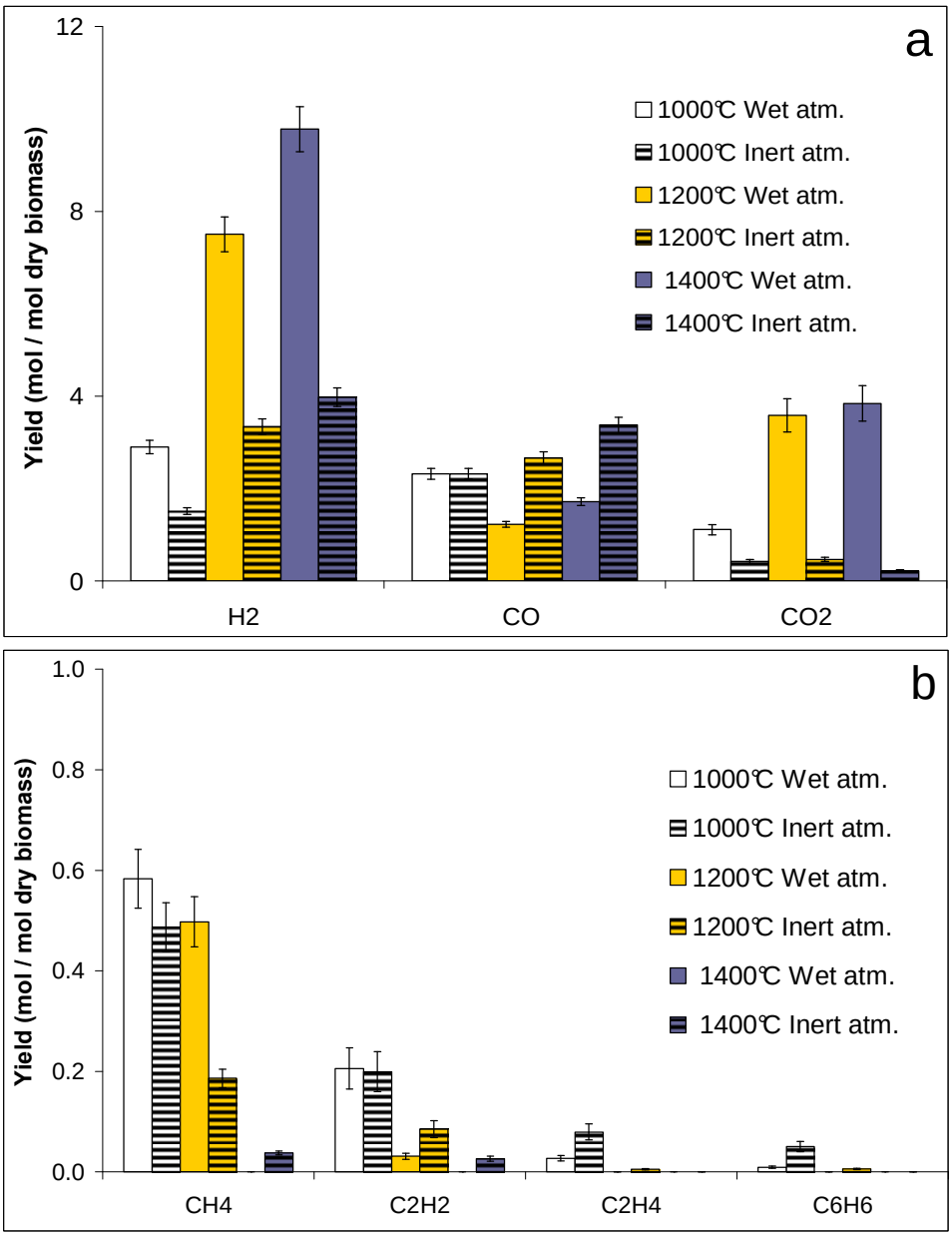


**Figure 53. Molar yields of non hydrocarbon gas (a) and light hydrocarbons (b) for the 0.35 mm particles thermal decomposition under inert and wet atmospheres at 1000°C, 1200°C and 1400°C**

### 1.2.3. Discussion

On the basis of the observations made in previous sections, an attempt to describe the effect of temperature under a wet atmosphere, and the effect of $H_2O$ on products yields is performed in this section.

#### 1.2.3.1. Influence of temperature

As shown before, as temperature increases from 1000°C to 1400°C, light hydrocarbons, tar and char yields decrease. This can be seen in Figure 54, which shows the repartition of carbon in the products for 0.35 mm wood particles under a wet atmosphere. The fraction of carbon in an oxidized form - CO and $CO_2$ - increases with temperature, and so the carbon fractions in char, hydrocarbons and soot decrease. Two types of chemical reactions can explain these changes: hydrocarbons reforming reactions and carbonaceous solid gasification, which both produce CO and $H_2$. Moreover, the water-gas shift reaction influences the balance between CO and $CO_2$ yields.

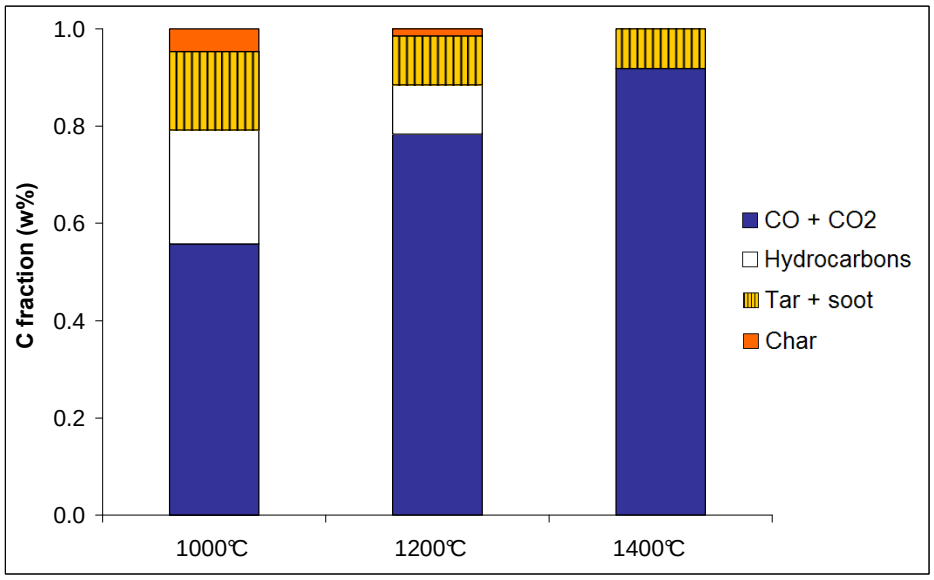


**Figure 54. Carbon repartition in the products from the 0.35 mm particles thermal decomposition under a wet atmosphere at 1000°C, 1200°C and 1400°C**

According to our results, gasification, reforming reactions, and the WGS reaction play a major role in the evolution of gas yields between 1000°C and 1400°C, and give a gas very rich in $H_2$.

#### 1.2.3.2. Influence of steam in the atmosphere

As shown before, the hydrocarbons, soot, char and CO yields are lower under a wet than under an inert atmosphere. In counterpart, the $H_2$ and $CO_2$ yields are higher.

The differences in hydrocarbons yields measured between an inert and a wet atmosphere are in agreement with the experimental results of Hiblot (2010) and Valin (2009) which are summarized in Table 23. In these studies, gas phase experiments on light hydrocarbons conversion under a wet atmosphere were performed, and showed that 25 mol% of $H_2O$ enables to lower the temperature of conversion of some representative light hydrocarbons.

**Table 23. Comparison of the temperature of complete conversion (temperature from which hydrocarbons are undetectable) for $CH_4$, $C_2H_2$ and $C_6H_6$ between an inert atmosphere and a wet atmosphere composed 25 mol% of $H_2O$ (Hiblot, 2010; Valin et al., 2009)**

| Compound | Complete conversion – inert atmosphere | Complete conversion – 25 mol% of $H_2O$ atmosphere |
|---|---|---|
| $CH_4$ | 1600°C | 1400°C |
| $C_2H_2$ | 1600°C | 1400°C |
| $C_6H_6$ | 1300°C | 1100°C |

The higher conversion of hydrocarbons under a wet atmosphere than under an inert one at a given temperature is probably due to steam reforming reactions, which depend on the $H_2O$ content in gas.

As for $CH_4$, as said before, its yield is surprisingly higher under a wet atmosphere than under an inert one at 1000°C and 1200°C. This same result was obtained in experiments focusing on methane reforming (Hiblot, 2010; Valin et al., 2009). Two possible explanations can be given: $H_2O$ favors the formation of $CH_4$ and/or it inhibits the decomposition of this hydrocarbon for temperatures below 1300°C, as proposed by Hiblot (2010).

At 1400°C, the temperature seems high enough for the decomposition of all hydrocarbons species, even $CH_4$ and $C_2H_2$ which were still detected at this temperature under an inert atmosphere.

The lower soot yield under a wet atmosphere than under an inert one can result from two main phenomena:

- reforming of the soot precursors hydrocarbons;
- soot gasification, which has a fast enough kinetics to occur from 1200°C under a wet atmosphere, according to the characteristic time analysis presented in section 2.1.2.3 of the previous chapter.

However, it is not possible to experimentally distinguish the individual contribution of each of these phenomena on the soot reduction observed under a wet atmosphere.

The char yield under a wet atmosphere shows that char can be gasified partly at 1200°C - around 80 % of conversion - and totally at 1400°C, whereas gasification under an inert atmosphere occurs only at 1400°C and at a lower conversion degree - around 50 % of conversion -. According to the characteristic time analysis in section 2.1.2.2 of Chapter "Materials and Methods" about gasification of char from 0.35 mm particles, gasification is very unlikely to occur under an inert atmosphere due to the low content of $H_2O$ which limits the chemical kinetic and external mass transfer rates. On the contrary, char gasification under a wet atmosphere was predicted to occur from 1200°C and to be completely achieved at 1400°C in the timescale of the DTR experiments. So the results of the characteristic time analysis agree with the experimental results here described.

As $H_2O$ is in large excess for experiments under a wet atmosphere, the WGS reaction occurs widely preferentially in the direct path according to Le Chatelier's principle. This explains why the $CO_2$ yield is then higher than the CO yield: a considerable part of the CO formed by reforming and gasification reactions is turned into $CO_2$ via the WGS reaction.

## 1.3. Comparisons with the thermodynamic equilibrium

In Figure 55, the main products yields obtained from the experiments under an inert and a wet atmosphere are compared to those calculated at thermodynamic equilibrium. These calculations were performed with the GEMINI software, and presented in section 2.2 of Chapter "Materials and Methods". As char and soot are both considered as graphitic carbon in GEMINI calculations, these compounds are represented by the term "$C_{solid}$" in Figure 55.

As mentioned in section 2.2 of Chapter "Materials and Methods", according to thermodynamic equilibrium calculations, the complete thermal decomposition of biomass into $H_2$ CO, and $CO_2$ or $C_{solid}$ is achieved from 1000°C under inert and wet atmospheres. Note that no $C_{solid}$ remains whereas $CO_2$ is present under a wet atmosphere

contrary to under an inert one. The yields of the final products - $H_2$, CO, $CO_2$, $H_2O$ - under a wet atmosphere are modified at each temperature following the WGS equilibrium.

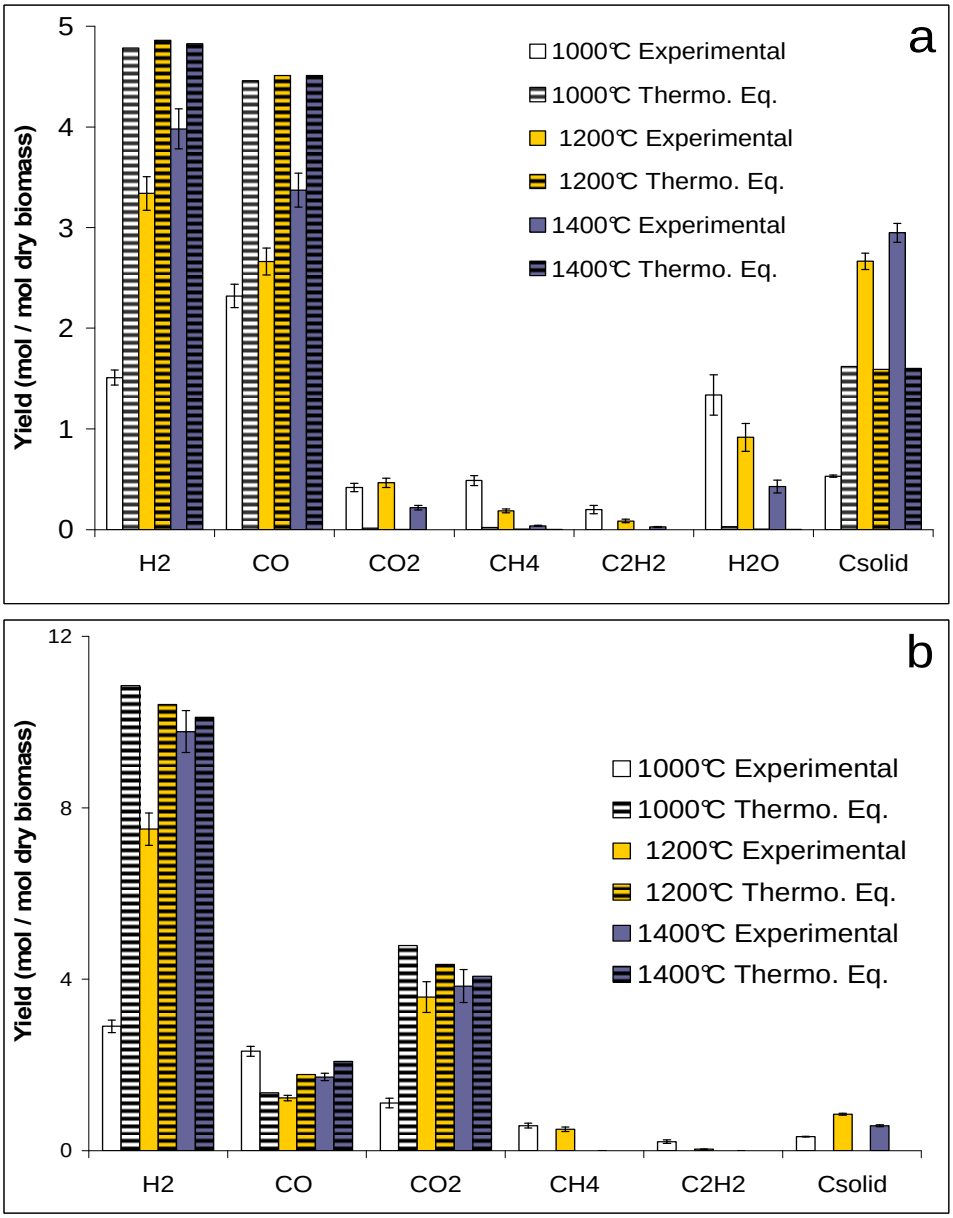


**Figure 55. Molar yields of the products from the particles thermal decomposition experiments and from thermodynamic equilibrium calculations under inert (a) and wet (b) atmospheres**

In Figure 55, it can be seen that when temperature increases, the experimental products yields get closer to those calculated at thermodynamic equilibrium. Only at 1400°C under a wet atmosphere, the experimental yields almost reach the values of thermodynamic equilibrium, as observed by other authors (Couhert et al., 2009). In this case, $H_2$ and $CO_2$ experimental yields are the same as those of equilibrium. However, the CO experimental yield is lower and $C_{solid}$ is still measured, even if its yield, of around 0.5 $mol/mol_{db}$, is low.

Concerning the products yields under an inert atmosphere, the experimental values and those at thermodynamic equilibrium are different even at 1400°C. The thermodynamic equilibrium calculations predict higher $H_2$ and CO yields and lower $C_{solid}$ yield than those experimentally obtained, as well as $CO_2$ and $H_2O$ yields very close to zero, which is not measured in the present study.

The differences between experimental results and thermodynamic equilibrium calculations can be explained by kinetic limitations of the involved reactions. The limiting reactions seem to be reforming and gasification reactions, which would lead to lower hydrocarbons, $C_{solid}$, $H_2O$ and $CO_2$ yields, and to higher $H_2$ and CO yields compared to those experimentally observed. Only at 1400°C and at 25 mol% of $H_2O$ the kinetics of these reactions is fast enough to almost reach the thermodynamic equilibrium.

Another phenomenon which could be limiting is the WGS reaction. This can be verified in Figure 56, which plots the equilibrium constant of the WGS reaction versus temperature. The experimental equilibrium constant was calculated from the experimental molar yields of $H_2O$, $CO_2$, $H_2$ and $H_2O$ obtained for 0.35 mm particles under inert and wet atmospheres. Note that the $H_2O$ yield used for the calculation of the WGS constant equilibrium under a wet atmosphere is calculated directly from the steam content in the injected gas, which is supposed not to change along the transformation as it is in high excess with respect to biomass (refer to section 1.2.2 of Chapter "Materials and Method").

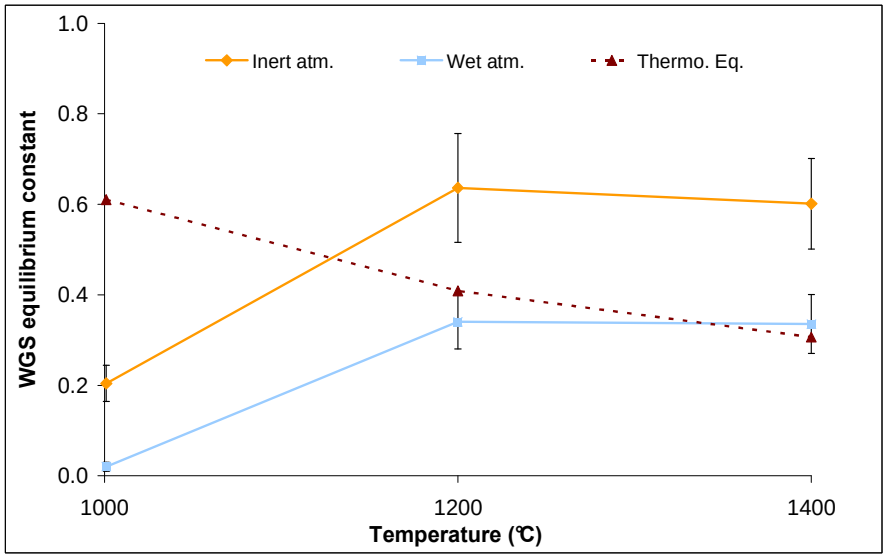


**Figure 56. WGS constant calculated from the experiments under inert and wet atmospheres, and from the thermodynamic equilibrium**

The WGS constant calculated with the experimental results corresponds to the thermodynamic equilibrium constant at 1200°C and 1400°C under a wet atmosphere. In the other cases, the WGS reaction is not at the equilibrium.

In summary, the thermodynamic equilibrium is more easily reached with the increases of both temperature and steam content in the atmosphere. In the present study, the system tends to thermodynamic equilibrium during experiments at 1400°C with 25 mol% of $H_2O$.

## 1.4. Summary

The thermal decomposition of wood particles under an inert atmosphere in the DTR can be decomposed into a complex series of interconnected chemical reactions.

The first stage is fast pyrolysis of the wood particles, which mainly produces volatile compounds, including tars and permanent gases, with an approximate yield of 0.95 $g/g_{db}$, and very low amounts of char, inferior to 0.05 $g/g_{db}$. The products from pyrolysis are then transformed by secondary reactions. The resulting products from these

reactions are the compounds which are observed at the reactor outlet. Between 800°C and 1400°C under an inert atmosphere, the predominant secondary reactions are hydrocarbons cracking and polymerization, which lead to the formation of PAH at 1000°C and soot from 1200°C, and to a massive release of $H_2$. Reforming reactions have a weaker role in products transformation and lead to a slight formation of $H_2$ and CO, from $H_2O$, $CO_2$ and hydrocarbons. The gas resulting from beech pyrolysis and gas phase reactions is then very rich in $H_2$ and CO, and poor in hydrocarbons. Char gasification by $H_2O$ and/or $CO_2$, which contributes to the formation of $H_2$ and CO, only partly occurs at 1400°C.

With the products yields measured from wood thermal decomposition under a wet atmosphere, it could be observed that the reactions involving $H_2O$ are highly favored under such conditions: hydrocarbons reforming, carbonaceous solid gasification and WGS reaction. Reforming and gasification reactions lead to the decrease of hydrocarbons, soot and char, and to the formation of $H_2$ and CO, which is then converted into $CO_2$ via WGS reaction, in particular from 1200°C. At 1400°C, where char is completely gasified and no hydrocarbons are detected, the thermodynamic equilibrium is almost reached. Only few soot remains under such conditions. The WGS reaction is at thermodynamic equilibrium from 1200°C.

## 2. Influence of residence time and particle size on the beech particles thermal decomposition

### 2.1. Influence of residence time of 0.35 mm particles

The influence of residence time was studied in experiments under an inert and a wet atmosphere, by sampling at the middle and at the bottom of the reactor, which corresponds to a respective gas residence time of approximately 2 s and 4 s. Note that the residence times of the gas and solid for the 0.35 mm particles pyrolysis are very close.

The “tar and soot” yield is not presented in this study as no interesting information could be retrieved from that measurement because of the too high error bar. Nor $H_2O$ yield under a wet atmosphere is represented, as its measurement at the reactor outlet is too imprecise.

#### *2.1.1. Products yields under an inert atmosphere*

The mass yields of the products from the thermal decomposition of 0.35 mm particles at two different residence times - 2 s and 4 s - are represented in Figure 57.

As observed in Figure 57, the residence time increase between 2 s and 4 s has an influence on several products yields:

- at 1000°C, increase of $H_2$ yield, and decrease of $C_2H_4$ yield;
- at 1200°C, increase of $H_2$ and $CO_2$ yields and decrease of $CH_4$, $C_2H_2$ and $C_6H_6$ yields.

Nevertheless, these differences are rather slight as they do not exceed 45% of relative difference. Note that the $H_2$ yield is the only compound to vary with residence time at the two temperatures, whereas CO and char yields do not change between 2 s and 4 s of residence time.

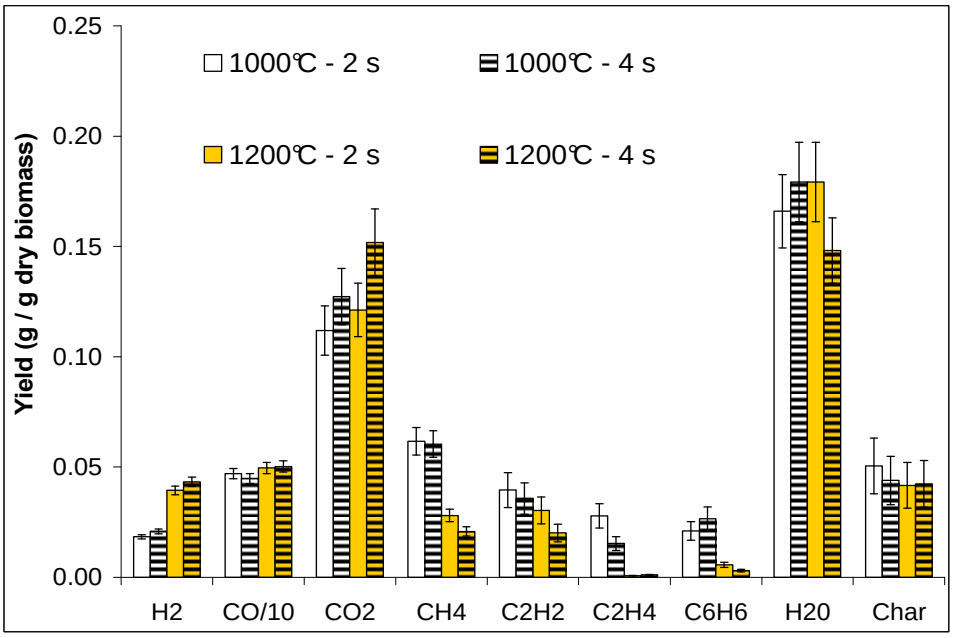


**Figure 57. Mass yields of the products from the 0.35 mm particles thermal decomposition under an inert atmosphere at 1000°C and 1200°C, after 2 s and 4 s of residence time**

### *2.1.2. Products yields under a wet atmosphere*

The products yields for 0.35 mm particles under a wet atmosphere at two residence times are compared in Figure 58.

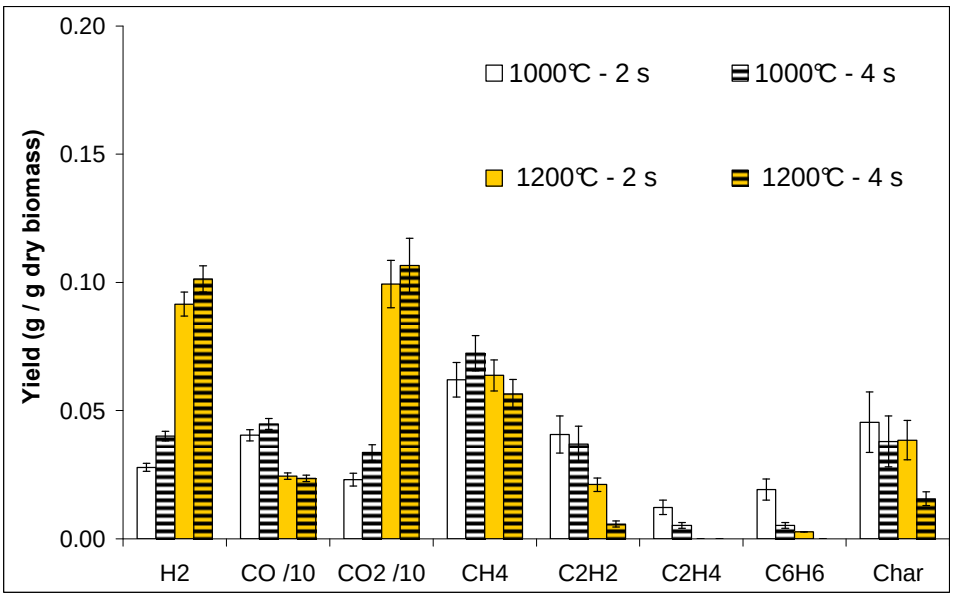


**Figure 58. Mass yields of the products from the 0.35 mm particles thermal decomposition under a wet atmosphere at 1000°C and 1200°C, after 2 s and 4 s of residence time**

At 1000°C, the $H_2$, CO and $CO_2$ yields are higher after 4 s, whereas the $C_2H_4$ and $C_6H_6$ yields are lower. The residence time influence is the same at 1200°C for $H_2$, $CO_2$, light hydrocarbons - here $C_2H_2$ and $C_6H_6$ -, but the CO yield stays steady. The char yield then clearly decreases between 2 s and 4 s.

Under a wet atmosphere, the $CH_4$ yield remains the same between the two residence times.

### 2.1.3. Discussion

The results of Figure 57 and Figure 58 show that the products yields slightly change between 2 s and 4 s of residence time. Homogeneous reactions, particularly concerning light hydrocarbons, seem to be mainly responsible for these changes, as well as char gasification.

The constant char yield between 2 s and 4 s of residence time observed in Figure 57 suggests that the 0.35 mm particles are completely pyrolysed in less than 2 s under the explored conditions. Tar cracking reactions also seem to be approximately achieved in less than 2 s: no increase of the CO, $CH_4$ and $C_2H_4$ yields are observed as residence time increases under an inert atmosphere, while these products are the main products from tar cracking.

According to the yields at 2 s and 4 s of residence time, the conversion of some light hydrocarbons, which was already discussed in section 1, takes place during several seconds and is probably still evolving at the end of the reaction length.

Note that the $CH_4$ yield under a wet atmosphere is steady at 1200°C. This result may confirm the assumption that $CH_4$ conversion is inhibited by $H_2O$ at temperatures above 1300°C, as discussed in section 1.2.3.2.

The char yield decrease at 1200°C under a wet atmosphere as residence time increases is due to char gasification, in agreement with the discussion of section 1.2.3.2. If the final char yield obtained from pyrolysis is supposed to be 0.045 $g/g_{db}$, the gasification conversion at 1200°C is approximately 70 % under 4 s of residence time whereas the conversion is only 15 % at 2 s.

The evolution of hydrocarbons conversion and char gasification with residence time has an impact on the CO, $CO_2$, $H_2O$ and more particularly $H_2$ yields. The WGS reaction also progress with residence time, as it can be seen with the evolution of the equilibrium constant. At 1200°C under a wet atmosphere, this one gets closer to the value predicted at the thermodynamic equilibrium, which is 0.41: 0.35 ± 0.07 at 4 s of residence time, compared to 0.16 ± 0.04 at 2 s.

In general, the progress of hydrocarbons decomposition, gasification and WGS reaction leads to the $H_2$, CO and $CO_2$ yield increase, and to the $H_2O$ yield decrease. Nevertheless, the exact contribution of each reaction to the gases yields evolution with residence time is not possible to be estimated on the basis of the experimental results only.

## 2.2. Influence of particle size

The influence of particle size, 0.35 mm and 0.80 mm, was studied with experiments under an inert and a wet atmosphere, by sampling at the middle and at the bottom of the reactor. Owing to the same reasons as mentioned in section 2.1, the sum of tar and soot yields is not presented in this study.

The term “long residence time” refers to a sampling at the bottom of the reactor and the term “short residence time” refers to a sampling at the middle of the reactor. Note that the residence times of volatiles and solid from the 0.80 mm particles thermal decomposition are evaluated respectively at ~ 4 s and ~ 2.7 s for sampling at the bottom, and at ~ 2 s and ~ 1.3 s for sampling at the middle of the reactor.

### 2.2.1. Influence of particle size on products yields in a inert atmosphere

Figure 59 compares the mass yields of the products from the thermal composition of 0.35 mm and 0.80 mm particles under an inert atmosphere at two residence times.

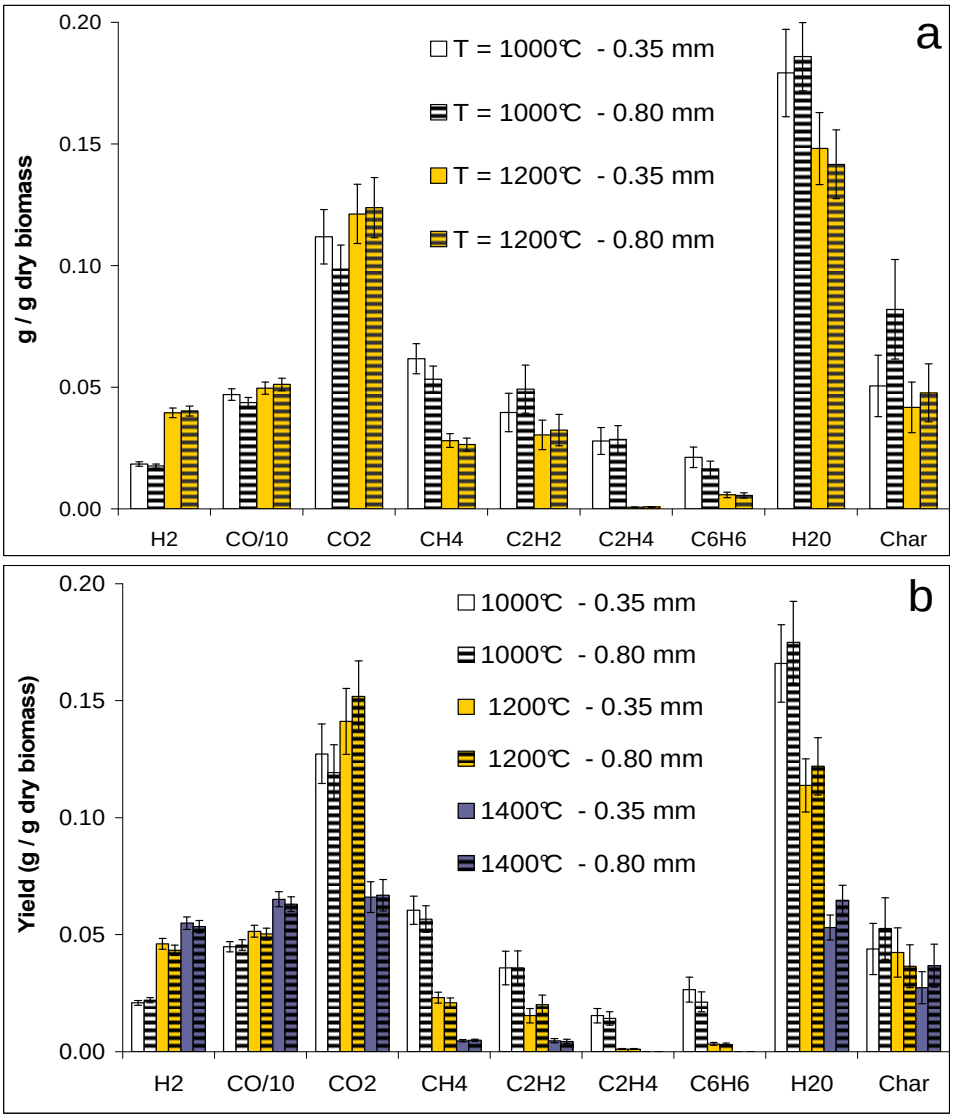


**Figure 59. Mass yields of the products from the 0.35 mm and 0.80 mm particles thermal decomposition under an inert atmosphere at 1000°C, 1200°C and 1400°C, after short (a) and long (b) residence times**

The mass yields in Figure 59 are very similar between the two samples. Only two exceptions can be noticed, with yields differences higher than the error bars:

- At short residence time and 1000°C, the char yield is lower for the 0.35 mm particles.
- At long residence time and 1400°C, the $H_2O$ yield is lower for the 0.35 mm particles.

### *2.2.2. Influence of particle size on products yields under a wet atmosphere*

The mass yields from the thermal decomposition of 0.35 mm and 0.80 mm particles under a wet atmosphere at two residence times are represented in Figure 60.

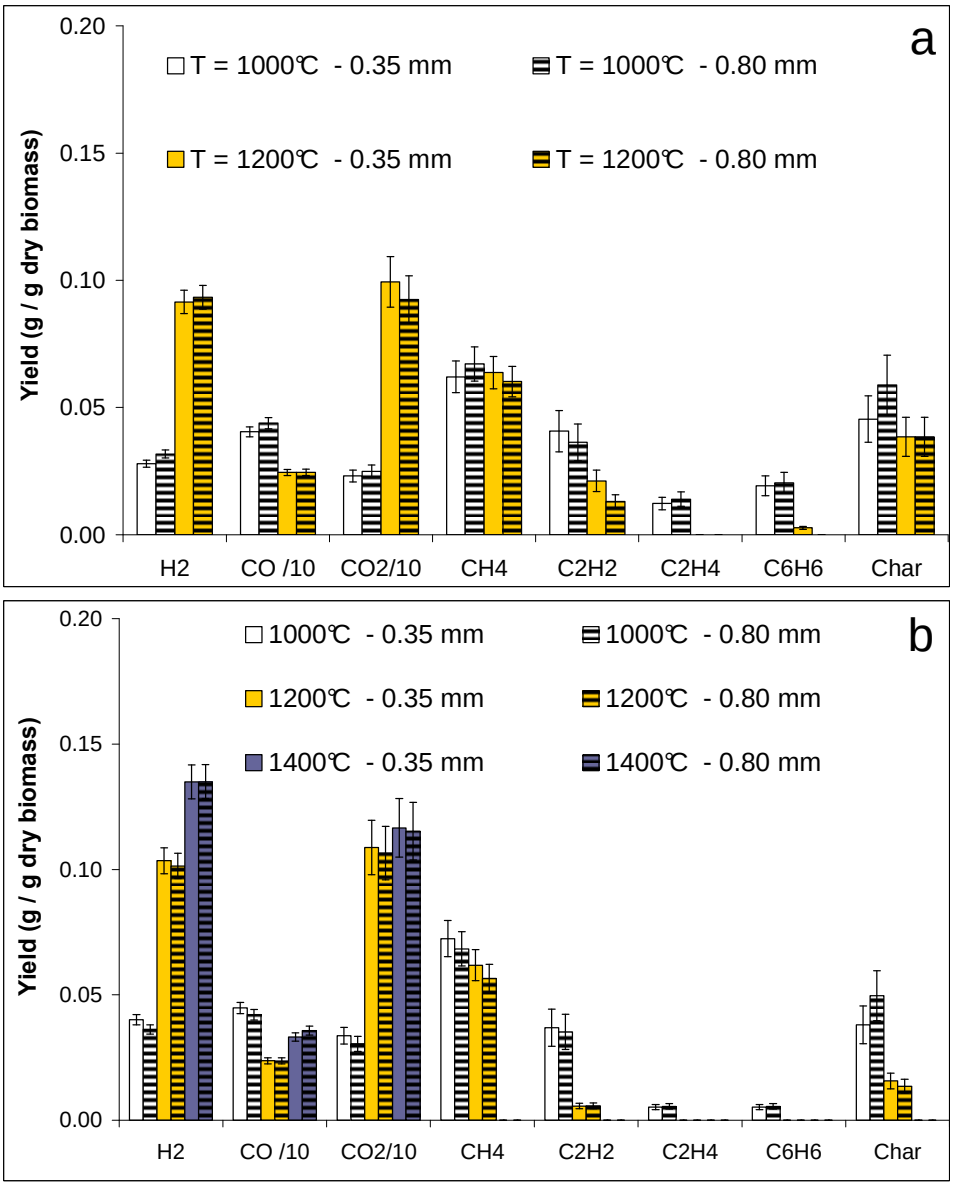


**Figure 60. Mass yields of the products from the 0.35 mm and 0.80 mm particles thermal decomposition under a wet atmosphere at 1000°C, 1200°C and 1400°C, after short (a) and long (b) residence times**

The mass yields of the products obtained from the thermal decomposition of 0.35 mm and 0.80 mm particles under a wet atmosphere present in most cases differences which are within the error bars. However, the differences concerning the $H_2$ yields at 1000°C and the $C_2H_2$ yield at 1200°C at short residence time slightly exceed the error bar.

### *2.2.3. Discussion*

Under the explored conditions, the particle size shows no significant effect on the products yields. Only one exception could be identified, for char yield at 1000°C under an inert atmosphere. This has a weak impact on the global results but it allows highlighting some interesting aspects for the understanding of wood thermal decomposition.

The char yields for the 0.35 mm and 0.80 mm particles under an inert atmosphere are the same at the bottom of the reactor: 0.05 $g/g_{db}$ which are supposed to be approximately the final char yield obtained from complete beech particles pyrolysis. No limitation of particle size on pyrolysis is then observed for 0.35 mm and 0.80 mm particles samples.

However, at the middle of the reactor, the 0.80 mm particles char yield is about 0.08 $g/g_{db}$ versus a yield of 0.05 $g/g_{db}$ for the 0.35 mm particles. This difference shows that pyrolysis is not completely achieved for 0.80 mm particles. A particle size of 0.80 mm is then limiting at 1000°C where pyrolysis is achieved after 2 s of residence time. This result was not predicted by the characteristic time analysis in 2.1.2.1 of Chapter "Materials and Methods", which gave an order of magnitude for the whole pyrolysis process of about 0.2 s for 0.80 mm particles at 1000°C. This means that the necessary time for particle heating was probably underestimated in the analysis. This limitation disappears at 1200°C and at 1000°C under a wet atmosphere, as the increase of temperature and $H_2O$ content improves the particle heating.

These results confirm that the 0.35 mm beech particles pyrolyze much faster than 0.80 mm particles. Besides, the 0.80 mm beech particles pyrolysis is achieved within the first 2 s of residence time, and thus it may occur at the same time as the rest of the phenomena.

On another hand, the difference of the $H_2O$ yield between the 0.35 mm and 0.80 mm samples at 1400°C under an inert atmosphere could be explained by higher char gasification conversion for the 0.35 mm particles. However, this cannot be directly confirmed by char yields because of the too high error bar. Note that our characteristic time analysis (section 2.1.2.2 of Chapter "Materials and Methods") shows that gasification rate is drastically limited by external mass transfer under low $H_2O$ concentration, and thus the possibility of gasification during experiments under an inert atmosphere is higher for char from the 0.35 mm sample than that from 0.80 mm.

Other slight differences between the two beech samples can be observed for the $H_2$ at 1000°C and the $C_2H_2$ yield at 1200°C, during experiments under a wet atmosphere. However, it is not possible to get a clear trend from these differences, which are in the limit of the error bar.

### 2.3. Summary

In this section, the results from the thermal decomposition of 0.35 mm particles at 1000°C and 1200°C were compared for two residence times, 2 s and 4 s. The yields of the major compounds, which are $H_2$, CO and $CO_2$, are very similar between the two residence times, with only some slight differences, especially in the case of $H_2$. Indeed, the most relevant changes during wood thermal decomposition occur in less than 2 s.

Slower phenomena, such as light hydrocarbons decomposition, char gasification and WGS reaction, are observed to occur during a few seconds and have a minor influence on the major gas yields.

Particle size can have an influence on two parameters during the beech sawdust gasification experiments: the transfer rates and the particle residence time. In general, an increase of the particle size leads to an increase of heat and mass external transfer rates, and to a decrease of the residence time. However, under the explored conditions, no major effect of particle size has been observed on the beech thermal decomposition.

## 3. Characterization of soot and char

Reminder: during experiments, the gas and 0.35 mm particles have approximately the same residence time, approximately 2 s and 4 s by sampling at the middle and the bottom of the reactor respectively. The 0.80 mm particles have a lower residence time, approximately 1.3 s and 2.7 s by sampling at the middle and the bottom of the reactor respectively.

## 3.1. Characterization of soot

The characterization was performed on soot obtained under an inert atmosphere at 1200°C and 1400°C, for the 0.35 mm and 0.80 mm beech samples. Soot is also present under a wet atmosphere and at 1000°C under an inert atmosphere, but not enough amounts of soot could be collected for its characterization.

### *3.1.1. Soot morphology*

Figure 61 presents the SEM images of soot samples collected at the bottom of the reactor, after experiments at 1200°C and 1400°C under an inert atmosphere, performed with 0.80 mm particles.

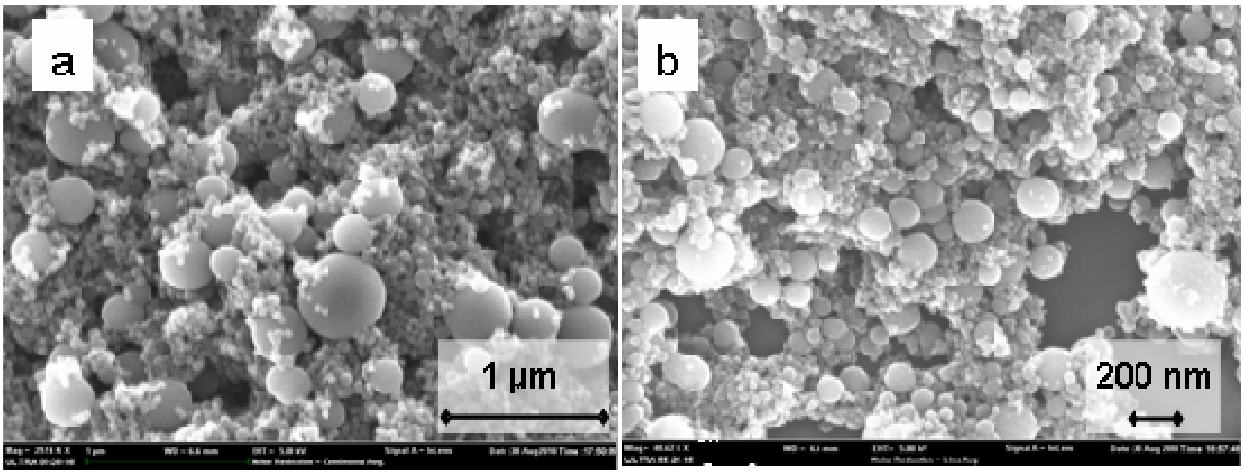


**Figure 61. SEM observations of soot samples from the 0.80 mm particles thermal decomposition at 1200°C (a) and 1400°C (b), after 4 s of residence time**

In Figure 61, soot appears as an agglomeration of very small units, which correspond to the spherules (refer to section 4.1.2. of Chapter "Fundamental Concepts"). Most of the spherules have a spherical shape and their surface seems to be smooth. The size distribution of spherules is very wide, varying from several nanometers to several hundreds of nanometers. No significant difference is observed between the soot samples obtained at different temperatures, which was expected as morphology is always quite the same for all kinds of soot.

Appendix G presents further SEM observation of soot samples.

### *3.1.2. Soot composition*

Table 24 presents the molar composition of soot from experiments at 1200°C and 1400°C under an inert atmosphere with 0.35 mm beech particles, after 2 s and 4 s of gas residence time.

**Table 24. Molar composition (daf) of soot samples from the 0.35 mm particles thermal decomposition at 1200°C and 1400°C, after 2 s and 4 s of gas residence time**

| Sample | 1200°C | | 1400°C |
|---|---|---|---|
| | 2 s | 4 s | 4 s |
| Carbon | 86 ± 5 % | 92 ± 4 % | 95 ± 5 % |
| Hydrogen | 14 ± 5% | 8 ± 2% | 5 ± 1% |

At 4 s of residence time, the soot samples from experiments at 1200°C and 1400°C have different compositions: their respective compositions give a mean formula for soot of $(C_{12}H)_n$ and $(C_{22}H)_n$. The soot formed at 1400°C is more concentrated in carbon than that formed at 1200°C.

At 1200°C, the soot sampled at 2 s of gas residence time has lower carbon content and higher hydrogen content than the soot sampled at longer residence time. Its composition gives a chemical formula of $(C_8H)_n$, which is very close to the formula of soot proposed by Palmer & Cullis (1965).

With these results, it can then be seen that the soot composition changes with temperature and residence time.

Note that the soots formed from the 0.80 mm and 0.35 mm particles have the same composition at given temperature and residence time.

### 3.1.3. Soot reactivity

#### 3.1.3.1. Influence of temperature and residence time on soot reactivity

The reactivity of soot samples to steam gasification measured by TGA experiments - 950°C and 20 mol% of $H_2O$ - in two conversion ranges, as described in section 1.3.3 of the previous chapter, is shown in Figure 62. The study was performed for soot obtained from experiments with 0.35 mm particles under an inert atmosphere:

- at 1200°C, by sampling at 2 s and 4 s of gas residence time;
- at 1400°C, by sampling at 4 s of gas residence time.

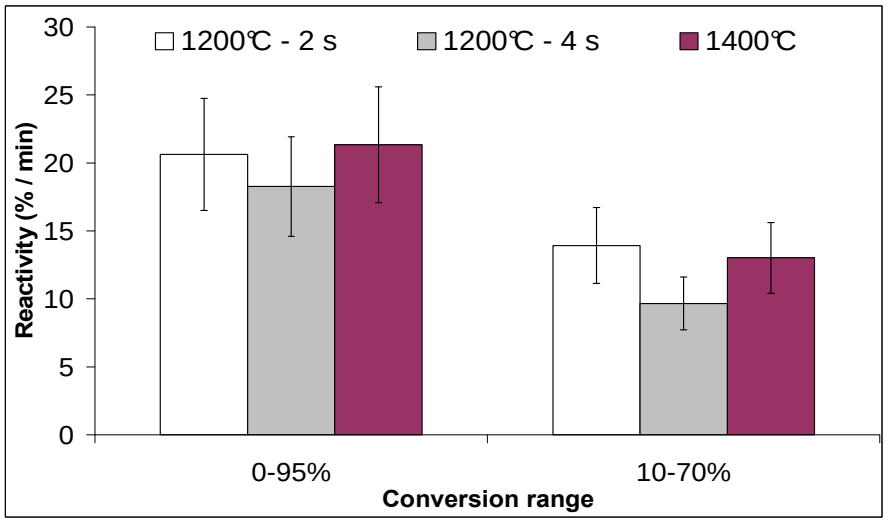


**Figure 62. Reactivity in two conversion ranges of soot samples from the 0.35 mm particles thermal decomposition at 1200°C and 1400°C, after 2 s and 4 s of gas residence time**

Figure 62 shows that temperature and residence time do not present a significative influence on soot reactivity in our experiments. Thereby, the soot composition change with temperature and residence time, discussed in section 3.1.2, does not influence reactivity. This result is not in agreement with results of the literature, where soot reactivity decreases with the temperature of its formation (Ruiz et al., 2007). Nevertheless, in that work, soot reactivity was measured in an $O_2$ containing atmosphere, and in a temperature range of 1000°C to 1200°C, which are different experimental conditions to ours.

#### 3.1.3.2. Influence of particle size on soot reactivity

The reactivity of soot samples - 950°C and 20 mol% of $H_2O$ -, obtained from the thermal decomposition of 0.35 mm and 0.80 mm particles at 1200°C and 1400°C under an inert atmosphere and sampled at 4 s of gas residence time, are presented in Figure 63.

At a given temperature, the 0.35 mm and 0.80 mm particles soot samples have a different reactivity in both conversion ranges, except for soot samples at 1200°C in a conversion range of 10 – 70%.

These differences of reactivities should be linked to differences of soot structures. So, the soot formation mechanism could change as a function of the initial particle size. As the wood pyrolysis duration depends on the particle size (refer to section 2.2.3), it could also have an influence on the composition of the hydrocarbons released by the particles, which participate to the soot formation process.

Note that soot composition does not change with particle size. So, soot composition and reactivity are not linked in that case either.

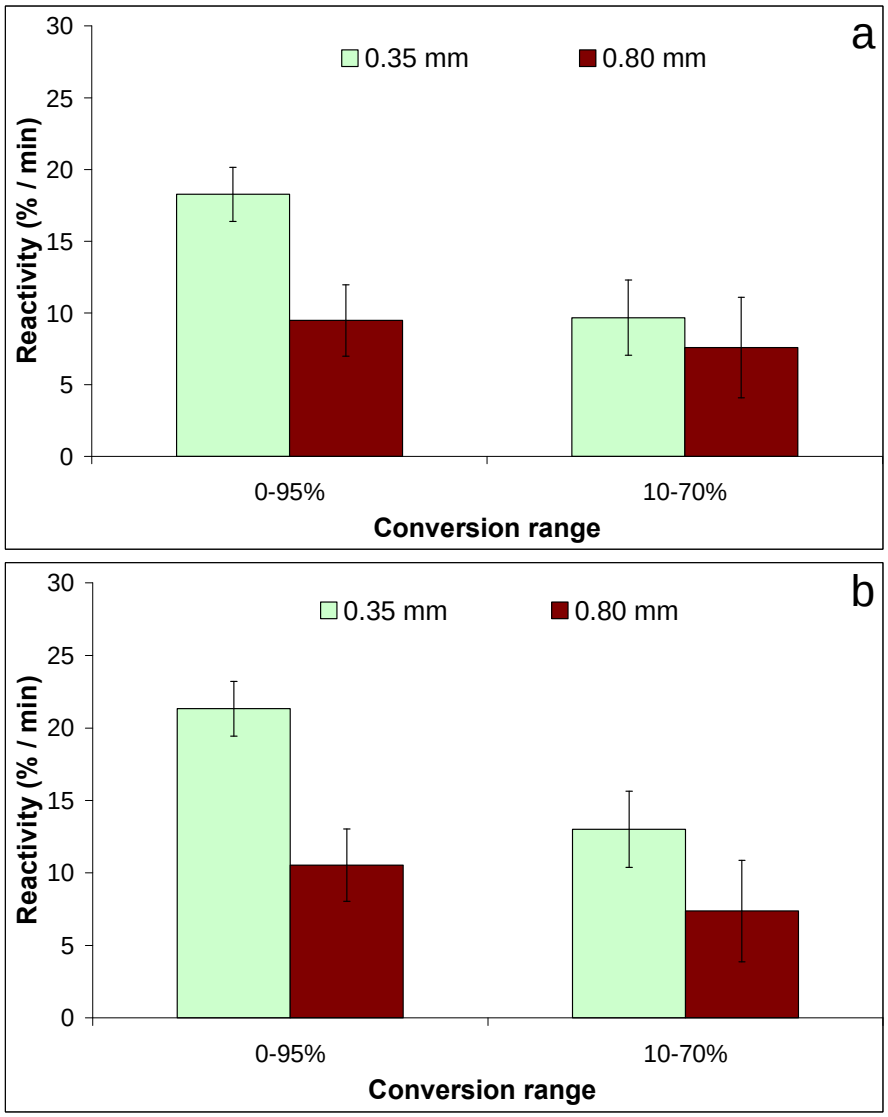


**Figure 63. Reactivity in two conversion ranges of soot samples from the 0.35 mm and 0.80 mm particles thermal decomposition at 1200°C (a) and at 1400°C (b), after 4 s of gas residence time**

## 3.2. Characterization of char

The char characterization presented here was performed on the samples collected under an inert atmosphere. The characterization results for char formed under a wet atmosphere are shown in Appendix H. In fact, a wet atmosphere does not have an influence on char characteristics during its formation but it can induce changes through gasification. Notably, the reactivity of a gasified char is much higher than that of a non reacted char.

### 3.2.1. Char morphology

Figure 64 shows a SEM image of char particles resulting from the pyrolysis of 0.35 mm particles at 1000°C and 1400°C under an inert atmosphere, by sampling at the bottom of the reactor.

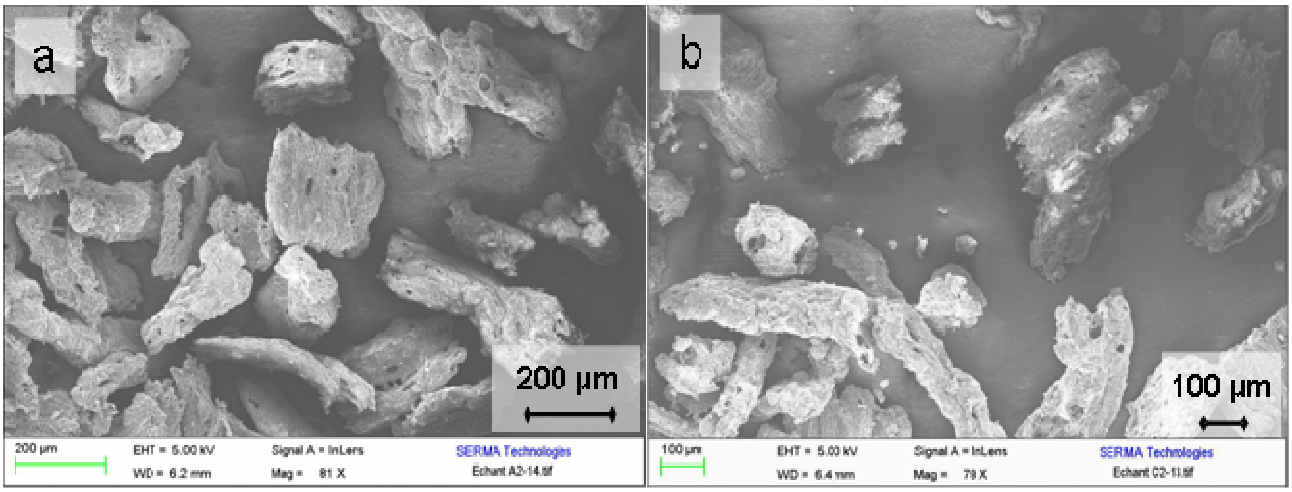


**Figure 64. SEM observations of char samples from the 0.35 mm particles thermal decomposition at 1000°C (a) and 1400°C (b), after 4 s of residence time**

Most of the char particles have a size in the same order of magnitude as the one of the initial biomass particle, as observed by Chen (2009) who suggested a shrinking factor of 0.7. Note that very small particles, surely corresponding to fragments from mother char particles, have also been observed. These fragments can be created during the devolatilisation process or during the sampling handling. No considerable effect of temperature on the char particles morphology is observed for samples at 1000°C, 1200°C and 1400°C.

Char particles present a different morphology from the one of the wood particles of origin. This can be explained by the brutal release of volatiles during the rapid pyrolysis in the DTR, which can damage the structure of the particle and thus deform it.

SEM images of chars obtained at 1000°C, 1200°C and 1400°C, with a higher zoom, provide more details of the char structure in Figure 65.

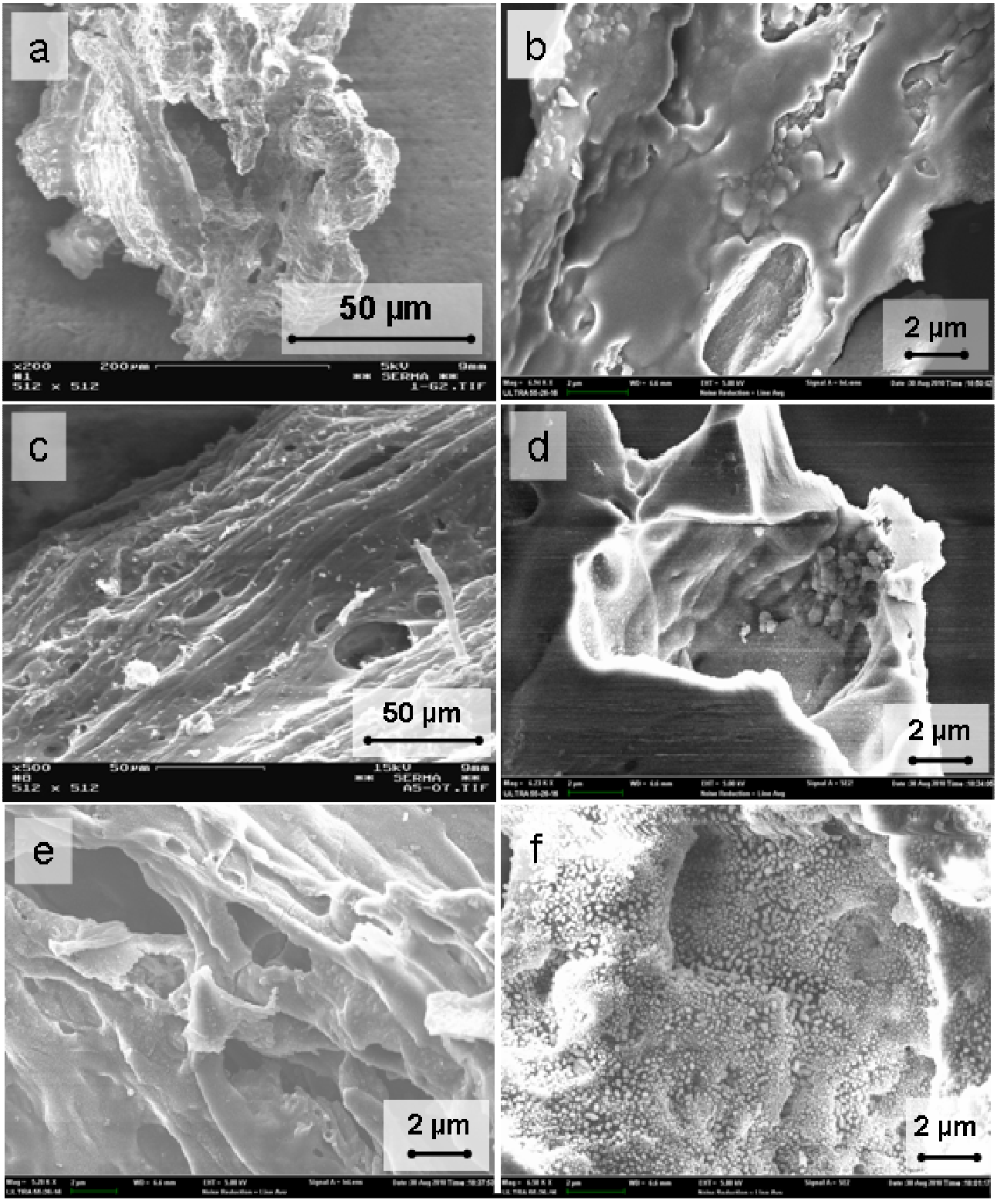


**Figure 65. SEM observations of char samples from experiments at 1000°C (a, b, c), 1200°C (d,e) and 1400°C (f)**

Some characteristics of char structure formation during pyrolysis are illustrated in Figure 65: formation of large cavities (a, d) and structure fracturing (e) due to the brutal release of volatiles; apparition of irregularities on char surface after char bubbling and fusion (b). Nonetheless, some char particles still present traces of the initial fibrous structure of wood (Figure 65– c).

Furthermore, some char particles present small grains with irregular shape emerging from the surface (Figure 65– f). These grains look like precipitated salts referring to literature (Petit, 2011). Figure 66 presents a typical XRD spectrum of char surfaces with and without grains.

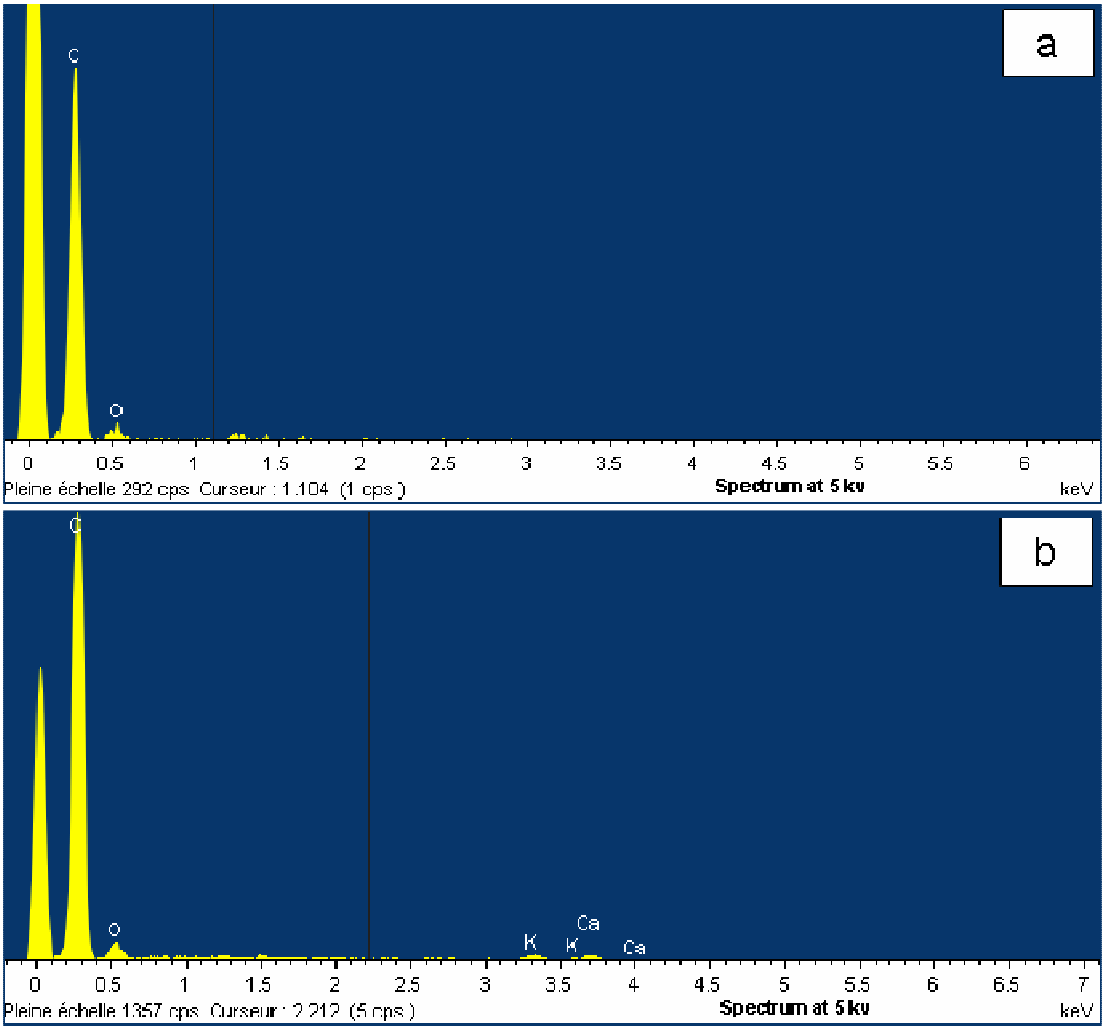


**Figure 66. XRD analysis of char samples from 1400°C experiments, without grains (a) and with grains (b) on its surface**

Through XRD analysis, a char surface with grains tend to present more inorganic compounds - here K and Ca - in its composition than a surface without, on which only C and O are usually detected. Therefore, the grains observed on char surfaces could be inorganic compounds which have migrated to the surface and coalesced after fusion (Richardson, 2010), or recondensed after evaporation during the quenching step (Petit, 2011).

Some soot particles are also observed in char samples at 1000°C, 1200°C, and 1400°C, as illustrated in Figure 67. This observation confirms that soot formation is already active at 1000°C, even if low amounts of soot are then produced. The segregation of char and soot in the experimental device is then not perfect. Nevertheless, during gasification experiments of char samples at successively 750°C and 950°C in the TGA, the char mass sample decreases at 750°C but not a 950°C, which means that only char gasification is measured. Soot observed in char samples can be then neglected in terms of quantity.

More SEM observation of char samples are shown in Appendix G.

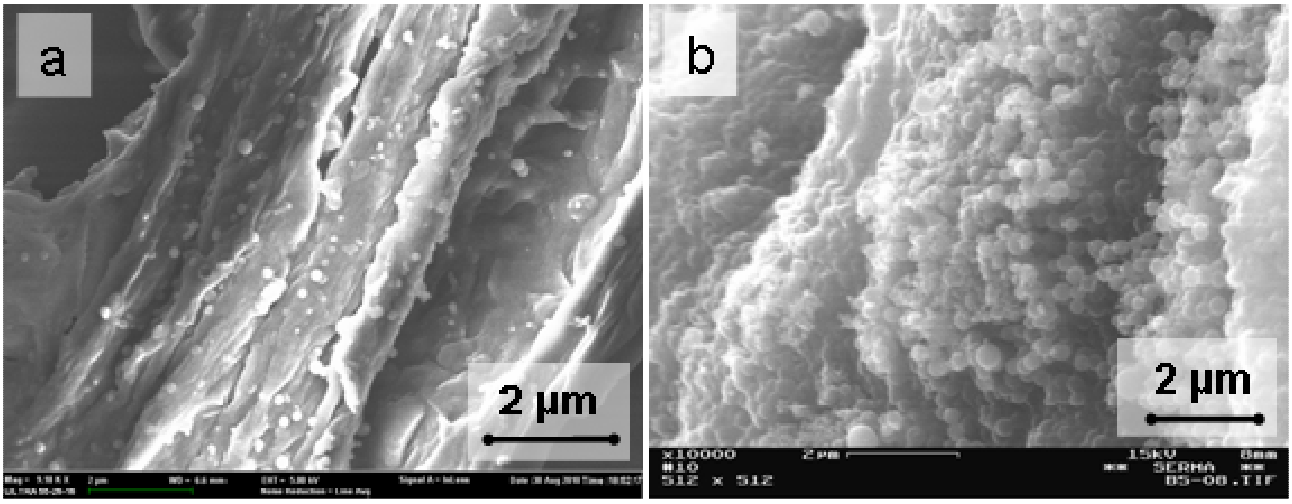


**Figure 67. Soot particles observed in char samples from 1000°C (a) and 1200°C (b) experiments**

### *3.2.2. Char composition*

#### *3.2.2.1. Influence of temperature on char composition*

The C, H and O molar compositions of the 0.35 mm particles char samples, obtained at 1000°C, 1200°C and 1400°C under an inert atmosphere and sampled at 4 s of residence time, are presented in Table 25.

**Table 25. Molar composition (daf) of char samples from the 0.35 mm particles thermal decomposition at 1000°C, 1200°C and 1400°C, after 4 s of residence time**

| Sample | 1000°C | 1200°C | 1400°C |
|---|---|---|---|
| Carbon | 74 ± 4 % | 78 ± 4% | 82± 4 % |
| Hydrogen | 19 ± 4% | 18 ± 4% | 17 ± 4% |
| Oxygen | 7 ± 4% | 4 ± 3% | 1 ± 1 % |

Char is mainly composed of carbon with a content highest than 70 mol% with also considerable amounts of hydrogen, around 20 mol %, and low amounts of oxygen, inferior to 10 mol %.

The composition of chars formed at 1000°C and 1400°C are different: the carbon content is higher in the sample formed at 1400°C than in the sample formed at 1000°C whereas the oxygen content is much lower. Note that the char formed at 1400°C contains almost no oxygen. The hydrogen content is similar between the three samples. The composition of char at 1200°C is intermediary between the compositions of the samples formed at 1000°C and 1400°C.

Chen (2009) measured the composition of char from the pyrolysis of 0.35 mm beech particles in a drop tube reactor for temperatures below 1000°C: the carbon, hydrogen and oxygen molar contents at 800°C were respectively of 67 mol%, 21 mol% and 12 mol%. This result complements ours: the char carbon content increases with temperature from 800°C to 1400°C.

The H/C and O/C molar ratios are plotted versus temperature in Figure 68. This graph includes the char compositions measured in the present study and in the study conducted by Chen (2009).

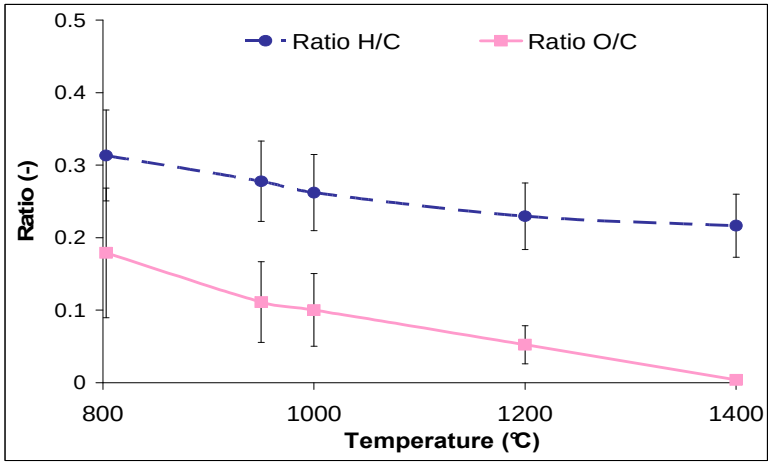


**Figure 68. H/C and O/C ratios versus temperature**

The H/C and O/C ratios decrease with temperature from 800°C to 1400°C. The difference of ratios can be clearly seen between 800°C and 1400°C: the O/C ratio decreases by a factor of 48, while the H/C is 30% lower at 1400°C than at 800°C.

So, the carbon concentration in chars increases with temperature between 800°C and 1400°C. This enrichment in carbon can be a consequence of the graphitization process which tends to rearrange the carbonaceous matrix into a more ordered structure of graphite type at high temperatures, according to literature (refer to section 1.2.3 of Chapter "State of the Art"). Graphitization implies the evolution of the material towards pure carbon, through which the hydrogen and oxygen atoms contained in the structure are released.

#### *3.2.2.2. Influence of residence time on char composition*

The molar compositions of the 0.35 mm particles chars at 1000°C and 1200°C under an inert atmosphere, collected at two different residence times - 2 s and 4 s -, are shown in Table 26.

**Table 26. Molar composition (daf) of char samples from the 0.35 mm particles thermal decomposition 1000°C and 1200°C, after 2 s and 4 s of residence time**

| Sample | 1000°C | | 1200°C | |
|---|---|---|---|---|
| | 2 s | 4 s | 2 s | 4 s |
| Carbon | 66 ± 3 % | 74 ± 4 % | 74 ± 4 % | 78 ± 4% |
| Hydrogen | 24 ± 5% | 19 ± 4% | 19 ± 4% | 18 ± 4% |
| Oxygen | 10 ± 5% | 7 ± 4% | 7 ± 4% | 4 ± 3% |

The composition of char from experiments at 1000°C varies between 2 s and 4 s of residence time: the char sample at 4 s of residence time has higher carbon content and a lower oxygen and/or hydrogen content than the char sample at 2 s of residence time. Note that it is not possible to have more details about the difference of hydrogen and oxygen composition between the two char samples due to the error bar. No significant difference of composition is observed between the char sample from 1200°C experiments at 2 s and 4 s of residence time.

#### *3.2.2.3. Influence of particle size on char composition*

The composition of chars from the thermal decomposition of 0.35 mm and 0.80 mm particles at 1000°C, 1200°C and 1400°C under an inert atmosphere can be seen in Table 27, by sampling at the bottom of the reactor.

**Table 27. Molar composition (daf) of char samples from the 0.35 mm and 0.80 mm particles thermal decomposition at 1000°C, 1200°C and 1400°C, by sampling at the bottom of the reactor**

| Sample | Char 1000°C | | Char 1200°C | | Char 1400°C | |
|---|---|---|---|---|---|---|
| | 0.35 mm | 0.80 mm | 0.35 mm | 0.80 mm | 0.35 mm | 0.80 mm |
| Carbon | 74 ± 4 % | 67 ± 3 % | 78 ± 4% | 74 ± 4 % | 82 ± 4 % | 81 ± 4 % |
| Hydrogen | 19 ± 4% | 24 ± 4 % | 18 ± 4% | 21 ± 4 % | 17 ± 4% | 13 ± 3 % |
| Oxygen | 7 ± 4% | 9 ± 4 % | 4 ± 2% | 5 ± 2 % | 1 ± 0.5 % | 6 ± 3 % |

The particles size has no influence on char composition for experiments at 1200°C and 1400°C, and a slight influence for experiments at 1000°C.

The particles size influence on char composition could be in fact a particles residence time effect. In section 3.2.2.2, we have shown that the composition of the 0.35 mm sample char varied between 2 s and 4 s of residence time at 1000°C, but above 1200°C no significant variations were observed. Here, the residence time of the 0.80 mm particles at the bottom of the reactor is shorter, about 2.7 s, than the residence time of the 0.35 mm particles, 4 s.

#### *3.2.2.4. Discussion*

In order to have a better comprehension of the char composition modification with residence time and temperature, a ternary diagram is plotted in Figure 69. This graph shows the molar composition of 0.35 mm particles char at 1000°C and 1200°C at 2 s and 4 s of residence time, and at 1400°C at 4 s of residence time. The char composition evolution measured by Chen (2009) at different residence times and for different beech particle sizes at 800°C and 950°C is represented by a dotted line in Figure 69.

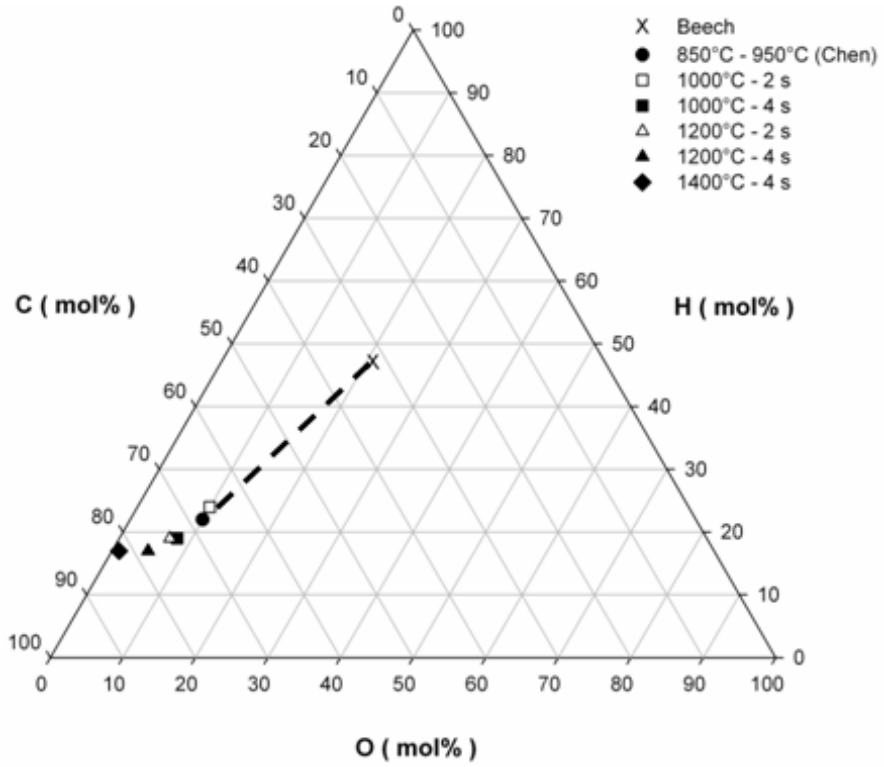


**Figure 69. Triangular diagram with the char molar composition from the 0.35 mm particles pyrolysis of at 800°C, 1000°C and 1200°C after different residence times**

Chen (2009) has proven that the char composition at 800°C and 950°C varies linearly in this diagram with the pyrolysis progress, from the wood composition until arriving to a composition of 67 mol% of carbon, 21 mol% of hydrogen and 12 mol% of oxygen, when devolatilisation is considered as finished. Our results show that the final composition of char continues to head towards a composition of 83 mol% of carbon and 17 mol% of hydrogen with the increase of temperature.

The increase of char carbon content, which is assumed to be a consequence of the carbonaceous structure graphitization, continues after pyrolysis achievement. Indeed, the composition of char at 1000°C changes between 2 s and 4 s of residence time, while pyrolysis has been demonstrated to be achieved in less than 2 s for 0.35 mm particles (refer to section 2.1.3). From 1200°C, char composition modification may be completely or almost achieved in less than 2 s.

### *3.2.3. Char reactivity*

#### *3.2.3.1. Influence of temperature on char reactivity*

Figure 70 shows the reactivity in two conversion ranges, measured by TGA experiments - 750°C and 20 mol% of $H_2O$ -, for char resulting from the pyrolysis of 0.35 mm particles at 800°C, 1000°C, 1200°C and 1400°C under an inert atmosphere.

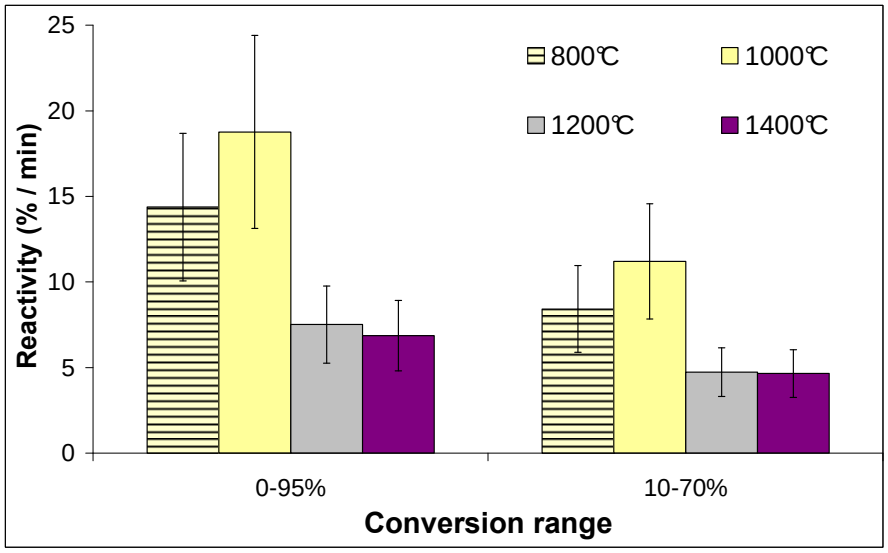


**Figure 70. Reactivity in two conversion ranges of char samples from the 0.35 mm particles thermal decomposition at 800°C, 1000°C, 1200°C and 1400°C, after 4 s of residence time**

The char samples from 800°C and 1000°C experiments have the same reactivities measured in a conversion range of 10 – 70% and 0 – 95%, which is the same for the char samples from 1200°C and 1400°C experiments. The reactivity of the chars formed at 800°C and 1000°C is twice that of the chars formed at 1200°C and 1400°C.

The lower reactivity measured for chars obtained above 1200°C can be explained by thermal annealing. This phenomenon is a consequence of the char graphitization, which leads to the decrease of the availability and of the intrinsic reactivity of reactive sites, due to a structure ordering (refer to section 1.2.3 of Chapter "State of the Art").

If thermal annealing was only to explain the reactivity differences between the char samples, a lower reactivity of char samples from 1400°C experiments than that of char samples from 1200°C experiments would be expected, as thermal annealing is enhanced by temperature. However, this is not what we measure in our experiments. In fact, char at 1400°C is partially gasified during the experiments in DTR under an inert atmosphere at 1400°C (Figure 49), while the reactivity of char is increased during its gasification, at least at the beginning of the conversion. This

assumption is confirmed by the high reactivity value of the gasified char sample from experiments at 1200°C under a wet atmosphere (see Appendix G). By consequence, the thermal annealing effects on char from 1400°C experiments may be attenuated by a reactivity increase due to the char gasification.

#### 3.2.3.2. *Influence of residence time on char reactivity*

Figure 71 compares the reactivity in two different conversion ranges of char from experiments at 1200°C under an inert atmosphere, sampled at 2 s and 4 s of residence time.

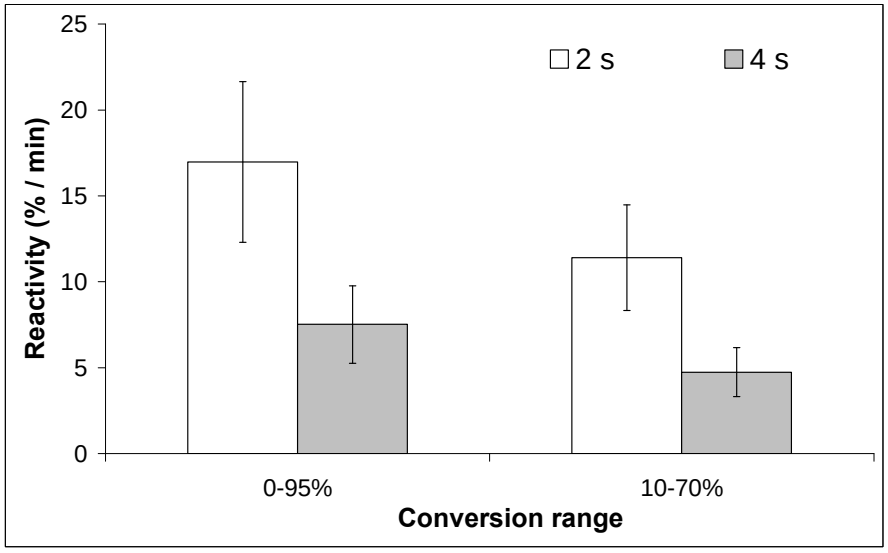


**Figure 71. Reactivity in two conversion ranges of char samples from the 0.35 mm particles thermal decomposition at 1200°C, after 2 s and 4 s of residence time**

Reactivity is 2.5 times higher for char sampled at 2 s of residence time than for char sampled at 4 s. This shows that char reactivity decreases as residence time increases at 1200°C, temperature at which char thermal annealing is thought to occur (refer to previous section). The progress of this phenomenon may then explain the difference of reactivity between the two char samples: as char is exposed to the heating flux during a longer time, it is more annealed and then its reactivity decreases.

#### 3.2.3.3. *Influence of particle size on char reactivity*

Figure 72 illustrates the effect of particle size on the reactivity, measured at 750°C and 20 mol% of $H_2O$ in two conversion ranges, for chars formed at 1000°C, 1200°C and 1400°C under an inert atmosphere, and sampled at the bottom of the DTR.

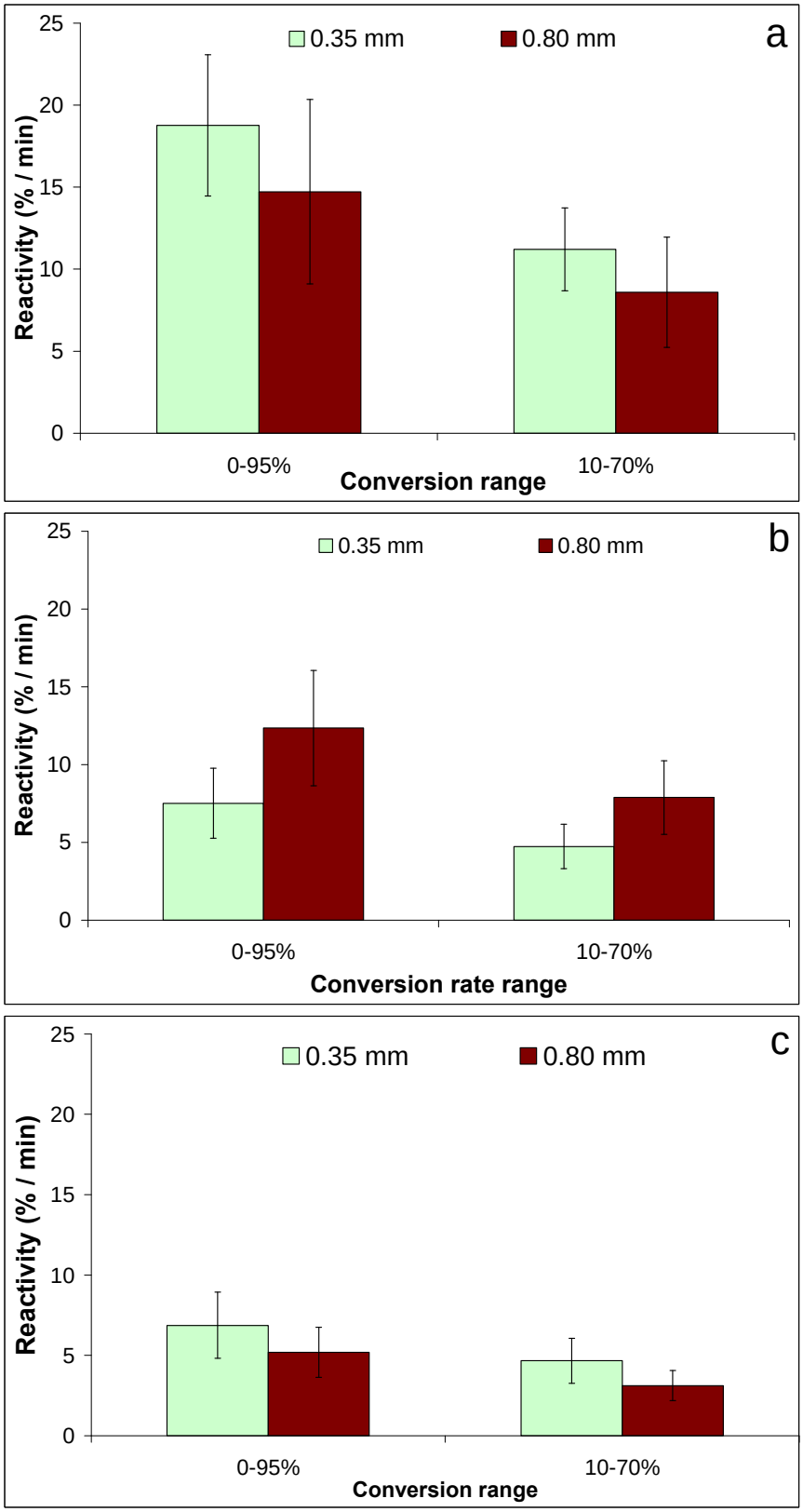


**Figure 72. Reactivity in two conversion ranges of char samples from the 0.35 mm and 0.80 mm particles thermal decomposition at 1000°C (a), 1200°C (b) and 1400°C (c), after 4 s of residence time**

The differences between samples are within the error bars. The particle size seems to have only a slight effect on char reactivity.

### 3.3. Summary

Even if soot always presents the same aspect in SEM observation, its composition and reactivity differ as a function of the operating conditions. Indeed, soot is enriched in carbon as temperature and residence time increase, and its reactivity depends on the initial particle size. The differences of composition and reactivity suggest different soot formation mechanisms depending on the experimental conditions. Regardless, composition and reactivity cannot be linked.

Chars formed between 1000°C and 1400°C show a typical morphology of a porous char from fast pyrolysis and keep a size in the same order of magnitude as that of the initial beech particles. Moreover, they present some soot and inorganic salts stuck on their surface. Char seems to be affected by graphitization a from 1000°C. This phenomenon, which consists in the rearrangement of the carbonaceous matrix into a more ordered structure and is enhanced with temperature, could not be directly identified by experiments, but its consequences could be detected: increase of the char carbon content and loss of reactivity, which arises from a more resistant char structure to gasification, with the increase of temperature. The loss of reactivity is known as thermal annealing or deactivation, and is in direct competition with gasification.

Note that the particle size has only a slight influence on char reactivity and composition.

## 4. Conclusion

Experiments in a DTR, which is the experimental device the best adapted to reproduce the operating conditions of an entrained flow reactor at a lab scale, were performed in order to study the thermal decomposition of beech sawdust. Several parameters were studied: temperature - 800°C to 1400°C -, steam concentration in the atmosphere - 0 mol% and 25 mol% -, residence time - 2 s and 4 s - and particle size - 0.35 mm and 0.80 mm -.

The thermal decomposition of beech particles in a DTR produces mainly volatiles - around 95 %w - and a very low amount of solid residue, char, remains - around 5 %w -. By consequence, the evolution of the gas phase controls the products yields in wood particles thermal decomposition.

The first step of the process is wood particle pyrolysis and tar cracking reactions. The resulting products are transformed by further reactions:

- cracking of $C_2H_4$ and $C_2H_6$ (dehydrogenation);
- hydrocarbons polymerization into PAHs and soot;
- hydrocarbons reforming;
- char and soot gasification;
- Water-gas shift.

According to products yields evolution, the most influencing transformations above 1000°C seem to occur in less than 2 seconds. Beyond 2 s, slight variations of the major gas yields - $H_2$, CO and $CO_2$ -, issued from the light hydrocarbons decomposition and char gasification taking several seconds to occur, are measured.

The biomass thermal decomposition reactions are considerably influenced by temperature and $H_2O$ concentration. The latter increases the kinetics of gasification, reforming and WGS.

Under an atmosphere with a poor $H_2O$, hydrocarbons cracking and polymerization play a major role, and lead to the subsequent formation of PAH and especially soot from 1200°C. Reforming, gasification and WGS reaction also occur under these conditions, but they have only a slight influence on the products yields because of their slow kinetics. The gas phase is then very rich in $H_2$ and CO issued from cracking and polymerization reactions, whereas $CO_2$, $H_2O$ and light hydrocarbons fractions are quite low.

On the contrary, in a 25 mol% of $H_2O$ atmosphere, the reforming, gasification and WGS reactions play a role as important as polymerization and cracking reactions on solid and gaseous products, particularly from 1200°C. The polymerization and reforming reactions are then in competition. All these reactions lead to low hydrocarbons, soot

and char yields, and to high $H_2$, CO and $CO_2$ yields. At 1400°C and 25 mol% of $H_2O$, the chemical kinetics of the reactions is fast enough to almost reach the thermodynamic equilibrium.

The beech particle size in the range of 0.30 mm - 0.80 mm has no considerable effect on the products yields from the beech thermal decomposition.

The collected solids from the experiments in the DTR, soot and char, were characterized by SEM observations, composition analyses and reactivity determinations by TGA experiments.

Soot characteristics appear to be very sensitive to the operating conditions, which lead to different soot formation pathways. Char is affected by the graphitization process from 1000°C, which leads to an enrichment in carbon content and thermal annealing. Graphitization and gasification, which have opposed influences on char reactivity, are competitive phenomena.

The next and last step in the present work is the modeling of the experiments, which will complement the study of wood gasification. Notably, modeling will be able to clarify some points for the biomass gasification understanding, as for example:

- the identification of soot precursors at each temperature;
- the individual contributions of reforming and gasification reactions on the soot yield reduction measured under a wet atmosphere compared to an inert one;
- the influence of chemical kinetics, of external mass transfer and thermal annealing on char gasification;
- the evolution of products yields at the early stage of the transformation.

# Résumé du Chapitre 4 : Résultats expérimentaux

Des expériences en four à chute ont été effectuées afin d'étudier la décomposition thermique de particules de hêtre en faisant varier plusieurs paramètres, qui sont: la température (800°C, 1000°C, 1200°C et 1400°C), la concentration de vapeur d'eau dans l'atmosphère (0% et 25% mol), le temps de séjour (2 s et 4 s pour le gaz) et la taille des particules (0,35 mm et 0,80 mm).

La décomposition thermique des particules de hêtre dans le four à chute produit principalement de la matière volatile (~ 95% en masse) et une très faible quantité de char (~ 5% en masse). Par conséquent, les rendements finaux des espèces sont principalement déterminés par l'évolution de la phase gazeuse.

La première étape de la transformation est la pyrolyse de particules de bois et le craquage des goudrons. Les produits résultants sont transformés par les réactions suivantes:

- le craquage de $C_2H_4$ et $C_2H_6$ (ou déshydrogénation),
- la polymérisation d'hydrocarbures en HAP et suie,
- le reformage des hydrocarbures,
- la gazéification du char et des suies,
- la réaction de water-gas shift.

D'après l'évolution des rendements mesurés, au-dessus de 1000°C, la plupart des transformations semblent se produire en moins de 2 s. Au-delà, de légères variations des rendements en gaz majoritaires ($H_2$, CO et $CO_2$) sont observées. Elles sont dues principalement à la conversion des hydrocarbures légers et à la gazéification du char et des suies, lesquels prennent plusieurs secondes pour se produire.

Les phénomènes liés à la décomposition thermique de la biomasse sont considérablement influencés par la température et la concentration en vapeur d'eau dans l'atmosphère.

Dans une atmosphère contenant peu de vapeur d'eau (c'est-à-dire une atmosphère inerte, contenant uniquement l'eau issue de la décomposition de la biomasse), le craquage et la polymérisation des hydrocarbures jouent un rôle majeur, et conduisent à des rendements élevés en HAP et/ou suies dès 1000°C. Les réactions de reformage, gazéification et WGS peuvent également se produire dans ces conditions, mais elles n'ont qu'une faible influence sur les rendements en raison de leur cinétique lente. La phase gazeuse est alors très riche en $H_2$ et CO, produits à partir des réactions de craquage et de polymérisation, tandis que les fractions de $CO_2$, $H_2O$ et hydrocarbures sont faibles.

Au contraire, dans une atmosphère contenant 25%mol de vapeur d'eau, les réactions de reformage, gazéification et WGS sont accélérés et jouent un rôle aussi important que la polymérisation et le craquage sur les produits solides et gazeux. Par ailleurs, la polymérisation et les réactions de reformage sont en compétition. L'ensemble de ces réactions conduit à de faibles rendements en hydrocarbures, suies et char, et à des rendements élevés en $H_2$, CO et $CO_2$. A 1400°C sous 25%mol de vapeur d'eau, la cinétique chimique des réactions est suffisamment rapide pour que l'équilibre thermodynamique soit presque atteint.

La taille des particules dans la gamme 0.30 mm – 0.80 mm n'a presque aucune influence sur les rendements en produits issus de la décomposition des particules.

Par ailleurs, les solides récupérés (suie et char) lors des expériences dans le four à chute ont été caractérisés grâce à des observations au microscope électronique à balayage, à des analyses de composition et à une détermination de leur réactivité par analyse thermogravimétrique.

Les caractéristiques des suies se montrent très sensibles aux conditions opératoires. Ceci suggère que les mécanismes concernant la formation des suies sont différents selon les conditions expérimentales, et donc que la décomposition thermique de la biomasse suit des chemins différents.

A partir de 1200°C, les caractéristiques du char subissent des modifications par le processus de graphitisation, qui conduit à une augmentation de la teneur en carbone et à une diminution de la réactivité quant la température augmente. La diminution de la réactivité du char, connue sous le nom de désactivation thermique, s'oppose à la gazéification qui a plutôt tendance à augmenter la surface réactive des particules et donc leur réactivité globale. Ainsi donc, la désactivation thermique et la gazéification sont des phénomènes compétitifs.

# Chapter 5: Modeling

This section describes the modeling associated to the experimental results obtained in the drop tube reactor (DTR), which were presented in the previous chapter. The main interest of this part is to have more complete information about the mechanisms of biomass thermal decomposition. The modeling was conducted using GASPAR, software originally developed for combustion applications and especially adapted for biomass gasification representation.

# 1. Description of GASPAR software

## 1.1. Description of the original model

### *1.1.1. Origins*

The GASPAR software, written in FORTRAN language, was initially developed by the research center RAPSODEE from the "Ecoles des Mines d'Albi - Carmaux" (Cancès, 2006; Commandré, 2002; Van de Steene, 1999). The initial objective of this software was the modeling of coal combustion and the interactions between the solid fuel and nitrogen oxides. GASPAR was then adapted by the CEA for a biomass gasification application (Peyrot et al., 2010).

### *1.1.2. Basic principles*

Figure 73 shows the particle and gas flows as represented in the GASPAR model.

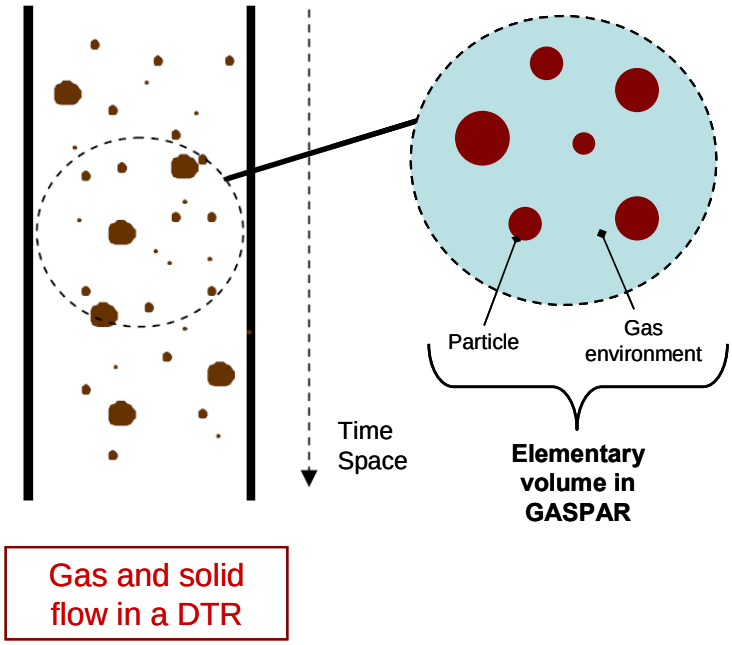


**Figure 73. Representation of the gas and solid flows in a DTR in GASPAR**

In the GASPAR software, the DTR is represented as a one-dimensional (1D) laminar plug flow reactor in a steady state regime where time and space are equivalent. Biomass particles in their gaseous environment are represented with a Lagrangian approach. The whole flow is simulated considering a single particle or a distribution of particles attached to a gas volume, which represent an elementary part of the flow. The particles are supposed to be spherical and their diameter can be unique or follow a size distribution of Rosin – Rammler type. No particle slip in the gas is considered in the model.

### 1.1.3. Modeling of physical and chemical processes

The GASPAR software couples the modeling of physical and chemical processes during the biomass thermal decomposition. The modeling includes gas and solid heating, moisture evaporation, biomass pyrolysis, gas phase reactions and char gasification.

The particle and gas heating is simulated by convection, conduction and radiation. A convective exchange is taken into account between the gas and the reactor walls fixed at a given temperature. As no particle slip is considered in the model, the heat exchange between the particles external surface and the gas is represented by conduction instead of convection. Radiative exchanges are considered between the hot reactor walls, the particles and the gas. The temperature of the gas and particles can be obtained at any moment of the transformation through a heat balance, which takes into consideration the heat exchanges between the particles, gas and the reactor walls, as well as the heat of the involved reactions and the heat transported by the volatiles leaving the particle.

Note that the internal heat transport within the particles is neglected because of their very small size, which implies that particles are isothermal. This assumption is questionable since the characteristic time of internal and external particle heating and that of pyrolysis have the same order of magnitude (refer to section 2.1.2.1 of Chapter "Materials and Methods"). Nevertheless, this assumption has no consequence when the whole pyrolysis process occurs almost instantaneously after the introduction of the particles in the reactor, as in the case of particles inferior to 500 µm. However, the use of this assumption can be hazardous when pyrolysis takes a few seconds to occur, as for instance for large particles, with a size higher than 500 µm.

Wood particle drying is represented by a simple Arrhenius law. The biomass devolatilization is represented by a one-step reaction (Equation 64) whose kinetics is of Arrhenius type. This reaction includes tar cracking because pyrolysis and cracking reactions cannot be experimentally uncoupled in a DTR, as they occur simultaneously in the temperature range of the present study. The solid particle size reduction during the transformation of biomass into char is represented by a shrinking factor.

$$BIOMASS\ (dry) \rightarrow a\ H_2 + b\ CO + c\ CO_2 + d\ H_2O + e\ CH_4 + f\ C_2H_2 + g\ C_2H_4 + h\ C_2H_6 + i\ C_3H_8 + j\ C_6H_6 + k\ CHAR + l\ TAR \qquad \textbf{Equation 64}$$

With: $a$, $b$, $c$, $d$, $e$, $f$, $g$, $h$, $i$, $j$ and $k$ determined from the experiments and $l$ deduced by difference from mass balance.

The gas phase reactions are represented using subroutines of CHEMKIN II software, which uses detailed chemical mechanisms (refer to section 2.2.1 of Chapter "State of the art").

Char gasification can also be modelled using a one-step reaction with a kinetics following an Arrhenius law, to which the Thiele diffusion model can be added in order to take into account the internal transport phenomena.

### 1.1.4. Input and output data of the model

Among the variables of the model, some are related to the process and others to the biomass characteristics. These can be listed in the following groups:

- operating conditions: temperature, pressure, inlet gas composition, biomass and inlet gas flowrates;
- reactor characteristics: dimensions, heat exchange coefficients;
- biomass composition: C, H, O, ash, moisture - w%;
- particles characteristics: size, physical properties, tortuosity, porosity;

- chemical reactions: kinetic parameters of pyrolysis and gasification, selection of the chemical scheme for gas phase reactions;
- repartition coefficients of the devolatilization products.

The results after the calculations are the gas and solid temperature, the molar and mass yields of the products, the molar fraction of each gas compound in the outlet gaseous stream, and the heat and mass balances.

#### *1.1.5. Limitation of the model*

The GASPAR software was successfully validated with the experimental results obtained by Chen (2009) concerning the 0.35 mm beech particles pyrolysis at 800°C and 950°C in a DTR (Peyrot et al., 2010). However, the model in its original version seems limited for its use above 950°C.

Indeed, the "tar" fraction in GASPAR represents the undetermined part of a mass balance which considers gaseous species and char (Equation 64). As it does not have any chemical signification, it cannot evolve with the operating conditions, whereas our experimental results clearly showed that tar yield decreases as temperature increases.

On the other hand, GASPAR does not include the soot species, whereas this compound is an important actor in biomass thermal decomposition from 1000°C.

Finally, the kinetic parameters of gasification available in GASPAR were determined from coal gasification experiments, while biomass char and coal have different properties and cannot be assimilated.

In summary, the model proposed in the GASPAR software is accurate for the description of wood devolatilization and of some gas phase reactions. However, it cannot describe further phenomena occurring at high temperature (> 950°C), as tar destruction and soot formation. Besides, the gasification kinetic parameters available in the model are not adapted for biomass char. So, some modifications of the model were performed in the present study in order to include tar and soot evolution, and to introduce a more appropriate approach for char gasification. Next section describes these modifications.

### 1.2. Modifications in GASPAR

#### *1.2.1. Modeling of tar evolution*

Tar fraction, as written in Equation 64, corresponds to all the unidentified compounds and thus its evolution is not possible in the original version of GASPAR. In order to improve its modeling, it can be represented by model compounds which are included in the chemical scheme and can then be transformed. The choice of the model tar compounds which will be used in our simulations is described and justified later in section 2.2.

#### *1.2.2. Modeling of soot formation and gasification*

##### *1.2.2.1. Modeling of soot formation*

One of the main objectives of the modeling was soot prediction, as the formation of this species is one of the key phenomena during the biomass gasification above 1000°C.

A simple approach was chosen for soot formation modeling. This consists in one-step reactions where the soot particle inception and surface growth steps are implicitly included. This approach is based on a global model proposed in literature (Ziegler, 2004), where soot formation is issued from the $C_2H_2$ decomposition, as shown by Equation 65.

$$C_2H_2 \rightarrow 2C_{soot} + H_2 \qquad \textbf{Equation 65}$$

As PAHs also contribute to soot formation, the same approach as the one used for $C_2H_2$ was applied for the most representative PAHs (Equation 66 – 69), which are: $C_{10}H_8$ (naphthalene), $C_{12}H_8$ (acenaphtalene), $C_{14}H_{10}$ (phenanthrene) and $C_{16}H_{10}$ (pyrene).

$$C_{10}H_8 \rightarrow 10\,C_{soot} + 4\,H_2 \qquad \textbf{Equation 66}$$

$$C_{12}H_8 \rightarrow 12\,C_{soot} + 4\,H_2 \qquad \textbf{Equation 67}$$

$$C_{14}H_{10} \rightarrow 14\,C_{soot} + 5\,H_2 \qquad \textbf{Equation 68}$$

$$C_{16}H_{10} \rightarrow 16\,C_{soot} + 5\,H_2 \qquad \textbf{Equation 69}$$

The kinetic parameters of Equation 65 to 69, based on those measured for soot formation from $C_2H_2$ during propane pyrolysis experiments (Ziegler, 2004), follow an Arrhenius law of first order with respect to $C_2H_2$ or PAHs concentration. The activation energy is the same as that obtained for propane pyrolysis - $Ea$ = 167 kJ.mol$^{-1}$ -, for all the cases, in order to keep the same relation of soot formation kinetics with temperature. However, the pre-exponential factor was adapted to our experimental conditions. As soot formation from $C_2H_2$ and PAHs occurs following a different mechanism, as explained in section 1.2.3 of "State of the art", a different pre-exponential factor was used for Equation 65 and Equation 66 to 69:

- The pre-exponential factor in Equation 65 was fitted so as to obtain the best agreement between the $C_2H_2$ yield experimentally measured under an inert atmosphere and that predicted by the model: $k_0 = 1.10^6$ s$^{-1}$.
- The pre-exponential factor in Equations 66 to 69, kept the same for all the PAHs, was fitted so that the soot yield from the simulation of experiments under an inert atmosphere agrees the best with the experimental yields: $k_0 = 5.10^6$ s$^{-1}$.

Note that this kinetic parameters set was found to be the only to give accurate predictions of both soot and $C_2H_2$ yields.

Equations 65 to 69 were integrated with their respective kinetic parameters into the chemical scheme selected to be used with CHEMKIN in GASPAR. Note that soot in the model is composed of carbon only. This approximation is acceptable for soot obtained after 4 s of residence time, as its carbon content is more than 92 mol% (refer to section 3.1.2 in the previous chapter). However, this is not the case for 'younger' soot with 2 s of residence time, which is composed of 83 mol% of carbon.

Besides the approach proposed in this section, soot formation will be also studied considering its formation by decomposition of $C_2H_2$ only and of PAHs only with the kinetic parameters determined above. A comparison between these three options is performed in section 2.3.2.

#### *1.2.2.2. Modeling of soot gasification*

Soot formation modeling has to be coupled with that of its gasification. This was modelled by a one step reaction of Arrhenius type, as seen in Equation 70.

$$\frac{dm_{soot}}{dt} = k_0 \cdot \exp\left(\frac{-Ea}{R \cdot T}\right) \cdot P_{H2O}^{n} \cdot m_{soot} \qquad \textbf{Equation 70}$$

With:

| | | |
|---|---|---|
| $m_{soot}$ | Mass of soot | kg |
| $k_0$ | Pre-exponential factor | $s^{-1}.bar^{-n}$ |
| $Ea$ | Activation energy | $J.mol^{-1}$ |
| $R$ | Constant of ideal gas | $J.mol^{-1}.K^{-1}$ |
| $T$ | Temperature | K |
| $P_{H2O}$ | Partial pressure of $H_2O$ | bar |
| $n$ | Order of the reaction | - |

The expression of gasification rate (Equation 70) does not take soot particles surface or a surface function (refer to section 2.3.1 of Chapter "State of the art") into account, as these parameters cannot be simply represented due to particles surface variations during surface growth and coagulation.

Mass transfer phenomena are neither included in soot gasification modeling. Indeed, our characteristic time analysis showed that soot gasification is kinetically controlled during the experiments in the DTR (refer to section 2.1.2.3 of Chapter "Materials and Methods").

The gasification kinetic parameters were determined from TGA experiments at three temperatures – 910°C, 950°C and 980°C – and two $H_2O$ molar concentration – 5 mol% and 20 mol% – for soot samples collected from the 0.35 mm particles thermal decomposition experiments at 1200°C. The mean reactivity measured in a conversion range of 10 - 70% ($R_{X=10\ -\ 70\%}$) was chosen to calculate the gasification kinetic parameters. This conversion range represents the middle of the reaction, which is for some authors the part of the transformation with the most accurate results related to gasification modeling (Barrio et al., 2001).

The gasification kinetic parameters, as calculated from the method in Appendix I, are then: $Ea$ = 178 $kJ.mol^{-1}$, $k_0$ = 345915 $bar^{-0.7}.s^{-1}$ and $n$ = 0.7. These kinetic parameters were determined for only one soot sample, as said just before. As shown in the previous chapter, reactivity $R_{X=10\ -\ 70\%}$ is approximately the same for all soot samples from the 0.35 mm particles whatever the temperature and residence time.

### 1.2.3. Modeling of char gasification

A char gasification model adapted to the experimental results was developed and added to GASPAR. This model establishes gasification kinetics proper to the char samples collected in the experiments.

The gasification rate can be written by the means of the conversion rate, which here is written as a function of the char kinetic parameters and the surface function (Equation 71).

$$\frac{dX}{dt} = k(T, P_{H2O}) \cdot f(X) \qquad \textbf{Equation 71}$$

With:

| | | |
|---|---|---|
| $X$ | Conversion | - |
| $t$ | Time | s |
| $k$ | Intrinsic kinetic parameter | $s^{-1}$ |
| $f$ | Surface function | - |

The kinetic parameter in Equation 71 was determined for a reference sample, which was the char obtained from the DTR experiments at 1000°C under an inert atmosphere.

Note that, as justified later through the validation in section 2.3.3, the modeling of char gasification during experiments in DTR did not require including:

- thermal annealing which was put into evidence with the reactivity measurements of char from 1000°C, 1200°C and 1400°C experiments in TGA (refer to section 3.2.3.1 of previous chapter);
- mass transfer phenomena, in particularly external transfer which could influence gasification rate as its characteristic time has the same order of magnitude as that of chemical kinetics under an inert atmosphere (refer to section 2.1.2.2 of Chapter "Materials and Methods").

#### 1.2.3.1. Modeling of the intrinsic kinetics

The intrinsic kinetics is expressed by the means of an Arrhenius law of order $n$ with respect to $H_2O$ partial pressure. The kinetic parameters were determined from the reactivities ($R_{X=10\ -\ 70\%}$) which were measured by TGA experiments in a conversion range of 10 - 70% at 750°C, 800°C and 850°C, and with a $H_2O$ concentration of 5 mol% and 20 mol%.

The gasification kinetic parameters, calculated by the method in Appendix I, are as follows: $Ea$ = 149 kJ.mol$^{-1}$, $k_0$=217893 s$^{-1}$.bar$^{-0.7}$ and $n$ = 0.7. The activation energy is in the range of the values reported in literature, which are 88 - 250 kJ.mol$^{-1}$ (Di Blasi, 2009), and the order of the reaction is very close to those found in literature, i.e. 0.4 – 0.6 (Di Blasi, 2009).

#### 1.2.3.2. Modeling of the surface function

The surface function used in this model corresponds to the Random Pore Model (RPM), which is the most suitable for char gasification modeling (refer to section 2.3.1.2 of Chapter "State of the art"). The surface function for the RPM is expressed as Equation 72.

$$f(X) = (1 - X) \cdot \sqrt{1 - \psi \cdot \ln(1 - X)} \qquad \textbf{Equation 72}$$

Where, $\Psi$ is a surface function parameter related to the pore structure of the non reacted sample ($X$ = 0). This parameter was fitted so as to obtain similar reactivities in a conversion range of 10 -70% between the experimental results in TGA and the model. This gives $\Psi \approx 1$, which is in the range of the values reported in literature concerning gasification of char from biomass fast pyrolysis: $\Psi$ = 0.5 – 50, (Fermoso et al., 2009; Matsumoto, 2009; Yuan et al., 2011).

### 1.3. Summary

The GASPAR software was chosen to simulate the beech particles thermal decomposition experiments in the DTR. This software was developed for thermochemical applications and modified in order to adapt it to biomass gasification at high temperatures (> 1000°C). The flow of particles in the carrier gas is represented in GASPAR by a 1D Lagrangian approach, and it includes thermal and chemical phenomena modeling:

- heating of carrier gas and wood particles;
- particles drying;
- chemical reactions: pyrolysis, gas phase reactions, soot formation and carbonaceous solids gasification.

Gas heating is modeled by convection and radiation, while particle heating is modeled by external conduction and radiation. The solid particles are supposed to be isothermal and not to slip in the gas. Pyrolysis, which also includes tar cracking as it is not possible to dissociate these phenomena in a DTR, is modelled by a one-step reaction with kinetics of Arrhenius type. The devolatilization products consist in permanent gases - $H_2$, CO, $H_2O$,

$CO_2$, $CH_4$, $C_2$ compounds, $C_6H_6$ -, char and tar. The latter can be represented by a mixture of model compounds. Gas phase reactions are described in details in CHEMKIN using a chemical scheme. Soot is assumed to be formed from $C_2H_2$ and/or PAHs decomposition reactions, which were added to the chemical scheme. The reactions of soot formation and gasification are modelled by global models reactions with kinetics following an Arrhenius law. Char gasification is represented by a global model with two terms: an Arrhenius kinetic law and a surface function.

The different parts of the modeling in GASPAR and their links are shown in Figure 74.

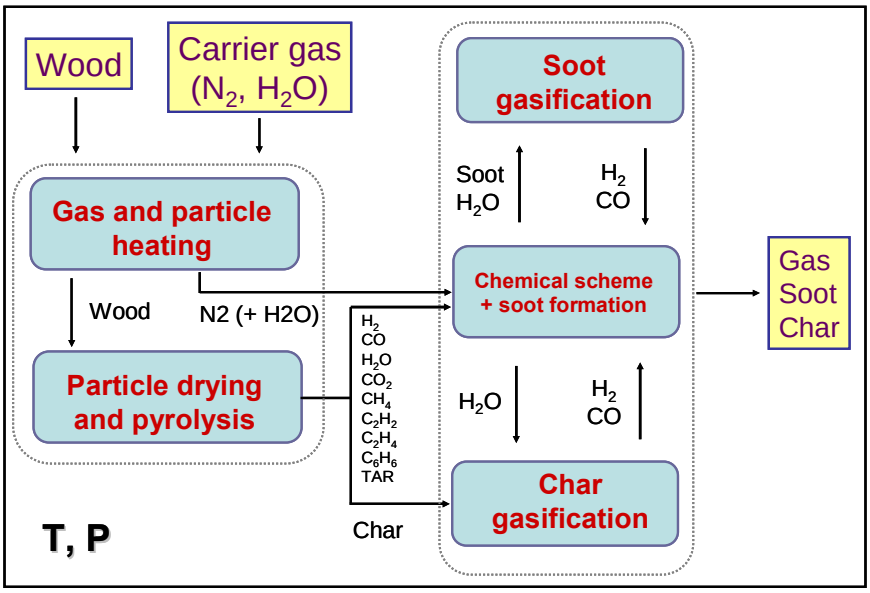


**Figure 74. Modeling principle of GASPAR software**

The results of the GASPAR simulations are shown and discussed in next section.

## 2. Validation and results of the modeling

### 2.1. Determination of variables of the model for the calculations

The experiments in the DTR were simulated with GASPAR. The pyrolysis kinetics, the particle shrinking factor and the heat exchange coefficient relative to gas heating by convection, were fixed from previous studies (Cancès, 2006; Chen, 2009; Commandré, 2008) and were not modified in the present study. The operating conditions and feedstock characteristics were fixed for our study.

The coefficients related to the repartition of the products after pyrolysis (Equation 64) were determined from our experiments under an inert atmosphere at 800°C and then were applied for all temperatures. This choice was based on the following assumptions:

- The products at 800°C are assumed to mainly result from pyrolysis and tar cracking, as further phenomena, such as soot formation, reforming and gasification, are limited at this temperature for a residence time of several seconds. This assumption was experimentally verified by Chen (2009), who showed that the gas yields stabilize in the first 0.3 m of the reactor, so just after pyrolysis and cracking have taken place.
- Pyrolysis and tar cracking give the same products distribution at any temperature, which is then modified by further gas phase reactions and by gasification.

The Skjoth-Rasmussen chemical scheme (Skjøth-Rasmussen et al., 2004) was selected for the gas phase modeling because it predicts with accuracy the PAHs formation and is then suitable for the soot formation

modeling. Note that this chemical scheme also includes the possibility to model soot formation from the collision of two pyrene molecules, which corresponds to the soot particle inception step.

As particle size does not present a significant effect on the particles thermal decomposition, as demonstrated in section 2.2 of Chapter "Experimental results", the modeling of the DTR experiments was only conducted for 0.35 mm particles. Besides, neglecting the particle slip in the gas and the solid internal heating may not be a correct approach for the 0.80 mm particles (refer to section 1.1.3).

## 2.2. Selection of the model tar compounds

We tried to select model tar compounds which were the most representative of our experiments. The tar mean formula determined for the experiments at 800°C (in section 1.1.3.1 of previous chapter), $C_nH_nO_{0.2n}$, suggests that tar is composed of a mixture of oxygen containing and aromatic hydrocarbons. This is in agreement with tar composition analyses performed by Zhang (2010), who studied thermal decomposition of Hinoki cypress sawdust in a DTR, under conditions very similar to those of the present study. These results are shown in Table 28.

**Table 28. Molar composition of tar from Hinoki cypress sawdust thermal decomposition experiments at 800°C in a DTR (Zhang et al., 2010)**

| Molar composition of tar | | | |
|---|---|---|---|
| **Oxygen containing HC** | **44 %** | **Aromatic HC** | **56 %** |
| - Methanol ($CH_3OH$) | 14 % | - Toluene ($C_6H_5CH_3$) | 12 % |
| - Phenol ($C_6H_5OH$) | 22 % | - Styrene ($C_6H_5CHCH_2$) | 6 % |
| - Benzofuran ($C_8H_6O$) | 4 % | - Indene ($C_9H_8$) | 7 % |
| - Others | 4 % | - Naphthalene ($C_{10}H_8$) | 12 % |
| | | - Biphenyl ($C_{12}H_8$) | 6 % |
| | | - Anthracene ($C_{14}H_8$) | 3 % |
| | | - Pyrene ($C_{16}H_8$) | 2 % |
| | | - Others | 8 % |

Table 28 shows that $C_6H_5OH$ (phenol) and $CH_3OH$ (methanol) are the major oxygen containing hydrocarbons, and that $C_{10}H_8$ (naphthalene) and $C_6H_5CH_3$ (toluene) are the major aromatic hydrocarbons. Therefore, these compounds were selected to represent tar in the model. Nevertheless, in practice, the decomposition of $C_6H_5OH$ was not correctly modeled by the Skjoth – Rasmussen scheme and thus only $CH_3OH$, $C_{10}H_8$ and $C_7H_8$ were considered for tar modeling.

The term "tar" in Equation 64 can then be replaced by a combination of $CH_3OH$, $C_{10}H_8$ and $C_7H_8$ in Equation 73.

$$l\ TAR = m\ CH_3OH + n\ C_{10}H_8 + o\ C_7H_8 + p\ TAR_{residual} \qquad \textbf{Equation 73}$$

Through a global and an elemental mass balance, the *m*, *n* and *o* coefficients were adjusted in order to minimize the coefficient *p*, which corresponds to the remaining fraction of the unidentified tar.

The best fitting, through which the residual tar yield was minimized to 5 mol%, was obtained for a tar composition of 30 mol% of $CH_3OH$ and 65 mol% of $C_{10}H_8$ and no $C_7H_8$. The resulting tar formula from this combination is $C_nH_{1.3n}O_{0.3n}$, which is very close to the tar mean formula obtained from our experiments at 800°C.

## 2.3. Validation of GASPAR

### *2.3.1. Validation of the devolatilization coefficients choice*

The devolatilization coefficients , which were determined from the experimental yields at 800°C under an inert atmosphere, were validated by comparing the modeling and experimental results under these conditions (Figure 75).

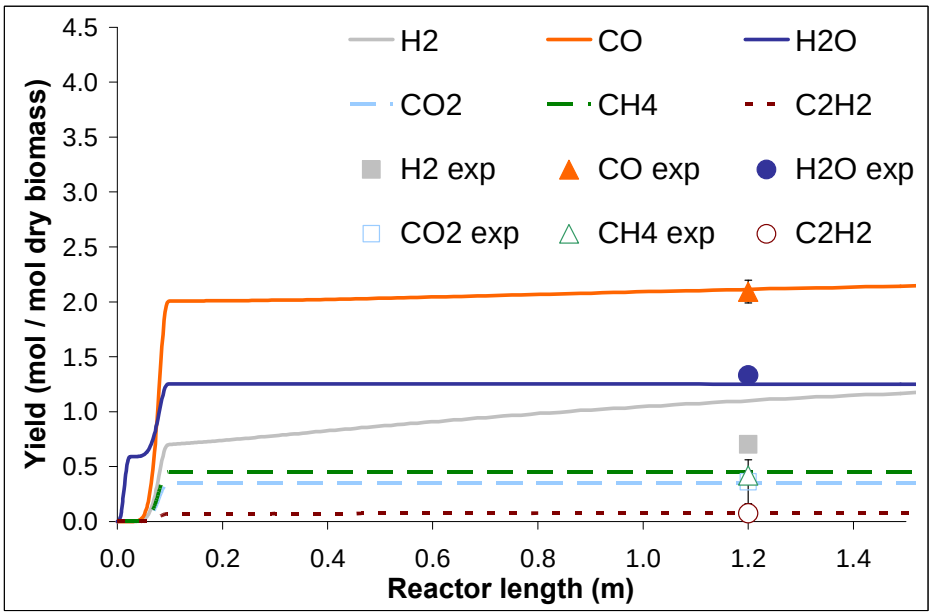


**Figure 75. Experimental and simulated molar yields of permanent gas from the particles thermal decomposition under an inert atmosphere at 800°C, versus reactor length**

According to the modeling results, pyrolysis and tar cracking occur in the first 0.30 m of the DTR, which agrees with the experimental results obtained by Chen (2009) for the 0.35 mm beech particles pyrolysis under the same conditions.

After pyrolysis and tar cracking, the $H_2O$, $CO_2$, $CH_4$ and $C_2H_2$ yields stabilize, as expected according to the assumptions of section 2.1, whereas $H_2$ and CO yields tend to increase. The increase of these yields is linked to the decomposition of the model tars, particularly methanol ($CH_3OH$), as shown in Figure 76. Therefore, the use of methanol as a model tar induces an overestimation of cracking reactions, and thus of the $H_2$ and CO yields at 800°C. However, this has no consequence from 1000°C, since all oxygen containing hydrocarbons are then supposed to be almost completely converted, as could be experimentally observed in section 1.1.3.1 of Chapter "Experimental results" and confirmed by Zhang (2010).

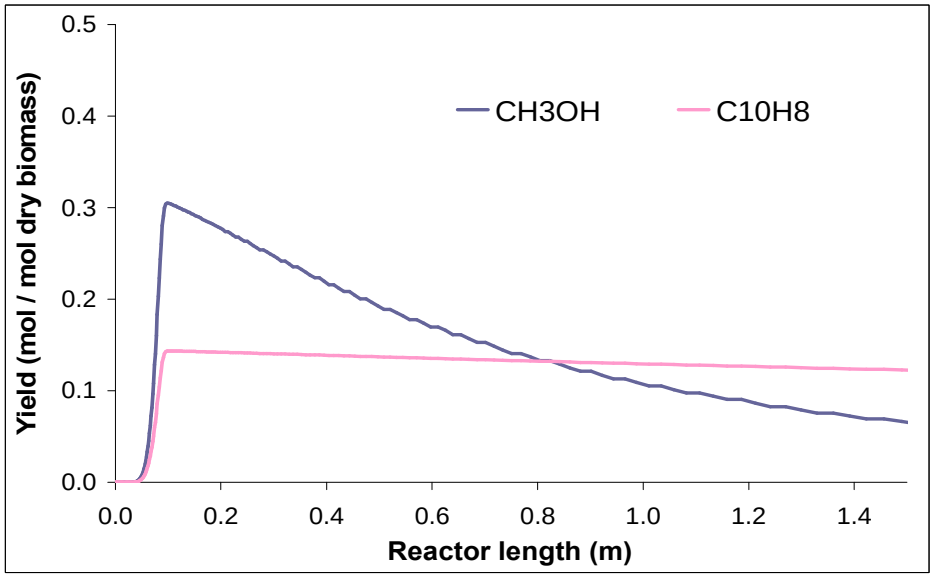


**Figure 76. Simulated molar yields of $CH_30H$ and $C_{10}H_8$ from the particles thermal decomposition under an inert atmosphere at 800°C, versus reactor length**

### *2.3.2. Validation of the soot modeling approach*

Figure 77 compares the soot yields measured for the 0.35 mm particles thermal decomposition under an inert atmosphere and the yields calculated using different soot formation pathways (refer to section 1.2.2.1):

- soot formation from $C_2H_2$ only;
- soot formation from PAHs only;
- soot formation from $C_2H_2$ and PAHs;
- soot formation from the collision of two pyrene molecules included in the initial Skjoth – Rasmussen chemical scheme (refer to section 2.1).

Note that the experimental soot yields could only be estimated at 1200°C and 1400°C but not at 800°C and 1000°C, as explained in the previous chapter.

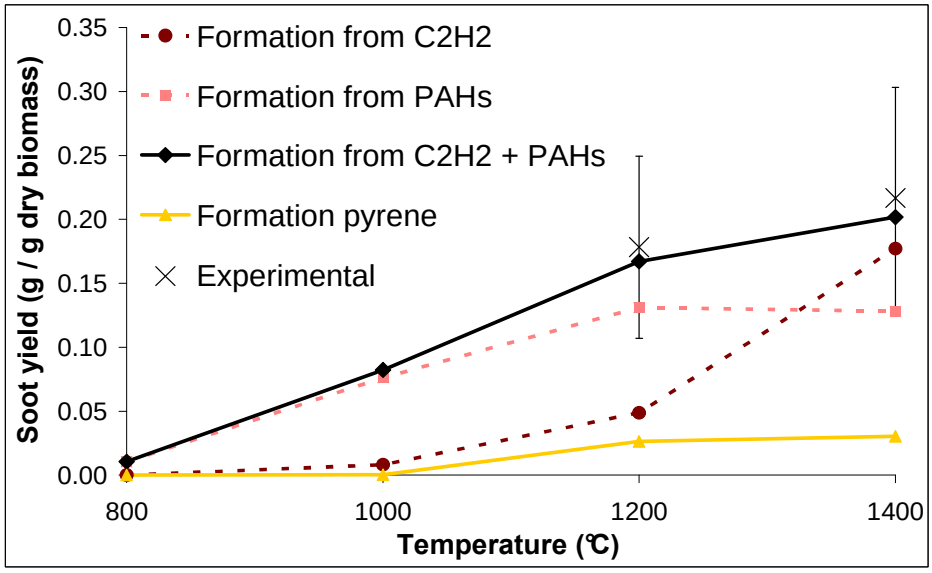


**Figure 77. Experimental and simulated (by using different modeling approaches) mass yields of soot from the particles thermal decomposition under an inert atmosphere at 800°C, 1000°C, 1200°C and 1400°C**

The model considering soot formation from both $C_2H_2$ and PAHs gives results which are in best agreement with the experimental results. So, the modeling of soot formation requires the consideration of both $C_2H_2$ and PAHs as soot precursors for accurate predictions in the wider temperature range.

Considering only $C_2H_2$ or PAHs can give a correct estimation of soot formation at respectively 1400°C and 1200°C. These results can be explained by simulations without considering soot formation at all (Figure 78). At 1200°C, the PAHs total mass yield is much higher than that of $C_2H_2$ along the reactor length. On the contrary, at 1400°C, the PAHs yield decreases and the $C_2H_2$ yield increases along the reactor length, which leads to a higher $C_2H_2$ yield from 0.35 m. The evolution of these compounds may be related to the decomposition of PAHs into $C_2H_2$ (Vander Wal & Tomasek, 2004).

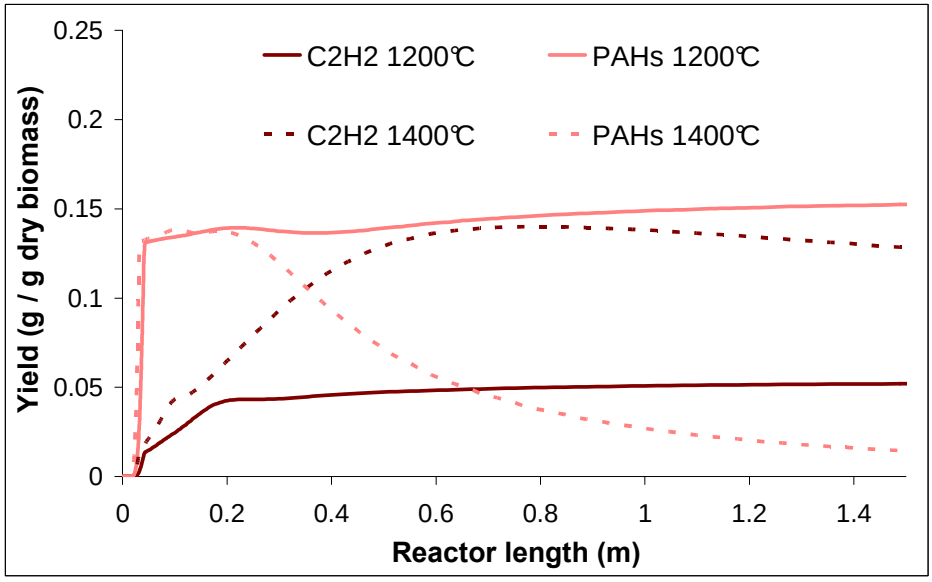


**Figure 78. Mass yields of PAHs and $C_2H_2$ yields from the simulation of experiments at 1200°C and 1400°C under an inert atmosphere without considering soot formation, versus reactor length**

The soot yields issued from the reaction proposed in the Skjoth – Rasmussen chemical scheme, corresponding to the particle inception, is much lower than the experimental results. In fact, soot formation modeling by particle inception only is not satisfactory for a complete description of the phenomena, and confirms that soot mass growth is mainly due to the addition of $C_2H_2$ and PAH on its surface (refer to section 3.1.2.2 of Chapter "Fundamental concepts").

Note that the soot yields at 800°C and 1000°C, which could not be experimentally determined, are estimated by the model at respectively 0.01 and 0.08 $g/g_{db}$ (Figure 77). This latter value is closed to the soot yield at 1000°C measured by Zhang (2006), which is 0.066 $g/g_{db}$.

### *2.3.3. Validation of char gasification modeling approach*

In Figure 79, the char yields obtained by the simulation of the experiments under inert and wet atmospheres are compared to the experimental yields.

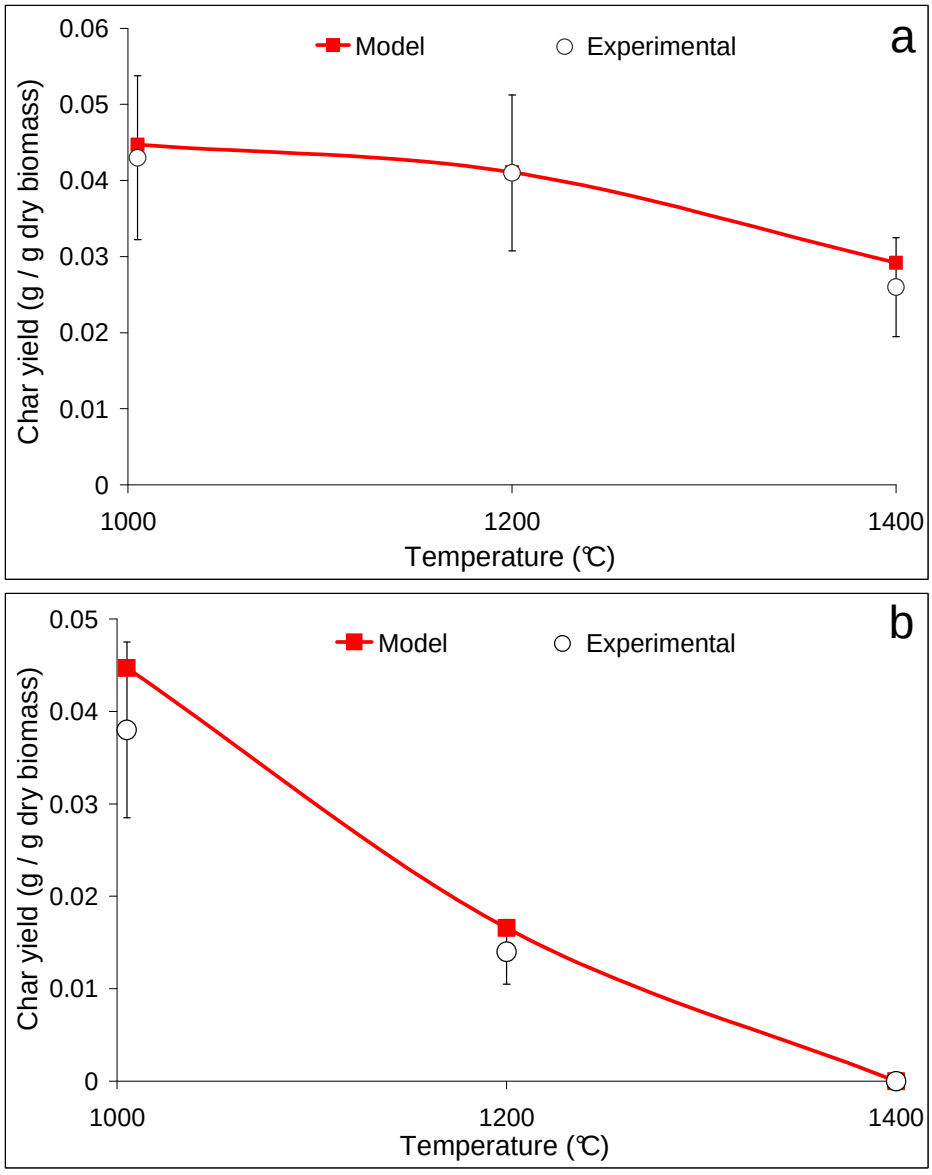


**Figure 79. Experimental and simulated mass yields of char from the particles thermal decomposition under inert (a) and wet (b) atmospheres at 1000°C, 1200°C and 1400°C**

For the simulation of experiments under inert (Figure 79a) and wet (Figure 79b) atmospheres, the gasification model gives char yields values within the error bars of the yields measured during DTR experiments. As mentioned in section 1.2.3, this result suggests that thermal annealing and external mass transfer are not limiting for char gasification under high temperatures and high heating rates. This suggests that thermal annealing and external mass transfer do not have a significant influence on char gasification during the experiments in the DTR. Indeed, thermal annealing is not seen in the experimental conditions in the DTR, where the temperature is much higher and the residence time much shorter than those of TGA experiments. Besides, the external mass transfer rate may occur much faster than the chemical kinetics, even under an inert atmosphere. Char gasification then occurs in a kinetically controlled regime for every DTR experiments with the 0.35 mm sample.

## 2.4. Results of the simulation

### 2.4.1. Results of the simulation for $C_2H_2$, PAHs and soot

Reminder: the sum of tar and soot yields in the experiments corresponds to the unmeasured fraction in the mass balance. At 1000°C, it is considered as a mixture of unknown proportions of PAHs and soot, whereas at 1200°C and 1400°C it is assumed to be only composed of soot (refer to section 1.1.3.1 of Chapter "Experimental results").

Note that the term "PAHs" in Figure 80, Figure 82 and Figure 83 refers to the sum of all the PAHs present in the Skjoth – Rasmussen chemical scheme, including the major ones (naphthalene, acenaphtalene, phenanthrene and pyrene).

#### 2.4.1.1. Simulation of experiments under an inert atmosphere

Figure 80 presents the $C_2H_2$, PAHs and soot yields obtained from the simulation of DTR experiments under an inert atmosphere at 1000°C, 1200°C and 1400°C. The soot formation was modeled considering $C_2H_2$ and PAHs as soot precursors, which show the best agreement with experiments (refer to section 2.3.2). The experimental $C_2H_2$ and sum of tar (PAHs) and soot yields, measured at the middle and the bottom of the reactor, are compared to the modeling results.

The calculated $C_2H_2$ and "PAHs + soot" yields are in good agreement with the experimental yields.

According to the model results, the soot yield clearly increases with temperature. At all temperatures, the PAHs decomposition into soot is faster than that of $C_2H_2$. At 1000°C, half of the initial PAHs are decomposed at the bottom of the reactor whereas the $C_2H_2$ yield remains almost steady. At 1200°C, the PAHs are completely converted at the reactor outlet whereas $C_2H_2$ is very slowly converted and its complete decomposition seems to be far. At 1400°C, the PAHs are decomposed very fast, just before the middle of the reactor, and the $C_2H_2$ complete conversion is almost achieved at the end of the reaction length. Note that the soot yield at 1400°C decreases very slightly after having reached its maximum value, which is probably due to a slight gasification.

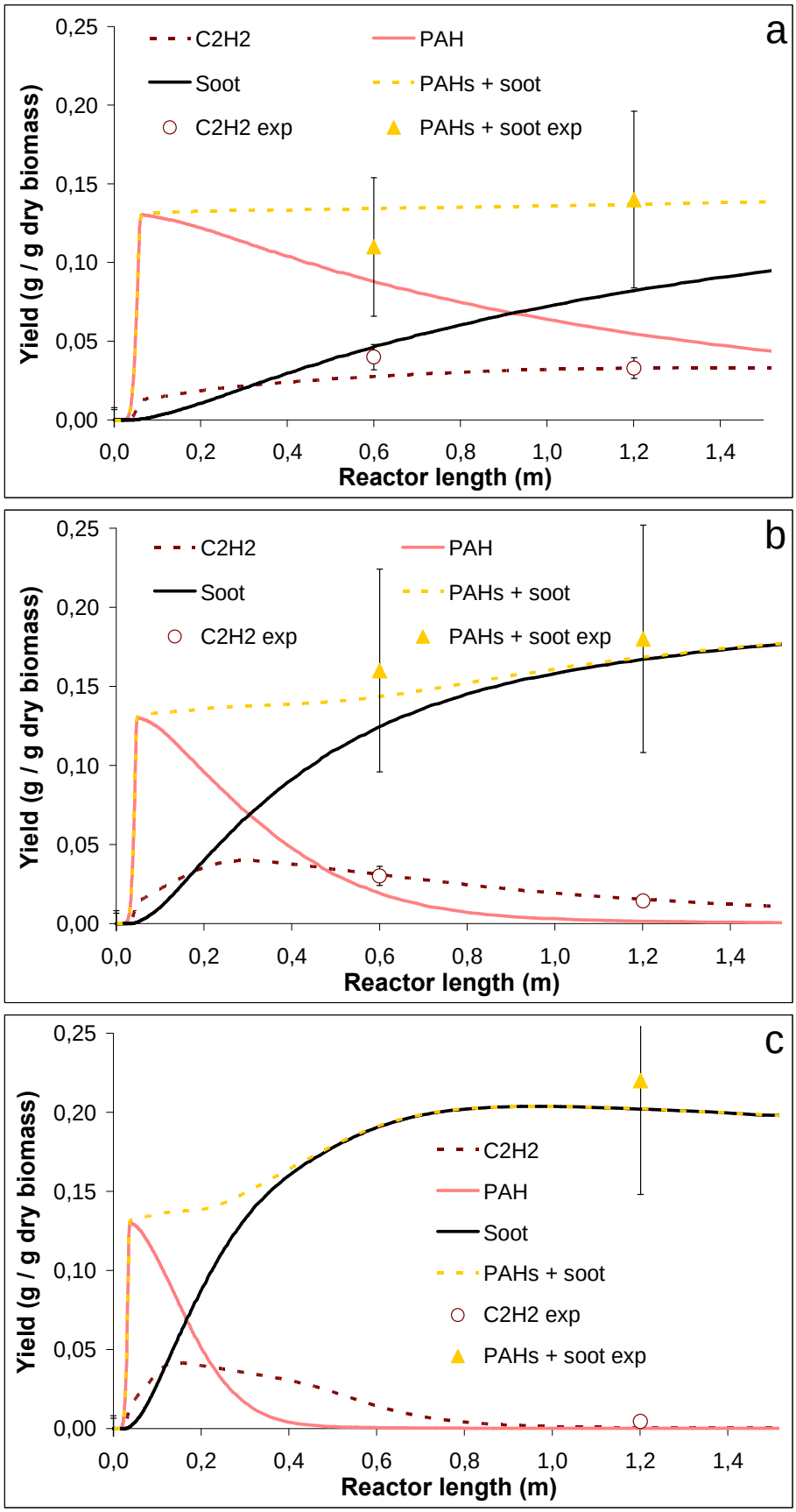


**Figure 80. Experimental and simulated mass yields of $C_2H_2$, PAHs and soot from the particles thermal decomposition under an inert atmosphere at 1000°C (a), 1200°C (b) and 1400°C (c), versus reactor length**

Interesting information about the soot formation mechanisms can be deduced from the modeling results. At 1000°C, soot mainly comes from PAHs decomposition, as $C_2H_2$ decomposition is very slow. At 1200°C and 1400°C, soot is issued from both $C_2H_2$ and PAHs. At 1400°C, PAHs can also alternatively decompose into $C_2H_2$ (Figure 78). Furthermore, at a given temperature, soot is firstly produced by PAHs decomposition and subsequently by $C_2H_2$ decomposition.

The difference of composition measured between soot samples in section 3.1.2 of the previous chapter can find an explanation in the difference of kinetics of $C_2H_2$ and PAHs decomposition into soot observed in Figure 80, and in the work of Vander Wal & Tomasek (2004). As already mentioned in section 1.2.3 in the Chapter "State of the Art", such study put soot nanostructure differences into evidence as a function of synthesis conditions, and suggests that soot mass growth by PAHs addition gives an amorphous structure whereas $C_2H_2$ addition leads to a more dense and graphitic structure. The aromatic complexes in soot structure are less interconnected in an amorphous structure than in a graphitic one, which leads to more C-H bonds within the particle and then to a higher hydrogen content. Figure 81 attempts to clarify this assumption: due to the branched PAH structure, its polymerization with soot surface can create void spaces, where C-H bonds are inaccessible for further polymerization. On the contrary, the polymerization of $C_2H_2$ with soot occurs uniformly on its surface, which minimizes the C – H bonds.

Therefore, the higher soot carbon content at 1400°C than at 1200°C, and after 4 s than after 2 s of residence time, could be related to a major contribution of $C_2H_2$ in soot formation as temperature and residence time are higher.

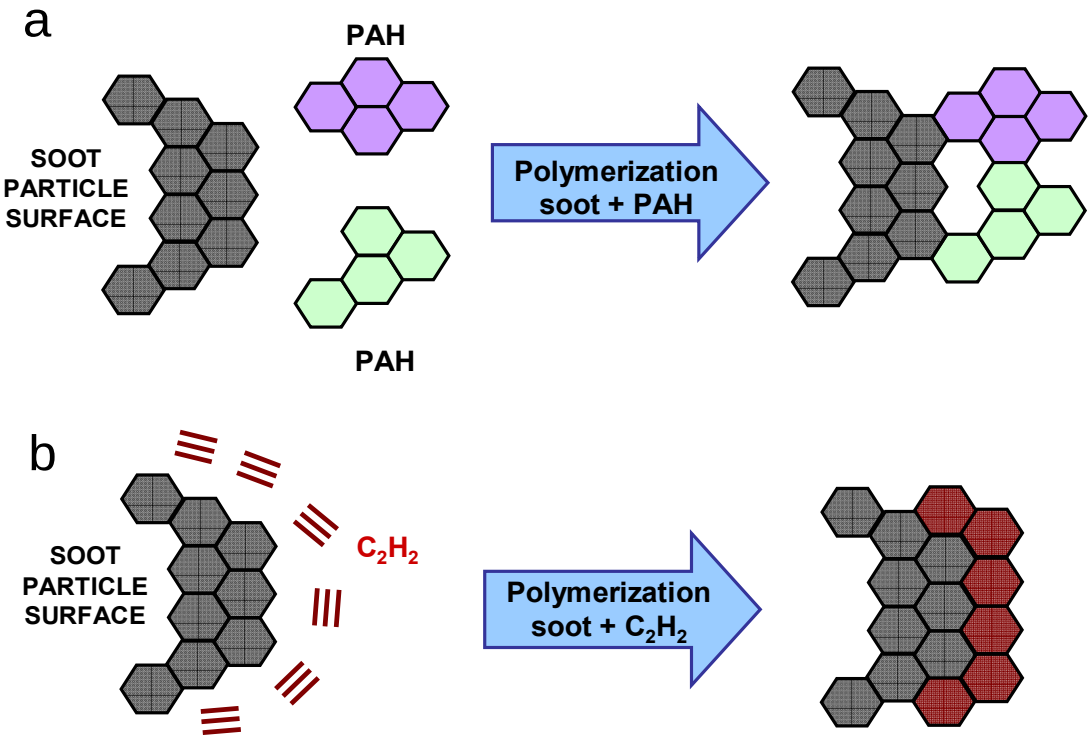


**Figure 81. Example of soot surface mass growth with PAHs (a) and $C_2H_2$ (b)**

#### 2.4.1.2. Simulation of experiments under a wet atmosphere

Figure 82 and Figure 83 present the $C_2H_2$, PAHs and soot yields obtained from the simulation of DTR experiments at 1000°C, 1200°C and 1400°C under a wet atmosphere. In order to better distinguish the contribution of soot gasification on the results, two different types of calculations were performed: one using the integral soot model developed in the present study (refer to section 1.2.2) presented in Figure 82, and one with soot gasification deactivated in Figure 83.

The $C_2H_2$, and the sum of tar and soot yields experimentally determined under a wet atmosphere, at the bottom and the middle of the reactor, are also represented in Figure 82.

The computed soot yields agree with experimental results only at 1400°C if gasification is considered. At 1000°C and 1200°C, the "PAHs + soot" yields given by the simulation are overestimated. Nonetheless, at 1200°C, the lower PAHs and soot yields under a wet atmosphere than under an inert one observed in experiments is also shown by simulation results, as seen through the comparison of Figure 80b and Figure 82b. This is not the case of simulation results at 1000°C, which give the same PAHs and soot yields under inert and wet atmospheres (comparison of Figure 80a and Figure 82a). Concerning $C_2H_2$, the simulation accurately predicts the yields measured during experiments at all temperatures.

A discussion about these results is proposed hereafter.

At 1400°C, according to the simulation results, the lower soot yield under a wet atmosphere than under an inert atmosphere is due to both soot gasification and hydrocarbons reforming. The respective contributions of each of these phenomena on soot yield reduction, with respect to the soot yield under an inert atmosphere, 0.22 $g/g_{db}$ (Figure 80c), are 35% and 65%.

At 1000°C and 1200°C, the lower soot yield under a wet atmosphere is mainly due to hydrocarbons reforming, as gasification seems to have no or only a slight influence, as seen through the comparison of Figure 82a and b with Figure 83a and b. Nevertheless, the model overestimates the PAHs and soot yields (Figure 82a and b), which seems to mainly come from the underestimation of hydrocarbons reforming reactions by the model. Thereby, more PAHs than expected are transformed into soot instead of being reformed at 1000°C and 1200°C in the model. The simulation of gas phase reactions experiments in a steam containing atmosphere, performed by Valin (2009), reaches the same conclusion for several chemical schemes, including the Skjoth – Rasmussen's one. Note that the possibility of soot gasification underestimation to explain the discrepancies at 1000°C and 1200°C is not likely to occur as soot gasification usually exhibits a slow kinetics at these temperatures (refer to section 2.1.2.3 of Chapter "Materials and Methods").

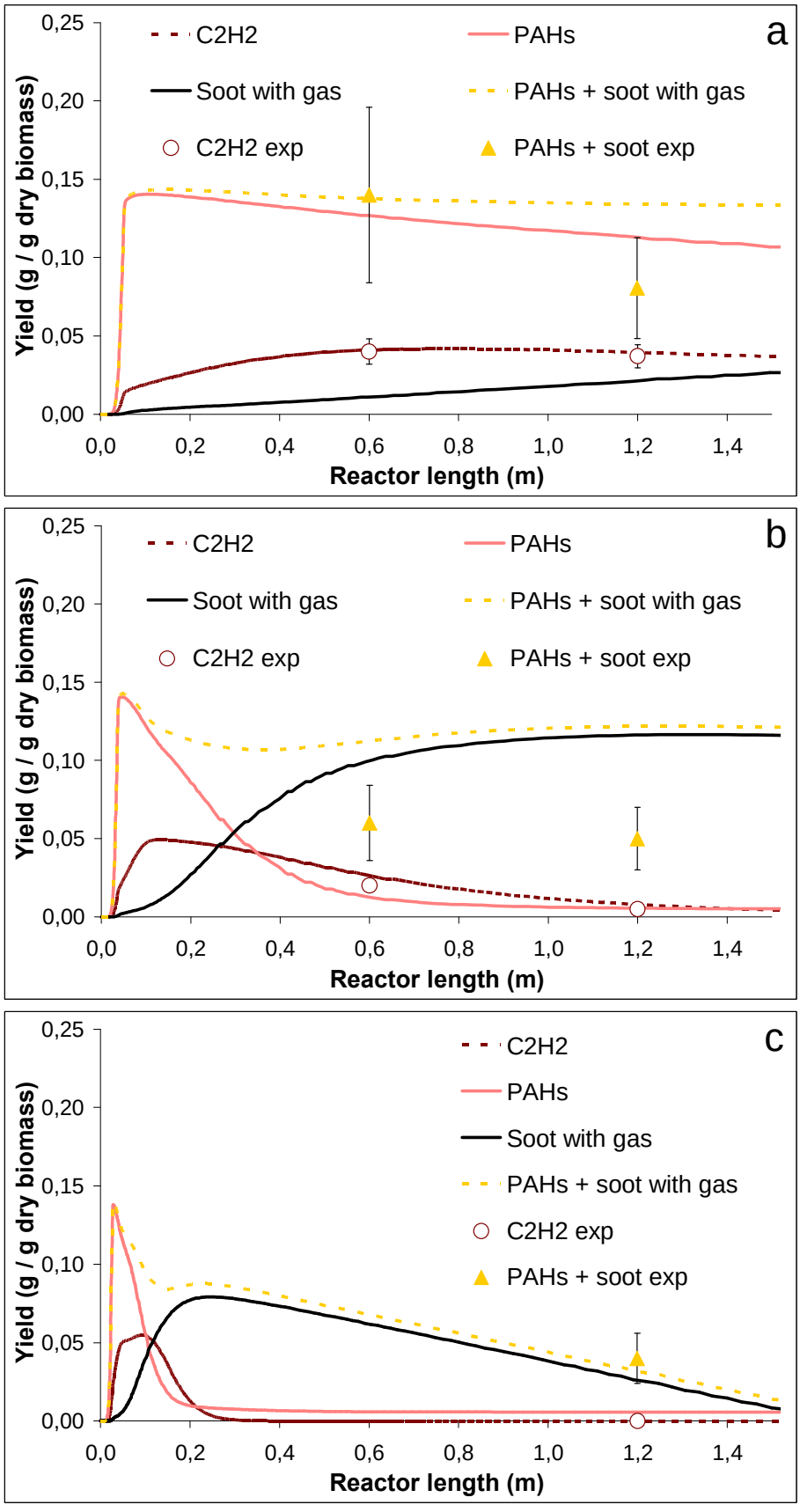


**Figure 82. Experimental and simulated (by considering soot gasification) mass yields of $C_2H_2$, PAHs and soot from the particles thermal decomposition under a wet atmosphere at 1000°C (a), 1200°C (b) and 1400°C (c), versus reactor length**

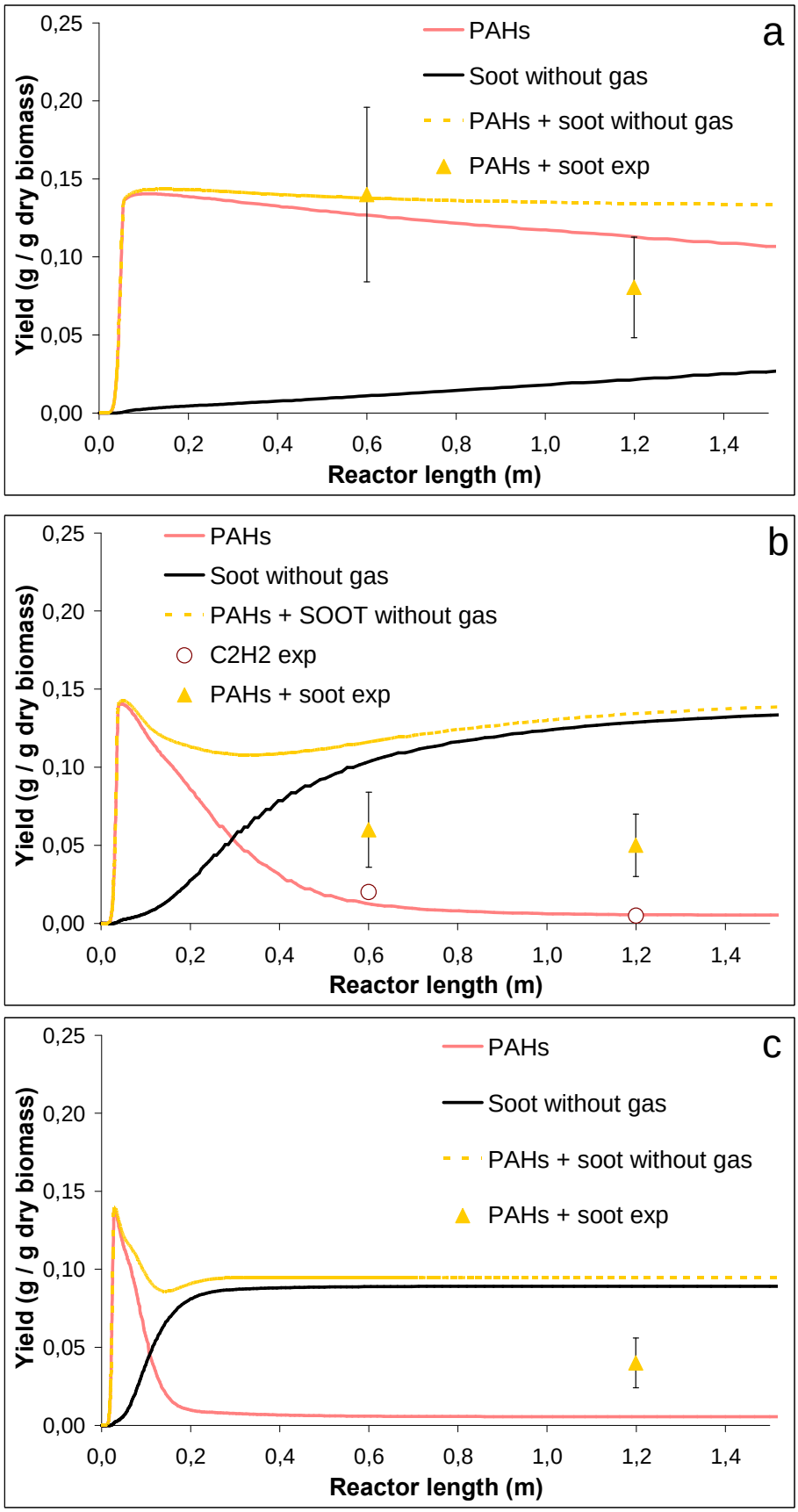


**Figure 83. Experimental and simulated (without considering soot gasification) mass yields of $C_2H_2$, PAHs and soot from the particles thermal decomposition under a wet atmosphere at 1000°C (a), 1200°C (b) and 1400°C (c), versus reactor length**

### 2.4.2. Results of the simulation for major gas

The major gas yields obtained from the simulation of DTR experiments under inert and wet atmospheres are presented in next sections. For this, the simulation in GASPAR was performed considering soot formation from $C_2H_2$ and PAHs, and soot and char gasification.

#### 2.4.2.1. Simulation of experiments under an inert atmosphere

Figure 84 shows the major gas molar yields computed by GASPAR for the DTR experiments under an inert atmosphere at 1000°C, 1200°C and 1400°C, and compared to the experimental yields measured at the middle and the bottom of the reactor.

The results from the model are globally satisfactory. The simulated gas yields follow the same evolutions as the experimental yields measured at the middle and the bottom of the reactor. Nevertheless, some discrepancies, not exceeding 20% of relative difference, can be observed for some yields.

At 1000°C, the $H_2$ yield obtained by the simulation is overestimated, which may be due to an overestimation of hydrocarbon polymerization.

At 1200°C, the $H_2$ yield is underestimated whereas the $CH_4$ yield is overestimated by the model. Part of the underestimation of $H_2$ yield can be related to the underestimation of $CH_4$ decomposition, which would tend to increase the $H_2$ yield and decrease the $CH_4$ yield.

At 1400°C, the simulated CO and $H_2$ yields are overestimated while the $H_2O$ yield is underestimated, which seems to be a consequence of the underestimation of reforming reactions (refer to section 2.4.1.2).

Note that the gas yields show a drastic increase within the first centimeters of the reactor with pyrolysis and tar cracking occurring very fast, at less than 0.05 s. The gas yields then stabilize or vary more slowly with the further reactions.

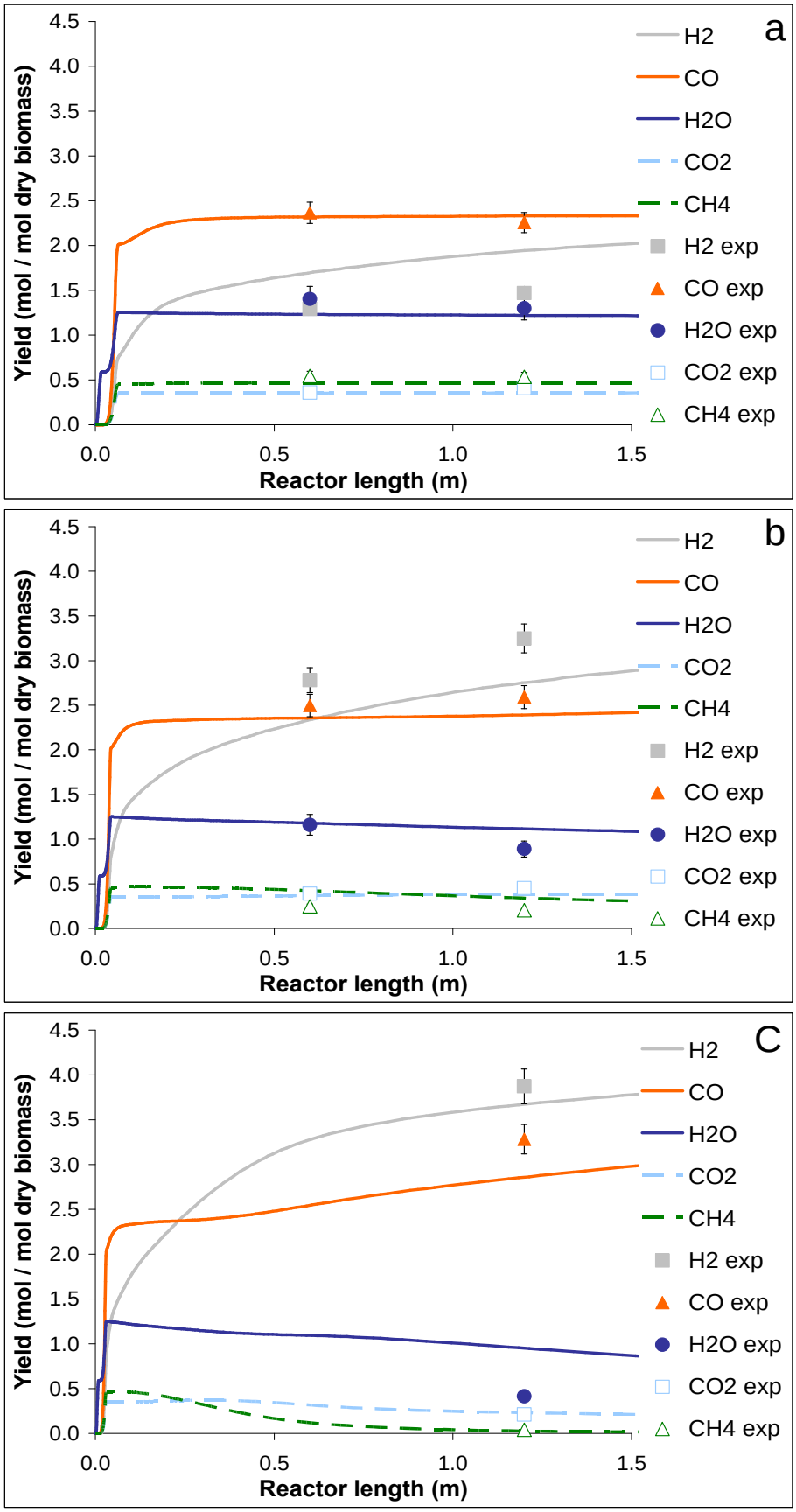


**Figure 84. Experimental and simulated molar yields of permanent gas from the particles thermal decomposition under an inert atmosphere at 1000°C (a), 1200°C (b) and 1400°C (c), versus reactor length**

#### 2.4.2.2. Simulation of experiments under a wet atmosphere

In Figure 85, the gas yields calculated by GASPAR at 1000°C, 1200°C and 1400°C are compared to those measured at the bottom and the middle of the reactor.

The simulation of the DTR experiments under a wet atmosphere gives acceptable results. The main trends experimentally observed are well represented in the simulation. Moreover, the predictions are in some cases very accurate, and the deviations between the calculated and experimental yields rarely exceed 20% of relative difference.

At 1000°C, the $CO_2$ and $H_2$ yields are underestimated, whereas the CO yield is overestimated at the middle of the reactor. At this temperature, the deviations between experiments and simulation are the highest, 50% for $CO_2$ and 25% for $H_2$ yields at the bottom of the reactor. At 1200°C, the $CO_2$ and $H_2$ yields are also underestimated by the model. The deviations concerning CO, $CO_2$ and $H_2$ yields can be mainly explained by the underestimation of the hydrocarbons reforming, which also leads to an underestimated soot yield (refer to section 2.4.1.2). A better representation of hydrocarbons conversion would increase the $H_2$ yield and indirectly that of $CO_2$ by the intermediary of CO via the WGS reaction.

At 1400°C, the simulation completely agrees with the experimental results. All the phenomena are then well represented under these conditions. Let us remind that thermodynamic equilibrium is almost reached under these conditions (refer to section 1.3 of Chapter “Experimental results”). At this temperature, the increase of gas yields occurs very fast in the first instant and then it gets slower since the middle of the reactor, where the only reaction still evolving is soot gasification.

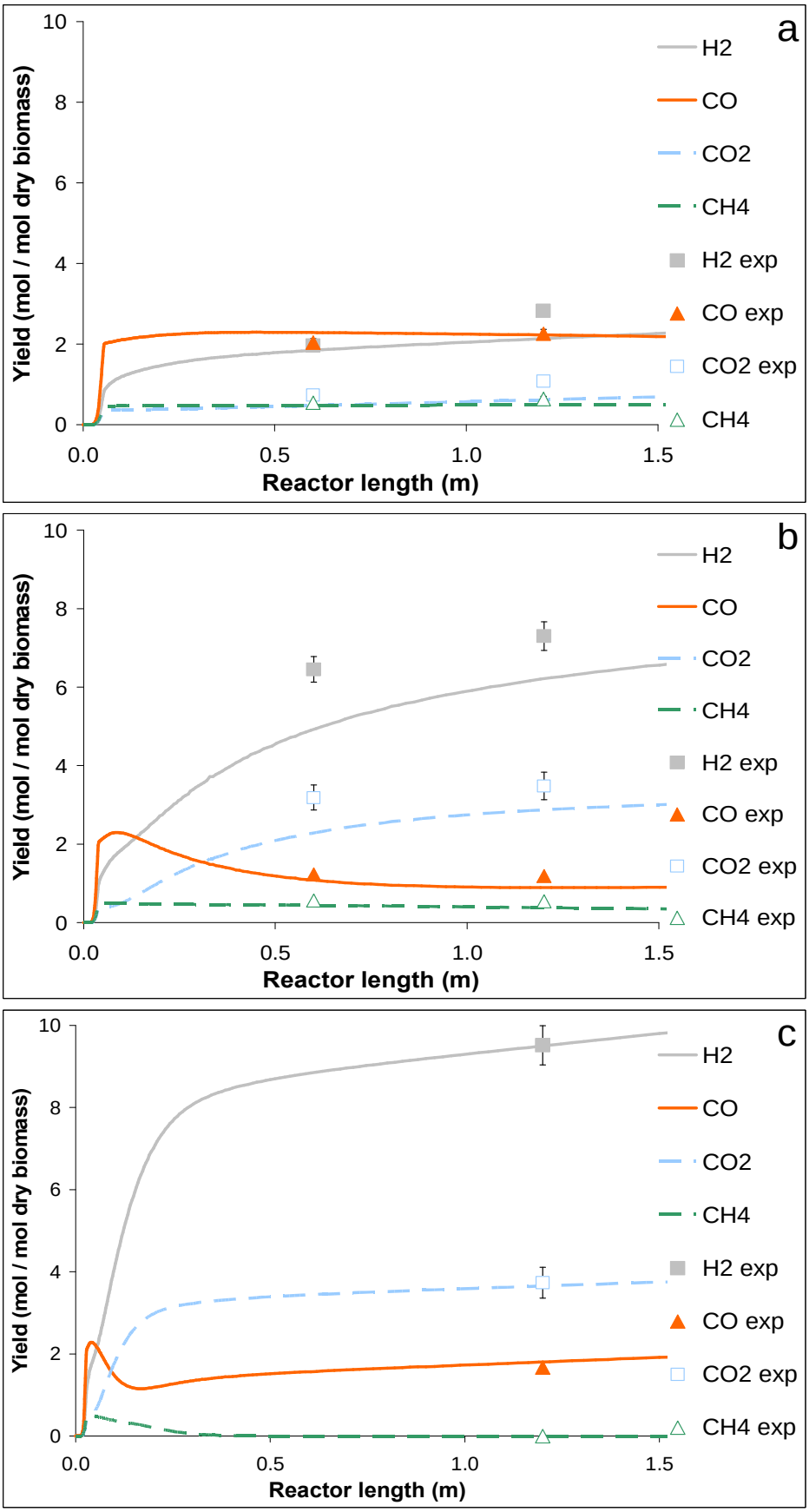


**Figure 85. Experimental and simulated molar yields of permanent gas from the particles thermal decomposition under a wet atmosphere at 1000°C (a), 1200°C (b) and 1400°C (c), versus reactor length**

### 2.5. Summary

The 0.35 mm particles thermal decomposition experiments in a DTR were simulated using an improved version of the GASPAR software.

The simulations give very accurate predictions for gas, PAHs, soot and char yields for the experiments under an inert atmosphere, at the exception of some cases which present slight deviations. However, the simulation results at 1000°C and 1200°C under a wet atmosphere are not in quite as good agreement with the experimental results as the results under an inert atmosphere. Indeed, the $H_2$ and $CO_2$ yields are lower, while the sum of PAHs and soot yield is higher than expected. These deviations seem to be mainly caused by the underestimation of hydrocarbons reforming. Hydrocarbons reforming underestimation is not visible for the simulation of experiments at 1400°C under a wet atmosphere as the system tends to the thermodynamic equilibrium. The best agreement between the simulation and the experiments is obtained in that case.

The results of the simulation bring us further information about the beech particles thermal decomposition.

As expected from the experimental results, particles pyrolysis and tar cracking occur very fast, within the first centimeters of the reactor (< 0.05 s of residence time). On the contrary, the polymerization, gasification, reforming and WGS reactions occur all along the reactor. Thereby, the yields of some products are still evolving at the bottom of the reactor...

The simulations results show that soot is formed from both $C_2H_2$ and PAHs. In literature, these compounds are assumed to be responsible for most of the soot mass growth after particle inception. According to the model, the conversion of $C_2H_2$ and that of PAHs into soot have different kinetics. Besides, according to literature, the soot formations from $C_2H_2$ and PAHs follow different pathways, which lead to different soot molecular structures. These observations can explain the differences of composition of soot samples experimentally measured.

On another hand, the lower soot yield under a wet atmosphere than under an inert one is mainly due to the reforming of the hydrocarbon precursors. From 1200°C, soot gasification also slightly contributes to soot reduction.

Finally, the thermal annealing of char formed in DTR experiments under an inert atmosphere, which was put into evidence with TGA experiments, does not have an influence on char gasification in the DTR conditions.

## 3. Conclusion and perspectives

The modeling of the experiments in the DTR was performed by GASPAR. This software presents a simplified modeling approach to describe in one dimension the phenomena involved in biomass particles thermal decomposition. Each simplification is justified and based on physical and chemical concepts. GASPAR is coupled to CHEMKIN, which provides a detailed description of the gas phase reactions.

The simulation results enable to complement the experimental analysis performed in previous chapter. In general, the simulations present correct predictions with a very low running time, inferior to 20 s.

However, the model underestimates hydrocarbon reforming, which probably comes from the Skjoth – Rasmussen chemical scheme, specialized in PAH formation and only validated for oxidation applications. Thereby, it would be suitable to adapt the Skjoth – Rasmussen chemical scheme or use a new one more appropriate for a gasification atmosphere.

Another point which could be improved in GASPAR is the modeling of soot formation, even if it presents acceptable predictions in its current state. The soot formation approach used here is simplified, by assigning the same kinetic parameters to the different PAHs and by not including the term of surface while most phenomena during soot formation occur in heterogeneous phase. A model, distinguishing the individual contribution of each PAH and including the soot surface, would give a fine description of the process. Thus, more detailed soot characteristics would be obtained, such as its composition and the spherule size.

The soot gasification approach used here apparently seems correct. Nevertheless, it could not be truly validated because its influence on soot yield was not clearly observed due to the reforming overestimation. Soot gasification modeling could still be improved by introducing the term of surface or better yet by inserting this reaction to the mass growth chemical scheme where it would be in competition with $C_2H_2$ surface addition.

Another interesting perspective is to model the 0.80 mm beech particles thermal decomposition in the DTR, which would require changes in the actual model. For 0.80 mm beech particles, internal heating and slip in the gas cannot be neglected. Besides, external mass transfer of $H_2O$ molecules into char would be necessary to be introduced in order to accurately model gasification under an inert atmosphere. The comparison of the results from the simulation of 0.80 mm beech particles thermal decomposition to those obtained for the 0.35 mm particles could allow identifying differences in the involved mechanisms, notably concerning soot formation, as experimentally observed.

# Résumé du Chapitre 5 : Modélisation

Le logiciel GASPAR a été choisi pour simuler les expériences en four à chute. Ce logiciel, développé initialement pour modéliser la combustion du charbon, a été modifié afin de l'adapter à la gazéification de la biomasse à haute température (> 1000°C). Le flux de particules et de gaz est représenté dans GASPAR par une approche 1D lagrangienne, qui considère des phénomènes thermiques et chimiques:

- Chauffage du gaz et des particules de bois,
- Séchage des particules,
- Réactions chimiques (pyrolyse, réactions en phase gazeuse, formation de suie et gazéification des solides carbonés).

Le chauffage du gaz et des particules est modélisé par de la convection (gaz), de la conduction externe (solide) et du rayonnement (gaz et solide). Les particules solides sont supposées être isothermes et ne pas glisser dans le gaz. La pyrolyse, qui comprend également le craquage primaire des goudrons puisque ce n'est pas possible de dissocier ces phénomènes dans un four à chute, est modélisée par une réaction en une seule étape dont la cinétique suit une loi d'Arrhenius. Les produits de la dévolatilisation sont des gaz permanents ($H_2$, CO, $H_2O$, $CO_2$, $CH_4$, les composés $C_2$, $C_6H_6$), le char et les goudrons, lesquels sont représentés par un mélange de composés modèles (méthanol et naphtalène). Les réactions en phase gazeuse sont modélisées par CHEMKIN, en utilisant un schéma cinétique détaillé. Les suies sont formées à partir du $C_2H_2$ et/ou des HAP. Les réactions de formation et la gazéification des suies sont représentées par des réactions en une seule étape suivant une loi d'Arrhenius. La gazéification du char est représentée par un modèle global comportant 2 composantes: une loi d'Arrhenius associée à une fonction de surface.

La décomposition thermique des particules de 0,35 mm dans le four à chute a été simulée en utilisant le logiciel GASPAR.

Les simulations donnent des prédictions assez précises concernant les rendements en espèces gazeuses, en HAP, en suies et char pour les expériences dans une atmosphère inerte, sauf dans quelques cas où les écarts entre expériences et simulation restent cependant inférieurs à 20%. Cependant, les résultats de simulation à 1000°C et 1200°C dans une atmosphère humide ne sont pas en si bon accord avec les résultats expérimentaux. Les rendements prédits en $H_2$ et de $CO_2$ sont alors trop faibles, tandis que la somme des rendements en HAP et en suies est trop élevée. Ces écarts semblent être principalement la conséquence de la sous-estimation du reformage d'hydrocarbures par ce modèle. A 1400°C dans une atmosphère humide, l'accord entre la simulation et les expériences est très bon, le système tendant alors vers l'équilibre thermodynamique.

Les résultats des simulations nous apportent des informations complémentaires à l'analyse expérimentale sur les mécanismes lors de la gazéification de la biomasse.

Comme prévu à partir des résultats expérimentaux, la pyrolyse des particules et le craquage des goudrons se produisent très rapidement, dans les premiers centimètres du réacteur (< 0,3 s de temps de séjour). Au contraire, la polymérisation, la gazéification, le reformage et la réaction de WGS se produisent tout au long du réacteur.

Les résultats des simulations confirment que les suies sont formées à partir du $C_2H_2$ et des HAP, ce qui est en accord avec la littérature. Selon le modèle, la conversion de $C_2H_2$ et celle des HAP en suie ont des cinétiques différentes: les HAP ont tendance à être convertis plus rapidement que le $C_2H_2$. Par conséquent, à 1000°C, les suies sont surtout formées à partir des HAP. A 1200°C et 1400°C, le $C_2H_2$ et les HAP participent à sa formation. La formation des suies à partir des HAP donne des propriétés différentes aux suies par rapport au $C_2H_2$, comme observé expérimentalement et dans la littérature. Notamment, le $C_2H_2$ conduit à une structure de suie plus dense et avec une teneur plus élevée en carbone.

Par ailleurs, le rendement en suies est plus faible dans une atmosphère humide que dans une atmosphère inerte, principalement à cause du reformage des hydrocarbures, précurseurs de suies. A partir de 1200°C, la gazéification des suies contribue également à la réduction des suies, mais son influence reste moins importante que celle du reformage.

Enfin, la désactivation thermique du char, mise en évidence à partir des expériences en ATG, n'a pas une influence significative sur la gazéification du char dans le four à chute.

# Conclusion

The present study was conducted in order to get a better comprehension of biomass particles gasification in the operating conditions characteristic of an entrained flow reactor. In order to achieve this goal, the influence of several parameters, namely reaction temperature, $H_2O$ content in the atmosphere, particle size and residence time, were carefully studied by the means of experiments and simulation. This work was organized in three steps.

First of all, thermal decomposition experiments were performed in a drop tube reactor under an inert or a wet atmosphere composed of 25 mol% of $H_2O$, with beech particles of two sizes: 0.35 mm and 0.80 mm. The products yields were measured at several temperatures - 800°C, 1000°C, 1200°C and 1400°C - and reaction zone lengths - 0.6 m and 1.2 m -.

Secondly, the carbonaceous solids collected during the DTR experiments, char and soot, were characterized with elementary composition analyses - C, H, O, ash -, scanning electron microscopy observations and steam reactivity measurements by thermogravimetric analysis.

Finally, the experimental observations were integrated into an existing model, GASPAR, which was modified to represent biomass gasification at high temperatures (> 1000°C). The modified model, which accurately predicts the products yields, remains simple and has enough physical meaning to be used for an investigation of the role of the different phenomena on the apparent kinetics of the process.

The most important information obtained with the analysis of experimental and modeling results are:

- Particles pyrolysis and tar cracking occur very fast and are completed in less than 0.3 s for the 0.35 mm particles and than 2 s for the 0.80 mm particles, at 1200°C or above. These phenomena mainly produce volatile compounds - around 95 w% - and very low amounts of char - around 5 w% - under high heating rates and high temperatures (> 800°C).
- From 1200°C, the light hydrocarbons and tar yields are very low, inferior to 0.05 $g/g_{db}$. Soot formation and reforming reactions are competing phenomena responsible for these low hydrocarbons yields. These phenomena occur in a few seconds.
- Soot is synthesized from 1000°C through $C_2H_2$ and PAH polymerization. These compounds also result from a complex series of cracking and polymerization reactions. Soot formation from PAHs occurs much faster than that from $C_2H_2$ and gives different characteristics to the solid. Notably, soot from $C_2H_2$ is very dense and has higher carbon content. The whole process releases high amounts of $H_2$.
- Steam reforming reactions play an important role in the prevention of soot formation, as they convert hydrocarbons into CO and $H_2$ instead of soot. Steam gasification also contributes to soot reduction but it has a secondary role compared to reforming reactions, due to the low soot reactivity.
- Water gas shift reaction has an important influence on gas yields. Under a wet atmosphere, the direct path of this reaction is favored due to the high $H_2O$ concentration, which leads to high $H_2$ and $CO_2$ yields. Note that this reaction is at thermodynamic equilibrium from 1200°C under a wet atmosphere.
- Char gasification significantly occurs from 1200°C in a steam containing atmosphere. Under an inert atmosphere, the $H_2O$ and $CO_2$ released by pyrolysis are to low for char to be significantly gasified. Char graphitization leads to a carbon content increase and to a reactivity decrease of the char as temperature increases. However, it does not have a significant influence on char yield in the DTR.
- The thermodynamic equilibrium is almost reached at 1400°C under an atmosphere containing 25 mol% of $H_2O$. The limiting phenomenon which can explain that this equilibrium is not perfectly reached is soot gasification.
- No significant difference of products yields was observed between the 0.35 mm and 0.80 mm particles. Nevertheless, the phenomena occur with a different pathway in the early stage of the transformation, which gives soot with different properties.

The results obtained in the present study enable to better understand the phenomena occurring in an entrained flow reactor and to give suggestions for the optimal operating conditions.

Particularly, the important role of high temperatures, above 1200°C, in an entrained flow reactor has been demonstrated, since hydrocarbon conversion is very high under these conditions, leading to very low light hydrocarbons and tar yields. In counterpart, high temperatures favor soot formation, while this compound is an undesirable product which leads to an efficiency loss in the process, filter clogging and system fouling. A high $H_2O$ content in the atmosphere can limit the presence of soot in the reactor outstream, as it avoids soot formation through the reforming of its precursors and enhance its gasification. Note that supplementary measures can be taken in the reactor in order to enhance reforming reaction before soot formation takes place. For example, the mixing between $H_2O$ and the gas released from the particle pyrolysis could be improved. High temperatures and high $H_2O$ concentrations can together allow thermodynamic equilibrium to be reached. The conversion of wood into CO and $H_2$ is then maximal, and the models for reactor design and operation are simpler.

Another important phenomenon in the entrained flow reactor is the WGS reaction, which determines the final concentrations of $H_2$, CO, $H_2O$ and $CO_2$. The operating conditions of the reactor, such as the steam content in the atmosphere, could be oriented to modify the WGS so as to adjust the $H_2$ and CO concentrations towards the required ratio for their further use, as for instance a ratio $H_2/CO = 2$ for Fischer-Tropsch synthesis. These measures could reduce costs related to the WGS post-treatment unit.

Finally, our results suggest that almost millimetric particles could be fed in an entrained flow reactor and be completely converted in a few seconds. This would considerably lower the pretreament cost and increase the process efficiency.

Some direct perspectives to this work have been identified, concerning experiments in the DTR, solids characterization and modeling:

Firstly, the quantification of tar and soot produced in the DTR would allow establishing a more precise mass balance. For this purpose, SPA tar sampling and analysis could be used to measure the yields of several tar compounds, as well as a laser system for soot quantification.

Solids characterization could be completed:

- by TEM observations for soot, in order to better understand the soot structure differences;
- by Raman spectroscopy for char, in order to confirm the assumption of graphitization.

Hydrocarbons steam reforming, which is not very accurately represented in GASPAR, could be improved. Moreover, a more realistic soot model could be developed and introduced in GASPAR. Such a model would bring additional information about soot, as the spherules size distribution or soot composition. Moreover, the modeling of the 0.80 mm particles thermal decomposition in a DTR would also be of great interest. This would require that additional phenomena, such as particles internal heating and sliding in the gas, are taken into account.

Further investigations about biomass gasification in an entrained flow reactor would be interesting to be performed. For instance, the influence of the presence of $O_2$ or $CO_2$ on the distribution and characteristics of products from biomass thermal decomposition could be the topic of the next research. These compounds are probably present in the reaction zone of an industrial reactor, as unreacted $O_2$ could leave the flame from the burner and $CO_2$ is a by-product of biomass combustion.

# Conclusion générale et perspectives

L'étude présent a été mené afin d'accéder à une meilleure compréhension de la gazéification de particules de bois dans les conditions opératoires caractéristiques d'un réacteur à flux entraîné. Afin d'atteindre cet objectif, l'influence de plusieurs paramètres, à savoir la température de réaction, la teneur en vapeur d'eau dans l'atmosphère, la taille des particules et le temps de séjour, a été étudiée en détails à partir d'expériences et de simulations. Ce travail a été organisé en trois étapes.

Tout d'abord, des expériences de décomposition thermique du bois dans un four à chute ont été effectuées sous une atmosphère inerte ou humide (composée 25 %mol de $H_2O$), avec deux tailles de particules de hêtre (0,35 mm et 0,80 mm). Les rendements des produits ont été mesurés à plusieurs températures (800°C, 1000°C, 1200°C et 1400°C) et prélevés après plusieurs longueurs de zone réactionnelle (0,6 m et 1,2 m).

Ensuite, les solides carbonés récupérés lors des expériences en four à chute, c'est-à-dire le char et les suies, ont été caractérisés par des analyses de composition élémentaire (C, H, O, cendres), par des observations au microscope électronique à balayage et par des mesures de réactivité en thermobalance.

Enfin, les observations expérimentales ont été intégrées dans un modèle existant (GASPAR) modifié afin de l'étendre aux conditions de notre étude. Le nouveau modèle, qui prédit de manière satisfaisante le rendement des produits, reste simple et possède suffisamment de sens physique pour être utilisée comme un moyen d'analyse.

Les informations les plus remarquables issues de l'analyse des résultats expérimentaux et de modélisation sont résumées dans les paragraphes ci-dessous:

- La pyrolyse et le craquage des goudrons, se déroulant presque simultanément, produisent principalement des composés volatiles (~ 95% en masse) et de très faibles quantités de char (~ 5% en masse) sous une vitesse de chauffage élevée et à température supérieure à 800°C. Ces phénomènes sont très rapides et sont achevés en moins de 0,3 s pour les particules de 0,35 mm et en moins de 2 s pour les particules de 0,80 mm, à 1200°C ou plus.
- A partir de 1200°C, les hydrocarbures sont très peu présents (moins de 0,05 g/g de biomasse sèche). La formation des suies et les réactions de reformage, qui sont des phénomènes concurrents, conduisent à de faibles rendements en hydrocarbures. Ces phénomènes se produisent en quelques secondes.
- Les suies sont produites dès 1000°C à partir des réactions de polymérisation faisant intervenir le $C_2H_2$ et les HAP, lesquels sont le résultat d'une série complexe de réactions de craquage et polymérisation. La formation de suies est beaucoup plus rapide à partir des HAP que du $C_2H_2$. Les caractéristiques des suies, telles que leur composition, sont très sensibles à la manière dont elles ont été synthétisées, laquelle est étroitement liée aux conditions opératoires. En général, les suies formées à partir du $C_2H_2$ sont plus denses et riches en carbone. L'ensemble du processus libère de grandes quantités de $H_2$.
- Les réactions de reformage des hydrocarbures jouent un rôle important pour la prévention de la formation des suies, puisque les hydrocarbures sont alors transformés en CO et $H_2$ à la place de former des suies. Ces réactions sont d'autant plus favorisées que la teneur en vapeur d'eau dans l'atmosphère est importante. Par ailleurs, comme la réactivité des suies est faible, leur gazéification a un rôle mineur dans leur réduction.
- La réaction de WGS a une influence importante sur les rendements en gaz. Dans une atmosphère contenant de la vapeur d'eau, le sens direct de cette réaction est favorisé en raison de la forte concentration en $H_2O$, ce qui mène à des rendements élevés de $H_2$ et de $CO_2$.
- La gazéification du char se déroule en quelques secondes à partir de 1200°C sous une atmosphère contenant 25 %mol $H_2O$. Dans une atmosphère inerte, le $H_2O$ et $CO_2$ produits par la pyrolyse sont en faibles concentrations, ce qui mène à des cinétiques de gazéification lentes. La graphitisation du char apparaît à partir de 1000°C, et conduit à l'augmentation de sa teneur en carbone et à la diminution de sa réactivité quand la température augmente. Cependant, ce phénomène n'influence pas significativement le rendement en char lors des expériences en four à chute.

- L'équilibre thermodynamique est presque atteint à 1400°C sous une atmosphère contenant 25%mol de vapeur d'eau. La gazéification des suies est le phénomène limitant qui explique pourquoi l'équilibre n'est pas parfaitement atteint après 4 s de temps de séjour.
- Aucune différence significative n'a été observée concernant les rendements des produits issus de la décomposition des particules de 0,35 mm et 0,80 mm. Cependant, le processus peut se dérouler de manière différente avec chaque taille de particule, ce qui attribuerait des propriétés différentes aux suies.

Des mesures complémentaires (analyse de la composition des goudrons et quantification des suies, observations au microscope électronique à transmission de la structure des suies, mesure de la fraction de carbone sous forme graphite dans le char) et des améliorations du modèle (meilleure représentation du reformage des hydrocarbures, utilisation d'une approche basée sur des fondements plus réels pour modéliser la formation et la gazéification des suies) pourraient être envisagées pour compléter cette étude. D'autres axes de recherche sur la gazéification de la biomasse dans un réacteur à flux entraîné pourraient également être explorés (exemple : étude de l'influence de l'$O_2$ et du $CO_2$).

# References

**Antal, M.J., Gronli, M. 2003. The Art, Science, and Technology of Charcoal Production. *Industrial & Engineering Chemistry Research*, 42(8), 1619-1640.**

**Baker, E.G., Brown, M.D., Elliott, D.C., Mudge, L.K. 1988. Characterization and Treatment of Tars from Biomass Gasifiers. *AIChE 1988 Summer National Meeting*, Denver, CO. pp. pp. 1–11.**

**Bar-Ziv, E., Kantorovich, I.I. 2001. Mutual effects of porosity and reactivity in char oxidation. *Progress in Energy and Combustion Science*, 27(6), 667-697.**

**Barrio, M., Gøbel, B., Rimes, H., Henriksen, U., Hustad, J.E., Sørensen, L.H. 2001. Steam Gasification of Wood Char and the Effect of Hydrogen Inhibition on the Chemical Kinetics. in: *Progress in Thermochemical Biomass Conversion*, Blackwell Science Ltd, pp. 32-46.**

**Barrio, M., Gøbel, B., Rimes, H., Henriksen, U., Hustad, J.E., Sørensen, L.H. 2008. Steam Gasification of Wood Char and the Effect of Hydrogen Inhibition on the Chemical Kinetics. in: *Progress in Thermochemical Biomass Conversion*, Blackwell Science Ltd, pp. 32-46.**

**Bellais, M. 2007. Modelling of the pyrolysis of large wood particles, Vol. PhD thesis, Royal Institute of Technology.**

**Bhaskaran, K.A., Roth, P. 2002. ChemInform Abstract: The Shock Tube as Wave Reactor for Kinetic Studies and Material Systems. *ChemInform*, 33(15), no-no.**

**Bhatia, S.K., Perlmutter, D.D. 1980. A random pore model for fluid-solid reactions: I. Isothermal, kinetic control. *AIChE Journal*, 26(3), 379-386.**

**Bitowft, B., Andersson, L.A., Bjerle, I. 1989. Fast pyrolysis of sawdust in an entrained flow reactor. *Fuel*, 68(5), 561-566.**

**Blyholder, G., Binford, J.S., Eyring, H. 1958. A Kinetic Theory for the Oxidation of Carbonized Filaments. *The Journal of Physical Chemistry*, 62(3), 263-267.**

**Bohm, H., Jander, H. 1999. PAH formation in acetylene-benzene pyrolysis. *Physical Chemistry Chemical Physics*, 1(16), 3775-3781.**

**Boroson, M.L., Howard, J.B., Longwell, J.P., Peters, W.A. 1989. Heterogeneous cracking of wood pyrolysis tars over fresh wood char surfaces. *Energy & Fuels*, 3(6), 735-740.**

**Boutin, O., Ferrer, M., Lédé, J. 2002. Flash pyrolysis of cellulose pellets submitted to a concentrated radiation: experiments and modelling. *Chemical Engineering Science*, 57(1), 15-25.**

**Branca, C., Blasi, C.D., Elefante, R. 2005. Devolatilization and Heterogeneous Combustion of Wood Fast Pyrolysis Oils. *Industrial & Engineering Chemistry Research*, 44(4), 799-810.**

**Bridgwater, A.V., Meier, D., Radlein, D. 1999. An overview of fast pyrolysis of biomass. *Organic Geochemistry*, 30(12), 1479-1493.**

**Brink, D.L., Massoudi, M.S. . 1978. A flow reactor technique for the study of wood pyrolysis.I. Experimental. *Journal of Fire&Flammability* 9, 176-188.**

**Bunsell, A.R. 1988. *Fibre Reinforcements for Composite Materials*. Elsevier Science Publishers B.V., Amsterdam, The Netherlands.**

**Burghoffer, P. 2009. Preliminary experiments of wood pyrolysis in a induction furnace. CEA, Grenoble.**

**Cancès, J. 2006. Formation et réduction de NOx par un charbon, un lignite, un anthracite et un coke de pétrole dans les conditions d'un précaclcinateur de cimenterie. in: *Thèse de l'Institut National Polytechnique de Toulouse*, Vol. PhD thesis. Toulouse.**

**Cetin, E., Gupta, R., Moghtaderi, B. 2005. Effect of pyrolysis pressure and heating rate on radiata pine char structure and apparent gasification reactivity. *Fuel*, 84(10), 1328-1334.**

**Cetin, E., Moghtaderi, B., Gupta, R., Wall, T.F. 2004. Influence of pyrolysis conditions on the structure and gasification reactivity of biomass chars. *Fuel*, 83(16), 2139-2150.**

**Chen, G., Yu, Q., Sjöström, K. 1997. Reactivity of char from pyrolysis of birch wood. *Journal of Analytical and Applied Pyrolysis*, 40-41, 491-499.**

**Chen, L. 2009. Fast pyrolysis of millimetric particles between 800°C and 1000°C, Vol. PhD thesis, Université de Claude Bernard - Lyon 1 pp. 171.**

**Chern, J.-S., Hayhurst, A.N. 2004. Does a large coal particle in a hot fluidised bed lose its volatile content according to the shrinking core model? *Combustion and Flame*, 139(3), 208-221.**

**Chilton, T.H., Colburn, A.P. 1934. Mass Transfer (Absorption) Coefficients Prediction from Data on Heat Transfer and Fluid Friction. *Industrial & Engineering Chemistry*, 26(11), 1183-1187.**

**Commandré, J.-M. 2002. Formation des oxydes d'azote lors de la combustion de cokes de pétrole dans des conditions de précalcinateur de cimenterie, Vol. PhD Thesis.**

**Commandré, J.M., Couhert, C., Salvador, S. 2008. Compte-rendu des essais de gazéification de bois et de char dans le Réacteur à Flux Entraîné Haute Température. Ecole des Mines d'Albi-Carmaux, centre RAPSODEE.**

**Coppens, F.H.V., De Ruyck, J., Konnov, A.A. 2007. The effects of composition on burning velocity and nitric oxide formation in laminar premixed flames of CH4 + H2 + O2 + N2. *Combustion and Flame*, 149(4), 409-417.**

**Couhert, C. 2007. Pyrolyse Flash à Haute Température de la Biomasse Ligno-Cellulosique et de Ses Composés-Production de Gaz de Synthèse, Vol. PhD thesis, Ecoles des Mines de Paris.**

**Couhert, C., Salvador, S., CommandrÃ©, J.M. 2009. Impact of torrefaction on syngas production from wood. *Fuel*, 88(11), 2286-2290.**

**D'Alessio, A., D'Anna, A., Minutolo, P., Sgro, L.A., Violi, A. 2000. On the Relevance of Surface Growth in Soot Formation in Premixed Flames. *28th Symposium (International) on Combustion*. pp. 2547-2554.**

**Damköhler, G. 1936. Einflüsse der Strömung, Diffusion und des Wärmeüberganges auf die Leistung von Reaktionsöfen.: I. Allgemeine Gesichtspunkte für die Übertragung eines chemischen Prozesses aus dem Kleinen ins Große. *Zeitschrift für Elektrochemie und angewandte physikalische Chemie*, 42(12), 846-862.**

**De Diego, L.F., García-Labiano, F., Abad, A., Gayán, P., Adánez, J. 2002. Coupled drying and devolatilisation of non-spherical wet pine wood particles in fluidised beds. *Journal of Analytical and Applied Pyrolysis*, 65(2), 173-184.**

**De Jong, W., Di Nola, G., Venneker, B.C.H., Spliethoff, H., Wójtowicz, M.A. 2007. TG-FTIR pyrolysis of coal and secondary biomass fuels: Determination of pyrolysis kinetic parameters for main species and NOx precursors. *Fuel*, 86(15), 2367-2376.**

**De Soete, G. 1988. Catalysis of soot combustion by metal oxides. IFP.**

**DeGroot, W.F., Shafizadeh, F. 1984. Kinetics of gasification of Douglas Fir and Cottonwood chars by carbon dioxide. *Fuel*, 63(2), 210-216.**

**Di Blasi, C. 2009. Combustion and gasification rates of lignocellulosic chars. *Progress in Energy and Combustion Science*, 35(2), 121-140.**

**Di Blasi, C. 1997. Influences of physical properties on biomass devolatilization characteristics. *Fuel*, 76(10), 957-964.**

**Di Blasi, C. 1993. Modeling and simulation of combustion processes of charring and non-charring solid fuels. *Progress in Energy and Combustion Science*, 19(1), 71-104.**

**Di Blasi, C. 2008. Modeling chemical and physical processes of wood and biomass pyrolysis. *Progress in Energy and Combustion Science*, 34(1), 47-90.**

**Dobbins, R.A., Subramaniasivam, H. 1994. Soot Precursor Particles in Flames, Soot Formation in Combustion. *Springer Series in Chemical Physics*, 59, 290-301.**

**Du, Z., Sarofim, A.F., Longwell, J.P., Mims, C.A. 1991. Kinetic measurement and modeling of carbon oxidation. *Energy & Fuels*, 5(1), 214-221.**

**Dupont, C. 2006. Vapogazéification de la biomasse : Contribution à l'étude de la phénoménologie entre 800 et 1000°C, Vol. Doctorate Thesis, Université Claude Bernard - Lyon.**

**Dupont, C., Boissonnet, G., Seiler, J.-M., Gauthier, P., Schweich, D. 2007. Study about the kinetic processes of biomass steam gasification. *Fuel*, 86(1-2), 32-40.**

**Dupont, C., Commandré, J.-M., Gauthier, P., Boissonnet, G., Salvador, S., Schweich, D. 2008. Biomass pyrolysis experiments in an analytical entrained flow reactor between 1073 K and 1273 K. *Fuel*, 87(7), 1155-1164.**

**Durán, A., Carmona, M., Monteagudo, J.M. 2004. Modelling soot and SOF emissions from a diesel engine. *Chemosphere*, 56(3), 209-225.**

**Dworkin, S.B., Zhang, Q., Thomson, M.J., Slavinskaya, N.A., Riedel, U. 2011. Application of an enhanced PAH growth model to soot formation in a laminar coflow ethylene/air diffusion flame. *Combustion and Flame*, In Press, Corrected Proof.**

**Ekstrom, C., Rensfelt, E. 1980. Flash Pyrolysis of Biomass in Sweden. *Proceedings of the Specialists' Workshop on Fast Pyrolysis of Biomass*, Copper Mountain, Colorado, USA.**

**Elliott, D.C. 1988. Relation of reaction time and temperature to chemical composition of pyrolysis oils. in: *Pyrolysis oils from biomass*, (Ed.) A.s.s. 376. Denver, USA.**

**Evans, R.J., Milne, T.A. 1987a. Molecular characterization of the pyrolysis of biomass. 1. Fundamentals. *Energy & Fuels*, 1(2), 123-137.**

**Evans, R.J., Milne, T.A. 1987b. Molecular characterization of the pyrolysis of biomass. 2. Applications. *Energy & Fuels*, 1(4), 310-319.**

**Feng, B., Bhatia, S.K. 2000. Percolative Fragmentation of Char Particles during Gasification. *Energy & Fuels*, 14(2), 297-307.**

**Feng, B., Bhatia, S.K., Barry, J.C. 2002. Structural ordering of coal char during heat treatment and its impact on reactivity. *Carbon*, 40(4), 481-496.**

**Feng, B., Jensen, A., Bhatia, S.K., Dam-Johansen, K. 2003. Activation Energy Distribution of Thermal Annealing of a Bituminous Coal. *Energy & Fuels*, 17(2), 399-404.**

**Fermoso, J., Stevanov, C., Moghtaderi, B., Arias, B., Pevida, C., Plaza, M.G., Rubiera, F., Pis, J.J. 2009. High-pressure gasification reactivity of biomass chars produced at different temperatures. *Journal of Analytical and Applied Pyrolysis*, 85(1-2), 287-293.**

**Fisher, T., Hajaligol, M., Waymack, B., Kellogg, D. 2002. Pyrolysis behaviour and kinetics of biomass derived materials. *Journal of Analytical and Applied Pyrolysis*, 62, 331-349.**

**Font, R., Marcilla, A., Devesa, J., Verdu, E. 1994. Gas production by almond shell pyrolysis at high temperature. *Journal of Analytical and Applied Pyrolysis*, 28, 13-27.**

**Frenklach, M., Wang, H. 1994. *Detailed mechanism and modeling of soot particle formation.***

**Frenklach, M., Wang, H. 1990. Detailed Modeling of Soot Particle Nucleation and Growth. *23rd Symposium (International) on Combustion*, University of Orleans, France. pp. 1559-1566.**

**Fujita, O., Ito, K. 2002. Observation of soot agglomeration process with aid of thermophoretic force in a microgravity jet diffusion flame. *Experimental Thermal and Fluid Science*, 26(2-4), 305-311.**

**Fusco, A., Knox-Kelecy, A.L., Foster, D.E. 1994. Application of a Phenomenological Soot Model to Diesel Engine Combustion. in: *Comodia 94*. Yokohama, Japan, pp. 571-576.**

**Fushimi, C., Araki, K., Yamaguchi, Y., Tsutsumi, A. 2003. Effect of heating rate on steam gasification of biomass. 1. Reactivity of char.** ***Industrial and Engineering Chemistry Research*****, 42(17), 3922-3928.**

**Galgano, A., Di Blasi, C. 2004. Modeling the propagation of drying and decomposition fronts in wood.** ***Combustion and Flame*****, 139(1-2), 16-27.**

**Gilot, P., Bonnefoy, F., Marcuccilli, F., Prado, G. 1993. Determination of kinetic data for soot oxidation. Modeling of competition between oxygen diffusion and reaction during thermogravimetric analysis.** ***Combustion and Flame*****, 95(1-2), 87-100.**

**Girods, P., Dufour, A., Rogaume, Y., Rogaume, C., Zoulalian, A. 2009. Comparison of gasification and pyrolysis of thermal pre-treated wood board waste.** ***Journal of Analytical and Applied Pyrolysis*****, 85(1-2), 171-183.**

**Gøbel, B., Henriksen, U., Qvale, B., Houbak, N. 2008. Dynamic Modelling of Char Gasification in a Fixed-Bed. in:** ***Progress in Thermochemical Biomass Conversion*****, Blackwell Science Ltd, pp. 92-108.**

**Gómez-Barea, A., Ollero, P., Arjona, R. 2005. Reaction-diffusion model of TGA gasification experiments for estimating diffusional effects.** ***Fuel*****, 84(12-13), 1695-1704.**

**Gonzalez Saiz, J. 1988. Gasificacion de biomasas con vapor de agua en lecho fluidizado. in:** ***Departamento de Ingenieria quimica y tecnologias del medio ambiente*****, Vol. PhD thesis, Universidad de Zaragoza.**

**Gosse, J. 1991. Propriétés de transport des gaz à pression modérée, pp. 15 p.**

**Groeneveld, M.J., van Swaaij, W.P.M. 1980. Gasification of char particles with CO2 AND H2O.** ***Chemical Engineering Science*****, 35(1-2), 307-313.**

**Gronli, M.G. 1996. A theoretical and experimental study of the thermal degradation of biomass. in:** ***Faculty of Mechanical Engineering*****, Vol. PhD Thesis, The Norwegian University of Science and Technology.**

**Gronli, M.G., Vorhegyi, G.b., Di Blasi, C. 2002. Thermogravimetric Analysis and Devolatilization Kinetics of Wood.** ***Industrial & Engineering Chemistry Research*****, 41(17), 4201-4208.**

**Guerrero, M., Ruiz, M.P., Alzueta, M.U., Bilbao, R., Millera, A. 2005. Pyrolysis of eucalyptus at different heating rates: studies of char characterization and oxidative reactivity.** ***Journal of Analytical and Applied Pyrolysis*****, 74(1-2), 307-314.**

**Gutierrez, A., Karinen, R., Airaksinen, S., Kaila, R., Krause, A.O.I. 2005. Autothermal reforming of ethanol on noble metal catalysts.** ***International Journal of Hydrogen Energy*****.**

**Hajaligol, M.R., J. B. Howard, J. P. Longwell, W.A. Peters. 1982. Product Compositions and Kinetics for Rapid Pyrolysis of Cellulose.** ***Ind. Eng. Chem. Process Des. Dev*****, 21.**

**Hallgren, A., Andersson, L.A., Bjerle, I. 1993. High temperature gasification of biomass in an atmospheric entrained flow reactor. in:** ***Advances in thermochemical biomass conversion*****, (Ed.) A.V. Bridgwater, Vol. 1, Blackie Academic and Professional. Cambridge.**

**Harris, D.J., Smith, I.W. 1990.** ***Twenty-third international symposium on combustion*****, Philadelphia: The Combustion Institute. pp. 1185.**

**Hiblot, H. 2010. Etude cinétique du réformage thermique des produits issus de la gazéification de la biomasse, Vol. PhD thesis, University of Nancy.**

**Hurt, R., Sun, J.-K., Lunden, M. 1998. A Kinetic Model of Carbon Burnout in Pulverized Coal Combustion.** ***Combustion and Flame*****, 113(1-2), 181-197.**

**Hurt, R.H., Calo, J.M. 2001. Semi-global intrinsic kinetics for char combustion modeling.** ***Combustion and Flame*****, 125(3), 1138-1149.**

**Hüttinger, K.J., Merdes, W.F. 1992. The carbon-steam reaction at elevated pressure: Formations of product gases and hydrogen inhibitions.** ***Carbon*****, 30(6), 883-894.**

**Ibañez, F.E. 2002. Etude de la carbonisation et l'activation de précurseurs végétaux durs et mous, Vol. PhD Thesis, University of Neutchatel Neutchatel, Switzerland.**

**Ishiguro, T., Takatori, Y., Akihama, K. 1997. Microstructure of diesel soot particles probed by electron microscopy: First observation of inner core and outer shell. *Combustion and Flame*, 108(1-2), 231-234.**

**Janse, A.M.C., Westerhout, R.W.J., Prins, W. 2000. Modelling of flash pyrolysis of a single wood particle. *Chemical Engineering and Processing*, 39(3), 239-252.**

**Kajitani, S., Hara, S., Matsuda, H. 2002. Gasification rate analysis of coal char with a pressurized drop tube furnace. *Fuel*, 81(5), 539-546.**

**Kajitani, S., Suzuki, N., Ashizawa, M., Hara, S. 2006. CO2 gasification rate analysis of coal char in entrained flow coal gasifier. *Fuel*, 85(2), 163-169.**

**Kee, R.J., Rupley, F.M., Miller, J.A. 1989. CHEMKIN II: a fortran chemical kinetics package for the analysis of the gas-phase chemical kinetics. Sandia National Laboratories, Albuquerque NM, US.**

**Kee, R.J., Rupley, F.M., Miller, J.A. 1990. The CHEMKIN thermodynamic data base. Sandia National Laboratories, Albuquerque NM, US.**

**Khalil, R., Várhegyi, G., Jäschke, S., Grönli, M.G., Hustad, J. 2008. CO2 Gasification of Biomass Chars: A Kinetic Study. *Energy & Fuels*, 23(1), 94-100.**

**Khan, M.S., Crynes, B.L. 1970. Survey of Recent Methane Pyrolysis Literature. *Industrial & Engineering Chemistry*, 62(10), 54-59.**

**Kifani-Sahban, F., Belkbir, L., Zoulalian, A. 1996. Etude de la pyrolyse lente de l'Eucalyptus marocain par analyse thermiqueStudy of the slow pyrolysis of Moroccan eucalyptus by thermal analysis. *Thermochimica Acta*, 284(2), 341-349.**

**Klose, W., Wölki, M. 2005. On the intrinsic reaction rate of biomass char gasification with carbon dioxide and steam. *Fuel*, 84(7-8), 885-892.**

**Kojima, T., Assavadakorn, P., Furusawa, T. 1993. Measurement and evaluation of gasification kinetics of sawdust char with steam in an experimental fluidized bed. *Fuel Processing Technology*, 36(1-3), 201-207.**

**Konnov, A.A. 2000. Development and validation of a detailed reaction mechanism for the combustion of small hydrocarbons. *28-th Symposium (Int.) on Combustion*, Edinburgh. Abstr. Symp. Pap. . pp. 317.**

**Koufopanos, C.A., Lucchesi, A., Maschio, G. 1989. Kinetic modelling of the pyrolysis of biomass and biomass components. *The Canadian Journal of Chemical Engineering*, 67(1), 75-84.**

**Krestinin, A., Kislov, M., Raevskii, A., Kolesova, O., Stesik, L. 2000. On the mechanism of soot particle formation. *Kinetics and Catalysis*, 41(1), 90-98.**

**Kronholm, D.F., Howard, J.B. 2000. Analysis of Soot Surface Growth Pathways using Published Plug-Flow Reactor Data with New Particle Size Distribution Measurements and Published Premixed Flame Data. *28th Symposium (International) on Combustion*, University of Edinburgh, Edinburgh, Scotland. pp. 2555-2562.**

**Kumar, M., Gupta, R.C. 1994. Influence of carbonization conditions on the gasification of acacia and eucalyptus wood chars by carbon dioxide. *Fuel*, 73(12), 1922-1925.**

**Lahaye, J., Prado, G. 1981. Morphology and Internal Structure of Soot and Carbon Black, In Particulate Carbon, Plenum. New York, pp. 33-51.**

**Lee, K.B., Thring, M.W., Beér, J.M. 1962. On the rate of combustion of soot in a laminar soot flame. *Combustion and Flame*, 6, 137-145.**

**Leung, K.M., Lindstedt, R.P., Jones, W.P. 1991. A simplified reaction mechanism for soot formation in nonpremixed flames. *Combustion and Flame*, 87(3-4), 289-305.**

**Levenspiel, O. 1997. Chemical Reaction Engineering, third edition, John Wiley & Sons Inc. New York.**

**Li, W., Law, M.E., Westmoreland, P.R., Kasper, T., Hansen, N., Kohse-Höinghaus, K. 2011. Multiple benzene-formation paths in a fuel-rich cyclohexane flame. *Combustion and Flame*, In Press, Corrected Proof.**

**Lindstedt, P.R. 1994. Simplified Soot Nucleation and Surface Growth Steps for Non-Premixed Flames. in: *Soot Formation in Combustion*, (Ed.) Springer Series in Chemical Physics, Vol. 59, Springer-Verlag. Berlin, pp. 417-441.**

**Liu, G.-S., Niksa, S. 2004. Coal conversion submodels for design applications at elevated pressures. Part II. Char gasification. *Progress in Energy and Combustion Science*, 30(6), 679-717.**

**Liu, G.-s., Tate, A.G., Bryant, G.W., Wall, T.F. 2000. Mathematical modeling of coal char reactivity with CO2 at high pressures and temperatures. *Fuel*, 79(10), 1145-1154.**

**Liu, H., Luo, C., Toyota, M., Kato, S., Uemiya, S., Kojima, T., Tominaga, H. 2003. Mineral reaction and morphology change during gasification of coal in CO2 at elevated temperatures[small star, filled]. *Fuel*, 82(5), 523-530.**

**Lu, H. 2006. Experimental and Modelling Investigations of Biomass Particle Combustion. in: *Department Chemical Engineering*, Brigham Young University.**

**Luis, S., Amokrane, A., Peyrot, M., Septien, S. 2011. Simulation sous Fluent du four à chute de l'EMAC. CEA DRT/LITEN/DTBH/LTB.**

**Lussier, M.G., Zhang, Z., Miller, D.J. 1998a. Characterizing rate inhibition in steam/hydrogen gasification via analysis of adsorbed hydrogen. *Carbon*, 36, 1361-1369.**

**Lussier, M.G., Zhang, Z., Miller, D.J. 1998b. Characterizing rate inhibition in steam/hydrogen gasification via analysis of adsorbed hydrogen. *Carbon*, 36(9), 1361-1369.**

**Maa, P.S., Bailie, R.C. 1973. Influence of Particle Sizes and Environmental Conditions on High Temperature Pyrolysis of Cellulosic Material (Theoretical). *Combustion Science and Technology*, 7(6), 257 - 269.**

**Makarov, K.I., Pechik, V.K. 1974. Kinetics of methane pyrolysis under conditions of pyrolytic carbon formation. *Carbon*, 12(4), 391-403.**

**Maki, T., Takatsuno, A., Miura, K. 1997. Analysis of Pyrolysis Reactions of Various Coals Including Argonne Premium Coals Using a New Distributed Activation Energy Model. *Energy & Fuels*, 11(5), 972-977.**

**Manocha, S., Chauhan, V., Manocha, L. 2002. Porosity development on activation of char from dry and wet babbool wood. *Carbon Science*, 3(3), 133-141.**

**Marbán, G., Fuertes, A.B. 1997. Influence of percolation on the modification of overall particle properties during gasification of porous solids. *Chemical Engineering Science*, 52(1), 1-11.**

**Marsh, P.A., Voet, A., Mullens, T.J., Price, L.D. 1971. Quantitative micrography of carbon black microstructure. *Carbon*, 9(6), 797-805.**

**Matsui, I., Kojima, T., Kunii, D., Furusawa, T. 1987. Study of char gasification by carbon dioxide. 2. Continuous gasification in fluidized bed. *Industrial & Engineering Chemistry Research*, 26(1), 95-100.**

**Matsumoto, K., Takeno, K., Ichinose, T., Ogi, T., Nakanishib, M. 2009. Gasification reaction kinetics on biomass char obtained as a by-product of gasification in an entrained-flow gasifier with steam and oxygen at 900–1000°C. *Fuel*, 88(3), 519-527 p.**

**Mendiara, T., Domene, M.P., Millera, A., Bilbao, R., Alzueta, M.U. 2005. An experimental study of the soot formed in the pyrolysis of acetylene. *Journal of Analytical and Applied Pyrolysis*, 74(1-2), 486-493.**

**Mermoud, F. 2006. Gazéification de charbon de bois à la vapeur d'eau : de la particule isolée au lit fixe continu, Vol. PhD thesis, Institut National Polytechnique de Toulouse.**

**Mermoud, F., Golfier, F., Salvador, S., Van de Steene, L., Dirion, J.L. 2006a. Experimental and numerical study of steam gasification of a single charcoal particle. *Combustion and Flame*, 145(1-2), 59-79.**

**Mermoud, F., Salvador, S., Van de Steene, L., Golfier, F. 2006b. Influence of the pyrolysis heating rate on the steam gasification rate of large wood char particles. *Fuel*, 85(10-11), 1473-1482.**

**Miller. 1999. Structure of wood. in: *Wood Handbook* Forest products Laboratoy, USDA Forest Services. Madison, Wisconsin.**

**Miller, R.S., Bellan, J. 1997. A Generalized Biomass Pyrolysis Model Based on Superimposed Cellulose, Hemicelluloseand Liqnin Kinetics. *Combustion Science and Technology*, 126(1), 97 - 137.**

**Milosavljevic, I., Oja, V., Suuberg, E.M. 1996. Thermal Effects in Cellulose Pyrolysis: Relationship to Char Formation Processes. *Industrial & Engineering Chemistry Research*, 35(3), 653-662.**

**Misra, M.K., Ragland, K.W., Baker, A.J. 1993. Wood ash composition as a function of furnace temperature. *Biomass and Bioenergy*, 4(2), 103-116.**

**Mitsuoka, K., Hayashi, S., Amano, H., Kayahara, K., Sasaoaka, E., Uddin, M.A. 2011. Gasification of woody biomass char with CO2: The catalytic effects of K and Ca species on char gasification reactivity. *Fuel Processing Technology*, 92(1), 26-31.**

**Moe, J.M. 1962. Design of Water-Gas Shift reactors. *Chem. Eng. Progress*, 58, 33–36.**

**Moilanen, A. 2006. Thermogravimetric characterisations of biomass and waste for gasification processes, Vol. PhD thesis, VTT Finland.**

**Mok, W.S.L., Antal, M.J. 1983. Effects of pressure on biomass pyrolysis. II. Heats of reaction of cellulose pyrolysis. *Thermochimica Acta*, 68(2-3), 165-186.**

**Molina, A., Mondragón, F. 1998. Reactivity of coal gasification with steam and CO2. *Fuel*, 77(15), 1831-1839.**

**Mousquès, P., Dirion, J.L., Grouset, D. 2001. Modeling of solid particles pyrolysis. *Journal of Analytical and Applied Pyrolysis*, 58-59, 733-745.**

**Mühlen, H.-J., van Heek, K.H., Jüntgen, H. 1985. Kinetic studies of steam gasification of char in the presence of H2, CO2 and CO. *Fuel*, 64(7), 944-949.**

**Neeft, J.P.A., Knoef, H.A.M., Onaji, P. 1999. Behaviour of Tar in Biomass Gasification Systems, Tar Related Problems and Their Solutions. *Energy from Waste and Biomass*, The Netherlands.**

**Niksa, S. 2000. Predicting the rapid devolatilization of diverse forms of biomass with bio-flashchain. *Proceedings of the Combustion Institute*, 28(2), 2727-2733.**

**Niksa, S., Liu, G.-s., Hurt, R.H. 2003. Coal conversion submodels for design applications at elevated pressures. Part I. devolatilization and char oxidation. *Progress in Energy and Combustion Science*, 29(5), 425-477.**

**Nunn, T.R., J. B. Howard, J. P. Longwell, W. A. Peters. 1985. Product Comparaison and Kinetics in the Rapid Pyrolysis of Sweet Gum Hardwood. *Ind. Eng. Chem. Process Des. Dev*, 24.**

**Ogi, T., Nakanishi, M., Fukuda, Y., Matsumoto, K. 2010. Gasification of oil palm residues (empty fruit bunch) in an entrained-flow gasifier. *Fuel*, In Press, Corrected Proof.**

**Oh, M.S., Peters, W.A., Howard, J.B. 1989. An experimental and modeling study of softening coal pyrolysis. *AIChE Journal*, 35(5), 775-792.**

**Oliveira, A.A.M., Kaviany, M. 2001. Nonequilibrium in the transport of heat and reactants in combustion in porous media. *Progress in Energy and Combustion Science*, 27(5), 523-545.**

**Ollero, P., Serrera, A., Arjona, R., Alcantarilla, S. 2003. The CO2 gasification kinetics of olive residue. *Biomass and Bioenergy*, 24(2), 151-161.**

**Orfão, J.J.M., Antunes, F.J.A., Figueiredo, J.L. 1999. Pyrolysis kinetics of lignocellulosic materials--three independent reactions model. *Fuel*, 78(3), 349-358.**

**Ouyang, S., Yeasmin, H., Mathews, J. 1998. A pressurized drop-tube furnace for coal reactivity studies. *Review of Scientific Instruments*, 69(8), 3036-3041.**

**Palmer, H.B., Cullis, H.F. 1965. The formation of carbon from gases. *Chemistry and Physics of Carbon 1*, 265-325.**

**Passé-Coutrin, N., Jeanne-Rose, V., Ouensanga, A. 2005. Textural analysis for better correlation of the char yield of pyrolysed lignocellulosic materials. *Fuel*, 84(16), 2131-2134.**

**Perry, R.H., Green, D.W. 1997. Section 2 : Physical and Chemical Data. in: *Perry's Chemical Engineers' Handbook*, (Ed.) M. Hill.**

**Petit, M. 2011. Etude du comportement des espèces inorganiques dans une installation de gazéification de la biomasse : condensation des aérosols et dépôts, Vol. PhD thesis, Ecole Nationale Superieure des Mines de Nancy.**

**Peyrot, M., Dupont, C., Chen, L., Spindler, B., Valin, S., Cancès, J. 2010. Fast pyrolysis of millimetric wood particles between 1073K and 1273K: Modelling and experimental validation in the chemical kinetic regime. *18th European Biomass Conference and Exhibition*.**

**Please, C.P., McGuinness, M.J., McElwain, D.L.S. 2003. Approximations to the distributed activation energy model for the pyrolysis of coal. *Combustion and Flame*, 133(1-2), 107-117.**

**Qin, K., Lin, W., Jensen, P.A., Jensen, A.D., Egsgaard, H. 2009. Influence of operating conditions on gas composition, soot and tar in entrained flow gasification of biomass. *Joint Meeting of the Scandinavian-Nordic and French Sections of the Combustion Institute*, Copenhaguen, Danemark.**

**Ranzi, E., Cuoci, A., Faravelli, T., Frassoldati, A., Migliavacca, G., Pierucci, S., Sommariva, S. 2008. Chemical Kinetics of Biomass Pyrolysis. *Energy and Fuels*.**

**Rath, J., Wolfinger, M.G., Steiner, G., Krammer, G., Barontini, F., Cozzani, V. 2003. Heat of wood pyrolysis. *Fuel*, 82(1), 81-91.**

**Richardson, Y. 2010. Nouvelles stratégies ctalytiques pour la gazéification de la biomasse: Génération in-situ de nanoparticules à base de nickel ou de fer au cours de l'étape de pyrolyse, Vol. PhD thesis, Université de Montpellier.**

**Richter, H., Howard, J.B. 2000. Formation of polycyclic aromatic hydrocarbons and their growth to soot - a review of chemical reaction pathways. *Progress in Energy and Combustion Science*, 26(4-6), 565-608.**

**Roberts, D.G., Harris, D.J. 2007. Char gasification in mixtures of CO2 and H2O: Competition and inhibition. *Fuel*, 86(17-18), 2672-2678.**

**Roberts, D.G., Harris, D.J. 2006. A Kinetic Analysis of Coal Char Gasification Reactions at High Pressures. *Energy & Fuels*, 20(6), 2314-2320.**

**Roth, K. 2006. Soot formation during the production of syngas from the partial oxidation of diesel fuel, Vol. PhD thesis, Ruhr-Universität Bochum.**

**Ruiz, M.P., de Villoria, R.G., Millera, A., Alzueta, M.U., Bilbao, R. 2007. Influence of the temperature on the properties of the soot formed from C2H2 pyrolysis. *Chemical Engineering Journal*, 127(1-3), 1-9.**

**Russell, N.V., Gibbins, J.R., Williamson, J. 1999. Structural ordering in high temperature coal chars and the effect on reactivity. *Fuel*, 78(7), 803-807.**

**Salatino, P., Senneca, O., Masi, S. 1999. Assessment of Thermodeactivation during Gasification of a Bituminous Coal Char. *Energy & Fuels*, 13(6), 1154-1159.**

**Schingnitz, M., Mehlose, F. 2005. MEGA GSP Process, Entrained- Flow Gasification of coal, biomass and waste. in:** ***International Freiberg Conference on IGCC & XtL Technologies.*** **Freiberg.**

**Senneca, O., Salatino, P. 2011. A semi-detailed kinetic model of char combustion with consideration of thermal annealing.** ***Proceedings of the Combustion Institute*****, 33(2), 1763-1770.**

**Senneca, O., Salatino, P., Menghini, D. 2007. The influence of thermal annealing on oxygen uptake and combustion rates of a bituminous coal char.** ***Proceedings of the Combustion Institute*****, 31(2), 1889-1895.**

**Seo, D.K., Lee, S.K., Kang, M.W., Hwang, J., Yu, T.-U. 2010. Gasification reactivity of biomass chars with CO2.** ***Biomass and Bioenergy*****, 34(12), 1946-1953.**

**Septien, S. 2009. Compte rendu de la campagne d'essais du 11 au 20 mai 2009. CEA DRT/LITEN/DTBH/LTB.**

**Septien, S. 2007. Etude de la réactivité à la vapogazéification de différentes biomasses. CEA DRT/LITEN/DTBH/LTB.**

**Shafizadeh, F., Chin Peter P, S. 1977. Thermal Deterioration of Wood. in:** ***Wood Technology: Chemical Aspects*****, Vol. 43, AMERICAN CHEMICAL SOCIETY, pp. 57-81.**

**Sheng, C., Azevedo, J.L.T. 2002. Modeling biomass devolatilization using the chemical percolation devolatilization model for the main components.** ***Proceedings of the Combustion Institute*****, 29(1), 407-414.**

**Shim, H.-S., Hurt, R.H. 2000. Thermal Annealing of Chars from Diverse Organic Precursors under Combustion-like Conditions.** ***Energy & Fuels*****, 14(2), 340-348.**

**Shin, Y., Choi, S., Ahn, D.-H. 2000. Pressurized drop tube furnace tests of global coal gasification characteristics.** ***International Journal of Energy Research*****, 24(9), 749-758.**

**Shuangning, X., Zhihe, L., Baoming, L., Weiming, Y., Xueyuan, B. 2006. Devolatilization characteristics of biomass at flash heating rate.** ***Fuel*****, 85(5-6), 664-670.**

**Shurtz, R.C., Kolste, K.K., Fletcher, T.H. 2011. Coal Swelling Model for High Heating Rate Pyrolysis Applications.** ***Energy & Fuels*****, 25(5), 2163-2173.**

**Siau, J.F. 1984.** ***Transport processes in wood.*** **Springler-Verlag, New York.**

**Simmons, G.M., Gentry, M. 1986. Particle size limitations due to heat transfer in determining pyrolysis kinetics of biomass.** ***Journal of Analytical and Applied Pyrolysis*****, 10(2), 117-127.**

**Singh, S., Walawender, W., Fan, L., Geyer, W. 1986. Steam Gasification of Cottonwood (Branches) in A Fluidized Bed.** ***Wood and Fiber Science*****, 18(2), 327-344.**

**Sjostrom, E. 1993.** ***Wood chemistry. Fundamentals and applications. Second edition ed.*** **Academic press.**

**Skinner, G.B., Ruehrwein, R.A. 1959. Shock Tube studies on the Pyrolysis and Oxidation of Methane.** ***The Journal of Physical Chemistry*****, 63(10), 1736-1742.**

**Skjøth-Rasmussen, M.S., Glarborg, P., Østberg, M., Johannessen, J.T., Livbjerg, H., Jensen, A.D., Christensen, T.S. 2004. Formation of polycyclic aromatic hydrocarbons and soot in fuel-rich oxidation of methane in a laminar flow reactor.** ***Combustion and Flame*****, 136(1-2), 91-128.**

**Skjøth-Rasmussen, M.S., Glarborg, P., Østberg, M., Larsen, M.B., Sørensen, S.W., Johnsson, J.E., Jensen, A.D., Christensen, T.S. 2002. A study of benzene formation in a laminar flow reactor.** ***Proceedings of the Combustion Institute*****, 29(1), 1329-1336.**

**Smekens, A., Knupfer, M., Berghmans, P., Van Grieken, R. 2000. The elemental composition and microstructure of soot emitted by different sources.** ***Journal of Aerosol Science*****, 31(SUPPL.1).**

**Song, J., Jeon, C.H., Boehman, A.L. 2010. Impacts of Oxygen Diffusion on the Combustion Rate of In-Bed Soot Particles.** ***Energy & Fuels*****, 24, 2418–2428.**

**Song, Q., He, B., Yao, Q., Meng, Z., Chen, C. 2006. Influence of Diffusion on Thermogravimetric Analysis of Carbon Black Oxidation. *Energy & Fuels*, 20, 1895-1900.**

**Stanmore, B.R., Brilhac, J.F., Gilot, P. 2001. The oxidation of soot: a review of experiments, mechanisms and models. *Carbon*, 39(15), 2247-2268.**

**Struis, R.P.W.J., von Scala, C., Stucki, S., Prins, R. 2002. Gasification reactivity of charcoal with CO2. Part I: Conversion and structural phenomena. *Chemical Engineering Science*, 57(17), 3581-3592.**

**Sudo, S., Takahashi, F. 1989. Chemical properties of biomass. in: *Biomass Handbook*, (Ed.) O.K.a.C.W. Hall, Gordon & Breach. New York.**

**Svensson, K.I. 2005. EFFECTS OF FUEL MOLECULAR STRUCTURE AND COMPOSITION ON SOOT FORMATION IN DIRECT-INJECTION SPRAY FLAMES. in: *Department of Mechanical Engineering*, Vol. PhD thesis, Brigham Young University.**

**Tagutchou, J.P. 2008. Gazéification du charbon de plaquettes forestières : particule isolée et lit fixe continu, Vol. PhD thesis, Université de Perpignan.**

**Valin, S., Cances, J., Castelli, P., Thiery, S., Dufour, A., Boissonnet, G., Spindler, B. 2009. Upgrading biomass pyrolysis gas by conversion of methane at high temperature: Experiments and modelling. *Fuel*, 88(5), 834-842.**

**Van de Steene, L. 1999. Thermochimie de la combustion à basses températures de solides pulvérisés : application à un charbon, Vol. PhD Thesis, INPT. Toulouse.**

**Van der Drift, A., Boerrigter, H., Coda, B., Cieplik, M.K., Hemmes, K. 2004. Entrained flow gasification of biomass : ash behaviour, feeding issues and system analyses, (Ed.) ECN.**

**Vander Wal, R.L., Tomasek, A.J. 2004. Soot nanostructure: dependence upon synthesis conditions. *Combustion and Flame*, 136(1-2), 129-140.**

**Vandsburger, U., Kennedy, I., Glassman, I. 1984. Sooting Counterflow Diffusion Flames with Varying Oxygen Index. *Combustion Science and Technology*, 39(1-6), 263-285.**

**Villermaux, J., Antoine, B. 1980. Pyrolyse éclair de solides divisés dans un réacteur continu : 1. Un nouveau modèle de volatilisation thermique de particules solides. *Revue Générale de Thermique*, 227, 851-860.**

**Wang, F.Y., Bhatia, S.K. 2001. A generalised dynamic model for char particle gasification with structure evolution and peripheral fragmentation. *Chemical Engineering Science*, 56(12), 3683-3697.**

**Wei, L., Xu, S., Zhang, L., Liu, C., Zhu, H., Liu, S. 2007. Steam gasification of biomass for hydrogen-rich gas in a free-fall reactor. *International Journal of Hydrogen Energy*, 32(1), 24-31.**

**Wei, L., Xu, S., Zhang, L., Zhang, H., Liu, C., Zhu, H., Liu, S. 2006. Characteristics of fast pyrolysis of biomass in a free fall reactor. *Fuel Processing Technology*, 87(10), 863-871.**

**Wheeler, A. 1955. Fundamental Principle (Part 2). P.H. Emmett ed. in: *Catalysis*, Vol. 2, Reinhold Publishing Corporation. New York, pp. 143.**

**Whitaker, S. 1972. Forced convection heat transfer correlations for flow in pipes, past flat plates, single cylinders, single spheres, and for flow in packed beds and tube bundles. *AIChE Journal*, 18(2), 361-371.**

**Wolfesberger, U., Aigner, I., Hofbauer, H. 2009. Tar content and composition in producer gas of fluidized bed gasification of wood-influence of temperature and pressure. *Environmental Progress and Sustainable Energy*, 28(3), 372-379.**

**Woods, I.T., Haynes, B.S. 1994. Active Sites in Soot Growth, Soot Formation in Combustion. in: *Springer Series in Chemical Physics*, Vol. 59, Springer-Verlag. Berlin, pp. 275-289.**

**Wu, J. 2004. Soot Abatement Using Fuel Additives, Pennsylvania State University.**

**Yang, J., Malendoma, C., Roy, C. 2000. Determination of the Overall Heat Transfer Coefficient in a Vacuum Pyrolysis Moving and Stirred Bed Reactor. *Chemical Engineering Research and Design*, 78(4), 633-642.**

**Yuan, S., Chen, X.-l., Li, J., Wang, F.-c. 2011. CO2 Gasification Kinetics of Biomass Char Derived from High-Temperature Rapid Pyrolysis. *Energy & Fuels*, 25(5), 2314-2321.**

**Zanzi, R., Sjöström, K., Björnbom, E. 1996. Rapid high-temperature pyrolysis of biomass in a free-fall reactor. *Fuel*, 75(5), 545-550.**

**Zhang, Y., Ashizawa, M., Kajitani, S., Miura, K. 2008. Proposal of a semi-empirical kinetic model to reconcile with gasification reactivity profiles of biomass chars. *Fuel*, 87(4-5), 475-481.**

**Zhang, Y., Kajitani, S., Ashizawa, M., Miura, K. 2006. Peculiarities of Rapid Pyrolysis of Biomass Covering Medium- and High-Temperature Ranges. *Energy & Fuels*, 20, 2705--2712.**

**Zhang, Y., Kajitani, S., Ashizawa, M., Oki, Y. 2010. Tar destruction and coke formation during rapid pyrolysis and gasification of biomass in a drop-tube furnace. *Fuel*, 89(2), 302-309.**

**Ziegler, I. 2004. Modélisation cinétique des dépôts de pyrocarbone obtenus par pyrolyse d'hydrocarbures, Vol. PhD thesis, Institut National Polytechnique de Lorraine. Nancy.**

**Zolin, A., Jensen, A., Dam-Johansen, K. 2000. Kinetic analysis of char thermal deactivation. *Symposium (International) on Combustion*, 28(2), 2181-2187.**

# Appendixes

# APPENDIX A: Summary of actual energetic situation

- Figure 86 shows the energetic worldwide supply repartition in 2008 in which fossil fuels (oil, gas, coal and peat) represent about 81%. The renewable energy part, including hydroelectricity, is only 13 %.

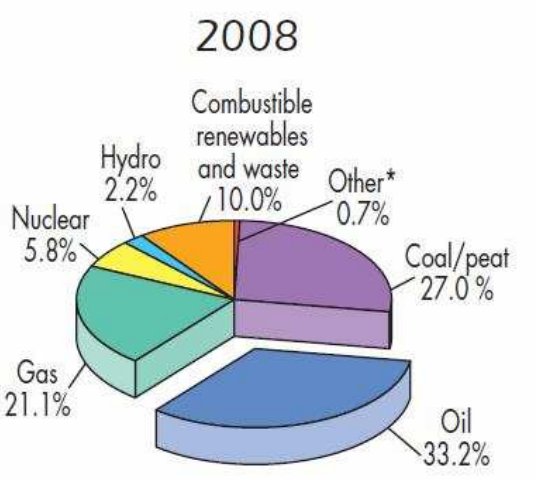


**Figure 86. Energetic worldwide supply in 2008 (*"other" includes geothermal, solar, wind, heat, etc...)**

- Figure 87 illustrates the increase of the energetic worldwide demand during the last 30 years, which is mainly linked to the demographic growth and to the change of way of life in the industrialized countries.

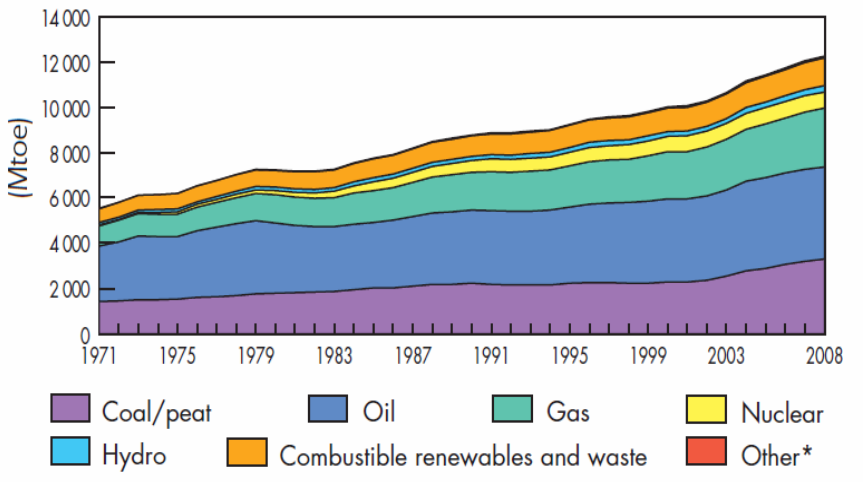


**Figure 87. Worldwide energy demand**

- Some indicators about fossil fuel exploitation are shown in Table 29. In 2009, the production of oil was the highest among fossil fuels, followed then by coal and gas. At the actual consumption rate, the oil and gas reserves are estimated to their depletion during the next 60 years. The reserves of coal, much higher than those of oil and gas, are abundant enough for their use during the next 170 years.

**Table 29. Indicators concerning fossil fuels exploitation**

| | Proven reserves (Gtoe) | Production in 2009 (Gtoe/year) | Time before depletion (year) |
|---|---|---|---|
| Oil | 181 | 3.8 | ~ 45 |
| Coal | 580 | 3.4 | ~ 170 |
| Gas | 168 | 2.7 | ~ 60 |

*BP Statistical Review of World Energy*

- In Figure 88, the unequal oil distribution in the globe can be observed. More than the half of the oil proven reserves is located in the Middle East, and an important part is in Southern countries (Latin America, Africa), Eastern Europe and Canada. The proven reserves in Western Europe, USA and Asia are low. The worldwide distribution of oil is a determining factor in the actual geopolitical context. Its depletion may lead to political tensions between countries and to the destabilization of the actual diplomatic order.

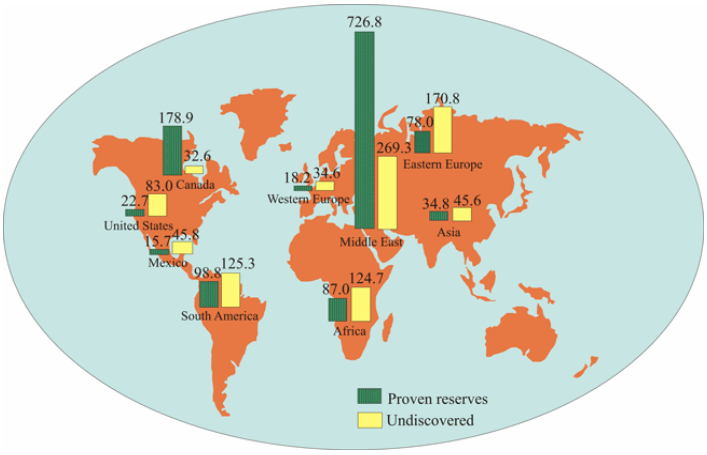


**Figure 88. Distribution of the proven and undiscovered oil reserves in the globe**

- The use of fossil energy is assumed to be the main cause of global warming, which would lead to the increase of temperatures on Earth and consequently to a climate change during the next decades. Among different scenarios showed in Figure 89, the most optimistic one predicts an increase of 2°C, whereas in the worst case the increase can reach 5°C.

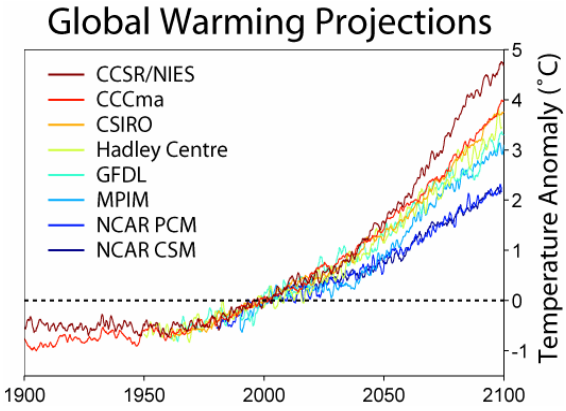


**Figure 89. Different scenarios about the increase of temperature on Earth due to global warming**

- Biomass can be used as a sustainable renewable energy source, which could contribute to the substitution of oil, gas and coal. This resource is abundant in the globe and more equally distributed than fossil fuels. Table 30 shows the potential of biomass as an energetic source in France.

**Table 30. Potential of biomass as a source of energy in France**

| Potential (MToe) | Lowest estimation | Highest estimation |
|---|---|---|
| Wood (remnant, products at end of life) | 5.5 | 11.6 |
| Agriculture residues | 1.4 | 8.7 |
| Energetic cultures | 0 | 8.2 |
| Waste | 0 | 2 |
| Total | ~7 | ~30 |

- Biomass has the advantage to present a wide variety of feedstock, which can be transformed into a wide variety of products through thermochemical or biological conversion, as illustrated in Figure 90.

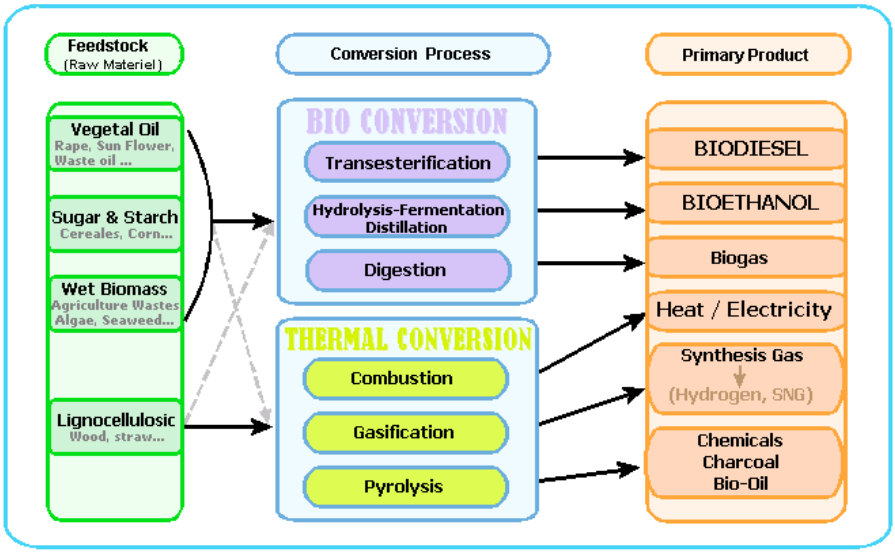


**Figure 90. Different routes of energetic valorization of biomass**

# APPENDIX B: Biomass gasification process

Figure 91 illustrates a prototype biomass gasification plant. Firstly, biomass feedstock is collected and carried to the gasification plant. There, before its introduction into the reactor, the raw feedstock has to be pretreated, which means grinding, moisture drying and an eventual heat treatment as torrefaction. After the gasifier, the produced gas undergoes several cleaning steps to remove pollutants such as tars or inorganic compounds, like $H_2S$. The gas is treated so as to separate the syngas, $H_2$ and CO, from the other gaseous species, such as $CO_2$, and to adjust the required $H_2/CO$ ratio for the further fuel synthesis.

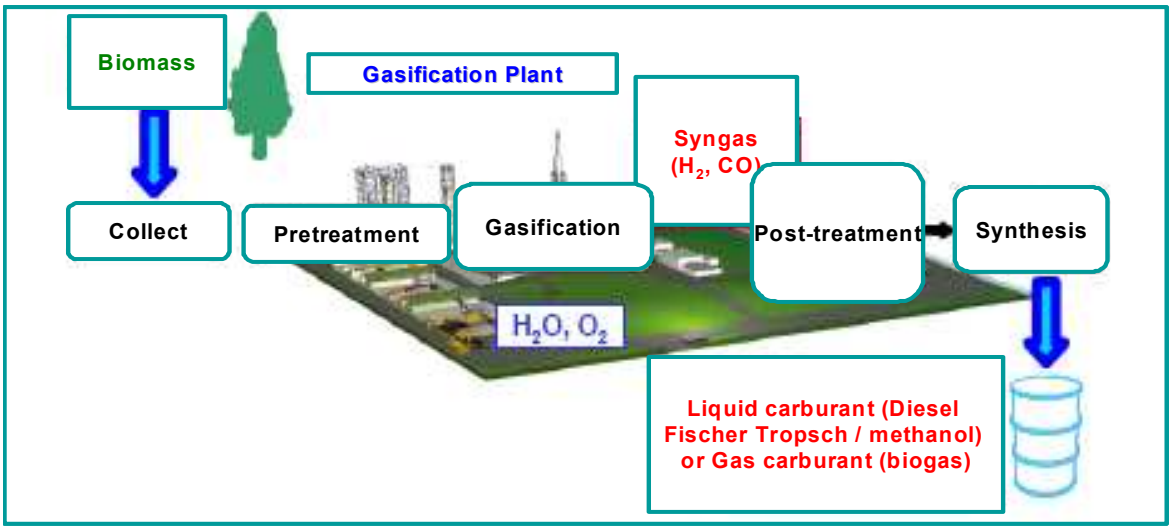


**Figure 91. Biomass gasification plant prototype for a BtL or BtG application**

Two main gasifier technologies could be used for a large scale biofuels production, namely fluidized bed reactor and entrained flow reactor. The main characteristics of the two reactors are compared in Table 31.

**Table 31. Operating conditions of a fluidized bed reactor and an entrained flow reactor**

| | Fluidized bed reactor | Entrained flow reactor |
|---|---|---|
| Temperature range | 800°C - 1000°C | 1200°C - 1500°C |
| Pressure | 1 - 4 bars | 30 - 80 bars |
| Heating rate | >500 °C.s$^{-1}$ | >1000 °C.s$^{-1}$ |
| Particle size | Centimetric | < 0.2 mm |
| Gaseous reagent | $H_2O/O_2$ / air (no flame) | $H_2O + O_2$ (flame) |
| Particle residence time | Several minutes | A few seconds |
| Gas residence time | A few seconds | A few seconds |

## APPENDIX C: List of the main soot precursors

$C_2H_2$ Acetylene

$C_6H_6$

Benzene

$C_{10}H_8$

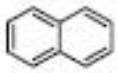

Naphtalene

$C_{12}H_8$

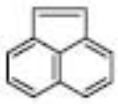

Acenaphtalene

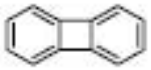

Biphenylene

$C_{13}H_{10}$

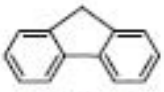

Fluorene

Phenalene

$C_{14}H_{10}$

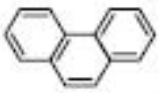

Phenanthrene

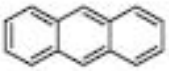

Anthracene

$C_{15}H_{10}$

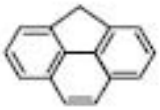

4H-Cyclopenta[def]-phenanthrene

$C_{16}H_{10}$

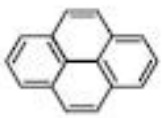

Pyrene

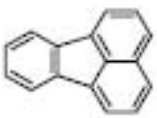

Fluoranthene

$C_{20}H_{12}$

Perylene

$C_{22}H_{12}$

Benzo[ghi]-perylene

Anthanthrene

$C_{24}H_{12}$

Coronene

$C_{28}H_{14}$

Dibenzo[fg,op]-anthanthrene

Dibenzo[hi,qr]-anthanthrene

$C_{30}H_{14}$

Naphto[8,1-abc]coronene

Dibenzo[bc, ef]coronene

Dibenzo[bc, kl]coronene

$C_{38}H_{16}$

Circobiphenyl

# APPENDIX D: Particle residence time during experiments in the drop tube reactor

The residence times used for the 0.35 mm and 0.80 mm particles thermal decomposition in the DTR experiments were calculated from the shrinking core model developed by Chen (2009). This model takes into account the evolution of particle size and density along the transformation and was validated for DTR experiments at 800°C and 950°C.

The residence times of 0.35 mm and 0.80 mm particles versus reactor length, at 1000°C, 1200°C and 1400°C are compared to that of gas in respectively Figure 92a, b and c.

The residence times of the 0.35 mm particles and of gas are close, unlike that of 0.80 mm particles which is much shorter. Note that the residence time of particles slightly increases with temperature.

These results can be explained by the evolution of particle slip velocity along the reactor length, as shown in Figure 93. During particle pyrolysis, the slip velocity firstly increases until reaching a maximum value and then, at the end of the transformation, it decreases until reaching its terminal velocity. The slip velocity reaches a lower maximum value and takes less time to stabilize as temperature increases and particle size decreases. Note that the slip velocity variations for the 0.35 mm particles do not considerably change with temperature.

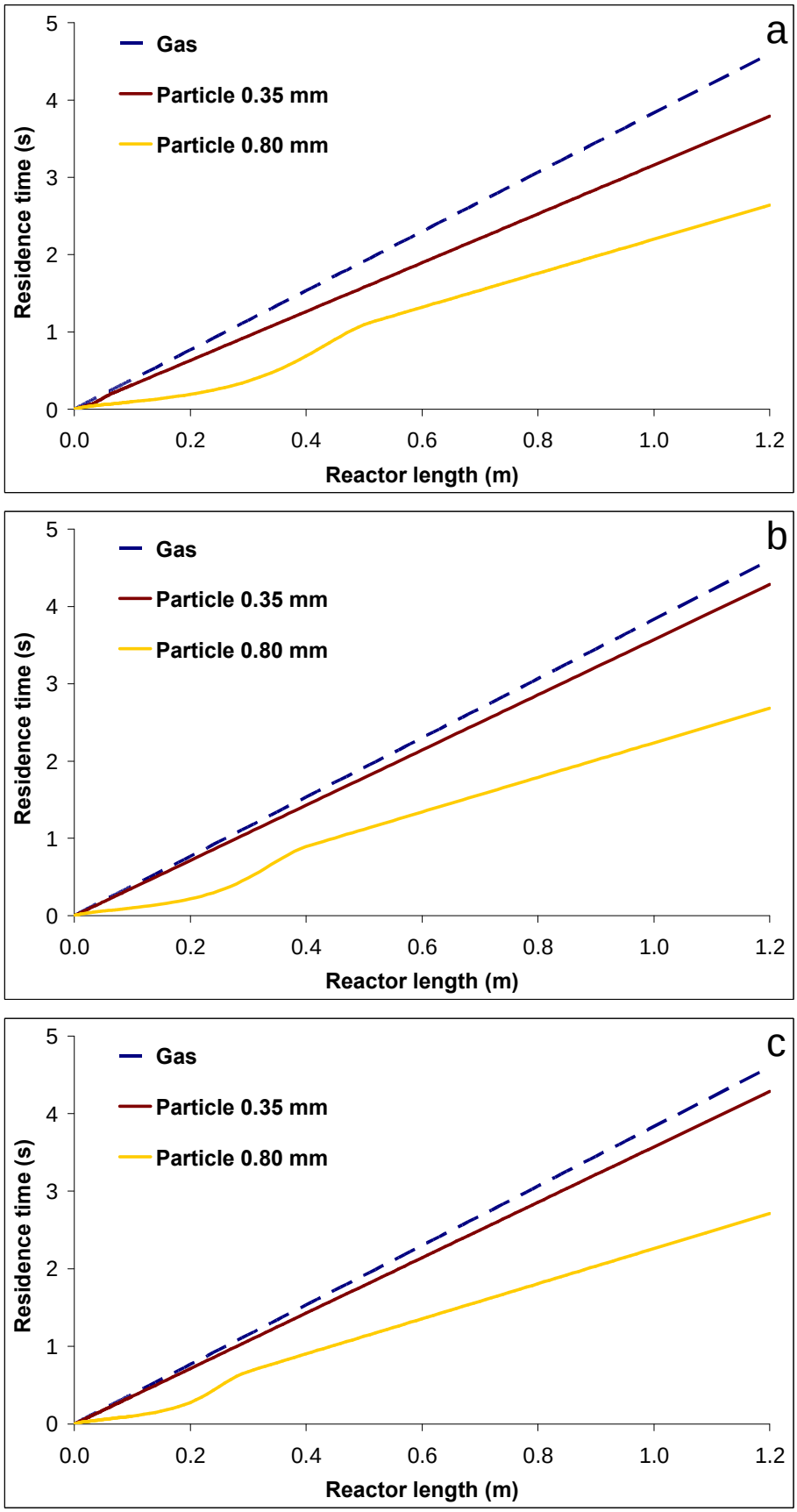


**Figure 92. Residence times of gas, 0.35 mm and 0.80 mm particles during experiments under an inert atmosphere at 1000°C (a), 1200°C (b) and 1400°C (c), versus reactor length**

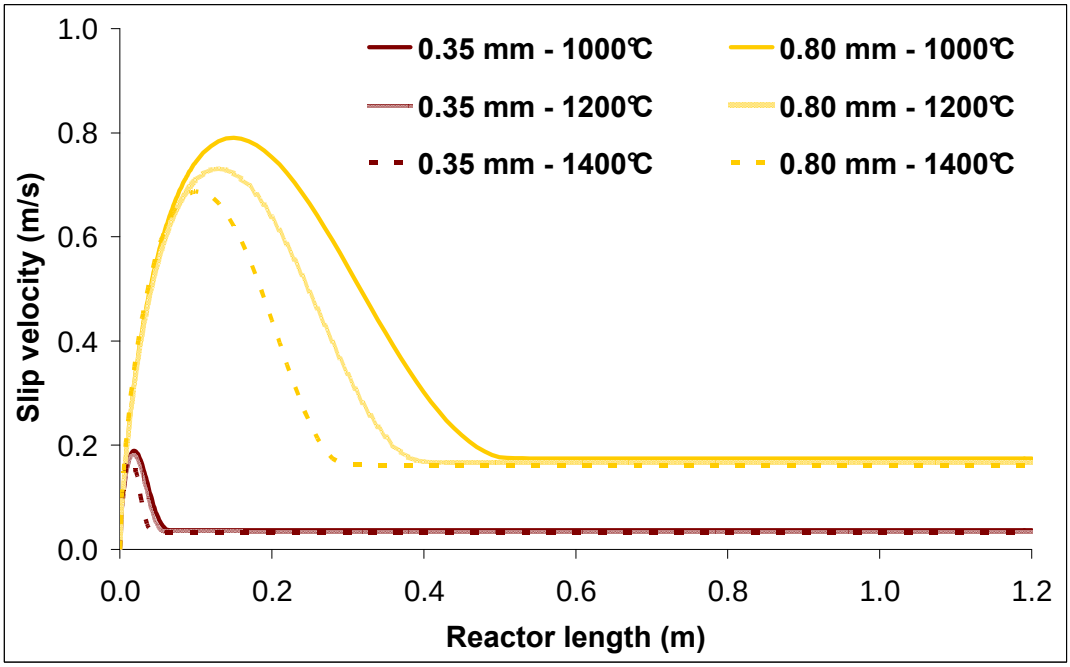


**Figure 93. Slip velocity of 0.35 mm and 0.80 mm particles during experiments under an inert atmosphere at 1000°C, 1200°C and 1400°C, versus reactor length**

# APPENDIX E: Regimes of pyrolysis and gasification during particles thermal decomposition

As described in Section 3.1 of Chapter "State of the Art", a characteristic time analysis can lead to the establishment of pyrolysis and gasification regimes in the DTR experiments conditions. Figure 94 shows the regime of wood particles pyrolysis for two different kinetic parameters set, and Figure 95a and b show that of char steam gasification under atmospheres with respectively 1 mol% and 25 mol% of $H_2O$. The regimes are presented in a temperature range of 1000°C to 1500°C and a particle size range of 0.1 mm to 1 mm.

Note that soot gasification is kinetically controlled in each experimental case.

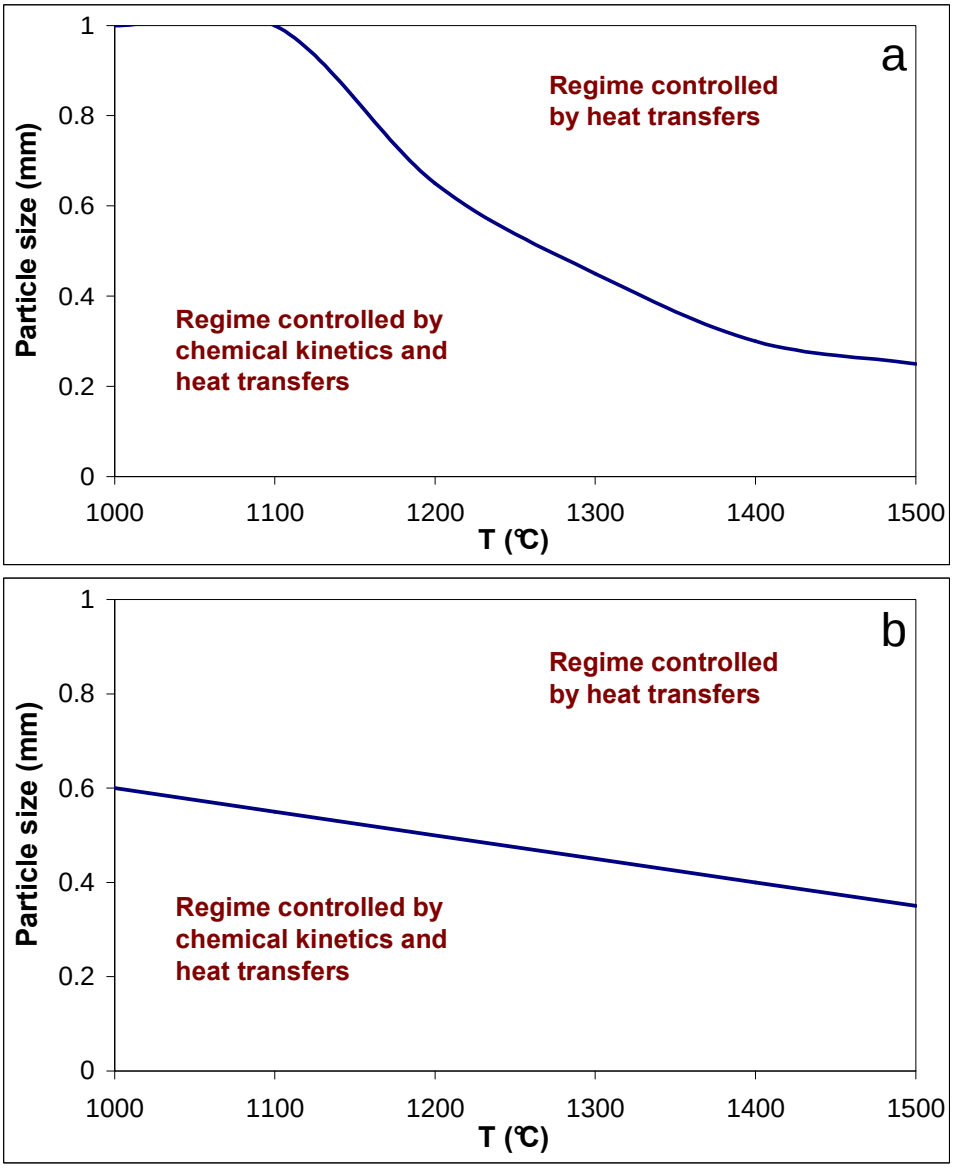


**Figure 94: Regimes of pyrolysis considering kinetic parameters set from Brink (1978) (a) and Shuaning et al. (2006) (b), as a function of temperature and particle size**

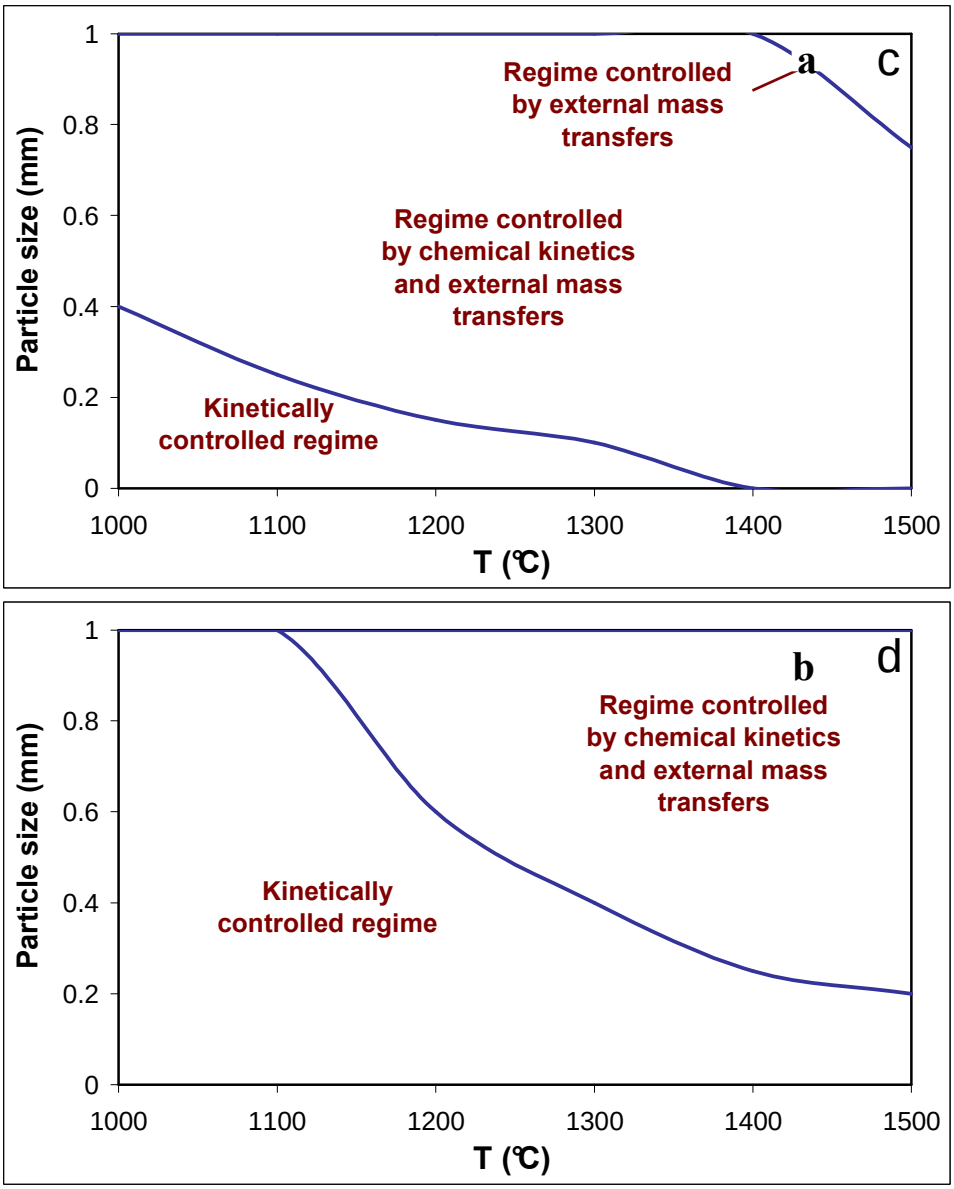


**Figure 95. Regimes of gasification under atmospheres containing 1 mol% (a) and 25 mol% (b) of $H_2O$, as a function of temperature and particle size**

# APPENDIX F: Experimental products yields results

| Inert atmosphere (100 mol% $N_2$) | | | | | |
|---|---|---|---|---|---|
| **Sample** | **0.35 mm particles** | | | | |
| **Temperature (℃)** | **1000** | | **1200** | | **1400** |
| **Gas residence time (s)** | **2 s** | **4 s** | **2 s** | **4 s** | **4 s** |
| **Yields ($g/g_{db}$)** | | | | | |
| $H_2$ | 0.018 | 0.021 | 0.039 | 0.046 | 0.055 |
| CO | 0.470 | 0.448 | 0.496 | 0.514 | 0.651 |
| $H_2O$ | 0.179 | 0.166 | 0.148 | 0.114 | 0.053 |
| $CO_2$ | 0.112 | 0.127 | 0.121 | 0.141 | 0.066 |
| $CH_4$ | 0.062 | 0.060 | 0.028 | 0.023 | 0.005 |
| $C_2H_2$ | 0.040 | 0.036 | 0.030 | 0.015 | 0.005 |
| $C_2H_4$ | 0.028 | 0.015 | 0.001 | 0.001 | 0.000 |
| $C_6H_6$ | 0.021 | 0.027 | 0.006 | 0.003 | 0.000 |
| Char | 0.044 | 0.044 | 0.042 | 0.042 | 0.027 |
| Tar + soot | 0.106 | 0.135 | 0.167 | 0.178 | 0.217 |

| Inert atmosphere (100 mol% $N_2$) | | | | | |
|---|---|---|---|---|---|
| **Sample** | 0.80 mm particles | | | | |
| **Temperature (℃)** | 1000 | | 1200 | | 1400 |
| **Gas residence time (s)** | 2 s | 4 s | 2 s | 4 s | 4 s |
| **Yields ($g/g_{db}$)** | | | | | |
| $H_2$ | 0.018 | 0.022 | 0.040 | 0.043 | 0.053 |
| CO | 0.436 | 0.455 | 0.511 | 0.503 | 0.630 |
| $H_2O$ | 0.186 | 0.175 | 0.142 | 0.122 | 0.065 |
| $CO_2$ | 0.099 | 0.119 | 0.124 | 0.152 | 0.067 |
| $CH_4$ | 0.053 | 0.057 | 0.026 | 0.021 | 0.005 |
| $C_2H_2$ | 0.049 | 0.036 | 0.032 | 0.020 | 0.004 |
| $C_2H_4$ | 0.028 | 0.014 | 0.001 | 0.001 | 0.000 |
| $C_6H_6$ | 0.016 | 0.021 | 0.005 | 0.003 | 0.000 |
| Char | 0.053 | 0.053 | 0.036 | 0.036 | 0.037 |
| Tar + soot | 0.141 | 0.127 | 0.160 | 0.177 | 0.218 |

| Wet atmosphere (75 mol% $N_2$ + 25 mol% of $H_2O$) | | | | | |
|---|---|---|---|---|---|
| **Sample** | **0.35 mm particles** | | | | |
| **Temperature (°C)** | **1000** | | **1200** | | **1400** |
| **Gas residence time (s)** | **2 s** | **4 s** | **2 s** | **4 s** | **4 s** |
| **Yields ($g/g_{db}$)** | | | | | |
| $H_2$ | 0.028 | 0.040 | 0.092 | 0.103 | 0.135 |
| CO | 0.404 | 0.447 | 0.245 | 0.237 | 0.331 |
| $CO_2$ | 0.231 | 0.336 | 0.994 | 1.087 | 1.165 |
| $CH_4$ | 0.062 | 0.072 | 0.064 | 0.062 | 0.000 |
| $C_2H_2$ | 0.041 | 0.037 | 0.021 | 0.006 | 0.000 |
| $C_2H_4$ | 0.012 | 0.005 | 0.000 | 0.000 | 0.000 |
| $C_6H_6$ | 0.019 | 0.028 | 0.003 | 0.000 | 0.000 |
| Char | 0.030 | 0.030 | 0.013 | 0.013 | 0.000 |
| Tar + soot | 0.136 | 0.082 | 0.055 | 0.051 | 0.048 |

| Wet atmosphere (75 mol% $N_2$ + 25 mol% of $H_2O$) | | | | | |
|---|---|---|---|---|---|
| **Sample** | **0.80 mm particles** | | | | |
| **Temperature (°C)** | **1000** | | **1200** | | **1400** |
| **Gas residence time (s)** | **2 s** | **4 s** | **2 s** | **4 s** | **4 s** |
| **Yields ($g/g_{db}$)** | | | | | |
| $H_2$ | 0.032 | 0.036 | 0.093 | 0.101 | 0.135 |
| CO | 0.438 | 0.420 | 0.245 | 0.236 | 0.357 |
| $CO_2$ | 0.249 | 0.304 | 0.925 | 1.065 | 1.153 |
| $CH_4$ | 0.067 | 0.068 | 0.060 | 0.056 | 0.000 |
| $C_2H_2$ | 0.036 | 0.035 | 0.013 | 0.006 | 0.000 |
| $C_2H_4$ | 0.014 | 0.006 | 0.000 | 0.000 | 0.000 |
| $C_6H_6$ | 0.020 | 0.022 | 0.000 | 0.000 | 0.000 |
| Char | 0.040 | 0.040 | 0.011 | 0.011 | 0.000 |
| Tar + soot | 0.107 | 0.105 | 0.088 | 0.063 | 0.041 |

**Reminder:** Uncertainty of the products yields for DTR experiments in dry and wet atmospheres

| $H_2$ | CO | $CO_2$ | $H_2O$ | $CH_4$ | $C_2H_2$ | $C_2H_4$ | $C_2H_6$ | $C_6H_6$ | Char | Tar + soot |
|---|---|---|---|---|---|---|---|---|---|---|
| 5% | 5% | 10% | 10% | 10% | 20% | 20% | 20% | 20% | 25% | 40% |

# APPENDIX G: SEM observations of soot and char from DTR experiments

- **Soot from the experiments at 1200°C and 1400°C with the 0.80 mm particles**

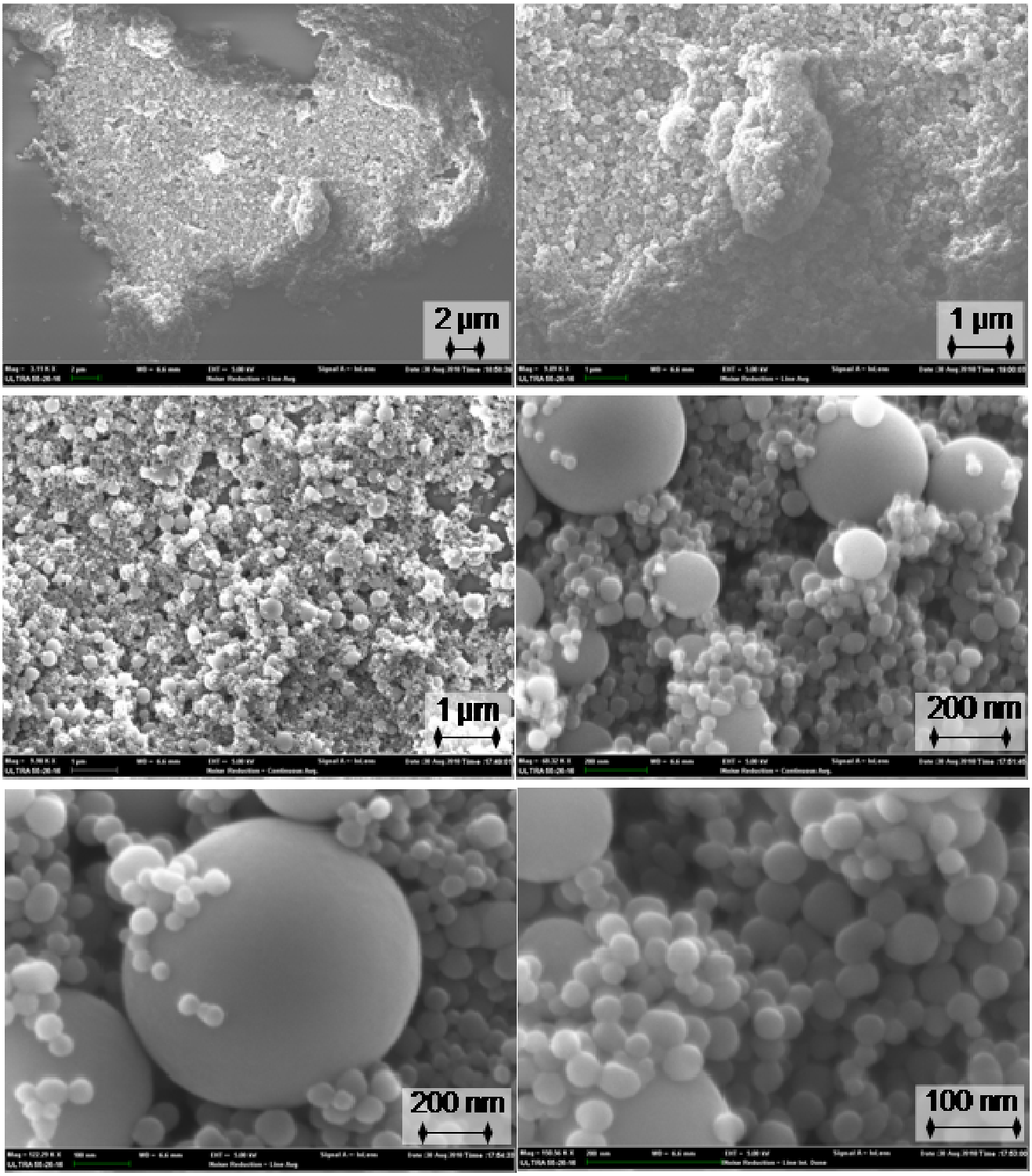

- **Char from the experiments at 1000°C, 1200°C and 1400°C with the 0.35 mm particles**

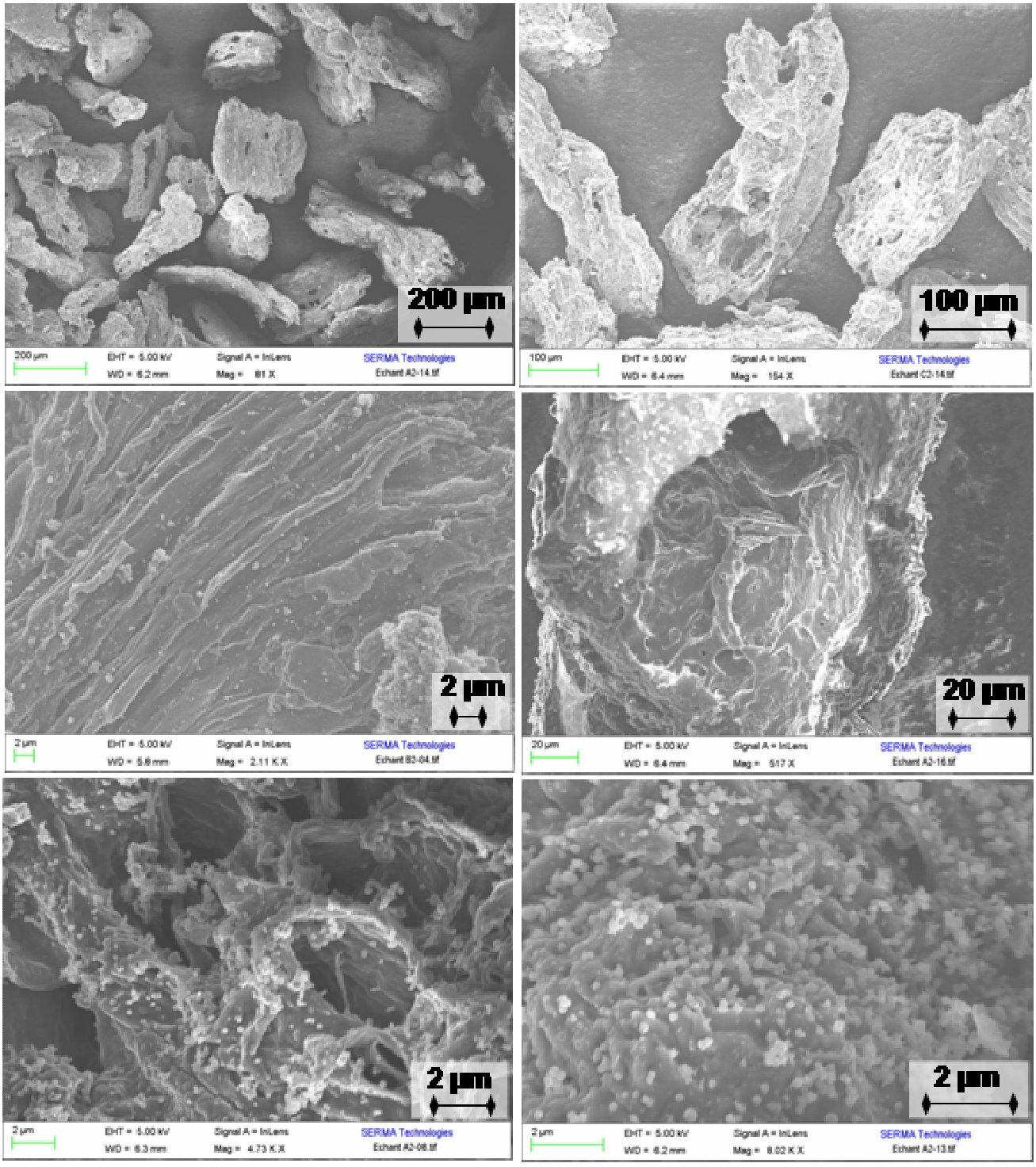

- **Char from the experiments at 1000°C, 1200°C and 1400°C with the 0.80 mm particles**

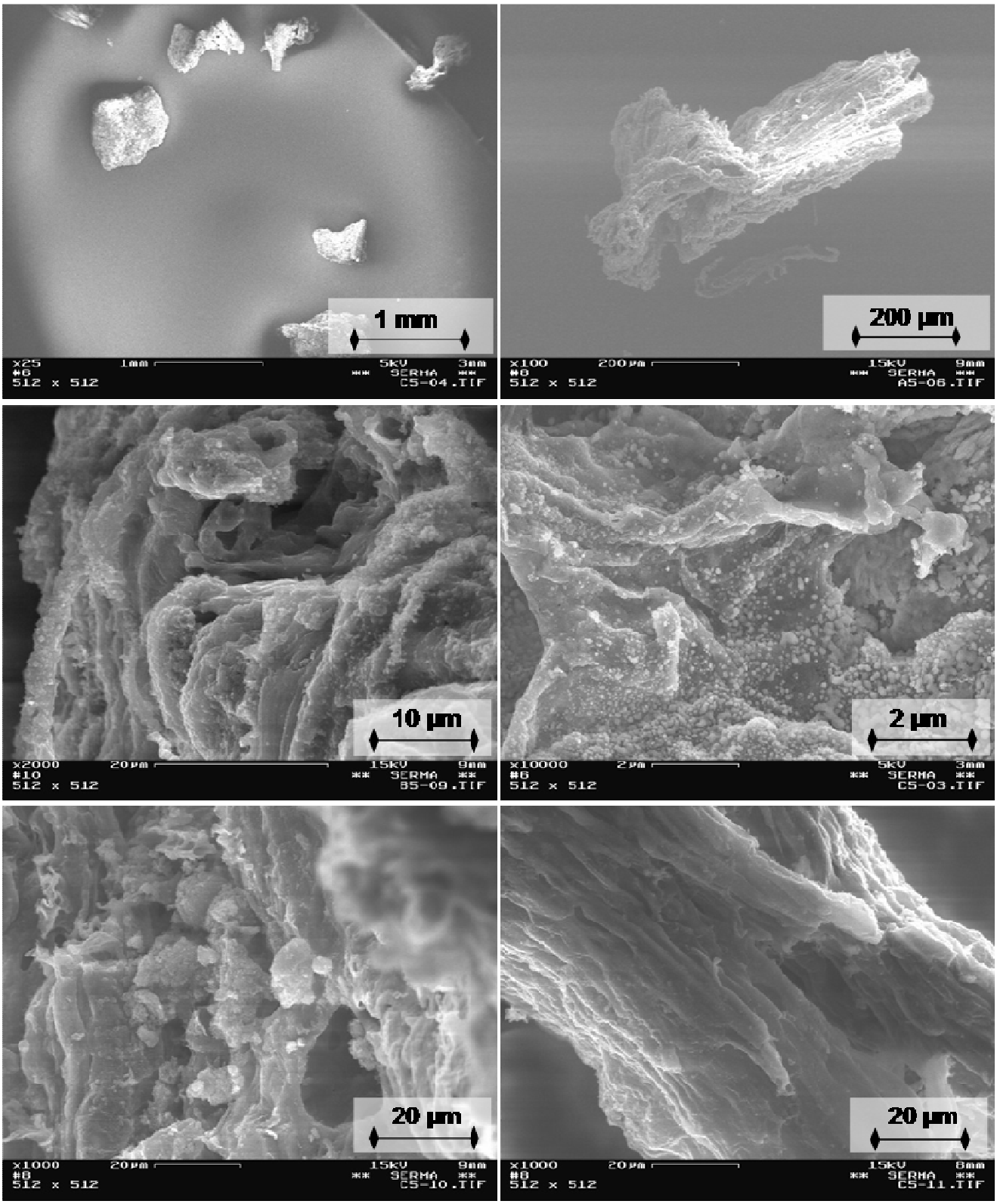

- **Char from the experiments under a wet atmosphere at 1000°C with the 0.35 mm particles**

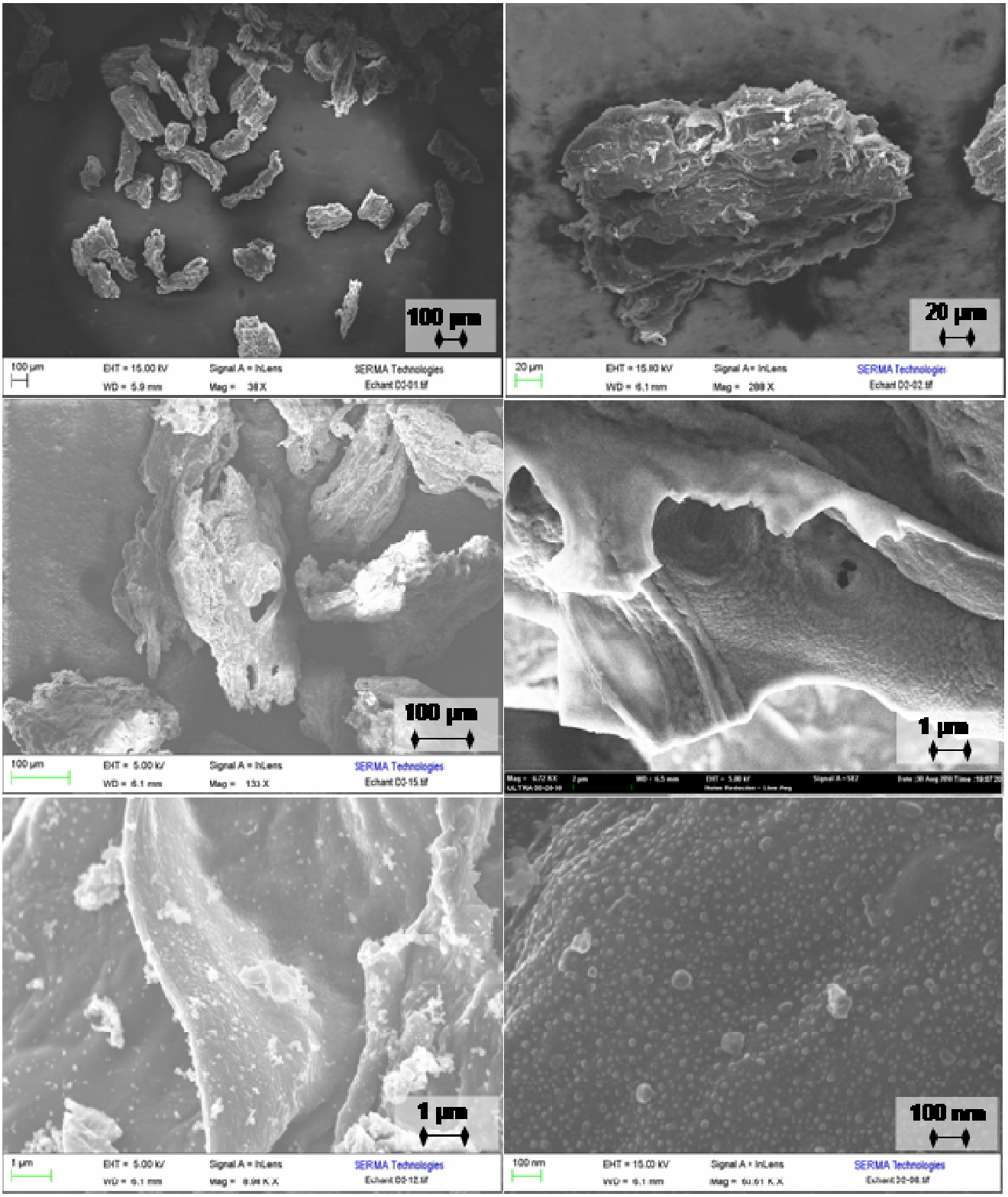

- **Char from the experiments under a wet atmosphere at 1200°C with the 0.80 mm particles**

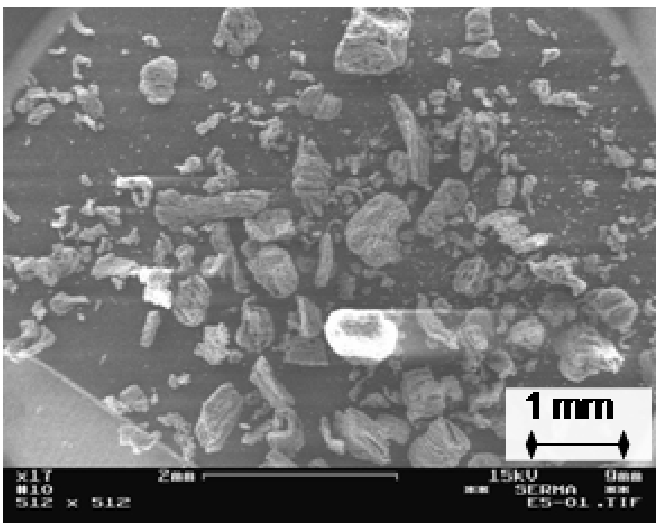


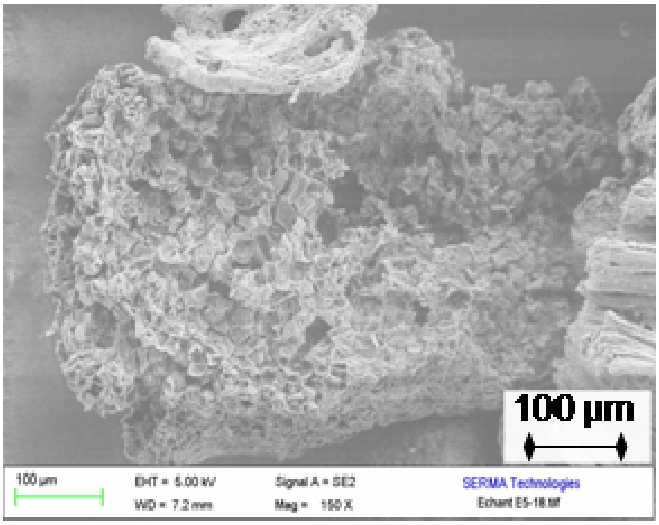


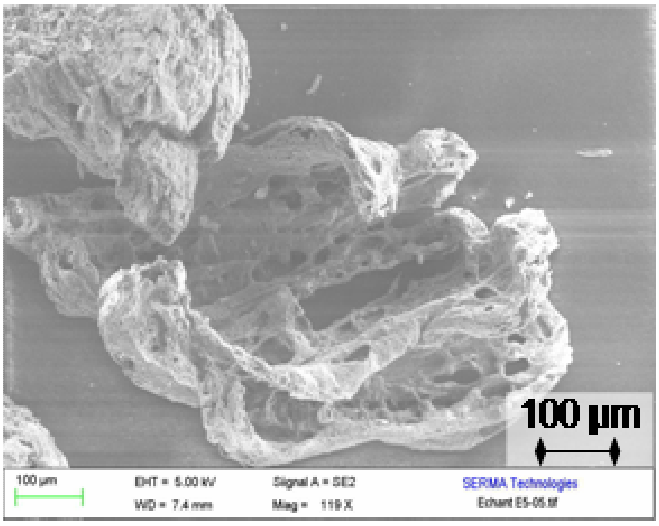


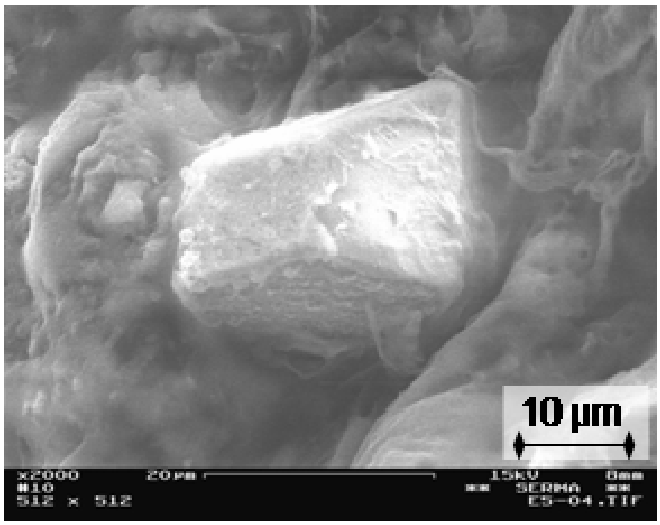


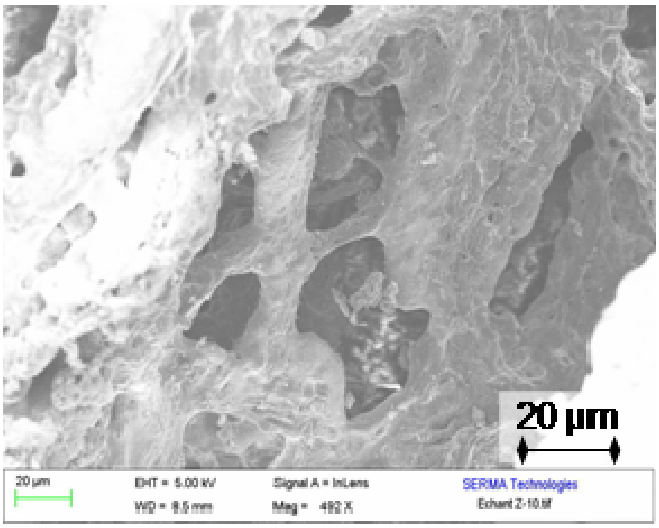


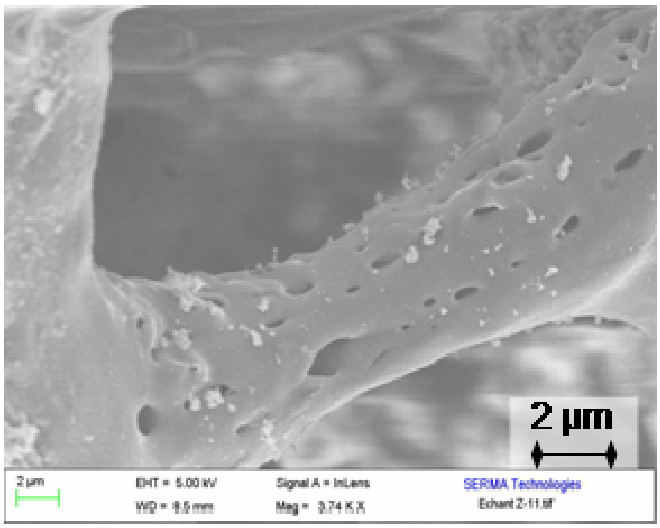

- **Char from the experiments under a wet atmosphere at 1400°C with the 0.35 mm and 0.80 mm particles**

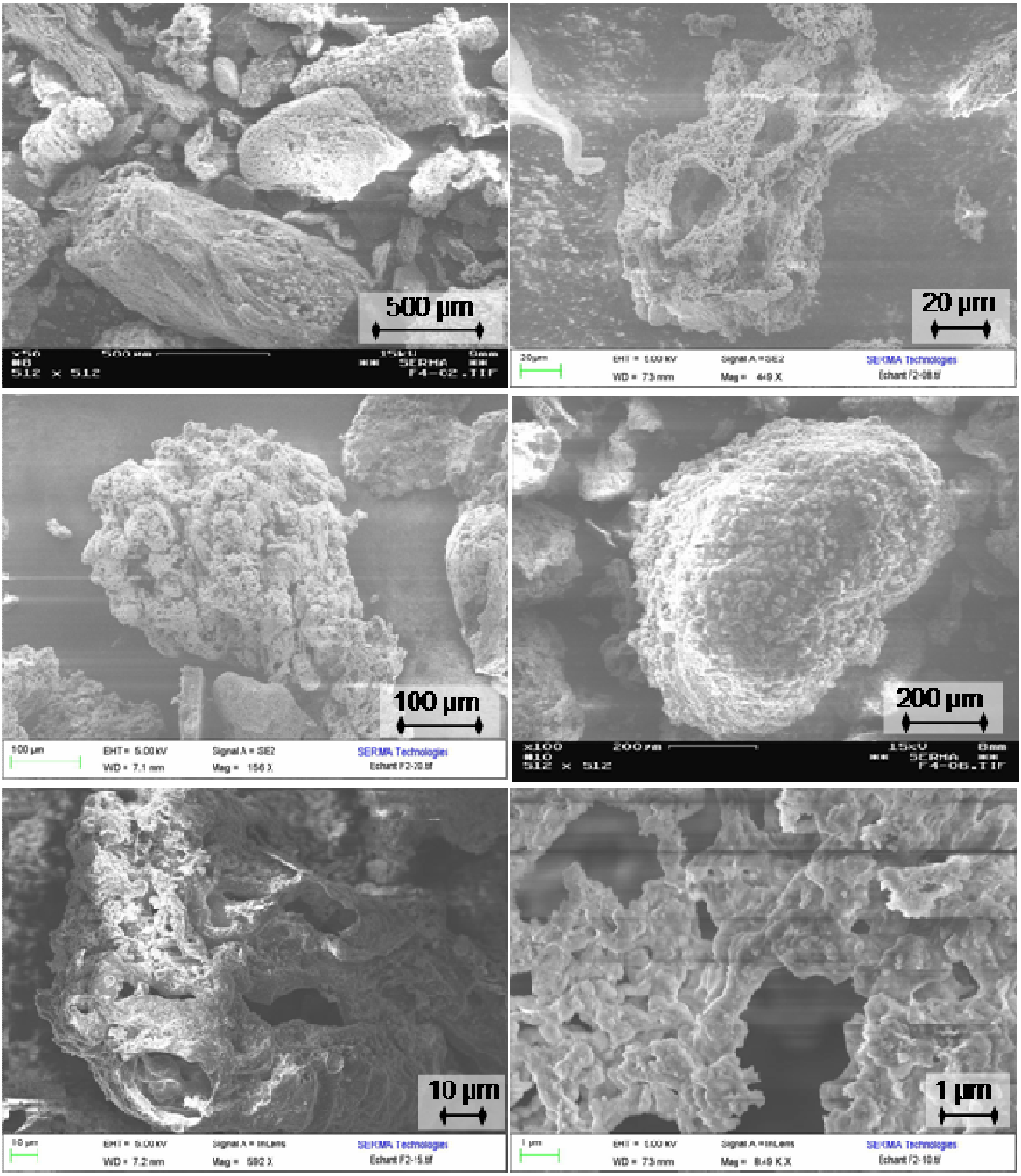

# APPENDIX H: Influence of a wet atmosphere on char characteristics

During the DTR experiments with 0.35 mm particles under a wet atmosphere, an enough quantity of char for a complete characterization was collected only at 1000°C. During the experiments at 1200°C and 1400°C, the collected amounts of char were hardly enough for C, H composition analysis, thermogravimetric experiments and electronic microscopy. For the char at 1400°C, only SEM observations could be performed.

- Char morphology

The morphology of char sample obtained under a wet atmosphere at 1000°C cannot be differenced from that of a char obtained under an inert atmosphere, as shown in Appendix G with the SEM observations.

Figure 96 shows the structure of the gasified char particles from 1200°C and 1400°C experiments under a wet atmosphere, observed by SEM, with their respective XRD analysis spectrum.

The char particles at 1200°C (Figure 96a) present a higher porosity and thinner walls than a non reacted char, which reflects a high conversion degree. As shown by the XRD analysis in Figure 96a, the char surface is still mainly composed of carbon but inorganic compounds are also detected – here Na, Mg and Si – in considerable amounts.

The char particles from 1400°C experiments (Figure 96b) present the aspect of a char at the end of conversion, with inorganic content on its surface – here Na, Mg, Si, Ca and K - in the same order of magnitude than the carbon content according to the XRD analysis. The ash particles (Figure 96c) can be identified by their small size which is inferior to 100 µm, their non porous structure and their composition rich in inorganics – here Mg and Si.

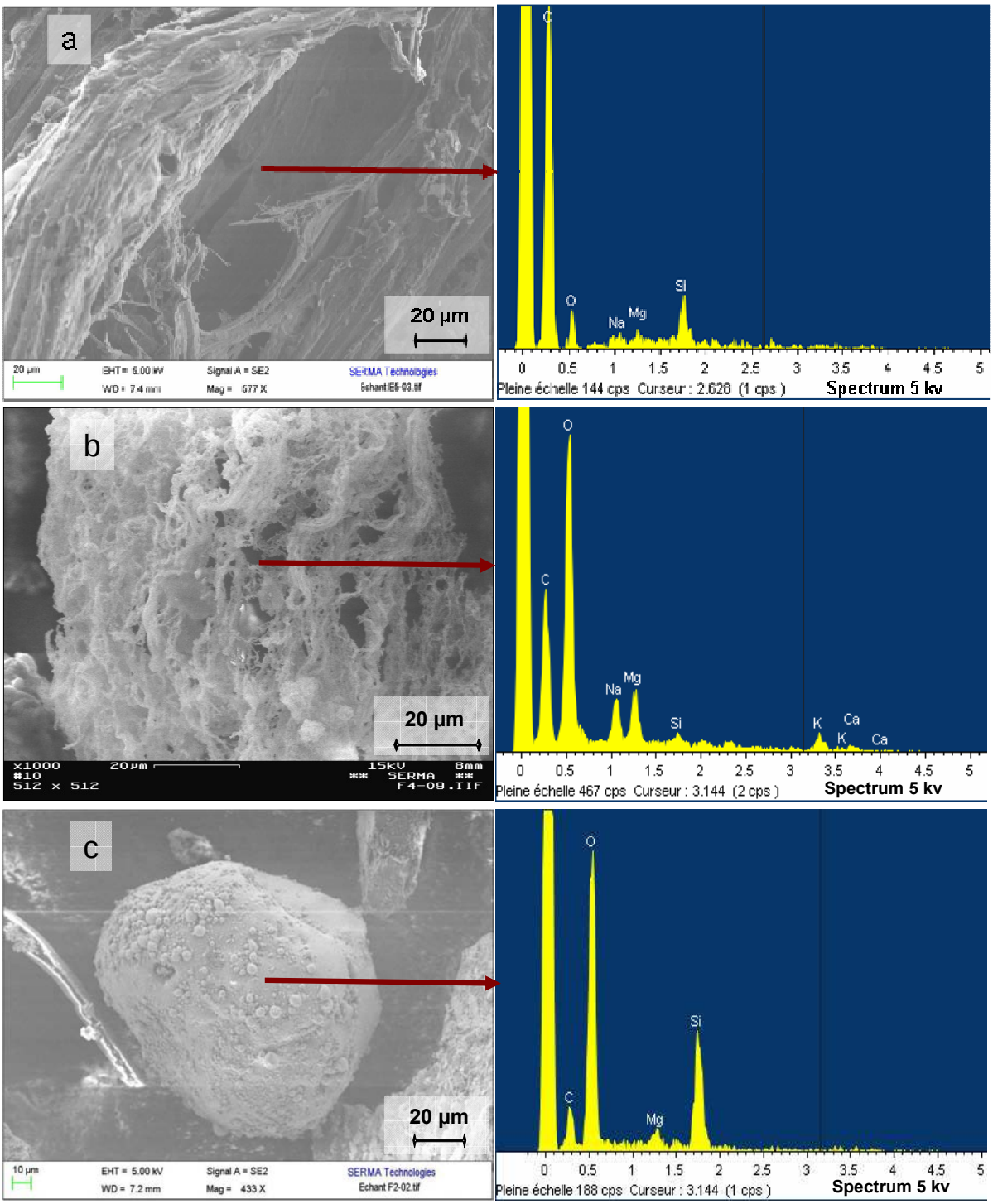


**Figure 96. SEM observations of char samples from experiments under a wet atmosphere at 1200°C (a) and 1400°C (b -c) with their respective XRD analysis spectrum**

- Char composition

The composition of chars obtained with 0.35 mm particles under inert and wet atmospheres at 1000°C are compared in Table 32.

**Table 32. Molar composition (daf) of chars samples from the 0.35 mm particle thermal decomposition under inert and wet atmospheres at 1000°C**

| Molar composition %, daf | Inert atmosphere | Wet atmosphere |
|---|---|---|
| Carbon | 66 ± 3 | 71 ± 4 |
| Hydrogen | 25 ± 5 | 23 ± 5 |
| Oxygen | 9 ± 5 | 6 ± 3 |

Chars formed under inert and wet atmospheres have the same composition, which suggests that $H_2O$ does not have a considerable influence on char chemical composition.

- Char reactivities

Figure 97 represents the reactivity of char from the 0.35 mm particles thermal decomposition at 1000°C under inert and wet atmospheres, and at 1200°C under a wet atmosphere. The reactivity is defined in two conversion ranges, 0 – 95% and 10 – 70%.

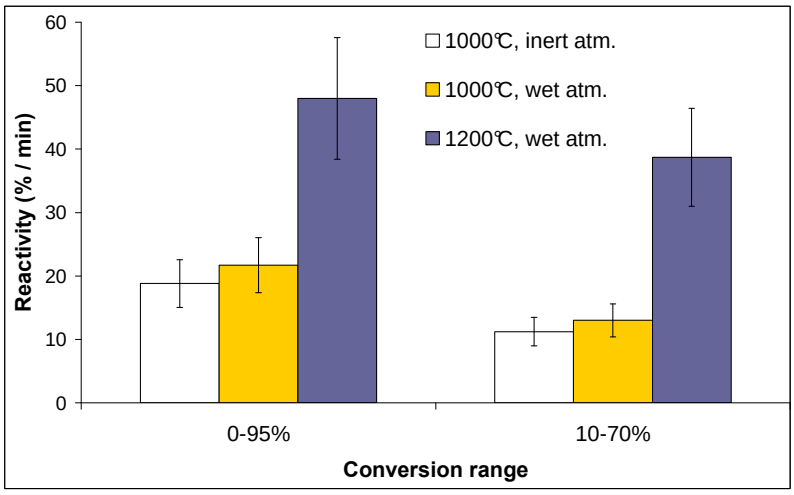


**Figure 97. Reactivity in two conversion ranges of char samples from the 0.35 mm particles thermal decomposition under inert and wet atmospheres at 1000°C and 1200°C**

The char samples from experiments at 1000°C have the same reactivity in the two conversion ranges. On the contrary, the reactivity of char from experiments under a wet atmosphere at 1200°C is 2 to 3 times higher than the reactivity of 1000°C samples.

According to these results, $H_2O$ has not a direct influence on char reactivity, as seen for samples at 1000°C. Nevertheless, it can indirectly lead to the increase of reactivity by the means of gasification, since it is widely accepted that reactivity increases with conversion during gasification. This trend is opposed to thermal annealing, from which a decrease of reactivity is expected to occur with temperature. Indeed, thermal annealing and gasification are competing phenomena. Therefore, the influence of gasification on char reactivity seems to be more important than that of thermal annealing for char from DTR experiments under a wet atmosphere at 1200°C.

# APPENDIX I: Kinetic parameters calculation for soot and char gasification

The gasification kinetic parameters for soot and char collected in DTR experiments were calculated with the classical kinetic method.

At first, soot and char reactivities to steam gasification were determined, using Equation 74, from the mass loss measured during TGA experiments at 3 different temperatures and with 2 different $H_2O$ contents in the atmosphere. The temperatures during TGA experiments were 750°C, 800°C and 850°C for char, and 910°C, 950°C and 980°C for soot. The $H_2O$ contents in the atmosphere were 5 mol% and 20 mol%. A mean reactivity was calculated in a conversion range of 10 - 70%.

$$r = \frac{dm}{dt} \cdot \frac{1}{m(t)} \qquad \textbf{Equation 74}$$

After the experimental reactivity determination, gasification kinetic parameters were obtained with Equation 75.

$$r = k_0 \cdot \exp\left(\frac{-Ea}{R \cdot T}\right) \qquad \textbf{Equation 75}$$

For this, $\ln(R_{X=10\text{ - }70\%})$ was plotted versus f(1/T) and $\ln(P_{H20})$, as shown in Figure 98 for soot and in Figure 99 for char.

The values of the activation energy, pre-exponential factor and of the order of the reaction could then be determined from the slopes of the graphs of Figure 98 and Figure 99, using the expression of Equation 76.

$$\ln\left(R_{X=10-70\%}\right) = -\frac{Ea}{R} \cdot \frac{1}{T} + n\ln\left(P_{H2O}\right) + \ln\left(k_0\right) \qquad \textbf{Equation 76}$$

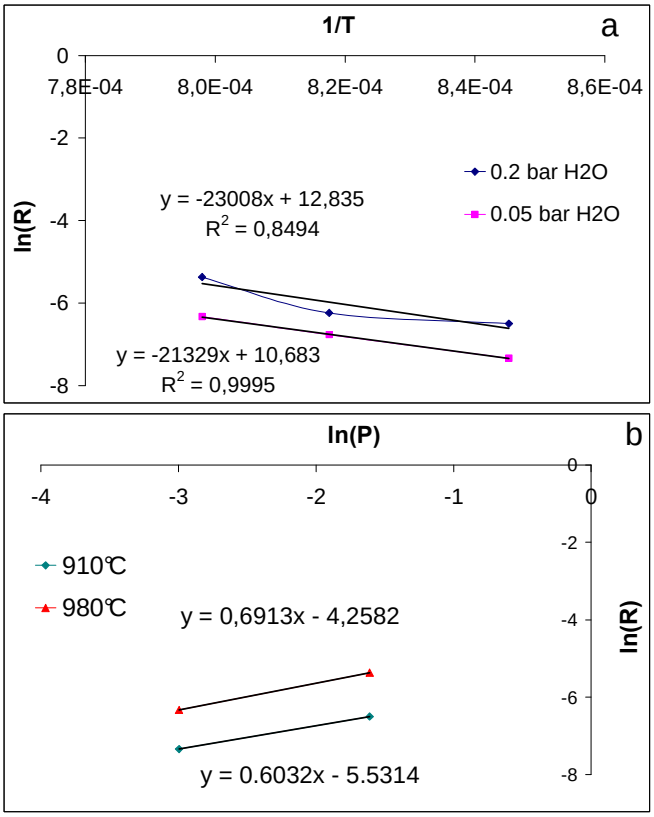


**Figure 98. Graphs [$\ln(R_{X=10-70\%})=f(1/T)$] (a) and [$\ln(R_{X=10-70\%}) = f(\ln(P_{H2O})$] (b) for soot**

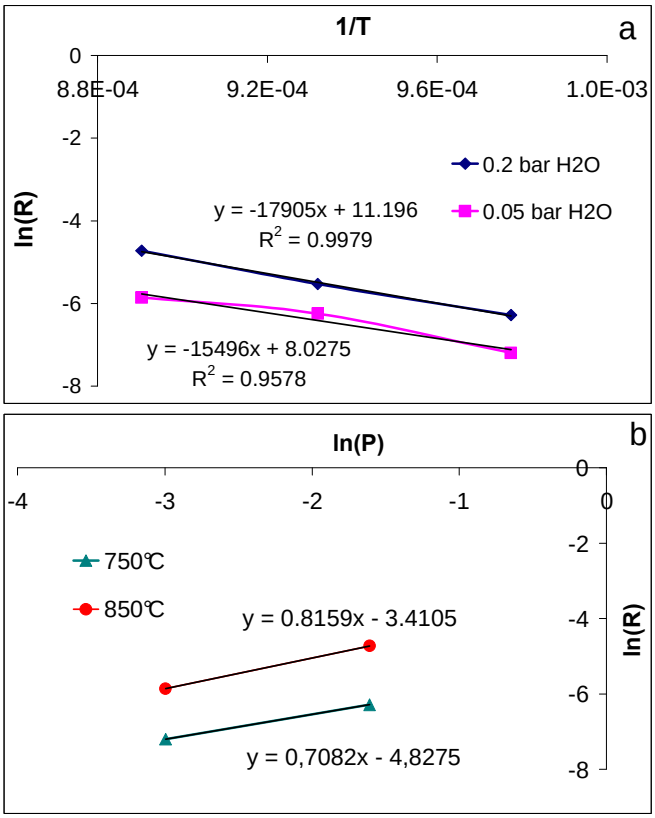


**Figure 99. Graphs [$\ln(R_{X=10-70\%})=f(1/T)$] (a) and [$\ln(R_{X=10-70\%}) = f(\ln(P_{H2O})$] (b) for char**